ASSESSMENT OF THE HOST POTENTIAL OF TETROL [(+)-(2*R*,3*R*)-1,1,4,4-TETRAPHENYLBUTANE-1,2,3,4-TETRAOL] FOR THE SEPARATION OF ISOMERS AND RELATED COMPOUNDS

S. DORFLING

Nelson Mandela University

2017

ASSESSMENT OF THE HOST POTENTIAL OF TETROL [(+)-(2*R*,3*R*)-1,1,4,4-TETRAPHENYLBUTANE-1,2,3,4-TETRAOL] FOR THE SEPARATION OF ISOMERS AND RELATED COMPOUNDS

by

SASHA-LEE DORFLING

Submitted in fulfilment of the requirements of the degree of

PHILOSOPHIAE DOCTOR

In the Faculty of Science to be awarded at the Nelson Mandela University,

South Africa

2017

PROMOTOR: DR. B. BARTON

NELSON MANDELA

UNIVERSITY

DECLARATION BY CANDIDATE

NAME: Sasha-Lee Dorfling

STUDENT NUMBER: 210075384

QUALIFICATION: PhD (Organic Chemistry)

TITLE OF PROJECT: Assessment of The Host Potential of TETROL [(+)-(2*R*,3*R*)-1,1,4,4- Tetraphenylbutane-1,2,3,4-Tetraol] for the Separation of Isomers and Related Compounds

DECLARATION:

In accordance with Rule G5.6.3, I hereby declare that the above-mentioned treatise/ dissertation/ thesis is my own work and that it has not previously been submitted for assessment to another University or for another qualification.

SIGNATURE:

DATE: 18th December 2017

ACKNOWLEDGEMENTS

The author wishes to express her sincere thanks to:

– Dr. B. Barton for her supervision, commitment, mentorship and enthusiasm throughout this project.

– Dr. E. Hosten for running of SCXRD experiments.

– Mr L. Bolo for help with thermal analysis experiments.

– Mr. E. Bashman for his assistance.

– My family for their constant support, love and encouragement

– To Daniel Jooste for his shared passion in chemistry, moral support and enduring love

– To Pieter Pohl, my best friend, for sharing this journey with me and for being a loyal friend

PUBLICATIONS AND CONFERENCES

- Chapter 4 of this thesis has been published: Barton, B., Dorfling, S. and Hosten, E. C., Cyclohexanone-Driven Discriminatory Behavior Change of Host Compound (+)-(2R,3R)TETROL for Isomeric Methylcyclohexanone Guests, *Cryst. Growth Des.*, 2017, DOI: 10.1021/acs.cgd.7b01334.

- Chapter 4 of this thesis was presented as a poster at the 18th Tetrahedron Symposium, Asia Edition held in Melbourne, Australia, on the 24–26th July 2017. The poster title was "Cyclohexanone-Driven Discriminatory Behaviour Change of Host Compound (+)-(2R,3R)-TETROL for the Isomeric Methylcyclohexanone Guests".

Table of Contents

SUMMARY

In this study, we investigated the potential of a host compound, (+)-(2*R*,3*R*)-1,1,4,4-tetraphenylbutane-1,2,3,4-tetrol (TETROL), for use in the separation of isomers and related compounds using host-guest chemistry. The synthesis of this host was carried out using a standard Grignard procedure, reacting naturally-occurring optically active tartaric acid with phenylmagnesium bromide. The feasibility of this host for separating isomers and structurally-related compounds was investigated by recrystallizing it from various potential cyclic, aromatic and aliphatic guest compounds. The extent of host inclusion and guest separation were determined using ^{1}H-NMR spectroscopy and GC-MS analyses.

Competition studies were conducted to establish the selectivity of TETROL for the various guest species and whether this host would be able to discriminate between them. In this instance, the host was recrystallized from equimolar amounts of binary, ternary, quaternary or quinary mixtures of the guests present in each target study. Subsequent binary or ternary competitions were conducted where the molar ratios of the guest species were varied beyond equimolar, and the guest selectivity of TETROL thus evaluated by means of selectivity profiles. Further analyses included single crystal X-ray diffraction (SCXRD), thermal analysis and Hirshfeld surface analysis. Any crystalline inclusion complex formed between host and guest, with suitable crystal quality, was analysed using SCXRD in order to determine the nature of any significant host–guest interactions present. Thermogravimetric and differential scanning calorimetry experiments provided further insight into complex stability by analysing the thermal events experienced by the complexes as they were heated at 10 °C/min. The data obtained from Hirshfeld surface analyses were used to determine whether host selectivity and/or thermal stability of the complexes were related to the number and types of interactions, observed from SCXRD, between host and guest.

The ability of TETROL to discriminate between related compounds was favourable. This host proved to have selective preference for aniline over its methylated derivatives, *N*-methylaniline and *N,N*-dimethylaniline. It was also selective for cyclohexylamine over cyclohexanol and cyclohexanone, and discriminated against the pyridine, piperidine and dioxane heterocyclics in favour of morpholine. Furthermore, this host was successful in the selective separation of isomers; for example, it

selectively showed discrimination between the three toluidine isomers (*p*-toluidine > *m*-toluidine > *o*-toluidine) and the cresols (*p*-cresol > *m*-cresol > *o*-cresol). Each guest mixture was selected based on data from experiments using either the industrial significance of its separation or because the mixture would add to the knowledge base of the host compound's preferences and selectivities.

In a separate study, TETROL and its derivative, (–)-(2*R*,3*R*)-2,3-dimethoxy-1,1,4,4-tetraphenylbutane-1,4-diol (DMT), were also allowed to compete for the inclusion of the guest cyclohexanone, where TETROL demonstrated superior ability. This host, in addition, showed potential for the separation of *cis*- and *trans*- 2-methylcyclohexanol.

Key Words:
- Host-Guest Chemistry
- Selectivity
- Isomer Separation
- Thermal Analysis
- SCXRD
- Hirshfeld Surface

ABBREVIATIONS AND SYMBOLS

H	Host
G	Guest
π–π	pi–pi
CH–π	CH–pi
TADDOL	α,α,α',α'-Tetraphenyl-2,2-dimethyl-1,3-dioxolan-4,5-dimethanol
TETROL	(+)-(2R,3R)-1,1,4,4-Tetraphenylbutane-1,2,3,4-tetraol
DMT	(−)-(2R,3R)-2,3-Dimethoxy-1,1,4,4-tetraphenylbutane-1,4-diol
Ton	Onset temperature of mass loss
Tb	Boiling point of a pure liquid guest
Tp	Peak temperature of mass loss
Tend	Peak endotherm temperature
CAM	Cyclohexylamine
CON	Cyclohexanone
COL	Cyclohexanol
2MCON	2-Methylcyclohexanone
3MCON	3-Methylcyclohexanone
4MCON	4-Methylcyclohexanone
MOR	Morpholine
PIP	Piperidine
PYR	Pyridine
DIO	Dioxane
ANI	Aniline
NMA	*N*-Methylaniline
NNMA	*N,N*-Dimethylaniline
o-TOLU	*ortho*-Toluidine
m-TOLU	*meta*-Toluidine
p-TOLU	*para*-Toluidine
PHO	Phenol
OC	*ortho*-Cresol
MC	*meta*-Cresol
PC	*para-Cresol*
2-MC	2-Methylcyclohexanol
BA	Butyric acid

IBA	*iso*-Butyric acid
3CPA	3-Chloropropionic acid
TG	Thermogravimetry
DSC	Differential scanning calorimetry
^{1}H-NMR	Proton nuclear magnetic resonance
GC-MS	Gas chromatography / mass spectroscopy
K	Selectivity coefficient
X	Mole fraction of guest in the mother liquor
Z	Mole fraction of guest in the crystal
PXRD	Powder X-ray diffraction
SCXRD	Single crystal x-ray diffraction
a, b, c	Unit cell axes
α	Angle between b and c unit cell axes
β	Angle between a and c unit cell axes
γ	Angle between a and b unit cell axes
V	Unit cell volume
Z	Number of formula units per cell

Hydrogen

H⋯Cl interaction

Carbon

Oxygen

Nitrogen

Chlorine

O⋯H/O⋯H interaction

N⋯H/N⋯H interaction

H⋯H/H⋯H interaction

C⋯H/C⋯H interaction
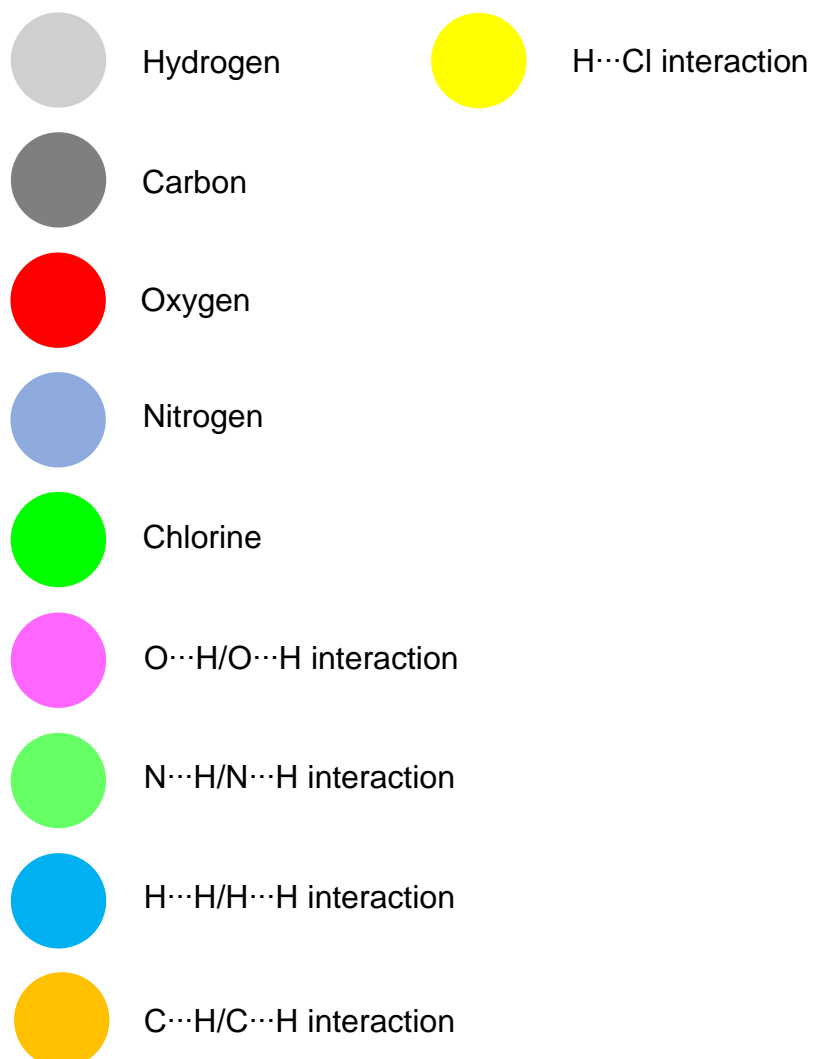
Chapter 1

1.   Introduction

1.1.   Supramolecular Chemistry

Supramolecular chemistry is a rapidly growing field that describes the "chemistry beyond the molecule" or "the chemistry of the non-covalent bond".[1-4] It is a discipline that studies the aggregation of molecules or ions that assemble and organize through non-covalent intermolecular interactions such as hydrogen bonding, metal coordination, hydrophobic forces, van der Waals forces, pi–pi interactions and electrostatic effects. Figure 1 is an example showing the self-assembly of $[Fe_5L_5)Cl]^{9+}$ from five tris-bipyridyl (bpy) ligand strands (L) and five molar equivalents of iron(II)chloride.[5,6]
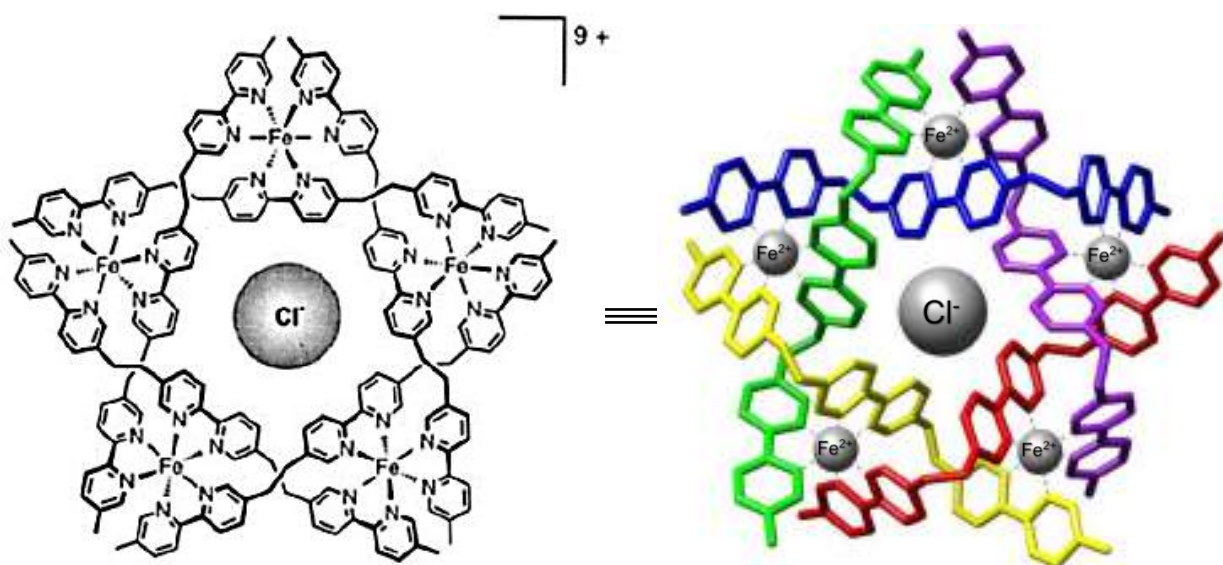
Figure 1: A supramolecular complex discovered by Jean-Marie Lehn *et al*[6]: the self-assembly of the circular helicate [(Fe₅L₅)Cl]⁹⁺ from five tris-bpy ligand strands and five equivalents of FeCl₂

The existence of intermolecular forces was first discovered by Johannes Diderik van der Waals in 1873.[7] In 1894, Nobel laureate Hermann Emil Fischer introduced the "lock and key" mechanism associated with enzyme-substrate interactions that

presently form the foundation of supramolecular chemistry and aid in the understanding of molecular recognition and "host-guest" chemistry.[8,9] In the early twentieth century, the recognition of non-covalent bonds progressively grew with the description of the hydrogen bond by Latimer and Rodebush in 1920.[10] With the support of these findings, supramolecular chemistry was established as a well-accepted chemical discipline by the work of Nobel laureates Donald J. Cram, Jean-Marie Lehn and Charles J. Pedersen "for their development and use of molecules with structure-specific interactions of high selectivity" in 1987.[11] Jean-Marie Lehn simply defined supramolecular chemistry as the "chemistry of molecular assemblies and of the intermolecular bond".[12,13]

Supramolecules are essentially aggregates formed by numerous components assembling together either spontaneously or by design. Consequently, supramolecular chemistry may be divided into two subsets, namely host-guest chemistry and self-assembly. Self-assembly is a process in which separate or linked components spontaneously form ordered aggregates under appropriate conditions.[14,15] These components may have ranging sizes from the molecular to the macroscopic.[16] However, a fundamental example of a supramolecular structure is a host-guest complex. Host-guest chemistry is a recognition-directed interaction involving a natural or sensibly designed synthetic structure (the host) which can recognize a target molecule (the guest), thus forming a supramolecular complex through non-covalent interactions. The host is generally a large organic molecule comprising of convergent binding sites and a large cavity volume that can accommodate the simpler guest molecule containing complementary divergent binding sites.[17] The study at hand focuses on host-guest chemistry while simultaneously using supramolecular chemistry principles to aid in the understanding of selectivities observed for various host-guest complexes.

1.2.   Non-covalent Interactions

Non-covalent, or non-bonding interactions, play a critical role in many chemical and biological systems. In biology, selectivity and recognition are achieved through non-covalent contacts, as well as the stabilization of large three-dimensional molecules, such as proteins and nucleic acids.[18] In chemistry, non-covalent interactions influence

a vast proportion of chemical reactions and the design of building blocks.[19] These non-covalent interactions include a variety of weak and reversible inter- or intra- molecular attractive forces. As previously stated, supramolecular chemistry is the chemistry of the non-covalent bond. Therefore, we will now discuss the non-covalent interactions frequently associated within the field of supramolecular chemistry.

The formation of a host-guest complex involves an extensive range of non-covalent attractive forces. The most prevalent intermolecular interactions are a) hydrogen bonding, b) cation⋯π, c) polar⋯π, d) C–H⋯π and e) aromatic C–H⋯π (T-shaped stacking) (Figure 2). These forces assist in controlling the packing of host-guest systems and can be classified according to their strength, directional influence and distance dependence.[20]
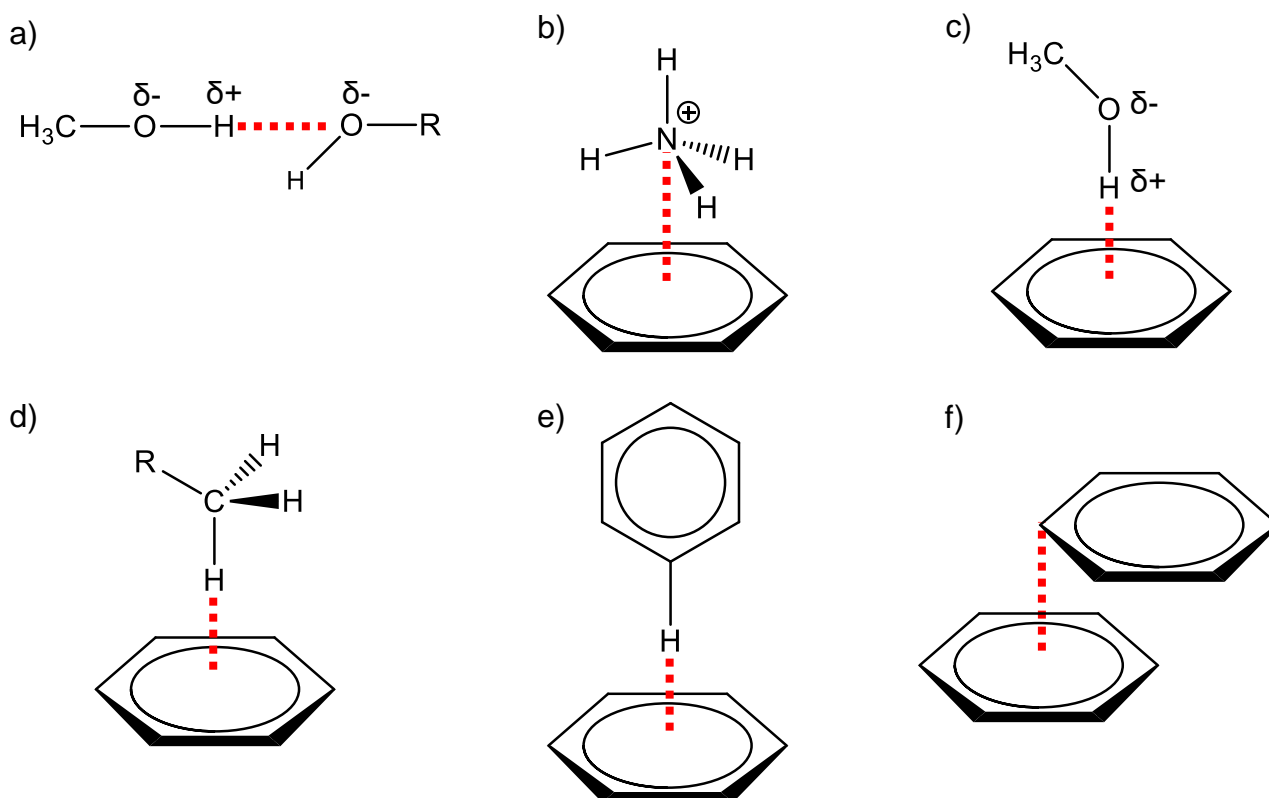
Figure 2: The most common non-covalent interactions are a) hydrogen bonding, b) cation⋯π, c) polar⋯π, d) C–H⋯π and e) aromatic C–H⋯π or T–shaped stacking

In this investigation, the hydrogen bond will be written as "X–H⋯A" and is defined as an interaction between a H-bond donor (X–H) and acceptor (A), where hydrogen

carries a partial positive charge and the acceptor (A) a full/partial negative charge (Figure 2a).[21,22] Hence, weak hydrogen bonds are a result of electrostatic attractive forces (δ+···δ-) owing to the differences in atom electronegativities. A strong hydrogen bond is quantified to range between 2.2–2.5 Å with angles of 175–180°, and is measured by the distance between X···X, from a X–H···X interaction (i.e., O–H··· O or N–H··· O). The hydrogen bond is the most prevailing and biologically-important non-covalent interaction,[23,24] and is used by nature to assist in the recognition of substrates via various enzymes, as well as to stabilize and assist in the formation of complex biological structures. The most renowned biological structure is the DNA double helix, which is stabilized by hydrogen bonding between its nucleotide base pairs and thus provides strong attractive forces that allow the two strands to be held together, which are important for the genetic information required for cellular function (Figure 3).[25–27]
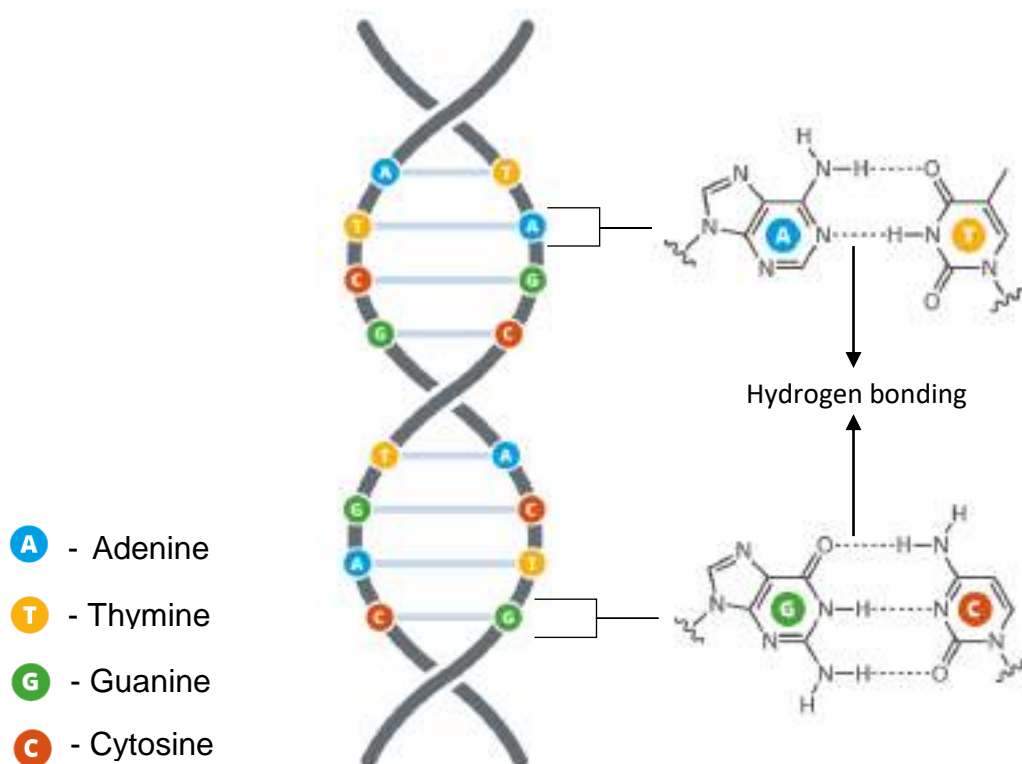
Figure 3: DNA stabilization by hydrogen bonding between its nucleotide base pairs adenine (blue, A), thymine (yellow, T), guanine (green, G) and cytosine (red, C)[27]

Most π interactions arise from the quadrupole of an aromatic system.[28–30] The benzene quadrupole in Figure 4a displays the partial positive (blue) charges situated near the hydrogen atoms and the partial negative (red) charges near the carbon atoms, as well as near the centre and above and below the ring. Aromatic rings are therefore considered to be adequate electron sources. The surface for a methanol molecule is shown in Figure 4b where the dipolar O–H bond is clearly visible with a partially negative oxygen atom and a partially positive hydrogen atom.
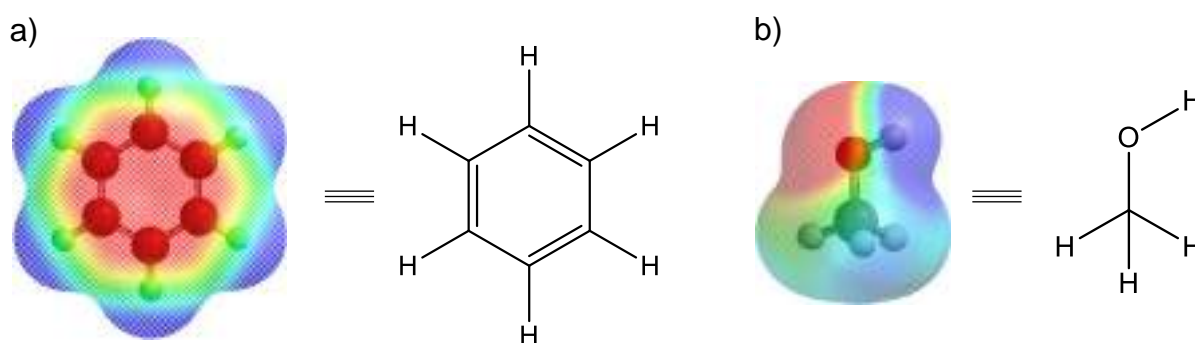
Figure 4: Electrostatic potential of a) a benzene ring and b) methanol; blue – partial positive charge, red – partial negative charge

Cation···π interactions are formed from the favourable electrostatic non-bonding attraction between the face of an electron-rich quadrupole (i.e., π system) and an adjacent monopole (i.e., a cation) (Figure 2b).[31] These interactions are relatively strong, with gas-phase binding energies of up to ~40 kcal/mol and aqueous-phase binding energies as high as 5 kcal/mol. Many studies have documented cation···π interactions in protein structures; there is an estimated one cation···π interaction for every 77 amino acids in a protein.[32]

Aromatic systems are able to interact with hydrogen bond donors such as N–H, giving rise to half of normal strength hydrogen bonds. These types of bonds are classified as polar···π interactions, abbreviated as "X–H···π", and arise from the common van der Waals and electrostatic interactions between atoms. More specifically, these interactions occur when a H-bond donor, having a large dipole, engages in the electrostatic interaction with the quadrupole moment of the ring π-system. Polar O–H···π and N-–H···π interactions are commonly observed in proteins and have calculated gas-phase interaction energies that range from 2–5 kcal/mol (Figure 2c).[34–

[36] Figure 5 shows an example of a N–H⋯π interaction occurring between the amino acids asparagine and tyrosine; the partially positive-charged amino proton of asparagine points directly at the electron-rich ring centroid of tyrosine.[33,37]
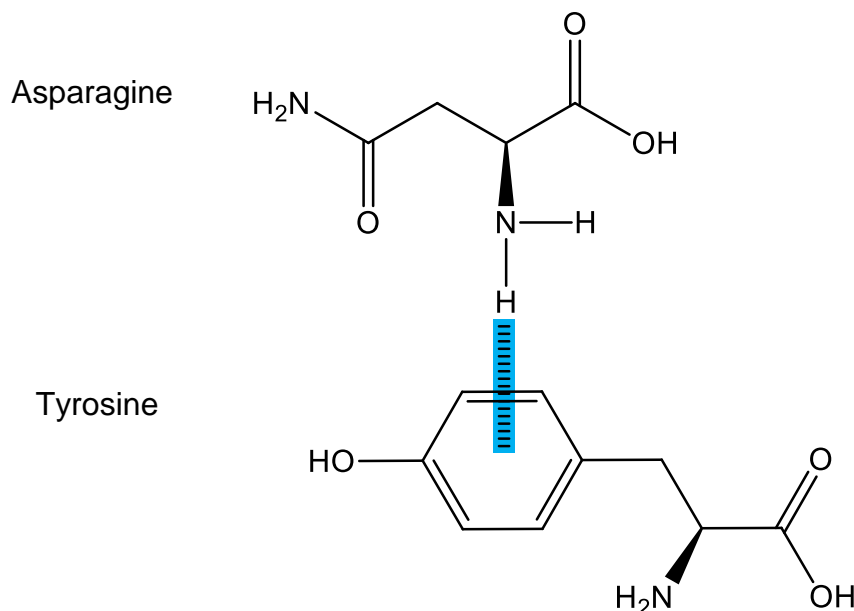
Figure 5: The partially positive-charged amino proton of asparagine forming a N–H⋯π interaction with the electron-rich centroid of the tyrosine aromatic ring; carbon – green, hydrogen – white, oxygen – red and nitrogen – blue

Unlike the electrostatic non-covalent bonds discussed previously, the strength of the C–H⋯π interaction arises primarily from dispersion (van der Waals attraction) between the C–H orbital and the π–system.[38–40] The geometry of this interaction requires that the C–H bond points directly toward the aromatic ring (Figure 2d). The C–H⋯π interaction is found in numerous molecular systems including organic crystals, proteins and nucleic acids, and is often a crucial driving force for crystal packing and molecular recognition.[38]

An important class of π interactions are π⋯π in nature, which is the attraction between arene rings.[35] These are involved in many diverse systems, such as crystal packing, complexation in host-guest systems and porphyrin aggregation, and have been shown to be of great importance in molecular and biomolecular assembly and engineering.[35,41,42] For example, significant studies have been conducted on π⋯π interactions between aromatic amino acids and DNA nucleobases. Mao *et al* were one

of the first research groups to consider the π⋯π interactions between adenosine-5'-triphosphate (ATP) and the aromatic amino acids.[43–45] Mao discovered that although hydrogen bonds occur almost three times more often than π⋯π, these latter interactions were vital for substrate binding. Although weaker than cation⋯π interactions, π⋯π contacts are characterised as being particularly strong. These aromatic ring interactions may occur in different orientations such as stacking, parallel-displaced, T-shaped or edge-to-face (Figures 6a–d, respectively). Edge-to-face and parallel stacking of aromatic rings are energetically unfavourable due to repulsion of the quadrupoles; however, stacking arenes in a T-shaped or parallel-displaced manner is energetically favourable.[46,35]
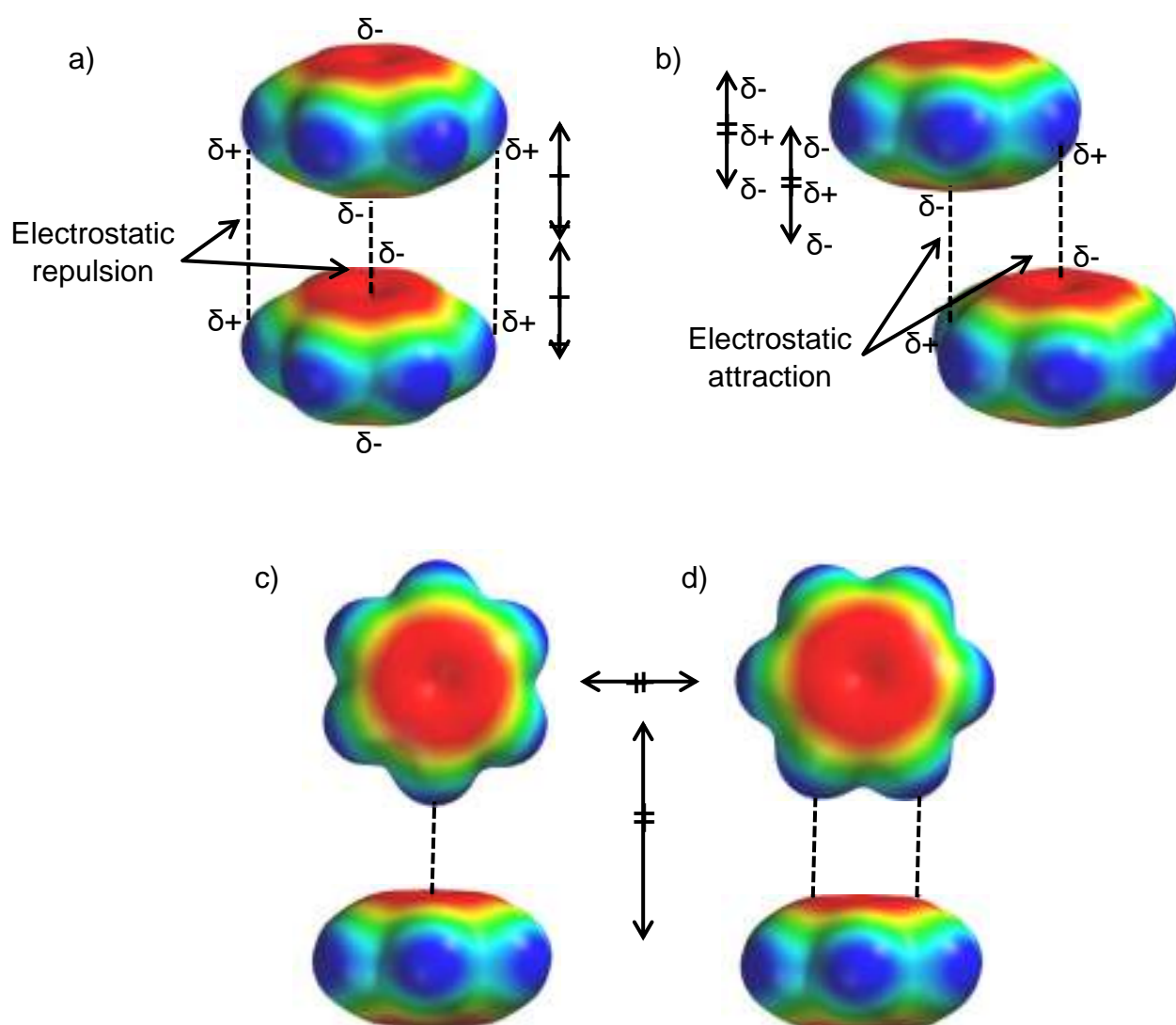
Figure 6: Different conformations of aromatic ring interactions, namely a) stacking b) parallel-displaced, c) T-shaped and d) edge-to-face

1.3. Host-guest Chemistry

1.3.1 Introduction

Host-guest chemistry involves the formation of an inclusion complex between a large organic molecule (the host) and a simpler molecule or ion (the guest) (Figure 7). Host and guest molecules organize into definable structural relationships via electrostatic forces; this in turn stimulates the idea of molecular recognition and interactions through non-covalent bonding. Such non-covalent bonds include ion-pairing, hydrogen bonding, metal ion-to-ligand attraction, π-π-stacking, dipole-dipole interactions and van der Waals attraction. As a result, host-guest chemistry permits further understanding of the underlying physics involved in these processes.[47]

Host   Guest   Complex
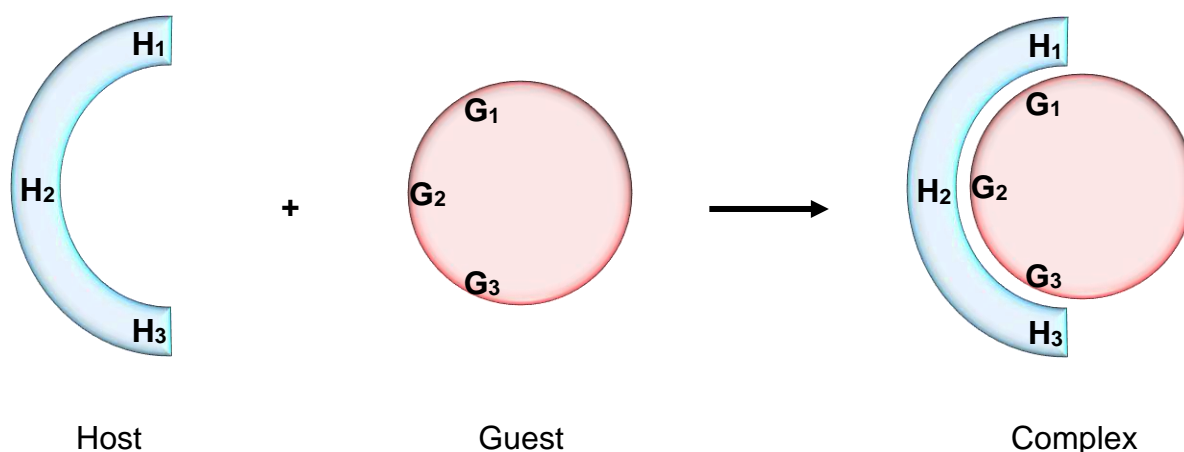
Figure 7: The establishment of an inclusion complex between host and guest

Non-covalent bonding is paramount in biological systems as it helps maintain the 3D structure of large molecules, such as proteins, and is involved in numerous biological processes in which large molecules bind specifically but transiently to one another.[48] Supramolecular chemistry and biology are two sciences dominated by weak interactions and molecular recognition. Due to this correspondence, supramolecular chemistry can aid in isolating and quantifying the interactions of the individual components of biological systems as they are often difficult to study due to their complexity. Biomolecules are invariably used as "guests" in host-guest chemistry; nevertheless, this field experiences a continuous development, and scientists are especially interested in synthesizing hosts to target proteins, nucleic acids,

carbohydrates and complex metabolites. It is important to note that host-guest chemistry has proven, probed, explored and expanded every fundamental type of weak interaction governing molecular recognition. However, the quest for the design and synthesis of simpler organic compounds that imitate working features of naturally-occurring compounds is very attractive. It is crucial that scientists thirst for new fundamental knowledge within the host-guest chemistry field.[49]

1.3.2   Host-guest Chemistry Definitions

One of the first formal definitions of a supramolecular cage-like host-guest structure was presented by H.M. Powell in 1948.[50] He coined the term 'clathrate' to describe a kind of inclusion, where "one component is enclosed within the framework of another".[48,50] This "kind of inclusion" may be described as a "molecular recognition" and defined as the specific binding of a host compound, whose shape is complementary to that of a given guest, thus forming a host-guest complex (Figure 7). The majority of host-guest compounds may be classified according to the type of host-guest interaction and the topological relationship between the host and the guest.[50] We will briefly define the concepts of these two distinct groups:

i.   Host-guest interactions:[48]
  a. **Complexes**: when host-guest aggregates are held together by primarily electrostatic forces (ion-dipole, dipole-dipole, hydrogen bonding, etc.), and
  b. **Clathrate**: when host-guest aggregates are held together by less specific and weaker non-directional interactions (hydrophobic, van der Waals, or crystal close-packing effects).

ii.   Host-guest topology:[47]
  a. **Cavitate**: the host (cavitand) possesses intramolecular cavities available for guest binding; this is an intrinsic molecular property of the host and exists both in solution and in the solid state, and
  b. **Clathrate**: the host (clathrand) possesses extramolecular cavities, producing a gap between two or more host molecules, which are only present in the crystalline or solid state.

Figure 8 is a depiction of the formation of cavitates and clathrates. Host-guest compounds that exhibit characteristics of both complexes and clathrates may be defined as follows:[48]

i.   **Inclusion compound**: the result of a host providing a hollow space or undefined cavity for a guest molecule,

ii. **Coordinatoclathrate**: the host–guest interaction is mostly defined as a clathrate but a small degree of coordinative binding exists, and

iii. **Clathratocomplexes**: the host–guest interaction is mostly defined as a complex but crystal close-packing does exist

| Larger molecules (cavitand hosts) | Small molecules (guests) | Cavitate host-guest complex (solution and solid-state) |

| Larger molecules (clathrand hosts) | Small molecules (guests) | Lattice inclusion host-guest complex or clathrate (solid-state only) |
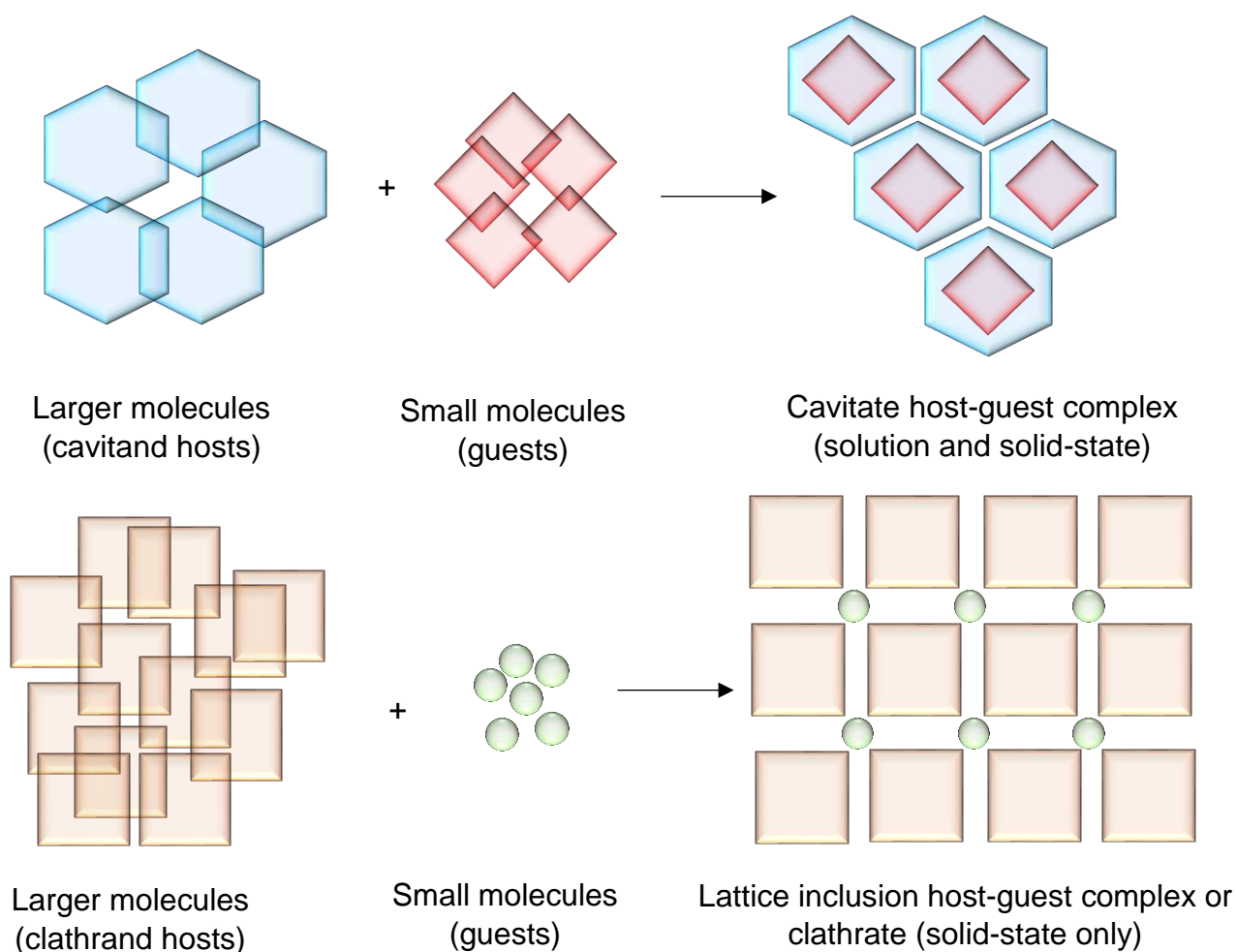
Figure 8: The formation of cavitates and clathrates

1.3.3 Directed Host-guest Design

Numerous "host" compounds have been discovered by chance, but great efforts have also been made in designing and synthesising host molecules with specific properties.[51,52] Weber has reviewed the principles of directed host design by delineating a strategy based on the formation of "coordinatoclathrates" in order to achieve efficient chemoselective guest inclusion (Figure 9).[53–56] He suggested that successful host molecules are usually bulky and rigid, since these characteristics furnish suitable cavities which can accommodate a guest; furthermore, successful hosts have additional functional moieties that can actively engage in specific host–guest interactions. Several successful host compounds have been designed based on Weber's principles.

COMPLEX

CLATHRATE

"Coordination-type" host/guest aggregate

"Lattice-type" host/guest aggregate

Binding sites
coordinative interaction, strong
(crystal, solution)

Steric barriers
topological interaction, weak
(crystalline state)

COORDINATIOCLATHRATE
coordination-assisted
clathrate

Completion of
donor/acceptor
groups

Sterical
host-guest fit

Variable co-
ordinating
sensor group

Bulky basic
skeleton

Chemoselectivity control,
controlled by functional
groups

Constitioselectivity control,
controlled by molecular
size and molecular
expanse

Figure 9: Schematic diagram of Weber's coordinatoclathrate concept (a directed host design) and abstracted structure of a coordinatoclathrate host – definitions, relations, and functions of control

1.3.4   Macrocyclic Host Types

1.3.4.1   Crown Ethers

In 1968, Pedersen developed a two-dimensional compound composed of a loose flexible ring of carbon and oxygen atoms that remained unbroken during chemical reactions. He discovered that this compound could "trap" atoms, chiefly alkali metal ions, via bonds formed within its ring structure. Pedersen named these compounds crown ethers.[57,58] Typically, crown ethers are a versatile class of macrocyclic ligands that are useful in supramolecular chemistry but also in a variety of research fields such as coordination chemistry, analytical chemistry and material sciences.[59] The mode of complex formation along with the selectivity towards cations are what distinguishes crown ethers from most non-cyclic ligands.[60] They are heterocycles that, in their simplest form, are characterized as cyclic oligomers of dioxane containing ethyleneoxy (i.e., $-CH_2CH_2O-$) repeating units.[61,62] Established crown ethers that exist are 12-crown-4, 15-crown-5, 18-crown-6, dibenzo-18-crown-6, and diaza-18-crown-6 (Figure 10). These compounds are flexible but can be rigidified by replacing the $-CH_2CH_2-$ groups by other rigid structures such as cyclohexane or benzene.[12]

The interior of a crown ether is hydrophilic with each oxygen atom bearing a partial negative charge, thereby generating a concentrated negative cavity.[63,64] Crown ethers can, therefore, coordinate to cations and neutral dipolar species owing to the free electron pairs of these oxygen atoms (Figure 11).[65] The exterior of the crown ether is hydrophobic, facilitating solubility in organic solvents. Hence they are extremely useful for increasing the solubility of ionic compounds in organic solvents which allows for reactions to be conducted with ease.[66] The diameter of the crown ether determines which ions are suitable for complexation, and their selective receptor properties, in conjunction with the relative ease of synthesis and structural modification, make crown ethers attractive targets as ionophores.[67]
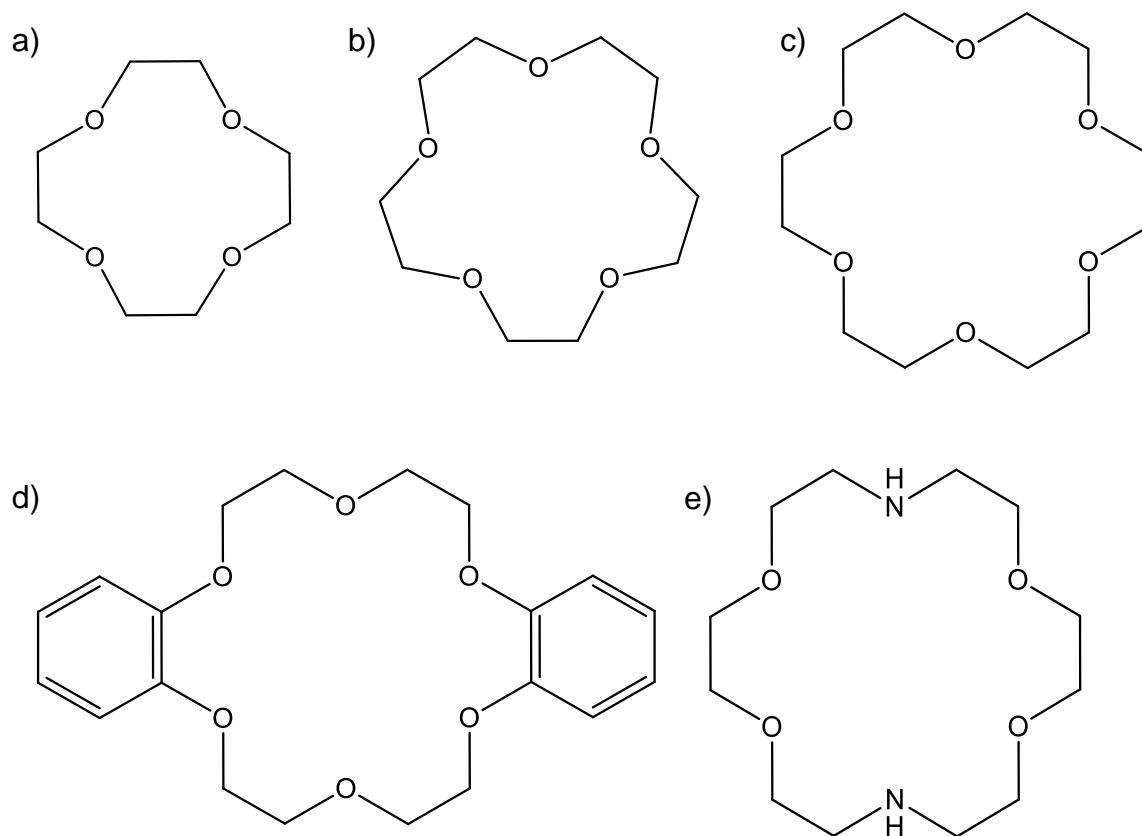
Figure 10: Common crown ethers are a) 12-crown-4, b) 15-crown-5, c) 18-crown-6, d) dibenzo-18-crown-6 and e) diaza-18-crown-6
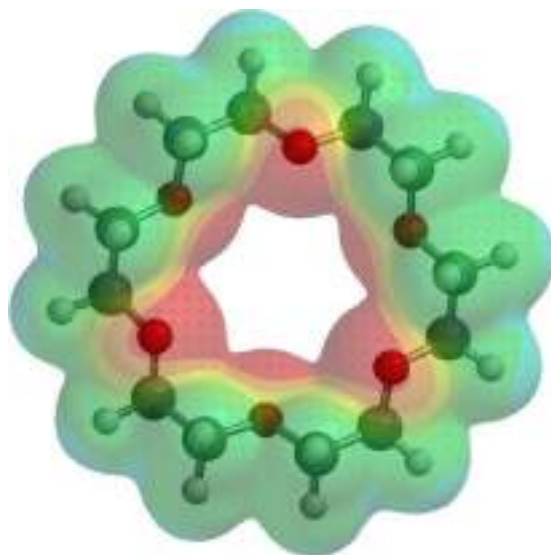
Figure 11: Electrostatic potential model of 18-crown-6; negative potential shown in red and positive potential shown in green-blue

The 'best fit' conceptualization applied in host-guest chemistry is analogous to the fundamental lock and key mechanisms used in biological systems.[68–70] Pedersen[71] and Izatt[72–74] have reported on the selectivity trends observed with certain crown ethers in solution. One of the most common models used to explain crown ether selectivity is the 'best fit' model. Accordingly, crown ethers have been predicted to preferentially bind ions whose sizes match well within the crown ether cavity. The 'best fit' model can be observed in Figure 12 from a study conducted by Rodriguez *et al.*[75,76]
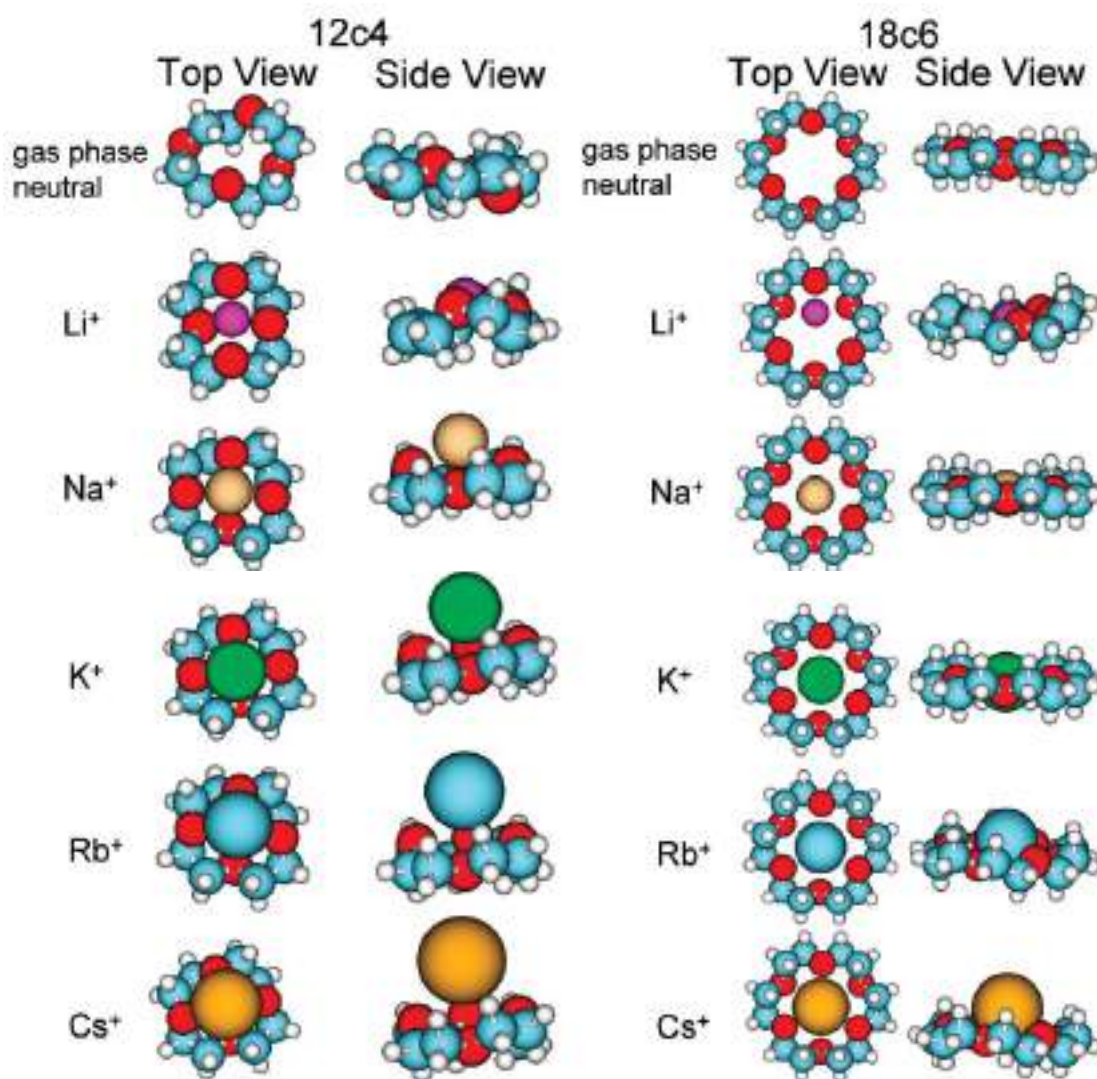
Figure 12: Space-filling representation of gas phase neutral 12-crown-4 (12c4) and 18-crown-6 (18c6), and M$^+$·(12c4) and M$^+$·(18c6) complexes based on B3LYP/6-3 1+G* geometry optimizations; the structures show how the crown ether configurations change as the ion size is increased[76]

Rodriguez reported the size-selective behaviour between the two crown ethers $M^+\cdot(12c4)$ and $M^+\cdot(18c6)$ where M^+ was Li, Na, K, Rb and Cs (Figure 12). The cavity of 12c4 (1.2–1.5 Å) could only accommodate Li^+ (1.36 Å) which adopted a symmetric orientation within the cavity. These remaining $M^+\cdot(12c4)$ complexes orient the M^+ ion above the macrocycle due to these being too large to fit inside the cavity. He observed that as the ion size increased, the $12c4\cdots M^+$ interaction weakened. The same was observed for 18c6, except the reduction in the $18c6\cdots M^+$ interaction was not as drastic as in the $12c4\cdots M^+$ interaction. The larger crown ether has additional macrocyclic oxygens which aid in increasing its flexibility and optimization of favourable interactions that might occur between the ion and etheric oxygens. The cavity of 18c6 (2.6–3.2 Å) was capable of accommodating Li^+, Na^+ and K^+ within its cavity. The Li^+ and Na^+ ions adopted an asymmetric orientation inside the cavity, while K^+ preferred to occupy a symmetrical binding site. The larger ions, Rb^+ and Cs^+, were too large to be an applicable fit. These results successfully indicated that the binding of the alkali metal ions in $M^+(12c4)$ and $M^+(18c6)$ were dependent on the dimensions of both the ion and crown ether.[76] Since crown ethers possess the ability to preferentially bind certain ions, they are used in a wide variety of applications such as drug delivery, nanotechnology and many environmental applications.[77–79]

1.3.4.2   Cryptands

Cryptands are preorganised derivatives of crown ethers.[80,81] They both possess comparable properties, but cryptands are more rigid three-dimensional polycyclic compounds and have higher association constants in comparison to crown ethers. Structurally, cryptands contain two nitrogen atoms connected by three bridged ethyleneoxy units (Figure 13).[82] Unlike the crown ethers, the addition of two nitrogen atoms provides further lone pairs available for coordination (eight for [2.2.2]cryptand compared with six for 18-crown-6); the bridging chain assists the cryptands to completely encapsulate a metal ion in a 'crypt', thus forming a cryptate (Figure 14).[83,84] These cryptates are characterized by high selectivity, slow exchange rates, higher stabilities and are therefore superior in forming complexes with guest alkali metal ions.[81,85] For example, the binding constant of [2.2.2]cryptand for potassium is approximately 10^4 times higher than that for 18-crown-6.[47]

[1.1.1]   [2.1.1]   [2.2.1]   [2.2.2]

[3.2.1]   [3.2.2]   [3.3.3]
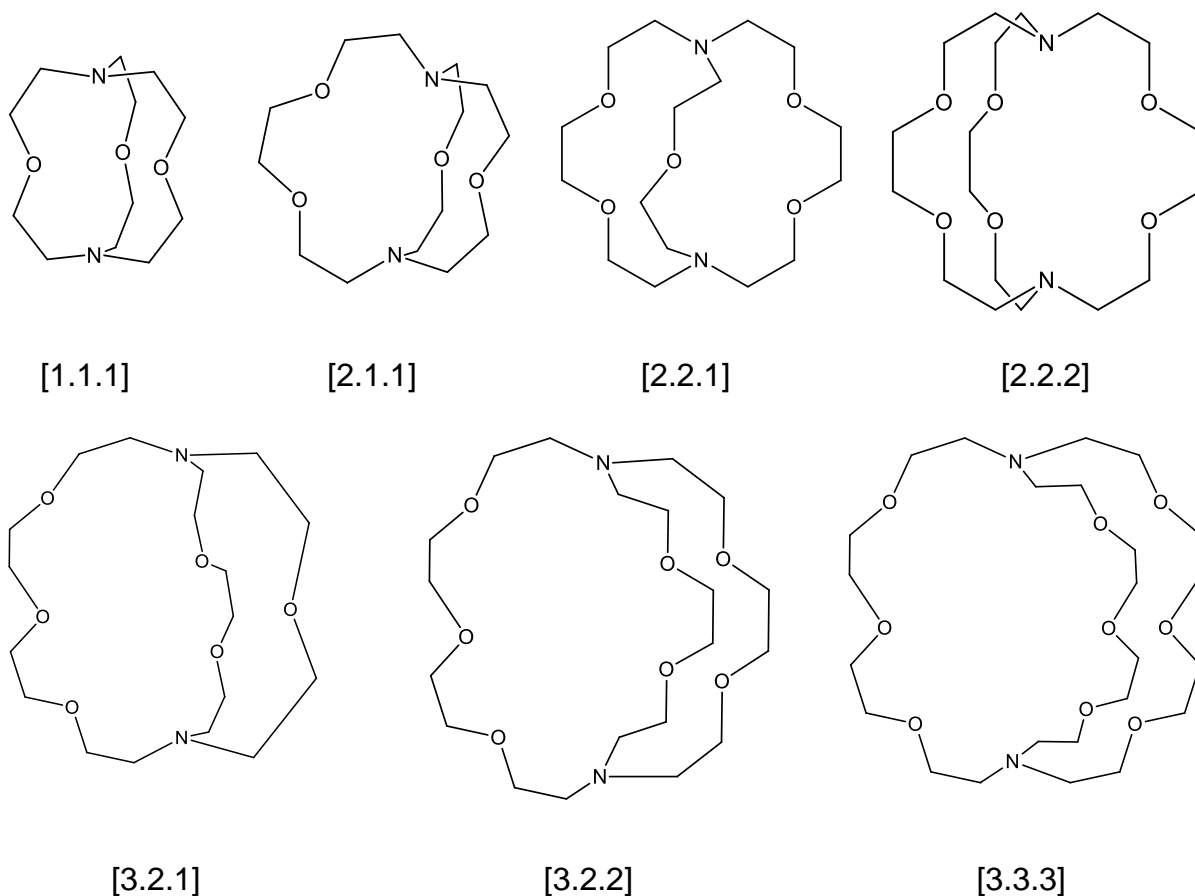
Figure 13: The various cryptands and their differing cavity sizes; the numbers between square brackets indicate the amount of ether oxygen atoms (and hence binding sites) in each of the three bridges between the amine nitrogen bridgeheads
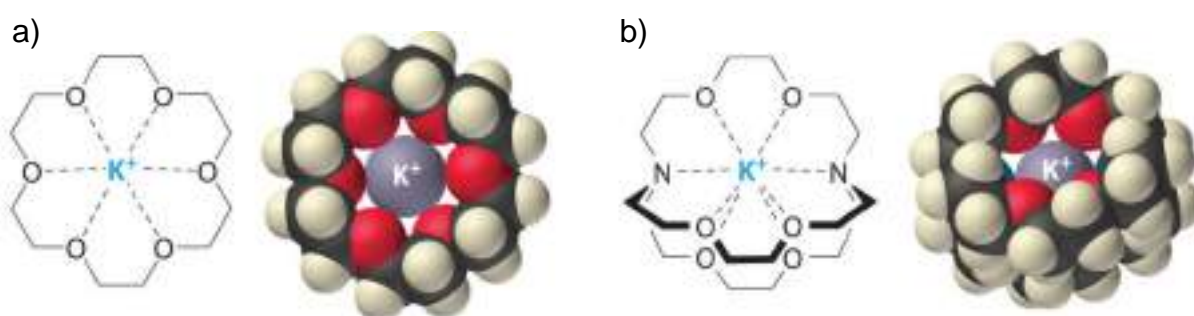
Figure 14: a) The potassium complex of the crown ether 18-crown-6; the cation is nestled within the central cavity of the molecule and interacts with lone pairs of electrons on the oxygen atoms, and (b) the potassium complex of [2,2,2]cryptand; the cation is almost hidden by the cryptand

The length of the bridging chain has an important effect on the binding strength of cryptands with guest molecules or ions. The size fit between the host and the guest is affected as well as the distances and angles that govern the strengths of the non-covalent interactions between host and guest.[81] The reason for the cryptand's enhanced metal cation binding ability compared with crown ethers is the defined, preorganised and three dimensional nature of the cavity. This defined cavity enables spherical recognition of the M^+ ion to take place.[47,83] As observed in Figure 14, the larger cryptands contain voluminous cavities that can incorporate sizeable ions. Lithium, sodium and potassium fit adequately in [2.1.1]cryptand, [2.2.1]cryptand and [2.2.2]cryptand, respectively.[86] Table 1 explains this phenomenon as the cavity radius of each cryptand is in close proximity to the size of the ionic radius.

Table 1: Cryptands and their preferred alkali metal ions: cavity and ionic radii

Cryptand	Cavity radius (pm)	Ion	Ionic radius (pm)
[2.1.1]	80	Li^+	74
[2.2.1]	110	Na^+	102
[2.2.2]	140	K^+	138
[3.2.2]	180	Rb^+	149
[3.3.3]	240	Cs^+	170

Positron emission tomography (PET) is a powerful, non-invasive imaging technique that enables the *in vivo* examination of physiological and biological phenomena at the molecular level.[87–89] PET imaging involves the introduction of radioactive tracers into the human body. Tracers are essentially biological compounds labelled with a positron-emitting isotope, such as carbon-11, nitrogen-13, oxygen-15 and fluoride-18. The PET system will detect pairs of gamma rays emitted indirectly by a positron-emitting radioactive tracer when it is in the presence of abnormal cells. The most commonly used PET tracer is 18F-fluorodeoxyglucose (FDG), a radioactive form of glucose (sugar). Tumor cells consume large amounts of sugar compared to normal surrounding tissues and therefore FDG-PET scanning can identify these cells as cancer cells.[90] Cryptand [2.2.2], commonly known as Kryptofix [2.2.2] (KRY), is used as a phase transfer catalyst in the nucleophilic substitution production of FDG (Figure

15). KRY enhances the reactivity/nucleophilicity of the fluoride anions by binding the potassium ion, thus preventing the formation of 18F-KF.[91–93] Consequently, potassium acts as a counter ion of 18-F to enhance its reactivity without interfering with the synthesis.
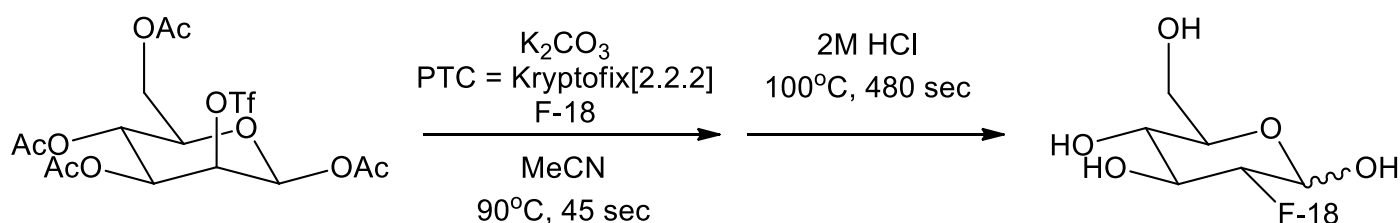
Figure 15: The production of 18F-2-fluoro-2-deoxyglucose (FDG) by labelling deoxyglucose with fluoride with the aid of Kryptofix[2.2.2]

1.3.4.3   Cyclodextrins

Cyclodextrins (CDs) are a family of macrocyclic oligosaccharides that are extensively used in a wide range of applications due to their capable host properties. These hosts find applications in food nutrition and flavours, agriculture, pharmaceutical products, drug delivery systems, cosmetics, textiles, and in the chemical industry.[94–96] Cyclodextrins are made up of at least six D-(+)-glucopyranosyl units situated in a chair conformation linked by α-1,4-glycosidic bonds, thus forming a ring shape.[97] There are over 1500 types of cyclodextrin derivatives mentioned in the literature and these are often classified according to the amount of glucopyranose units present, the internal cavity diameter and molecular mass, etc.[98,99] The most widely used natural cyclodextrins are α-, β- and γ- cyclodextrin that consist of 6, 7 and 8 glucopyranose units, respectively (Figure 16, Table 2).
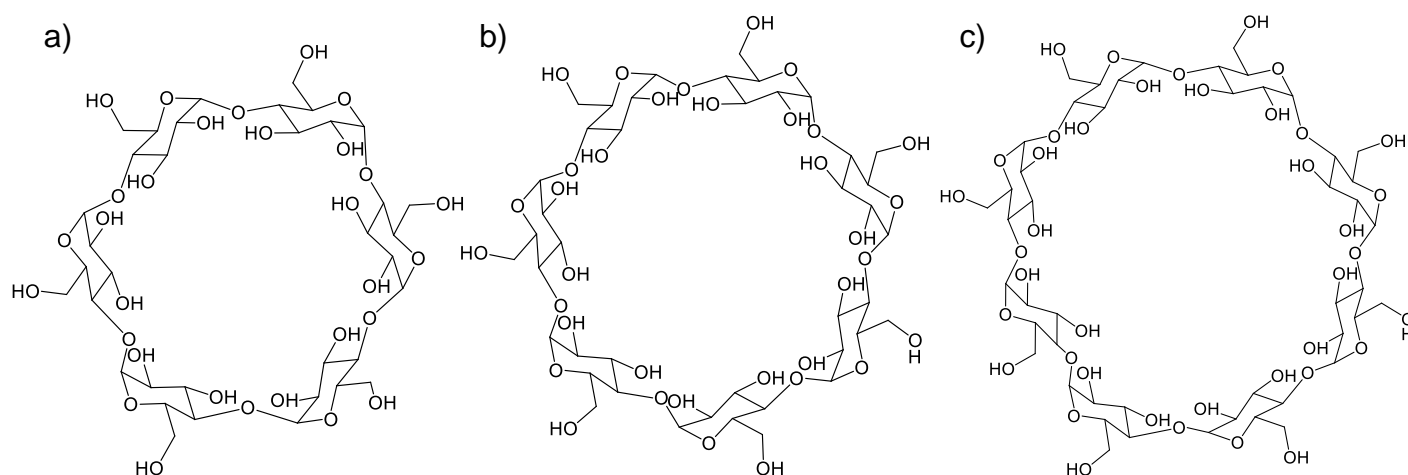
Figure 16: Structural representations of a) α-cyclodextrin, b) β-cyclodextrin and c) γ-cyclodextrin consisting of 6, 7 and 8 glucopyranose units, respectively

Table 2: The characteristic parameters of α-, β- and γ- cyclodextrin[100]

Parameters	α-CD	β-CD	γ-CD
Empirical formula	$C_{36}H_{60}O_{30}$	$C_{42}H_{70}O_{35}$	$C_{48}H_{80}O_{40}$
Glucose units	6	7	8
Molecular mass (g/mol)	973	1135	1297
Outer diameter (Å)	14.6	15.4	17.5
Cavity diameter (Å)	4.7–5.3	6.0–6.5	7.5–8.3
Minimum cross section of cavity (Å)	15	26	43
Cavity volume (Å^3)	174	262	427

Cyclodextrin has a unique truncated cone-shaped structure with a hydrophobic centre and a hydrophilic exterior. Hydrophilicity is a result of the presence of hydroxyl groups orientated towards the exterior of the cone, while the inner hydrophobic cavity is formed by the skeletal carbons and ethereal oxygens of the glucose residues (Figure 17). The hydrophobic cavity is able to encapsulate appropriately-sized non-polar/lipophilic/poorly water-soluble molecules forming stable host-guest complexes, while the hydrophilic exterior ensures water solubility of the complex.[100] Furthermore, encapsulation will change the physical and chemical properties of the guests, such as solubility and stability.[101] It is therefore not surprising that cyclodextrins have attracted so much attention and have been marketed worldwide in many industrial areas, especially in the pharmaceutical sector. One of the many examples is the improved

aqueous solubility of poorly water-soluble drugs due to cyclodextrin complexation.[102] Additional advantages include improved drug stability, bioavailability, oral administration, decreased toxic effects, alleviation of drug irritations often affecting the stomach, skin, or eye, and reduced drug interactions with biological membranes or cells.
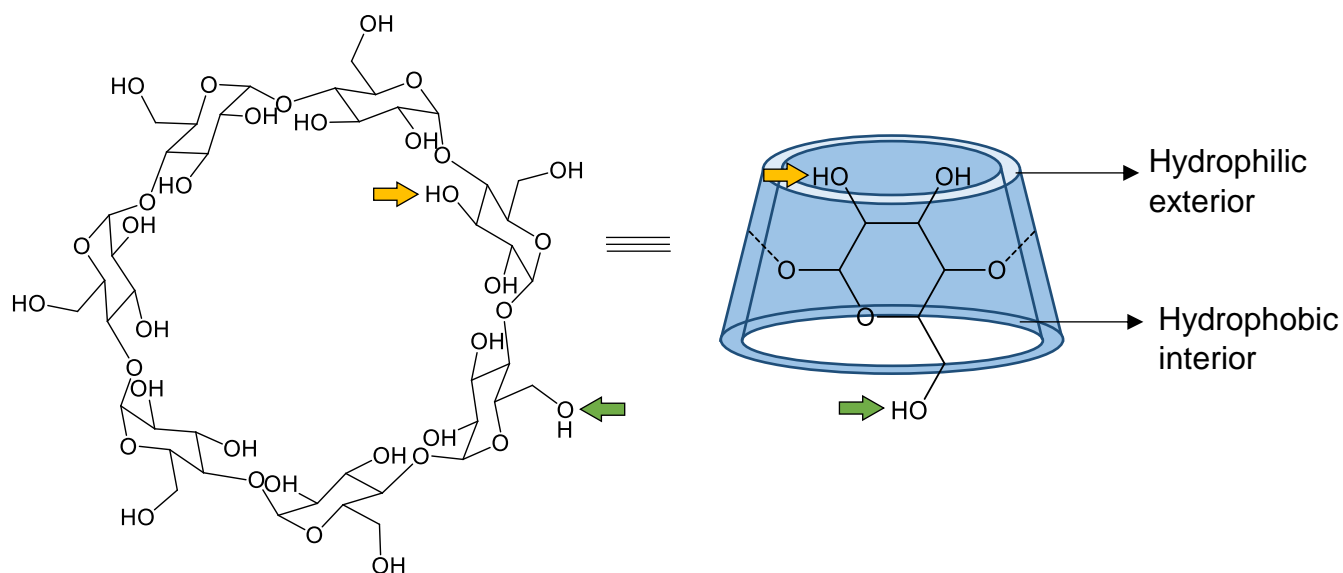
Figure 17: A representation of β-cyclodextrin's truncated cone-shaped structure illustrating the hydrophobic interior and hydrophilic exterior

To understand the effects of the cavity size of cyclodextrins (CDs), Kandoth *et al*[103] reported on the interaction of 1,4-dihydroxy-9,10-anthraquinone (quinizarin, QZ), with α-, β- and γ- CDs. In Figure 18, the dihydroxy-substituted ring of QZ has a dimension of about 6.3 Å, whereas the unsubstituted aromatic ring has a dimension of ~5 Å. The inner diameter of the α-CD cavity is ~5 Å and it was therefore expected that the dihydroxy-substituted ring of QZ could not enter the cavity. Instead, the inclusion of QZ with α-CD takes place with the unsubstituted ring entering the host cavity through its wider rim. The orientation of QZ in the β-CD cavity is similar to that seen with α-CD, but the unsubstituted ring was expected to be completely buried deep inside the host cavity. The cavity size of γ-CD was large enough to include almost the entire QZ molecule and the dihydroxy-substituted aromatic ring was encapsulated within this cavity.[104]
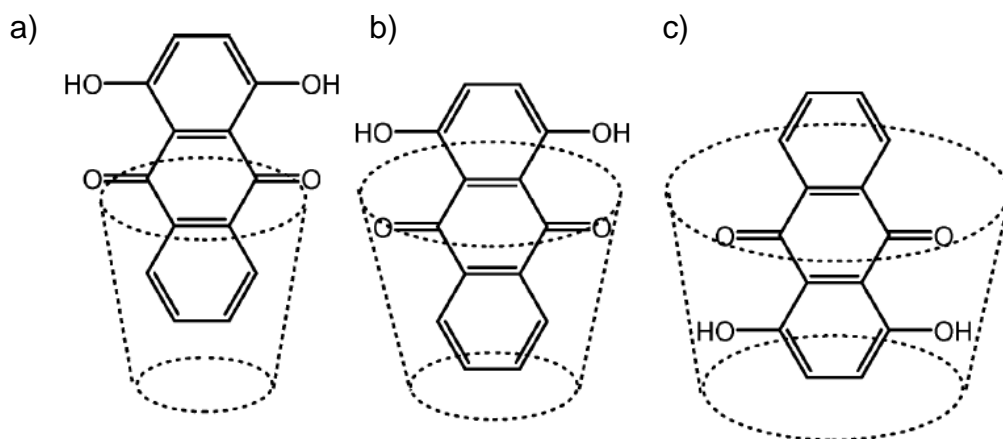
Figure 18: The orientation of QZ inside α-, β- and γ- CD cavities depending on their relative dimensions[103]

A recent study by Ezawa *et al*[105] analysed the changes in physicochemical properties of piperine when encapsulated by β-cyclodextrin. Piperine is a component found in black pepper that has previously been reported to have slight insecticidal and antibacterial activity, able to increase energy consumption of skeletal muscle and brown adipose tissue, and facilitates lipolysis in white adipose tissue (Figure 19). Therefore, piperine has drawn attention as a valuable spice for use in functional foods. Even though this compound is stable in black pepper, it is readily isomerized when exposed to ultraviolet light and has low aqueous solubility.
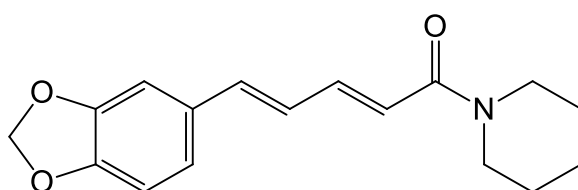
Figure 19: The structure of piperine (2*E*,4*E*)-1-[5-(1,3-benzodioxol-5-yl)-1-oxo-2,4-pentadienyl)piperidine]

The lipophilic aromatic ring of piperine is able to interact with the cavity of β-cyclodextrin forming a stable complex (Figure 20). This complex was fortunately observed to increase the solubility of piperine, thus allowing it to be used beneficially

in the development of health care supplements. Future studies will include the stability of piperine in food supplements.
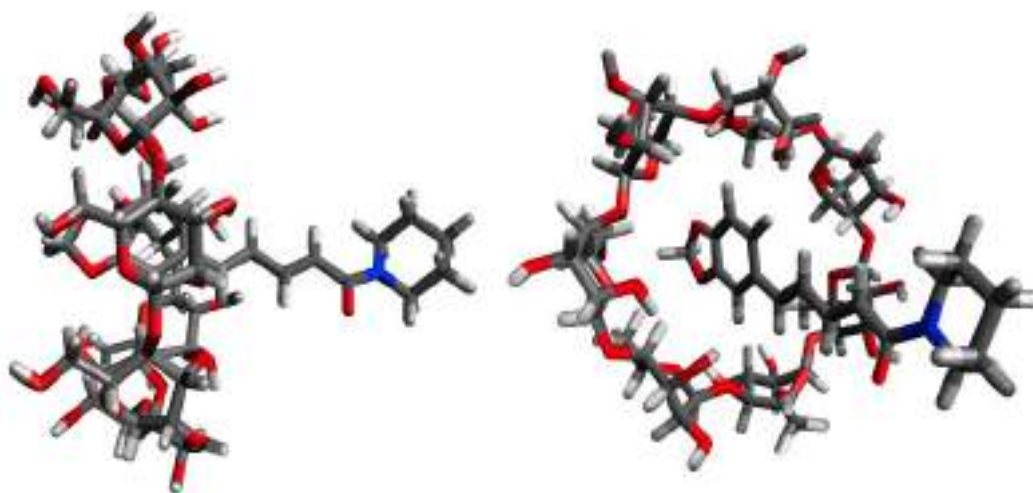
Figure 20: Molecular inclusion diagram of the complex formed between piperine and β-cyclodextrin

A great deal of research has been conducted on the complexation between cyclodextrins and coenzyme Q10 (CoQ10). CoQ10, also known as ubiquinone, is a lipid-soluble compound that is found in the mitochondria of almost all cells in the human body (Figure 21).[106] It is an essential cofactor for energy production as it is used as an electron carrier in the mitochondrial electron transport chain.[107] It is also a powerful antioxidant since it is able to regenerate vitamin E and reduces free radical-induced oxidative damage by quenching free radicals, thus maintaining and protecting the structural integrity and stability of mitochondrial and cellular membranes, including intracellular membranes.[106,108]
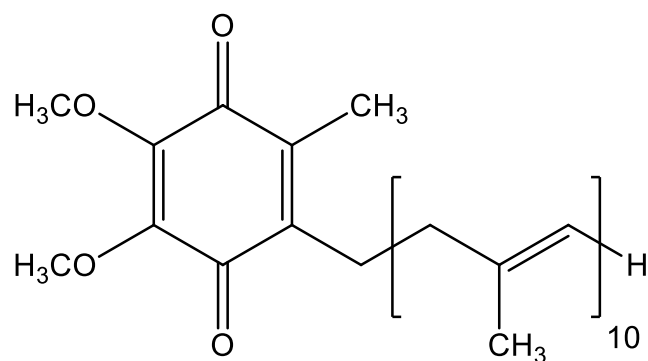
Figure 21: Structure of CoQ10 (ubiquinone)

In spite of the advantages of CoQ10, it presents several inconveniences for use in the food industry as a fortifier or nutraceutical. As a dietary supplement, it is poorly absorbed due to its hydrophobic nature and large molecular weight. Milivoievic *et al*[110] reported that the complexation of CoQ10 with β- and γ- CD in aqueous solutions leads to an increase in the water solubility, thermo- and photo- stability, and the consequent bioavailability of CoQ10. About 72.3 % of pure crystalline CoQ10 degrades after 120 min of exposure at 80 ˚C and UV light (λ = 254). However, under the same conditions, more than 64% of complexed CoQ10 remained unchanged. They concluded that the complex of CoQ10 with β-CD may be suitable as a pharmaceutical ingredient and food additive enabling the preparation of water-based functional foods. In fact, it is already used as a pharmaceutical ingredient in soft capsules and syrup, and as a food additive in milk, yoghurt, kefir, jam, marmalade and honey.[106,109]

There are many forms of CoQ10 on the market that claim enhanced bioavailability. However, the problem with these claims is that they do not apply to everyone. How well CoQ10 is absorbed varies from person to person. One person might be a "super-absorber", while another may only absorb small quantities. As a result, since bioavailability is calculated as the average absorption rate of all subjects in a study, uniformity is not guaranteed. One of the main goals of complexing CoQ10 with CDs is to increase its bioavailability. Terao *et al*[110] compared, in supplement form, a complex of CoQ10 and γ-CD with that of a CoQ10 and microcrystalline cellulose (MCC) mixture. Microcrystalline cellulose is one of the most commonly used fillers and binders in drug formulations, and is often used in the pharmaceutical industry in maximizing the drug bioavailability. After 6 and 8 h, mean CoQ10 plasma levels in

subjects given the CoQ10·γ-CD capsules were significantly higher than those given the CoQ10·MCC capsule. A 47.60 and 13.83% average rise from the baseline plasma CoQ10 level was observed with CoQ10·γ-CD and CoQ10·MCC, respectively. These effects were still observed 24 and 48 h later. As a result, it was shown that the oral absorption and bioavailability of CoQ10 may be enhanced by complexation with γ-CD. This result may be attributed to the solubilizing effect and fast dissolution rate of the CoQ10·γ-CD complex, thereby improving the potential of γ-CD use in oral capsule formulations.[106,110]

1.3.5 Host–guest Application: Selective Inclusion

When a host molecule specifically recognizes the shape of a guest molecule and can selectively include one isomer from a mixture of isomers, this process may be used to separate isomeric compounds, which oftentimes have similar physical properties, from one another.[111–114] Additionally, when a chiral and optically pure host molecule recognizes the chirality of a guest molecule and selectively includes one enantiomeric guest over the other, it is suitable for chiral/optical resolution.

The process of the separation of isomers or mixtures of different guests using host-guest chemistry is dependent on molecular recognition. This requires the recrystallisation of the host material from the guest mixture, and this process may be described by Equation 1:[115]

$$\text{H}(\alpha, s) + n\text{G}_{1(l)} + m\text{G}_{2(l)} \rightarrow \text{H} \cdot x\text{G}_1 \cdot y\text{G}_2(\beta, s) + (n-x)G_1^{(l)} + (m-y)G_2^{(l)}$$
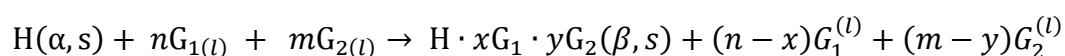
Equation 1

When a host compound H is recrystallized from pairs of guest molecules G_1 and G_2, the resulting inclusion compound, $\text{H} \cdot x\text{G}_1 \cdot y\text{G}_2(\beta, s)$, may have a host:$G_1$:$G_2$ ratio of $1 : x : y$. It is of great importance to establish accurate values of x and y to aid in the understanding of the site occupancy factors of these guests within the crystal structure. These values can be obtained using various analytical techniques such as thermogravimetry (TG), gas chromatography (GC), NMR spectroscopy and single crystal X-ray diffraction (SCXRD).[115]

A complete separation would involve a host that has a selectivity for only the one guest. In an example where the host includes G_1 exclusively over G_2, the inclusion compound formed would simply be $H \cdot xG_1$ (where $x = n$), and y would be zero. However, this seldom occurs in practice and therefore the extent of the selectivity must be calculated using the selectivity constant, $K_{G_1:G_2}$ (Equation 2):

$$K_{G_1:G_2} = Z_{G_1}/Z_{G_2} \; x \; X_{G_1}/X_{G_2} \quad (X_{G_1} + X_{G_2} = 1) \qquad \textbf{Equation 2}$$

The equation is explained as follows: X_{G_1} and X_{G_2} are the mole fractions of the guests G_1 and G_2 in the mother liquor from which crystallisation occurs, and Z_{G_1} and Z_{G_2} are their mole fractions in the resulting crystallized product. A selectivity curve can be generated by plotting Z_{G_1} versus X_{G_1} (Figure 22). Plot a) represents the case where the host is completely unselective; curve b) is obtained when the guest G_1 is preferentially enclathrated over the entire concentration range; curve c) results when the selectivity is guest-concentration dependent, and curve d) when there is preference for the minor guest component. For practical purposes, a selectivity constant ≥10 is regarded as efficient.[115–117]
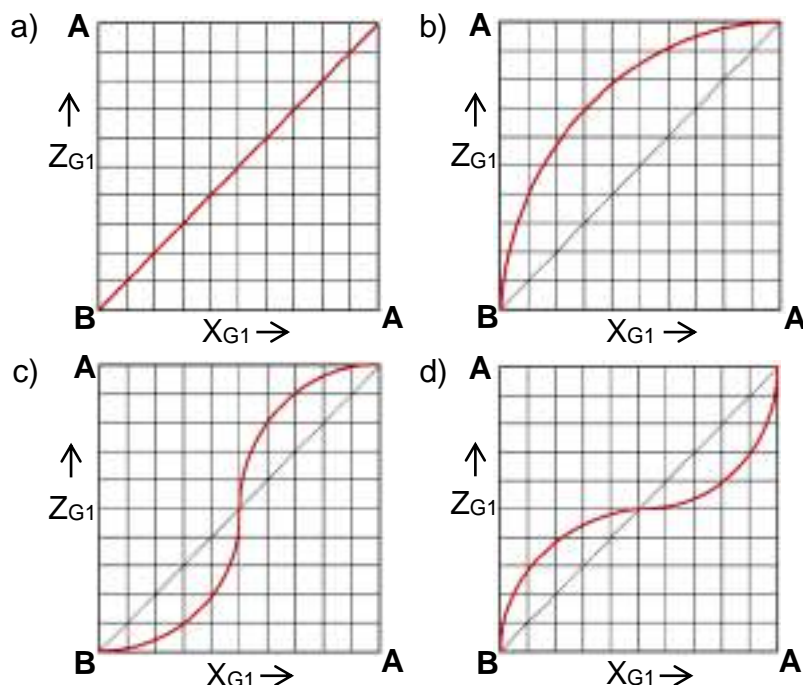
Figure 22: General selectivity curves showing a) zero selectivity, b) preference for one guest, c) dependence on concentration and d) preference for the minor component[117]

1.3.5.1 Separation of Isomers

The field of host-guest chemistry has successfully been applied in the separation of isomers and therefore is an important tool in separation technology.[112,118] Isomers can be divided into two broad categories, namely structural isomers and stereoisomers.[119] Structural isomers have the same molecular formula but different structural formulae, (i.e., the isomers have different constitutions). In contrast, stereoisomers only differ in the spatial orientation of their component atoms (i.e., the isomers have different shapes) (Figure 23).[119,120] The separation of isomeric mixtures into their individual components is important as each isomer may exhibit different chemical and/or biological properties; this is of great significance within the pharmaceutical industry.[121,122] Each of these isomers often serve as chemical precursors or synthetic intermediates to other compounds and materials, including plastics, pesticides, pharmaceuticals and dyes.[123]

```
                          ┌──────────┐
                          │ ISOMERS  │
                          └──────────┘
              ┌─────────────────┴─────────────────┐
    ┌────────────────────┐              ┌────────────────────┐
    │ STRUCTURAL ISOMERS │              │   STEREOISOMERS    │
    └────────────────────┘              └────────────────────┘
     ┌──────┬──────┴──────┐              ┌──────────┴──────────┐
  ┌───────┐┌──────────┐┌──────────┐  ┌─────────────┐  ┌───────────┐
  │ CHAIN ││POSITIONAL││FUNCTIONAL│  │ ENANTIOMERS │  │ CIS/TRANS │
  └───────┘└──────────┘└──────────┘  └─────────────┘  └───────────┘
```
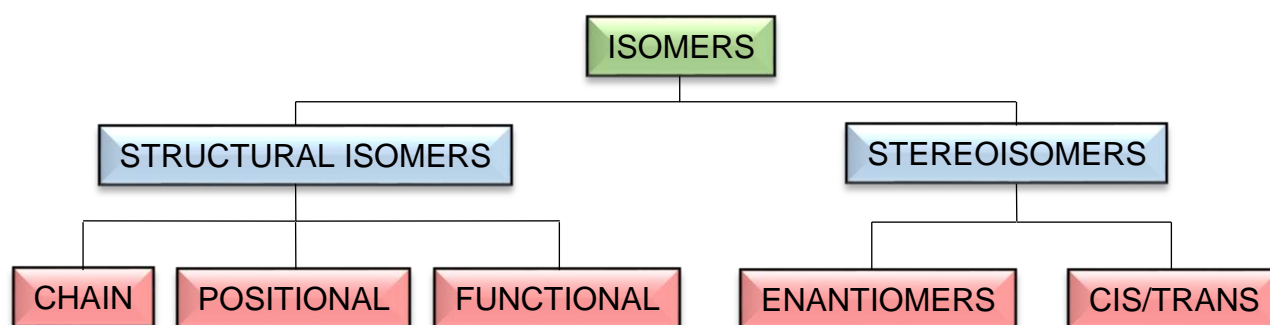
Figure 23: The classification of isomers[119]

Multi-component mixtures comprising compounds with different physical properties are readily separated and purified by virtue of these different properties, such as differences in volatility or solubility.[125,126] However, the separation of isomers remains a formidable task when they have similar physical properties. Oftentimes, distillation, crystallization, and liquid-liquid extraction techniques are, as a result, tedious, time-consuming and inefficient.[127,128] As an attractive alternative, a host may selectively and preferentially include a specific isomer during recrystallisation from a mixture. This isomer is then separated from the isomeric mixture by filtration of the so-formed crystallized inclusion compound, and the separated isomer may be retrieved from the host through dissolution and extraction, while the host may be recycled.[129] Despite the

success of host-guest chemistry, limitations still exist with respect to the design and optimization of the organic hosts for separation applications. There is a demand in this field to continuously design host molecules that are adaptable by means of facile structural modifications while being able to retain the general structural features.[130] By doing so, a variety of hosts may be synthesised which may behave even more favourably in isomer separation procedures.

1.3.5.2   The Physical Chemistry of Host-guest Inclusion Compounds

The following physical techniques are commonly used in the characterisation of inclusion compounds:

- Single crystal X-ray diffraction (SCXRD) is a common physical technique used in determining the crystal structures of inclusion complexes. Compounds crystallize because they form stable repeating patterns in three dimensions. The unit cell is the smallest three-dimensional repeating unit and contains information about the relative positions of all the atoms within the crystalline structure. This is useful in supramolecular chemistry where complexes may involve several components and solvent molecules. SCXRD relays important information such as geometry and the inter-atomic distances of non-covalent interactions between host and guest. It also illustrates the type of non-covalent interactions present and whether the guest is situated in channels, cavities, or layers within the host framework.[131]

- Thermal analysis, another important physical technique, measures changes in the physical properties of a substance as a function of temperature.[132] The two primary methods of thermal analysis are thermogravimetry (TG) and differential scanning calorimetry (DSC). Thermogravimetry measures the change in weight and the rate of this weight change as a substance is heated. In host-guest chemistry, TG can be used to obtain accurate host:guest ratios. Inclusion compounds are often non-stoichiometric, and the results of the TG can be used to assign practical site occupancy factors of the guests in the host framework.[132–134] DSC measures the thermal energy due to a thermal transition, which occurs when a chemical or physical change takes place and, as a result, heat is emitted or absorbed.[132] When

analysing an inclusion complex, DSC will yield both the onset temperatures of various thermal events such as guest release, polymorphic phase transitions and melting, as well as the associated enthalpy changes.[132] The desolvation of a host-guest complex with a volatile guest may be described by Equation 3:

$$H \cdot G_n(s, \beta) \rightarrow H(s, \alpha) + nG(g) \qquad \textbf{Equation 3}$$
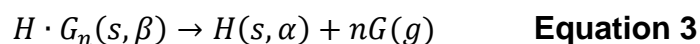
Figure 24 depicts the idealized TG and DSC curves resulting from an inclusion compound subjected to a constant heating rate. Here, the compound forms a stable intermediate γ-phase (not shown in Eqn. 3) after incomplete guest loss (−mG). The TG curve yields an accurate value of n and the host:guest ratio, while the area under the curves correspond to the enthalpy changes of the guest-release process. The DSC provides the onset temperatures of decomposition and shows two endotherms A and B, which correspond to the guest release from the β- and γ- phase, respectively. Endotherm C is associated with the melting of the host.[134] The onset temperature, T_{on}, is the onset temperature of guest release and is a reliable measure of thermal stability. The normal boiling point, T_b, of the guest is also important, as the difference $T_{on} - T_b$ is a useful measure of the relative thermal stabilities of isostructural inclusion compounds.[134,135]
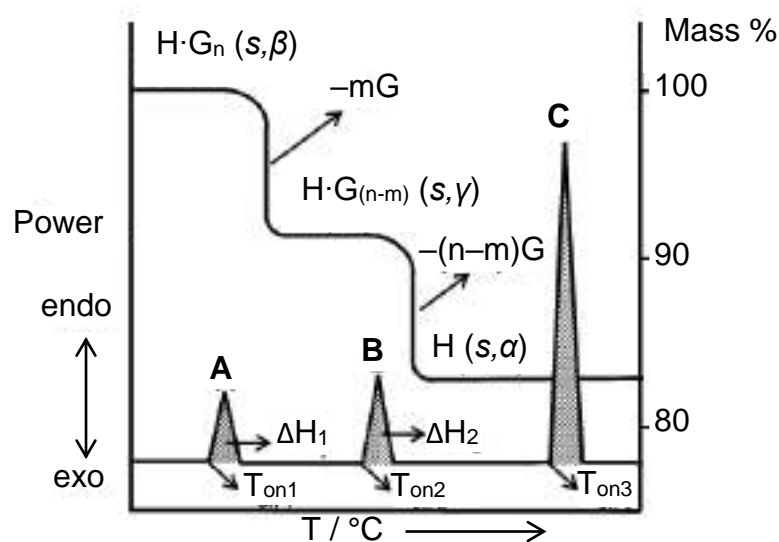
Figure 24: Idealized TG and DSC traces for the decomposition of an inclusion compound that forms a stable intermediate during the heating process[134]

- Proton nuclear magnetic resonance (^{1}H-NMR) spectroscopy is used to determine the stoichiometry of the host:guest inclusion complex. However, gas chromatography-mass spectroscopy (GC-MS) becomes the preferred method of quantification when host and guest proton signals overlap.

1.3.6   Diol Host Types

Many versatile host compounds are diols. A variety of these have been successful in the formation of inclusion compounds with a multitude of guest molecule types, usually with concomitant hydrogen bonding.[136] Knowing the history of diol host development, one may be equipped to design and synthesise new host systems that possess some of the functional groups and structural features of well-known and successful host compounds. In 1968, Toda designed two efficient diol hosts with a particular structural design. He found that 1,1,6,6-tetraphenylhexa-2,4-diyne-1,6-diol (H1) and 1,1,4,4-tetraphenylbut-2-yne-1,4-diol (H2) formed crystal inclusions with an assortment of organic guest compounds with 1:2 and 1:1 host:guest (H:G) ratios, respectively (Figure 25). The enclathrated organic guests were aromatic hydrocarbons, halogeno compounds, ketones, aldehydes, ethers, amines, amides, sulfoxides and alkaloids.[137] An inclusion with acetone proved that hydrogen bonds between the hydroxyl groups of H1 and H2 and the carbonyl oxygen of acetone plays an important stabilizing role in the crystal. However, due to the differing sizes of the hosts, H1 has sufficient space between the two diphenylcarbinol moieties to include two acetone molecules, while H2 has space enough for only one acetone molecule, which is then surrounded by phenyl groups. Rigidity was key in the formation of stable crystalline complexes as H2 included fewer guest compounds than H1, whereas the free rotating 1,1,6,6-tetraphenylhexane does not form any inclusion complexes whatsoever. Altogether, these observations suggest a means to design new potential host compounds that consist of rigid, bulky groups that, in turn, provide suitable cavities within the crystal structure to accommodate a guest under recrystallization conditions. Also, the diol function can engage in hydrogen bonding, giving rise to coordinatoclathrates.[138] The successful design of a host compound is based on molecular rigidity, bulkiness and, oftentimes, the possession of hydrogen-bonding functionalities.[139]
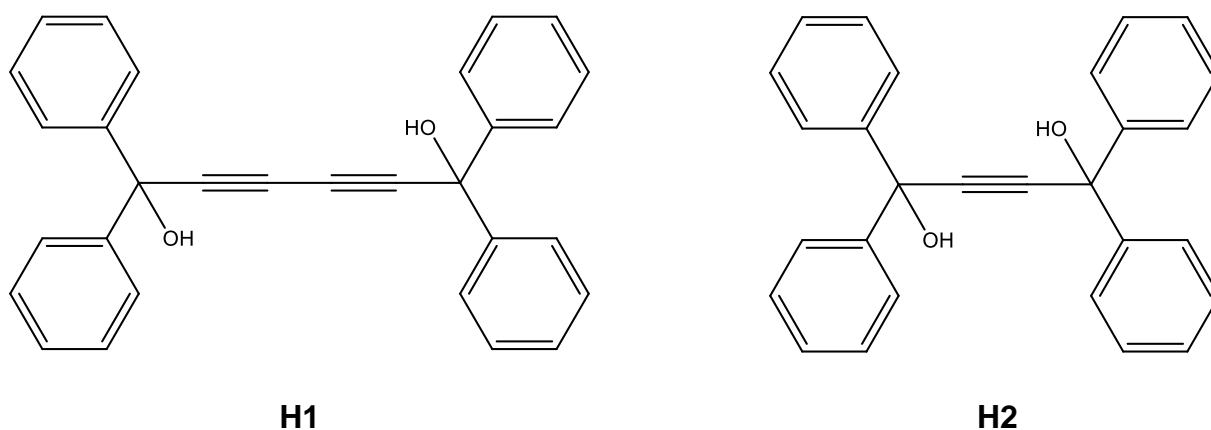
Figure 25: Bulky diol hosts synthesised by Toda: 1,1,6,6-tetraphenylhexa-2,4-diyne-1,6-diol (H1) and 1,1,4,4-tetraphenylbut-2-yne-1,4-diol (H2)

Toda subsequently designed and synthesised three new and different hosts. Firstly, 9,10-dihydroxy-9,10-diphenyl-9,10-dihydroanthracene (H3) was observed to form a variety of inclusion compounds with both aromatic and aliphatic guest molecules.[140] Enclathration and desolvation kinetics of this host have been studied with acetone,[141] 1,3-dioxolane,[142] and cyclohexanone.[143] 1,1-Bis(4-hydroxyphenyl)cyclohexane (H4) has been used to separate the isomers of phenylenediamine, benzenediol and picoline.[138] This host was successfully investigated by Goldberg *et al*[144] for the separation of *m*-cresol from the other cresol isomers. Upon conducting competition studies, he found that H4 showed preferential complexation with the guests according to the sequence *m*-cresol > *p*-cresol > phenol > *o*-cresol. This was a significant result since the separation of cresols obtained from coal tar has long been an important subject in the chemical industry. Most challenging to separate is *m*- (b.p. 202.0 ˚C) from *p*- cresol (b.p. 201.8 ˚C) because of their very similar boiling points. Crystallographic analyses revealed that intermolecular arrangements were characterised by layers of hydrogen-bonded entities (host-to-host, host-to-guest and guest-to-guest) with every OH group being involved in two H-bonds.[144] 1,1,2,2-Tetraphenylethane-1,2-diol (H5) has been used to separate the picoline, methylquinoline and lutidine isomers.

H3   **H4**   **H5**
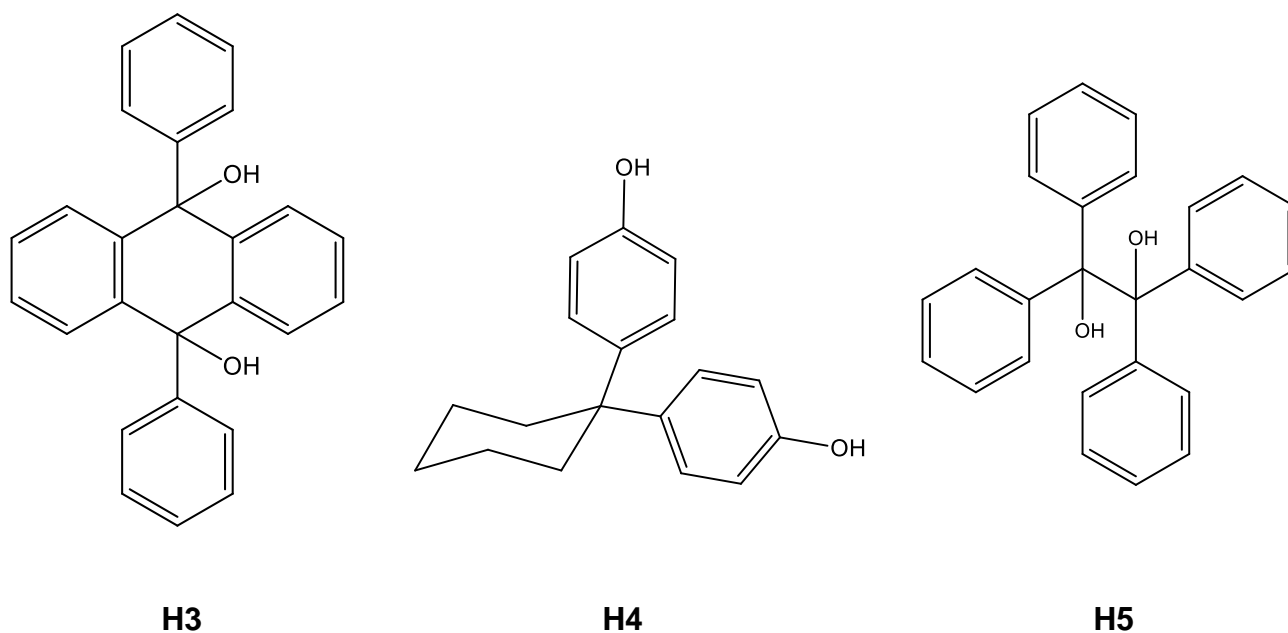
Figure 26: Diol hosts used for isomer enclathration: 9,10-dihydroxy-9,10-diphenyl-9,10-dihydroanthracene (H3), 1,1-bis(4-hydroxyphenyl)cyclohexane (H4) and 1,1,2,2-tetraphenylethane-1,2-diol (H5)

1.3.6.1   A Substituted Binaphthyl Diol Host: Enclathration of the Picoline Isomers

The host compound 3,30-bis(9-hydroxy-9-fluorenyl)-2,20-binaphthyl (H6) comprises a central biaryl unit with the bulky 9-hydroxy-9-fluorenyl moiety attached. It is a versatile host compound, including a variety of guest molecules with differing host:guest ratios (Figure 27).[145] In 2013, this host was investigated for the separation of the picoline (PIC) isomers by selective enclathration.[117] Competition experiments were conducted between guest pairs 2PIC/3PIC, 2PIC/4PIC and 3PIC/4PIC (Table 3). Separation of these isomers by selective inclusion is of great interest as these isomers are difficult to separate by distillation due to their very similar boiling points. In the two-guest competition experiment of 2PIC/3PIC, 3PIC was preferentially enclathrated. For guest mixtures 2PIC/4PIC and 3PIC/4PIC, 4PIC was preferentially included in both. These results were confirmed by ternary competition experiments resulting in the selective enclathration of 4PIC by H6. It is interesting to note that individual crystals derived from the competition experiments contained either only a single guest or a mixture of

the two guests, and these guests shared the same site in the crystal. It is therefore very important to carry out careful analyses of the crystals arising from the guest mixtures.

Normally the host:guest ratios of complexes H6·2PIC and H6·3PIC are 1:2. However, in the H6·2PIC·3PIC mixed complex, the overall host:guest ratio was 1:1. Both intramolecular host–host O–H···O and host–guest O–H···N hydrogen bonds stabilize the host packing and complex (Figure 28). A different situation arose for the crystals derived from the 3PIC/4PIC competition experiments. Consider the sigmoidal selectivity curve provided in Figure 29: between points Y1 and Y2, the host selectivity changes from 3PIC to 4PIC. The crystals that resulted were found to be of two types: large block-like crystals were those of H6·3PIC, while smaller, flat plate crystals were those of H6·4PIC. Both of these were subjected to X-ray diffraction and each turned out to be identical in structure to the crystals obtained from the single solvent experiments.

H6
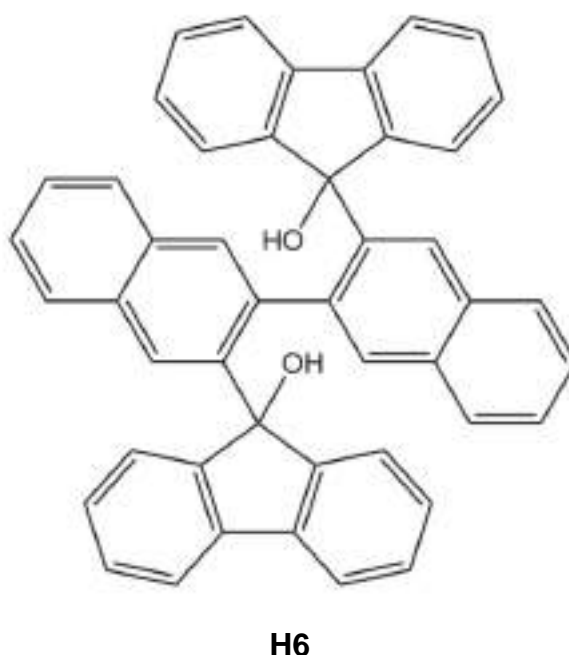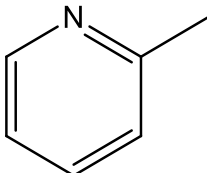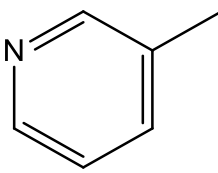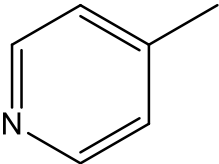
Figure 27: 3,30-Bis(9-hydroxy-9-fluorenyl)-2,20-binaphthyl (H6)

Table 3: Structure and boiling points of the picoline isomers

Guest	2-Picoline	3-Picoline	4-Picoline
Guest structure			
Boiling point (˚C)	128.5	144.0	144.5
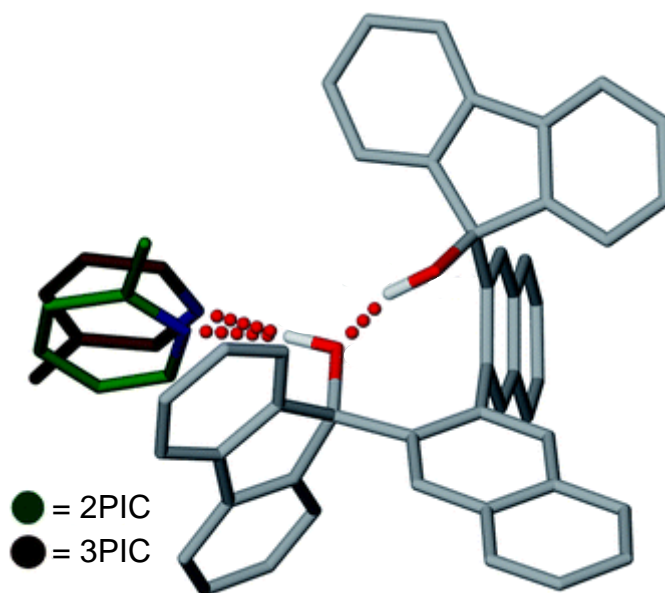
● = 2PIC
● = 3PIC

Figure 28: The asymmetric unit of H6·2PIC·3PIC which shows that both the picolines are hydrogen bonded to the host[117]
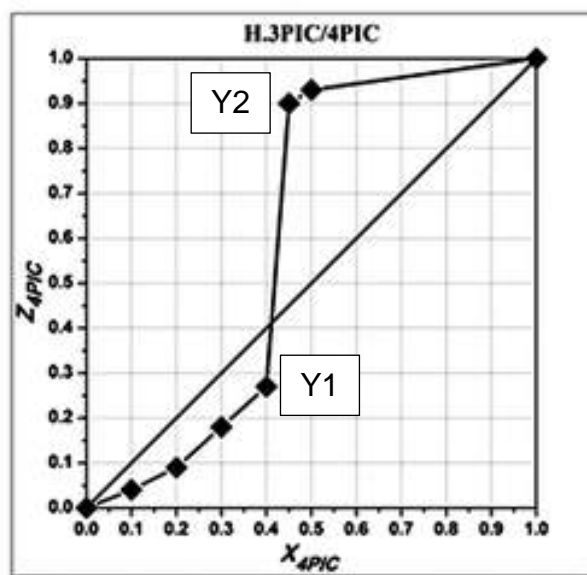
Figure 29: The selectivity curve of H6·3PIC/4PIC

1.3.6.2 Three Related Fluorenyl Diol Hosts: Enclathration of the Lutidines

Host compounds H7, H8 and H9 were individually recrystallised from binary equimolar mixtures of the lutidines (LUT, Figure 30, Table 4). In the present discussion, the host in a host-guest complex containing greater than 85% of one particular guest will be considered as completely selective.

H7 **H8** **H9**
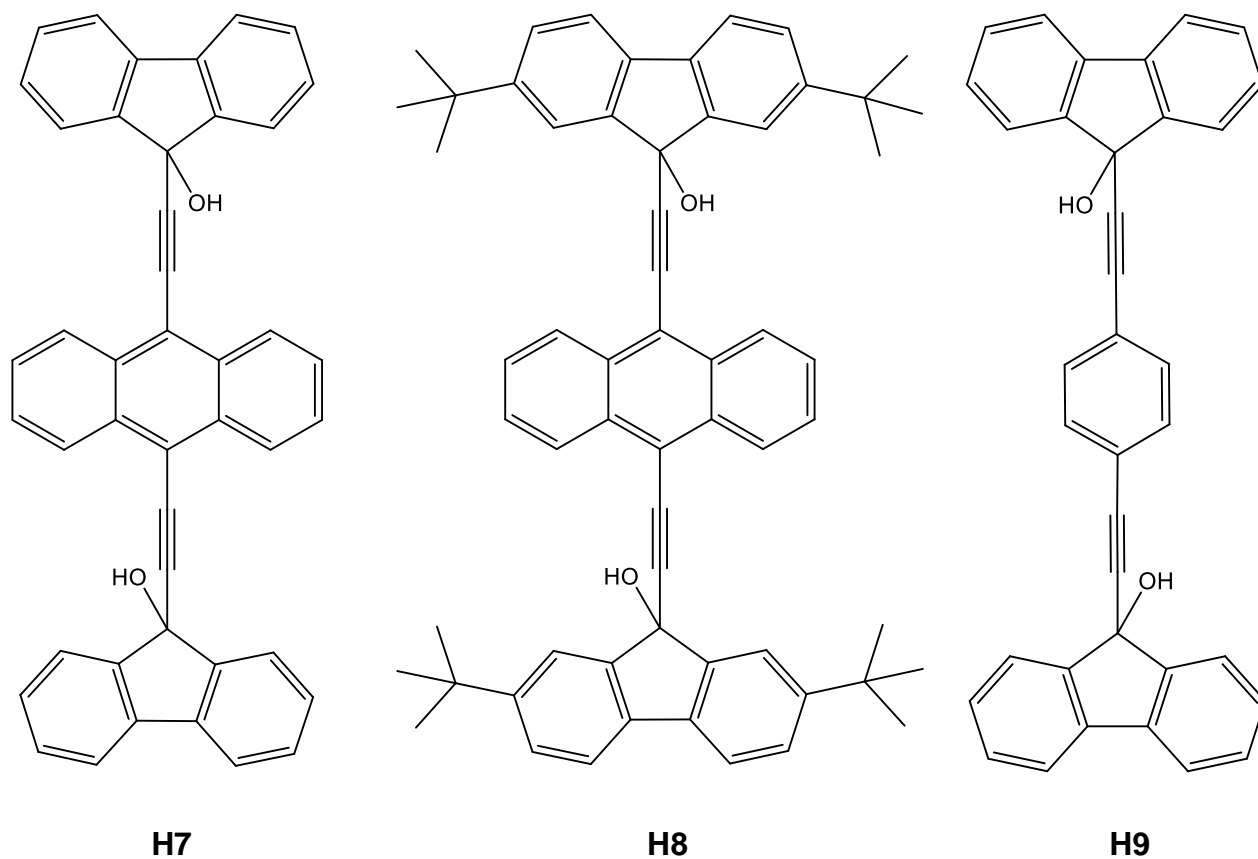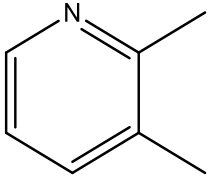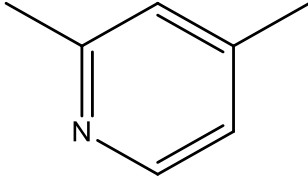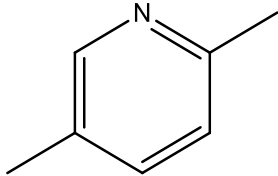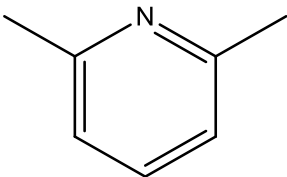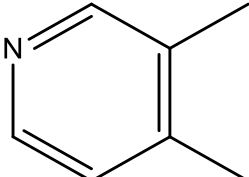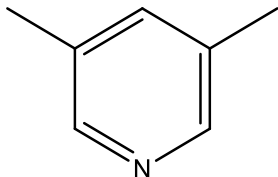
Figure 30: Structure of 9,10-bis[2-(9-hydroxy-9-fluorenyl)ethynyl]anthracene (H7), 9,10-bis[2-(2,7-*di-tert*-butyl-9-hydroxy-9-fluorenyl)ethynyl]anthracene (H8), and 1,4-bis[2-(9-hydroxy-9-fluorenyl)ethynyl]benzene (H9)

Table 4: Structure and boiling points of the lutidine isomers

Guest	2,3-Lutidine	2,4-Lutidine	2,5-Lutidine
Guest Structure			
Boiling point (˚C)	162	159	157
Guest	2,6-Lutidine	3,4-Lutidine	3,5-Lutidine
Guest Structure			
Boiling point (˚C)	144	163	169

Samipillai *et al*[116] discovered that host compound H7 displayed poor selectivity in the 2,3-LUT/3,4-LUT competition experiment enclathrating 62% 2,3-LUT and 38% 3,4-LUT. When analysing the crystal structures of the single-guest inclusion compounds H7·2(2,3-LUT) and H7·2(3,4-LUT), it was observed that both guests are hydrogen bonded to the host via (host)O–H···N(guest) interactions, with O···N bond lengths of 2.811 Å and 2.791 Å, respectively (Figure 31). The crystal structure of the mixed complex H7·2(2,3-LUT·3,4-LUT) was isostructural with that of H7·2(2,3-LUT), the more preferred of the two guests. Both 2,3-LUT and 3,4-LUT occupy the same site in the crystal with site occupancy factors of 0.62 for 2,3-LUT and 0.38 for 3,4-LUT.[116]
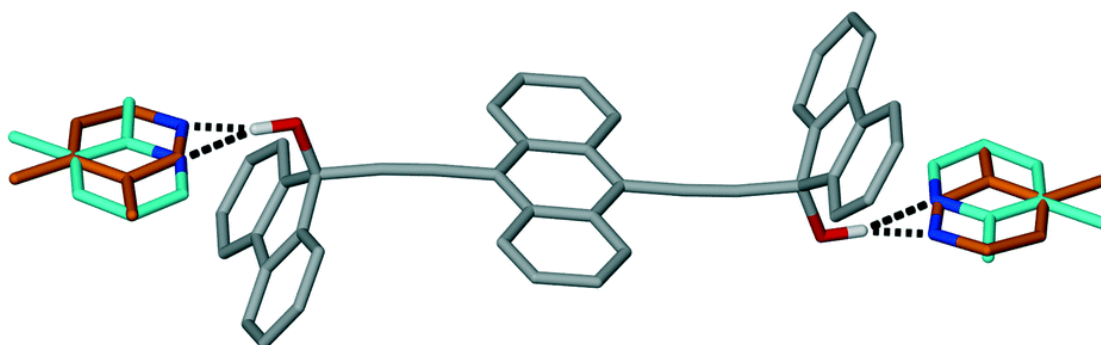
Figure 31: The asymmetric unit of H7·2(2,3-LUT·3,4-LUT) showing the positions of 2,3-LUT and 3,4-LUT; 2,3-LUT (green) and 3,4-LUT (brown)[116]

Host compound H8 also displayed poor selectivity in the 2,3-LUT/3,4-LUT competition; 2,3-LUT was preferred, 69% being extracted from the mixture compared to 31% of the 3,4-LUT guest. A structure elucidation of the three relevant crystals H8·2(2,3-LUT), H8·2(3,4-LUT) and H8·2(2,3-LUT/3,4-LUT) showed the guests in H8·2(2,3-LUT) to be disordered over two positions, both with site occupancies of 0.5. Both guests in this complex are hydrogen bonded to the host, with bond lengths of 2.796 Å and 2.769 Å. The structure of H8·2(3,4-LUT) has the host hydroxyl moieties in the *cis* conformation. Only one of these experiences a hydrogen bond with one lutidine guest while the hydroxyl is involved in another hydrogen bond with a neighbouring host molecule (Figure 32). The structure of H8·2(2,3-LUT·3,4-LUT) had unit cell dimensions similar to those of H8·2(2,3-LUT) (the preferred guest once more), yielding overall site occupancy factors of 0.69 for 2,3-LUT and 0.31 for 3,4-LUT.[116]
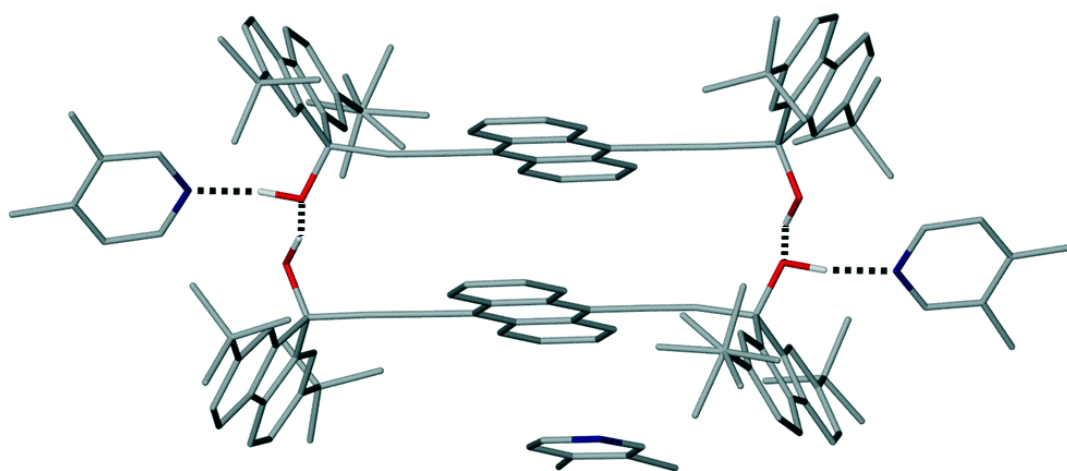
Figure 32: Hydrogen bonding pattern observed in H8·2(3,4-LUT)[116]

Interestingly, host compound H9 is completely selective for 3,4-LUT in a 3,4-LUT/2,3-LUT competition experiment. The H9·2(2,3-LUT) and H9·2(3,4-LUT) crystal structures revealed that both guests are H-bonded to the host compound. They also found that the H-bond energy of H9·2(2,3-LUT) was 14.69 kJ.mol^{-1}, while 15.06 kJ.mol^{-1} was measured for H9·2(3,4-LUT), the latter being associated with the stronger H-bond. Even though these differences are small, they are consistent with the host showing selectivity for 3,4-LUT. This was possibly as a result of steric hindrance of the methyl group at the *ortho* position of the 2,3-LUT guest compared with 3,4-LUT.[116]

1.3.6.3 Other Fluorenyl Diol Hosts: Enclathration of Methyl- and Dimethyl-Piperidines

Previously we discussed the separation of lutidine isomers using three similar diol hosts. Here we will summarise research conducted by Sykes *et al*,[115] focusing on host ability for methyl- and dimethyl- piperidines using two fluorenyl hosts, H10 and H11, with subtly different structures (Figure 33, Table 5).

H10   **H11**
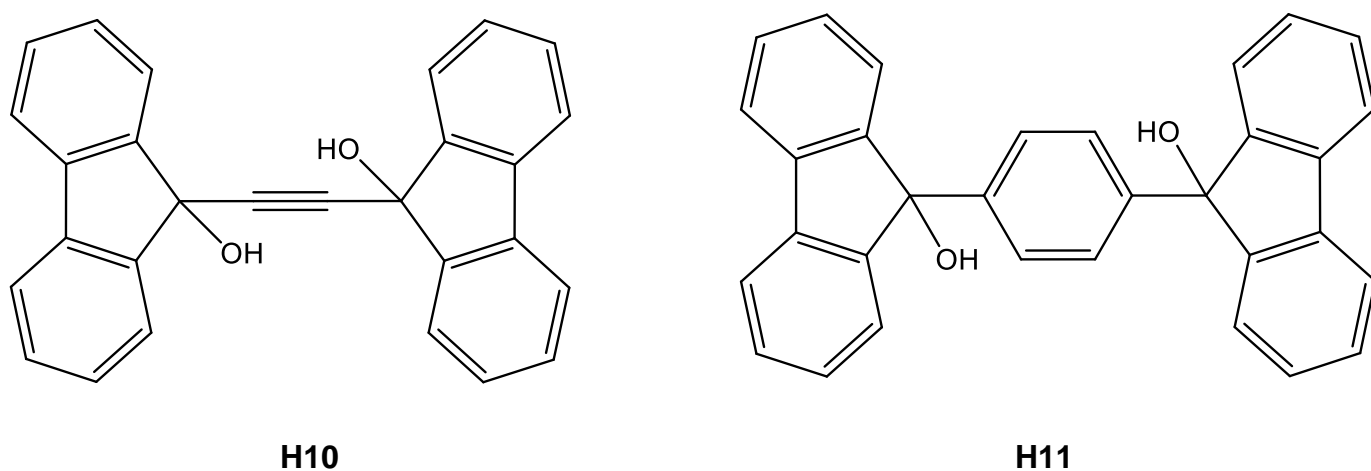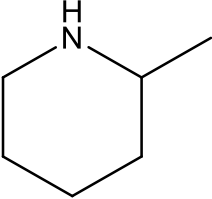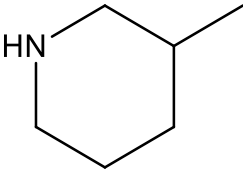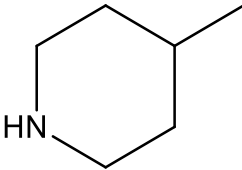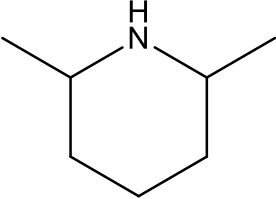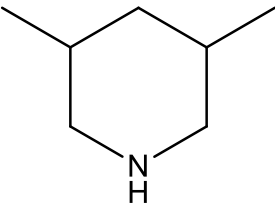
Figure 33: Structures of 9,9'-(ethyne-1,2-diyl)-bis(fluoren-9-ol) (H10) and 9,9'-(1,4-phenylene)-bis(fluoren-9-ol) (H11)

Table 5: Structure and boiling points of the methylpiperidine isomers

Guest	2-Methylpiperidine	3-Methylpiperidine	4-Methylpiperidine
Guest Structure			
Boiling point (˚C)	118–119	125–126	124

Guest	2,6-Dimethylpiperidine	3,5-Dimethylpiperidine
Guest Structure		
Boiling point (˚C)	113.2	125–126

The bulky diol compounds, H10 and H11, form inclusion compounds with a variety of guests including amines, aliphatic alcohols, ketones and aromatic hydrocarbons.[146] Both these hosts are typically dumbbell-shaped, containing fluorenyl groups separated by different spacers. The hydroxyl moieties of these hosts behave as hydrogen-bond donors to the piperidine guests.

H10·2(2-MP), H10·2(3-MP), H10·2(4-MP), H10·2(2,6-DMP) (MP = methylpiperidine, DMP = dimethylpiperidine) and H10·2(3,5-DMP) crystal structures were all observed to be stabilized by guest–host hydrogen bonds. The 3,5-dimethylpiperidine guest in H·2(3,5-DMP) is a mixture of 71/29% *cis*/*trans*, which was determined by ^{1}H-NMR spectroscopy and confirmed by SCXRD analysis.

H11·2(2-MP), H11·2(2,6-DMP) and H11·2(3,5-DMP)·H$_2$O crystal structures were also stabilized by these hydrogen bonds, and there was also evidence of C−H···π interactions. The ^{1}H-NMR spectrum of the H11·2(3,5-DMP)·H2O crystal showed that only a small percentage of the *trans*-3,5-DMP stereoisomer (15%) was present. However, crystal analysis could not confirm this. The packing of this crystal revealed

a chain of host molecules interconnected by hydrogen bonding pairs of 3,5-DMP and the water molecules. The structure is characterized by restricted channels accommodating the 3,5-DMP guests (Figure 34).
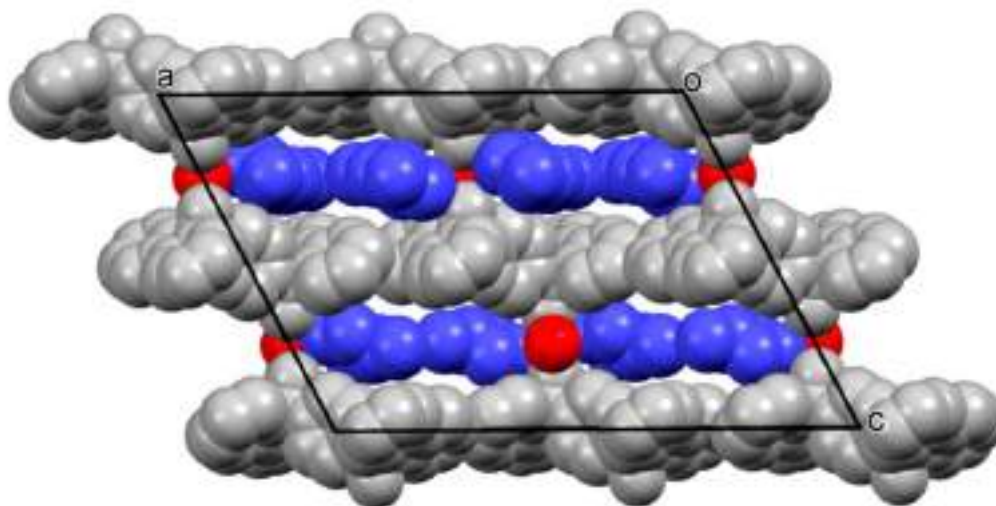
Figure 34: Packing of structure H11 as viewed along [010] showing the guests located in restricted channels along the *b*-axis[115]

Competition experiments conducted between H10 and equimolar 2-MP/3-MP yielded 90% 2-MP, while a 2-MP/4-MP experiment showed a decline in the selectivity for 2-MP (57%). To account for the sudden poor selectivity from the 2-MP/4-MP mixture, lattice energies were calculated and found to be –318.3 kJ/mol for H10·2(2-MP) and −312.0 kJ/mol for H10·2(4MP). Even though the difference was small, it was significant enough for the host to have a partial preference for the H10·2(4-MP) structure.

Each host was also recrystallised from equimolar mixtures of 2,6-DMP and 3,5-DMP. H10 showed a preference for 3,5-DMP while H11 preferred 2,6-DMP. This outcome could not be explained by X-ray analysis or lattice energy considerations but was found to be in accordance with thermal analytical TGA and DSC data. The DSC curves (Figure 35) were more informative than the TGA traces, and produced endotherms corresponding to the release of 3,5-DMP, with a peak temperature of 158.4 °C, while that of 2,6-DMP was lower at 143.0 °C for H10. 3,5-DMP was therefore more strongly retained in the crystal, correlating with the results from competition experiments. Opposingly, the order in which the two guest loss endotherms appeared was reversed for H11, with the 2,6-DMP release process having the higher peak temperature (151.8

°C), while that for 3,5-DMP occurred at only 129.2 °C. In conclusion, Sykes *et al*[115] suggested that the selectivity of the hosts may be governed by kinetic effects at the nucleation stage of host−guest aggregation.
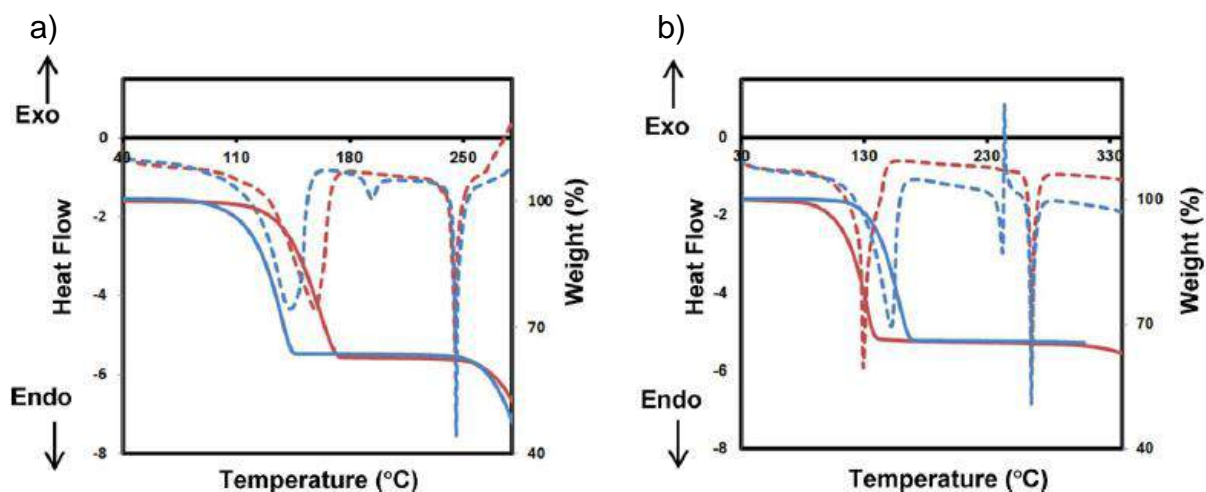
Figure 35: TGA (unbroken lines) and DSC (broken lines) traces for a) H10·2(3,5DMP) (red) and H10·2(2,6DMP) (blue), and b) H11·2(3,5DMP)·H$_2$O (red) and H11·2(2,6DMP) (blue)[115]

1.3.6.4　　　A Common Diol Host: TADDOL

TADDOLs (α,α,α',α'-tetraphenyl-2,2-dimethyl-1,3-dioxolane-4,5-dimethanol), introduced in 1982 by *Seebach et al,*[148] are characterized as diol hosts in which the diol unit is appended to heterocyclic moieties (Figure 36).[149] TADDOLs are an extremely versatile group of host compounds that possess efficient inclusion abilities, enclathrating a wide range of organic guest species.[150,151] These compounds are readily derived from dimethyl or diethyl tartrate, or from naturally-occurring optically pure tartaric acid. As a result, TADDOLs are optically pure and have been exploited for the efficient separation of racemic mixtures into their constituent enantiomers via simple recrystallization procedures.[152,153] TADDOLS are chiral hydrogen-bond donors and thus crystallize with hydrogen-bond acceptors, with which they form inclusion compounds.[154] Furthermore, TADDOL and its optically pure derivatives have the ability to behave as chiral auxiliaries and catalysts in asymmetric transformations.[148]

(*R*,*R*) - TADDOLs   (*S*,*S*) - TADDOLs

H12   **H13**
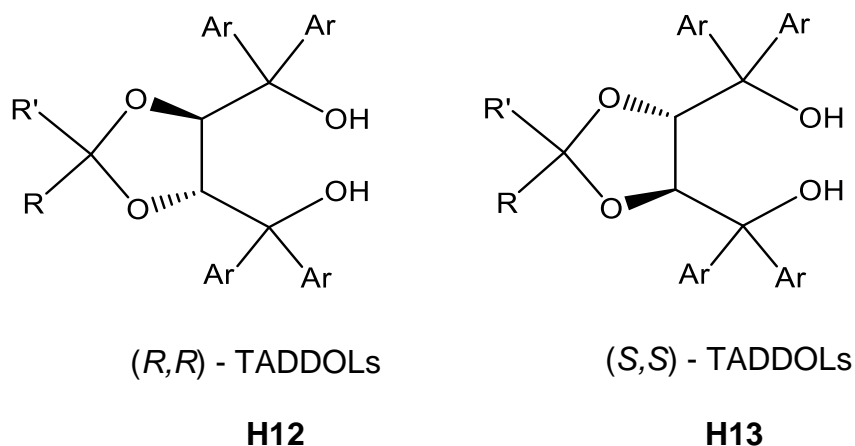
Figure 36: General structure of the TADDOLs: R or R' = H, Me, Ph etc.; Ar = Ph, *p*-MePh, naphthyl, etc.

A novel chiral separation process utilizing TADDOL as a host species was reported by Ghazali *et al.*[155] This process combined enantioselective inclusion complexation (EIC) with organic solvent nanofiltration (OSN). Ghazali focused on the chiral resolution of racemic 1-phenylethanol using (*R*,*R*)-TADDOL (H12) as the chiral host. The process is outlined in Figure 37 and can be summarised as follows: racemic 1-phenylethanol was added to H12 suspended in a resolution solvent. The (*S*)-enantiomer preferentially complexed with the host while the (*R*)-enantiomer remained in solution (Step A). The remaining suspension was nanofiltered using OSN, allowing the (*R*)-enantiomer to permeate the OSN membrane (Step B). The solid host-guest complex was retained and further resolution solvent added to encourage the full elution of the *R*-enantiomer. Thereafter, a decomplexation solvent was added to the suspension containing the solid host-guest complex, thereby dissolving and dissociating the complex into the (*S*)-enantiomer and host (Step C). The solution was subsequently nanofiltered to elute the (*S*)-enantiomer, while the soluble host was retained by the membrane (Step D). By removing the decomplexation solvent via filtration with the resolution solvent, the host was allowed to recrystallize (Step E), and returned to the next cycle. Ghazali concluded a successful first-time novel enantioseparation process using this combined EIC-OSN process.[156] He suggested that this method obviates the need for distillation to recover enantiomers from enantio-enriched solid complexes. In summary, a decomplexation solvent is used to dissociate enantiomers from the

complex, and a further separation of enantiomers from the chiral host is conducted using OSN.

Host in resolution solvent returned to subsequent cycle

| Resolution solvent | Decomplexation solvent | Decomplexation solvent | Resolution solvent |

R,S

| Step A: resolution | Step B: elution of *R* | Step C: decomplexation | Step D: elution of *S* | Step E: host precipitation |
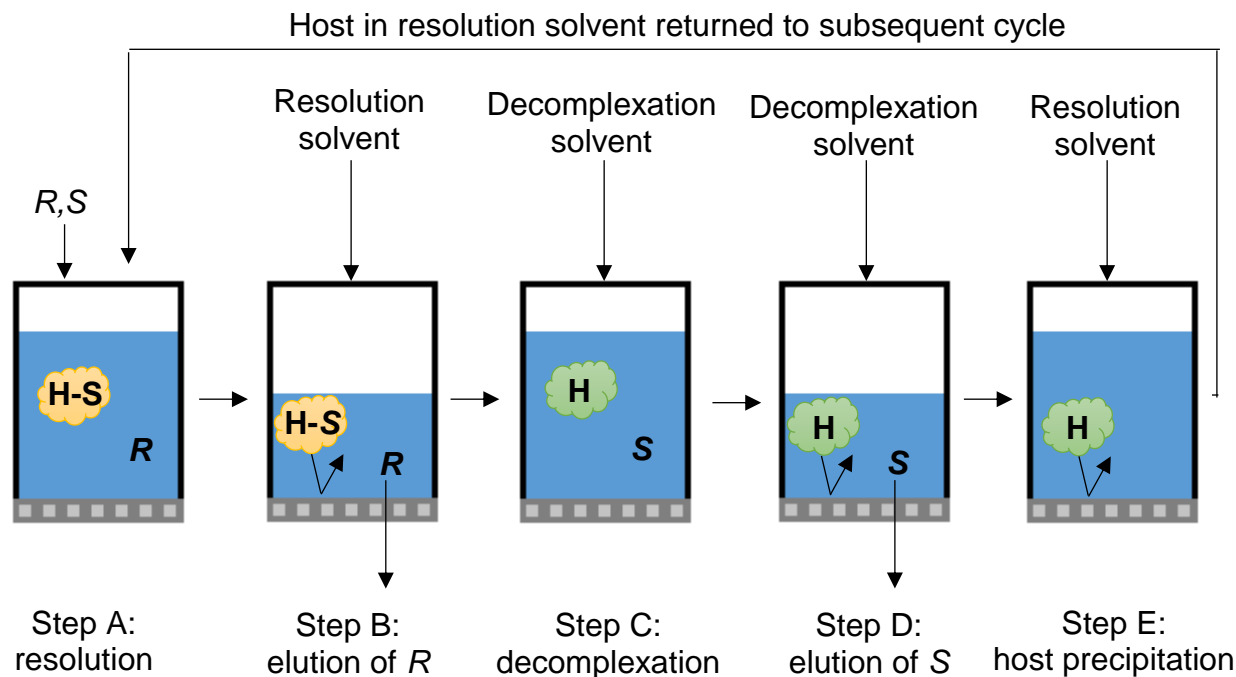
Figure 37: The process of enantioselective inclusion complexation-organic solvent nanofiltration[155]

1.3.6.5 TETROL as a Diol Host

(+)-(2*R*,3*R*)-1,1,4,4-Tetraphenylbutane-1,2,3,4-tetraol [(+)-TETROL, H14] was synthesized in our laboratories in December 2012 (Figure 38).[157] Subsequent to this synthesis, it was discovered that the preparation of H14 had previously been achieved by Hu *et al*[158] by using enantiomerically-pure diethyl tartrate, which was protected in the 2- and 3- positions with phenylboronic acid [PhB(OH)$_2$]. The protected diethyl tartrate was subsequently reacted with an excess of phenylmagnesium bromide (PhMgBr) in THF, followed by hydrolysis under acidic conditions in an ice-water bath. This afforded H14 in moderate yield (50%). The deprotection of diethyl tartrate to yield the final 2,3-diol products proved, however, quite difficult and required expensive reagents and rigorous conditions.

H14
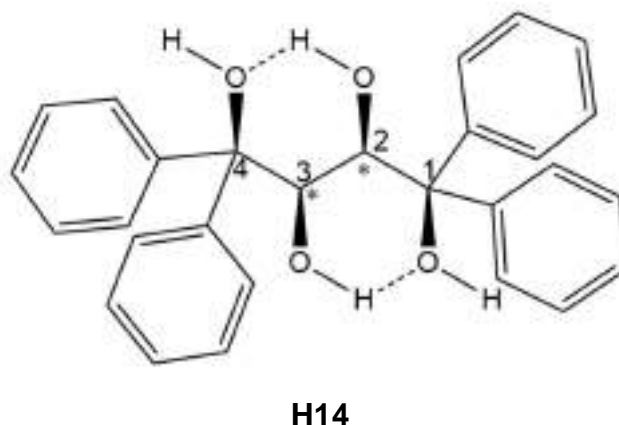
Figure 38: The structure of (+)-TETROL (H14, TET)

A simplification of that procedure was conducted in our laboratories, where standard Grignard conditions were used to promote direct phenylation of unprotected diethyl tartrate with excess PhMgBr, thus forming TETROL in also moderate yields (45%) (Figure 39).[157]

H14
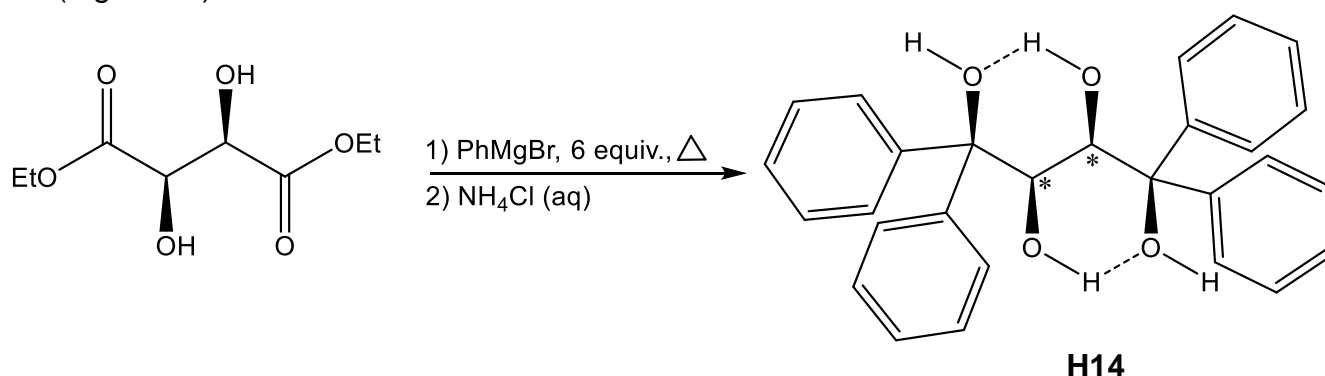
Figure 39: The synthesis of TETROL (H14) in our laboratories in December 2012

The TADDOLs have similar structural characteristics to H14 and, due to the widely modified and immensely successful TADDOL host class of compounds, it was envisaged that TETROL may be similarly effective. The TETROL molecule is well suited for applications as a host compound: the butane chain is significantly constrained due to the four hydroxyl groups where stabilisation through a pair of 1,3-hydrogen bonding interactions exists (Figure 39). Chirality of the C2 and C3 atoms influences the directionality of the hydrogen bonding array, increasing the possibility that TETROL may behave enantioselectively. This allows for extensive future investigations on its capabilities as both a host compound and as a chiral mediator in

asymmetric transformations.[157] Since our synthesis of H14 in 2012, we have communicated its use as a host compound for the separation of equimolar mixtures of pyridine and isomeric methylpyridines, and have noted its inclusion of 3- and 4-methylcyclohexanones in their energetically disfavoured axial conformations.[159,160]

(−)-(2*R*,3*R*)-2,3-Dimethoxy-1,1,4,4-tetraphenylbutane-1,4-diol [DMT, H15] is a TETROL derivative that has recently shown significant potential in our laboratories as a host compound; DMT has been applied in the separation of the xylene isomers and has proven to be remarkably selective for the methylated anilines (Figure 40).[161,162] This derivative is substituted with methoxy moieties that replace the secondary hydroxyl groups belonging to TETROL.
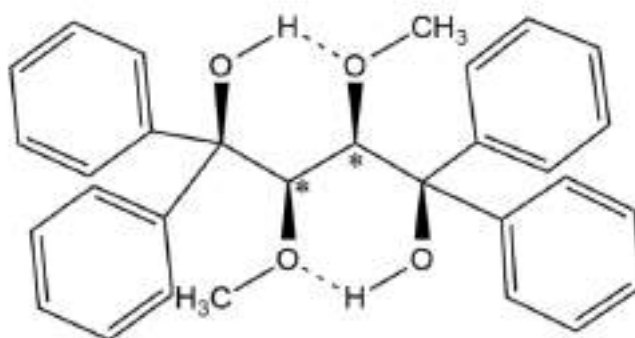
H14

Figure 40: The structure of dimethoxyTETROL (H15, DMT)

1.3.7   Aims and Objectives

The objective of this study is to investigate the feasibility of separating isomers and structurally-related compounds, with similar physical and chemical properties, by employing host-guest chemistry. The extent of host inclusion and guest separation will be determined using ^{1}H-NMR spectroscopy and GC-MS analyses. Host selectivities will be further assessed by constructing selectivity profiles. Any crystalline complexes formed successfully and with suitable crystal quality will be analysed using SCXRD to determine the nature of any significant host–guest interactions present. Thermogravimetric and differential scanning calorimetry experiments will provide information on the thermal events experienced by the complexes as they are heated

at 10 °C/min, and an attempt will be made to relate these back to complex stability and host selectivity.

The host compound TETROL will be investigated in this study with the following guest mixtures:

1) Cyclohexanone (CON), cyclohexanol (COL) and cyclohexylamine (CAM),
2) Cyclohexanone (CON), 2-methylcyclohexanone (2MCON), 3-methylcyclohexanone (3MCON) and 4-methylcyclohexanone (4MCON),
3) Pyridine (PYR), piperidine (PIP), morpholine (MOR) and dioxane (DIO),
4) Aniline (ANI), cyclohexylamine (CAM), cyclohexanol (COL) and phenol (PHO),
5) Aniline (ANI), *N*-methylaniline (NMA) and *N,N*-dimethylaniline (NNMA),
6) Aniline (ANI), toluene (TOLU), *o*-toluidine (*o*-TOLU), *m*-toluidine (*m*-TOLU) and *p*-toluidine (*p*-TOLU),
7) *o*-Cresol (OC), *m*-Cresol (MC) and *p*-Cresol (PC).

Each guest mixture was selected based on data from experiments using either the industrial significance of its separation or because the information provided by experiments conducted on the mixture would add to the knowledge base of the host compound's preferences and selectivities.

An additional aim is to acknowledge the importance of the secondary hydroxyl groups belonging to TETROL. The objective is to compete this host with DMT in the presence of cyclohexanone to asses which host preferentially crystallizes with this guest.

Chapter 2

Experimental

2.1 General methods

- The host melting point was recorded on a Stuart SMP10 melting point apparatus and is not corrected.

- ^{1}H- and ^{13}C- NMR spectra were obtained using a Bruker Ultrashield Plus 400 MHz spectrometer and examined using TopSpin 3.2 software.

- The optical rotation was measured using an A. Krüss Optronic polarimeter (Germany) furnished with a sodium lamp.

- Thermogravimetric (TG) and differential scanning calorimetry (DSC) traces were obtained using a TA SDT Q600 module system and analysed using TA Universal Analysis 2000 data analysis software. High purity nitrogen was used as a purge gas. An open platinum pan containing the sample and an empty platinum pan as reference were used during TG experiments. The heating rate was 10 °C·min^{-1}.

- Single crystal X-ray diffraction studies (SCXRD) were performed using a Bruker Kappa Apex II diffractometer with graphite-monochromated Mo Kα radiation (λ = 0.71073 Å). (see Section 2.6)

- Chiral gas chromatography (GC) was performed using an Agilent Technologies 7890 A gas chromatograph system fitted with an Agilent Technologies 5975 C VL MSD mass spectrometer (MS) with a Triple-Axis Detector. High purity helium was used as the carrier gas. An Agilent J&W GC Cyclodex-B column, Agilent J&W GC CycloSil-B column, Agilent J&W GC DB-WAX column and Agilent J&W GC HP-5 column were utilized, all 30 m in length, 0.25 mm in

diameter and having a film thickness of 0.25 µm. The following GC methods were conducted as per chapter:

- Chapters 3 and 4: a DB-WAX column (30 m) was used. The method involved an initial 1 min hold time at 55 °C, followed by a ramp of 1 °C/min until 150 °C was reached, and then a hold time at this temperature for 10 min. This was followed by a ramp of 1 °C/min until 160 °C was reached, and then a hold time at this temperature for 10 min, and lastly a ramp of 20 °C/min until 220 °C was reached, and then a final hold time at this temperature for 10 min. The split ratio was 2:1 and inlet temperature 250 °C.

- Chapter 5: a CycloSil-B column (30 m) was used. The method involved an initial 2 min hold time at 35 °C, followed by a ramp of 2 °C/min until 180 °C was reached, and then a hold time at this temperature for 5 min. The split ratio was 100:1 and inlet temperature 220 °C.

- Chapter 6: a HP-5 column (30 m) was used. The method involved an initial 2 min hold time at 40 °C, followed by a ramp of 2 °C/min until 160 °C was reached, and then a hold time at this temperature for 5 min, and lastly a ramp of 20 °C/min until 220 °C was reached, and then a final hold time at this temperature for 10 min. The split ratio was 100:1 and inlet temperature 250 °C.

- Chapters 7 and 8: a CycloSil-B column (30 m) was used. The method involved an initial 2 min hold time at 50 °C, followed by a ramp of 2.5 °C/min until 130 °C was reached, and then a hold time at this temperature for 1 min. The split ratio was 100:1 and inlet temperature 220 °C.

- Chapter 9: a CycloSil-B column (30 m) was used. The method involved an initial 1 min hold time at 55 °C, followed by a ramp of 1 °C/min until 150 °C was reached, and then a hold time at this temperature for 10 min. This was followed by a ramp of 1 °C/min until 160 °C was reached, and then a hold time at this temperature for 10 min, and lastly a ramp of 20 °C/min until 220 °C was reached, and then a final hold time at this temperature for 10 min. The split ratio was 100:1 and inlet temperature 220 °C.

- Chapter 10: a CycloSil-B column (30 m) was used. The method involved an initial 1 min hold time at 50 °C, followed by a ramp of 5 °C/min until 160 °C

was reached, and then a hold time at this temperature for 5 min. The split ratio was 2:1 and inlet temperature 220 °C.

- Chapter 11: a Cyclodex-B column (30 m) was used. The method involved an initial 5 min hold time at 80 °C, followed by a ramp of 5 °C/min until 110 °C was reached, and then a hold time at this temperature for 5 min, and lastly a ramp of 5 °C/min until 120 °C was reached, and then a final hold time at this temperature for 5 min. The split ratio was 100:1 and inlet temperature 220 °C.

2.2 (+)-(2*R*,3*R*)-1,1,4,4-Tetraphenylbutane-1,2,3,4-tetraol (H14, TETROL)

H14
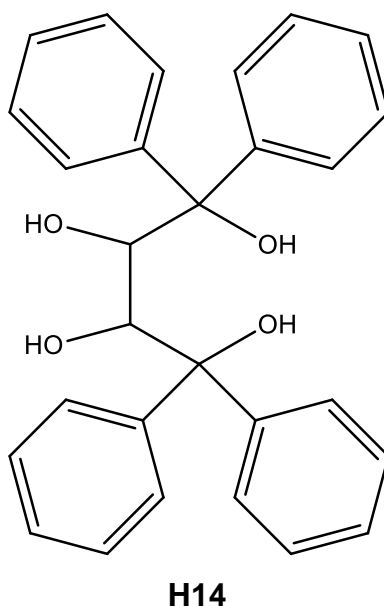
The host compound, (+)-TETROL (H14), was synthesized using a standard Grignard procedure. A two-necked 250 mL round-bottomed flask containing a stirrer bar was charged with excess magnesium turnings (4.0571 g, 0.1669 mol) and an iodine crystal, that were both covered with anhydrous THF. To this mixture was added a portion of bromobenzene (23.1243 g, 0.1473 mol) diluted in anhydrous THF. Through gentle heating and stirring, the reaction became colourless. The reaction was cooled to room temperature whereupon the remainder of the brominated compound was added dropwise so as to maintain a steady reflux. Upon completion of addition, the reaction was heated under reflux for 1 hr. The resultant reaction was cooled in an ice-water bath and (+)-diethyl-L-tartrate (5.7058 g, 0.02767 mol), in anhydrous THF, was added dropwise to the stirred reaction. After addition was complete, the reaction was heated

under reflux for an additional hour. Thereafter, the mixture was cooled to room temperature and poured into a 10% ammonium chloride solution (200 mL). This mixture was filtered through kieselguhr to remove any unreacted magnesium. The filtrate was extracted with 3 x 50 mL portions of diethyl ether. The combined organic extracts were dried using anyhydrous Na_2SO_4, and the solvent removed under reduced pressure to yield an orange gum which was crystallized and recrystallized from CH_2Cl_2/hexane/MeOH to afford (+)-(2*R*,3*R*)-1,1,4,4-tetraphenylbutane-1,2,3,4-tetrol as a white solid (45 %), mp 147–149 °C (lit.,[158] mp 150−151 °C); $[α]^{23}_D$ +166 (c = 9.32, CH_2Cl_2) {lit.,[158] $[α]^{25}_D$ +154 (c = 1.2, $CHCl_3$)}; v_{max}(solid)/cm^{-1} 3440 (br, OH), 3294 (br, OH), 3057 (Ar), 3033 (Ar), 1598 (Ar) and 1494 (Ar); $δ_H$($CDCl_3$) 3.82 (4H, br, 2HCO<u>H</u>, 2CPh₂O<u>H</u>), 4.31 (2H, s, 2<u>H</u>COH) and 7.05–7.30 (20H, m, Ar); $δ_C$($CDCl_3$) 72.1 (H<u>C</u>OH), 81.7 (<u>C</u>Ph₂OH), 125.0 (Ar), 126.1 (Ar), 127.1 (Ar), 127.3 (Ar), 128.4 (Ar), 128.6 (Ar), 143.9 (quaternary Ar) and 144.2 (quaternary Ar).

The (+)-diethyl tartrate and bromobenzene were purchased from Sigma-Aldrich and used as received. The guest compounds under investigation are presented in Table 1 and categorised under their respective target studies. Each guest, apart from 2-methylcyclohexanol (Chapter 11), was obtained from Sigma-Aldrich and used without further purification (Table 1).

Table 1: Guest mixtures investigated*a*

Chapter	Guests employed	Abbreviation
	Cyclohexanone	**CON**
3	Cyclohexanol	**COL**
	Cyclohexylamine	**CAM**
	Cyclohexanone	**CON**
4	2-Methylcyclohexanone	**2MCON**
	3-Methylcyclohexanone	**3MCON**
	4-Methylcyclohexanone	**4MCON**
	Pyridine	**PYR**
5	Piperidine	**PIP**
	Morpholine	**MOR**
	1,4-Dioxane	**DIO**
	Aniline	**ANI**
6	*N*-Methylaniline	**NMA**
	N,*N*-Dimethylaniline	**NNMA**
	Aniline	**ANI**
7	*o*-Toluidine	***o*-TOLU**
	m-Toluidine	***m*-TOLU**
	p-Toluidine	***p*-TOLU**
	Cyclohexylamine	**CAM**
8	Aniline	**ANI**
	Cyclohexanol	**COL**
	Phenol	**PHO**
	o-Cresol	**OC**
9	*m*-Cresol	**MC**
	p-Cresol	**PC**
10	Cyclohexanone	**CON**
	Butyric acid	**BA**
12	*iso*-Butyric acid	**IBA**
	3-Chloropropionic acid	**3CPA**

*a*Guests were obtained from Sigma-Aldrich and used without further purification

2.3 (–)-(2*R*,3*R*)-2,3-Dimethoxy-1,1,4,4-tetraphenylbutane-1,4-diol (H15, DMT) (See Chapter 11)
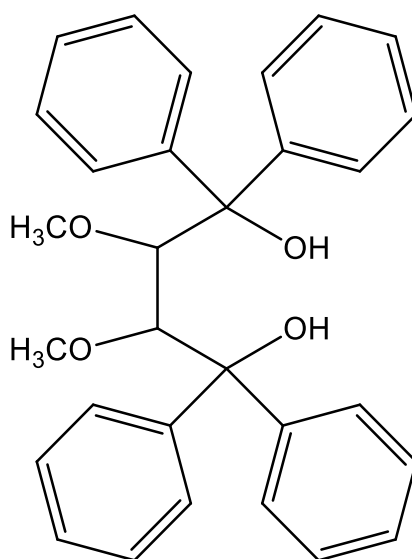
H15

A two-necked round-bottomed flask was equipped with a stirrer bar, dropping funnel, condenser and $CaCl_2$ drying tube. To this flask was added anhydrous THF and excess sodium hydride (6.1424 g, 55–65% suspension in mineral oil). The flask was cooled in an ice bath and the hydroxy-containing compound (H14) slowly added. Upon completion of this addition, a stoichiometric amount of dimethyl sulfate (3.5796 g, 0.02838 mol) was added slowly. The mixture was allowed to stir for 24 h whereafter it was poured into an ice-cold saturated solution of $NaHCO_3$ and stirred for an additional hour. The mixture was poured into a separatory funnel and extracted with ethyl acetate (3 x 50 mL). The combined organic extracts were dried over anhydrous Na_2SO_4, and solvent removed under reduced pressure to afford a gum which was crystallized from petroleum ether (40–60 °C) and recrystallized from ethanol to yield (–)-(2*R*,3*R*)-2,3-dimethoxy-1,1,4,4-tetraphenylbutane-1,4-diol (H15, DMT) as a white solid (4.6456 g, 0.01022 mol, 72%), mp 124–126 °C (lit.,[163] mp 125–126 °C); $[\alpha]_D^{23}$ – 154.5 (*c*. 0.27, CH_2Cl_2) {lit.,[163] –153 (*c*. 0.8, $CHCl_3$)}; ν_{max}(solid)/cm^{-1} 3576–3271 (br, OH), 3025 (Ar), 2836 (CH_3) and 1567 (Ar); δ_H($CDCl_3$)/ppm 2.60 (6H, s, 2OC$\underline{H}_3$), 4.46 (2H, s, 2$\underline{H}$COCH$_3$), 4.87 (2H, s, 2CPh$_2$O$\underline{H}$), 7.17 (2H, m, Ar), 7.26 (4H, m Ar), 7.32 (2H, m, Ar), 7.46 (4H, m, Ar) and 7.63 (8H, m, *ortho*-Ar); δ_C($CDCl_3$)/ppm 61.00 (OC$\underline{H}_3$),

80.09 ($\underline{C}$Ph$_2$OH), 85.27 (H$\underline{C}$OCH$_3$), 125.89 (Ar), 126.05 (Ar), 126.79 (Ar), 127.22 (Ar), 127.95 (Ar), 128.46 (Ar), 144.92 (quaternary Ar) and 145.64 (quaternary Ar).

2.4   2-Methylcyclohexanol (Mixture of *cis* and *trans*)
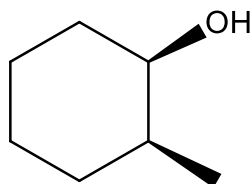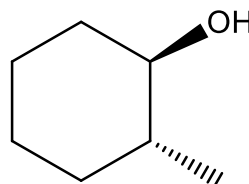
cis-2-methylcyclohexanol   **trans-2-methylcyclohexanol**

To a two-necked round-bottomed flask containing 25 mL MeOH and a stirrer bar, 2-methylcyclohexanone (5.63 mL, 5.202 g, 0.04638 mol) was added. The flask was immersed in an ice bath and NaBH$_4$ (0.9375 g, 0.02467 mol) added slowly. The mixture was allowed to stir for 5 min whereafter the flask was removed from the ice bath and stirred at room temperature for 30 min. The resultant mixture was poured into a separatory funnel and extracted with dichloromethane (40 mL), water (10 mL) and a 3 M sodium hydroxide solution (25 mL). The organic layer was removed, and the aqueous layer washed twice with dichloromethane (2 x 40 mL). The combined organic layers were dried with anhydrous Na$_2$SO$_4$, and the solvent removed under reduced pressure to yield the 2-methylcyclohexanol product as a clear, colourless liquid (4.910 g, 0.04638 mol, 94%) [47.59% (*cis*) and 52.41% (*trans*), determined using GC-MS], bp 164 °C (lit.,[164] bp 163–166 °C); v_{max}(solid)/cm^{-1} 3630–3500 (br, OH) and 2930 (CH$_3$) and 1500–600 (cyclic C–H); δ_H(CDCl$_3$)/ppm 0.96–1.93 (26H, m, 2C$\underline{H}$, 2C$\underline{H}_3$, 8C$\underline{H}_2$, 2O$\underline{H}$), 3.09 (1H, m, $\underline{H}$COH, *trans*) and 3.75 (1H, m, $\underline{H}$COH, *cis*).

2.5   Crystal Growth

2.5.1   Formation of Host-guest Complexes

TETROL (0.3 mmol) was dissolved independently in an excess (10−15 mmol) of each guest compound. Dissolution was ensured by heating the mixtures at 75 °C using a hot-water bath. These experiments were conducted in glass vials which were left open to the ambient atmosphere to facilitate evaporation of some of the solvent, after which crystallization ensued and the vials closed and left overnight to enforce further crystallization. The crystals were recovered by means of vacuum filtration and, to remove superficial guest solvent, carefully washed with small quantities of petroleum ether (40−60 °C) followed by ethanol. The compounds were analysed using ^{1}H-NMR spectroscopy with $CDCl_3$ as the NMR solvent. The recovery of host from the solutions in this way ranged between 60 and 72%.

2.5.2   Guest Competition Experiments

TETROL (0.3 mmol) was dissolved and recrystallized from equimolar amounts (5 mmol each) of binary, ternary, quaternary or quinary mixtures of the guests present in each target study. The vials were closed and stored at 0 °C in order to maintain these equimolar conditions. Crystallization occurred over a period of 1−5 days, whereafter the crystals were recovered and treated in an identical manner to the single solvent experiments mentioned previously. The methods of analysis was ^{1}H-NMR spectroscopy; where this was not a suitable technique due to resonance overlap of the various guest and/or host signals in the crystals, GC-MS was selected as the suitable method for analysis, with dichloromethane being used to dissolve each sample after crystal recovery.

Molar ratios of binary or ternary mixtures of the guests were also varied beyond equimolar [the mol% ratios that were used were approximately 10:90, 20:80, 30:70, 40:60, 50:50, 60:40, 70:30, 80:20 and 90:10, for guest 1:guest 2 (G1:G2), respectively] and the host (0.3 mmol) recrystallized from each of these mixtures. Vials were treated in an identical manner to the equimolar experiments mentioned previously, and both

the mother liquor from which crystallization had occurred and the crystalline solids were analysed by ^{1}H-NMR spectroscopy or GC-MS, where applicable. Data obtained in this way were used to construct selectivity curves, as well as the selectivity coefficients (Equation 2, Chapter 1).

2.6   X-Ray Crystallography

Each of the complexes of host H14 with the respective guests were subjected to single crystal X-ray diffraction experiments, where crystal quality was adequate. The experimental conditions for the guests in Chapter 4 have been published previously and these structures deposited at the Cambridge Crystallographic Data Centre [CCDC 989251 (H14·Cy), 989081 (H14·2MeCy), 989004 (H14·3MeCy) and 1007403 (H14·4MeCy)].[159] Suitable crystals that resulted from the single solvent recrystallization of TETROL from the various guests were analysed by SCXRD and the crystal structures reported. This experiment was conducted at 200 K using a Bruker Kappa Apex II diffractometer with graphite-monochromated Mo Kα radiation (λ = 0.71073 Å). APEXII and SAINT were used for data collection, and cell refinement and data reduction, respectively.[165] SHELXT-2014[166] was used to solve the structures, and refined by least-squares procedures using SHELXL-2016;[166] here, SHELXLE[166] served as a graphical interface. All non-hydrogen atoms were refined anisotropically, and the hydrogen atoms were added in idealized geometrical positions in a riding model. Data were corrected for absorption effects using the numerical method implemented in SADABS.[165] The H atoms of the hydroxyl groups of TETROL were allowed to rotate with a fixed angle around the C−O bonds to best fit the experimental electron density (HFIX 147 in the SHELX program suite).[166] The structure of TETROL has been deposited at the Cambridge Crystallographic Data Centre (CCDC 1541279).

2.7   Hirshfeld Surface Analysis

Hirshfeld surface analyses were conducted on the formed complexes to assist in summarising, quantitatively, the multiple intermolecular interactions present.[167] This information allows for a quantitative comparison of host–guest interactions between different host-guest complexes. The computer package, CrystalExplorer,[168] explores the different modes of packing and the various host–guest interactions within a

complex by utilizing the calculated Hirshfeld surfaces, which display the immediate environment of a molecule, to determine the percentage and type of intermolecular interactions between the molecules or for the entire crystal structure as a whole.[167]

2.8   Programs

The following programs were used in this investigation and for the analysis of crystal structures:

- ConQuest (CSD)[169]
- POV-RAY[170] used to create images of a few molecular and packing diagrams
- X-seed[171] used to create stereoviews
- Crystal Explorer[168]

2.9   Files Submitted

The Supplementary Information (SI) contains .cif, .lis and .res files for all X-ray experiments. (See submitted disc.)

Chapter 3

The Selectivity of TETROL for Three Selected Cyclic Compounds
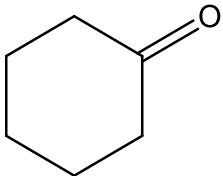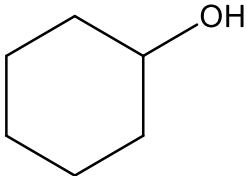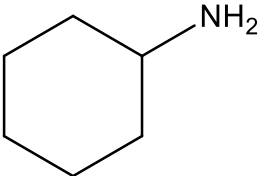
3.1   Introduction

Cyclohexanone (CON), cyclohexanol (COL) and cyclohexylamine (CAM) are structurally-similar cyclic compounds differing solely by their H-bond donor/acceptor functional groups (Table 1). Cyclohexanone is prepared industrially by either a homogeneously-catalysed oxidation of cyclohexane or by partial hydrogenation of phenol. The former process produces a reaction mixture containing a large amount of cyclohexane, cyclohexanol and cyclohexanone (also known as KA oil).[172] Consequently, three-step distillation procedures and membrane separation have been used to separate cyclohexanone and cyclohexanol from one another. This distillation process is disadvantageous as the distillation of cyclohexane results in the formation of cyclohexanone condensation products and, on a production scale, is therefore regarded as uneconomical. Alternatively, cyclohexanol can be dehydrogenated around 720 K over copper or zinc oxide catalysts to afford cyclohexanone. Cyclohexanone and cyclohexanol are important materials in the nylon industry and are used in the production of adipic acid for nylon and caprolactam, where over a billion pounds of cyclohexanone is used annually.[173–175] Cyclohexylamine is produced by the reaction of ammonia and cyclohexanol at elevated temperature and pressure in the presence of a silica-alumina catalyst, as well as from the catalytic hydrogenation of anilines.[176,177] In the former process, the cyclohexylamine is separated from the reaction mixture by distillation, leaving behind a small amount of residue including a crude cyclohexanone-derived Schiff base and/or residual oxygenated cyclohexane material.[178] Cyclohexylamine is primarily used as a corrosion inhibitor in boiler water treatment and in oil field applications, and also as a chemical intermediate for rubber processing chemicals, dyes, cyclamate artificial sweeteners and herbicides. It also finds application as a processing agent for nylon fibre production.[179]

In this study we analyse the ability of TETROL to separate CON, COL and CAM from one another, and to possibly provide an alternative method for their separation from

their starting materials during industrial syntheses. The three cyclic compounds were all enclathrated when crystals of this host compound were grown from each of these guest solvents, forming TET·CON, TET·COL and TET·2CAM complexes as viewed in Table 1, together with the boiling points of the pure guests.

Table 1: The structure and properties of the three cyclic compounds

	CON	COL	CAM
Structure			
Host (H):guest (G) ratio	1:1	1:1	1:2
Boiling point (°C)	155.6	161.8	134

3.2   Competition Experiments

Competition studies were conducted to establish the selectivity of TET for the three cyclic guests and whether this host would be able to discriminate between them. In Table 2, we summarize data obtained from the recrystallization of TET from various equimolar binary and ternary combinations of CON, COL and CAM. The so-formed crystal inclusions were analysed using proton NMR spectroscopy and GC-MS. The preferred guest species is given in bold red font face.

Table 2: Competition experiments of TET in the presence of equimolar mixtures of CON, COL and CAM [a,b]

CON	COL	CAM	Guest ratios	Overall H:G ratio
X	X		**89.2**:10.9 (0.8)	1:1
X		**X**	34.5:**65.5** (1.0)	1:2
	X	**X**	6.5:**93.5** (1.0)	1:2
X	X	**X**	35.3:11.7:**53.0** (1.5)(1.3)(0.2)	1:2

[a]Ratios determined using NMR and gas chromatography

[b]Experiments were conducted in triplicate; %e.s.d.'s are provided in parentheses

From Table 2, it is apparent that CAM was the preferred guest in all equimolar competition experiments whenever it was present. CON/CAM and COL/CAM binary experiments showed the selective inclusion of cyclohexylamine with molar ratios of 65.5% and 93.5%, respectively. In the absence of CAM, CON was selected for, as observed in the CON/COL experiment (Table 2, 89.2%). Finally, the equimolar ternary experiment showed the host to have a selectivity order of CAM (53.0%) > CON (35.3%) > COL (11.7%) for these guests. The overall host:guest ratio remained 1:2 for all competition experiments conducted with CAM, and 1:1 when this guest was absent (Table 2).

Subsequent binary competitions were conducted where the molar ratios of the three cyclic compounds were varied beyond equimolar, and the guest selectivity of TETROL thus evaluated by means of selectivity profiles for CON/COL, CON/CAM and CAM/COL combinations (Figures 1a−c, respectively). Analyses were carried out using NMR and GC-MS as before. In each figure, the straight-line plot (red data points) is a theoretical one, representing the case where the host is completely unselective towards both guests and is inserted for ease of comparison with the experimentally-determined data points (blue).
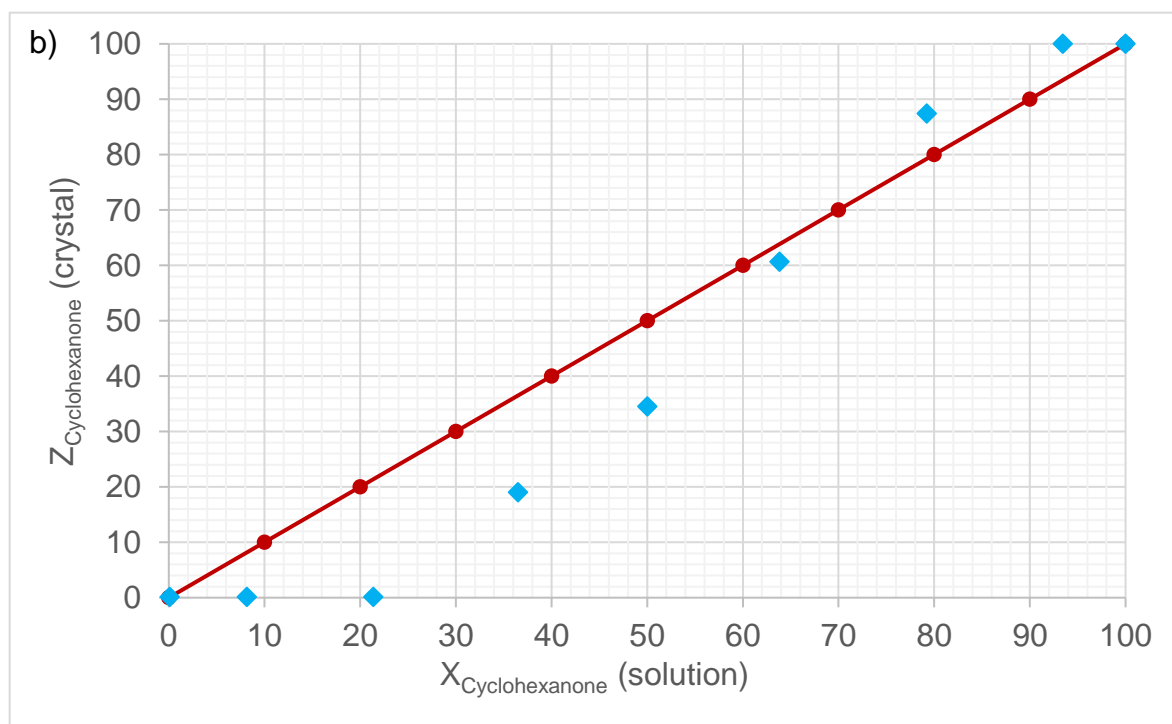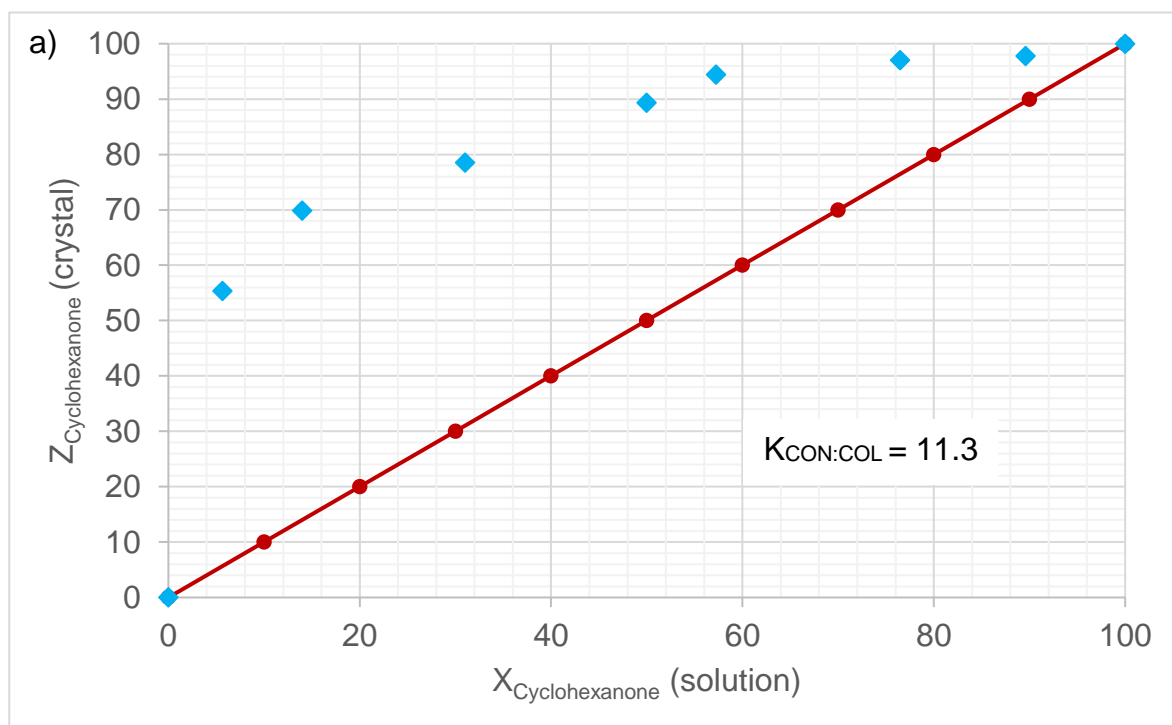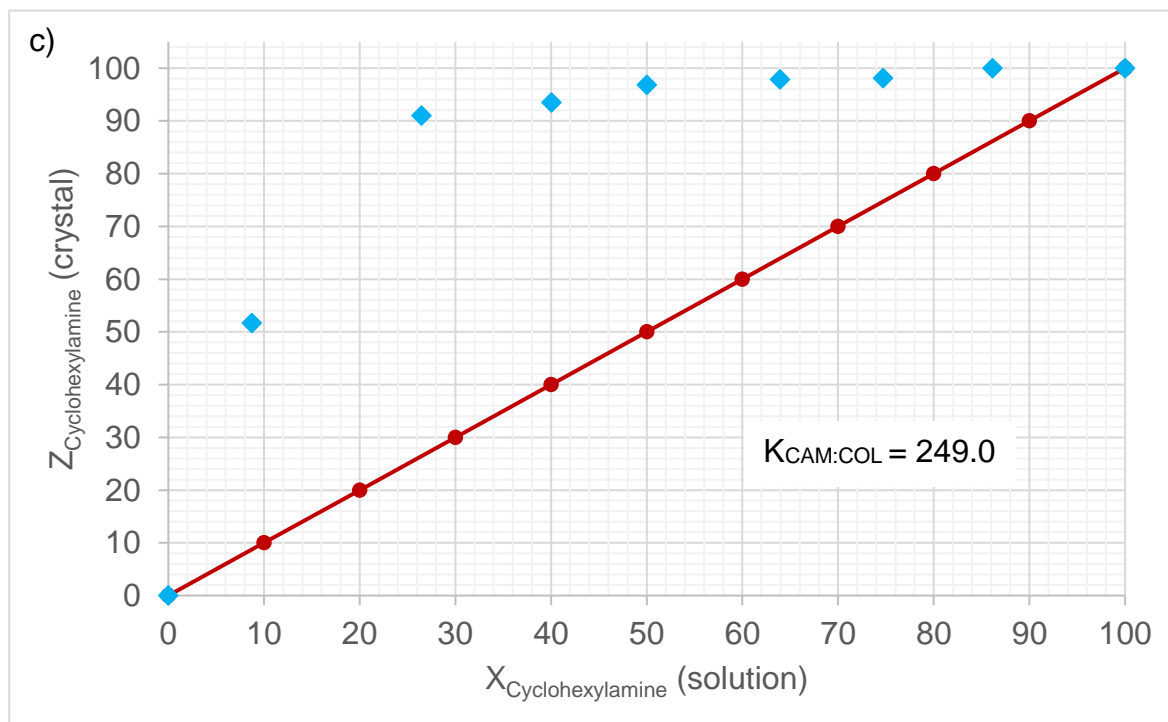
Figure 1: Selectivity curves for a) CON/COL, b) CON/CAM and c) CAM/COL

High host selectivity was observed for TET when recrystallised from the CON/COL binary mixture with CON being preferred over the entire concentration range investigated (Figure 1a, $K_{CON:COL}$ = 11.3). According to Figure 1b, the selectivity of the host was guest-concentration dependent: at low to moderate concentrations of CON (up to approximately 65.0%), the host was selective for CAM. Soon after this point, the host showed selectivity towards CON (Figure 1b). A selectivity coefficient for this profile is not provided here as the value obtained would be misleading due to the observed host selectivity change with guest concentration change. For combinations of CAM/COL (Figure 1c, $K_{CAM:COL}$ = 249.0), a consistent host preference for CAM over COL was observed for the entire concentration range assessed.

3.3   Single Crystal X-ray Diffraction (SCXRD)

To further interpret the results obtained from competition experiments, SCXRD analyses were carried out on suitable crystals from successfully-formed TET·CON, TET·COL and TET·2CAM complexes. The crystal data and refinement parameters for the three complexes are provided in Table 3. All complexes formed crystallize in the

monoclinic crystal system and *P*2$_1$ space group with Z = 2. It is noted that in the complex of TET·2CAM, one of the two guests is disordered [Figure 2, green, CAM(dis)]. It is clear that both guests occupy the same site within the crystal and that their NH$_2$ orientations are identical, but each cyclohexyl ring carbon atom differs slightly (Figure 2). It was observed that the CON and COL inclusion complexes crystallize with very similar unit cell dimensions, and their host frameworks are isostructural (Table 3). (This phenomenon is strikingly evident from Figures 3 and 4.) The guest accommodation type was analysed using the Mercury CSD 3.5.1 software package and the guests omitted from the packing calculation, and the remaining voids displayed (Figures 3–5). The crystal packing for the TET·CON and TET·COL complexes are characterized by guest molecules occupying isolated cavities within their respective host crystals (Figures 3 and 4), while TET·2CAM has its guests occupying channels (Figure 5). The stereoview for each complex with TETROL is displayed in Figure 6.
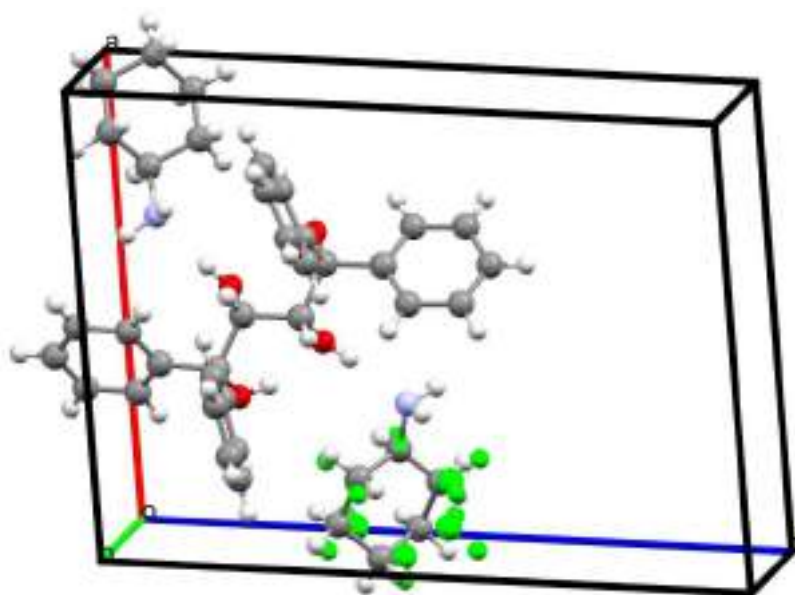
Figure 2: The unit cell of TET·2CAM; the disordered guest is shown in green
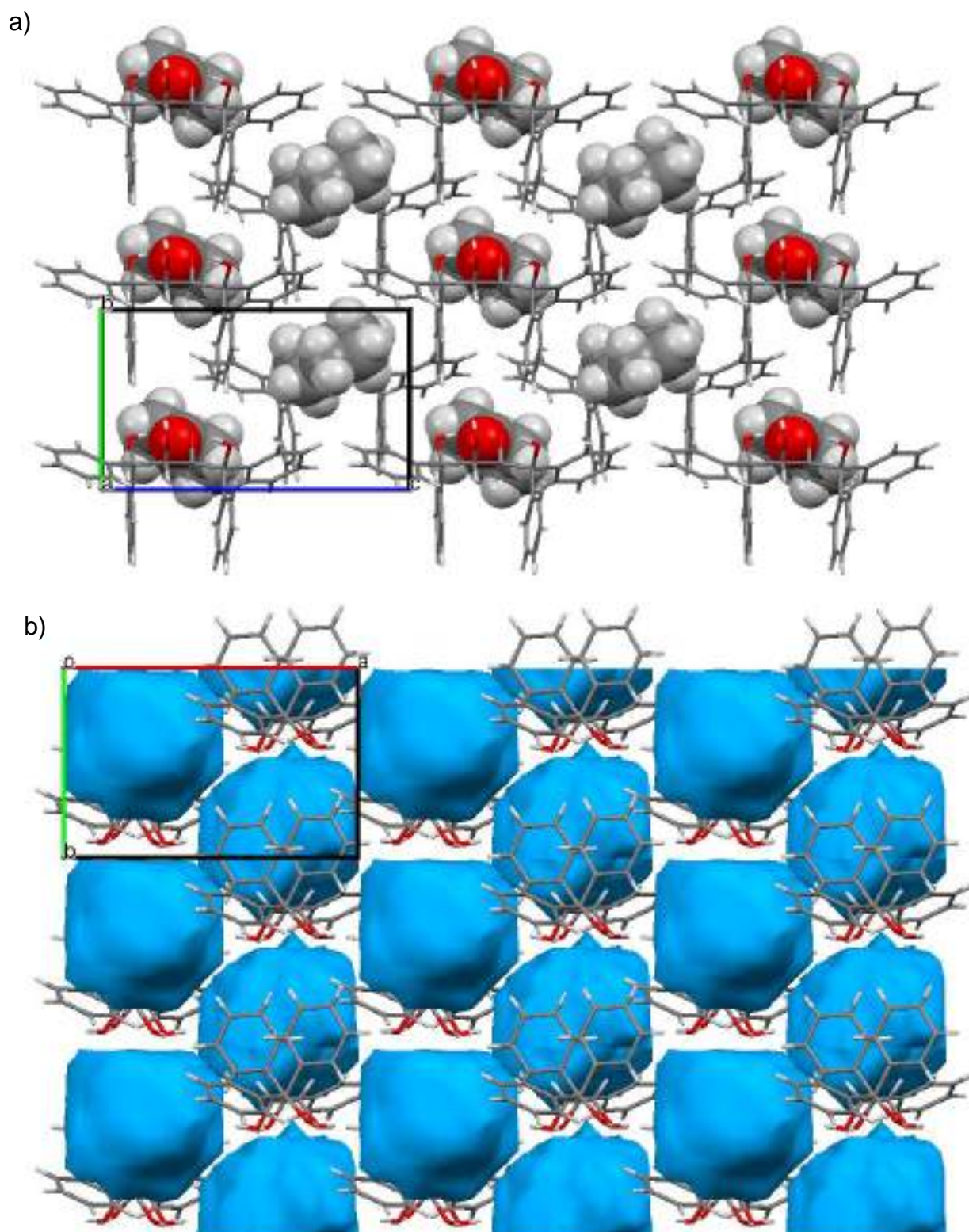
a)

b)

Figure 3: a) Crystal packing of the TET·CON inclusion complex with guests in spacefill form, b) calculated voids (blue) for TET·CON indicating guest accommodation in cavities; (oxygen – red, carbon – grey and hydrogen – light grey)
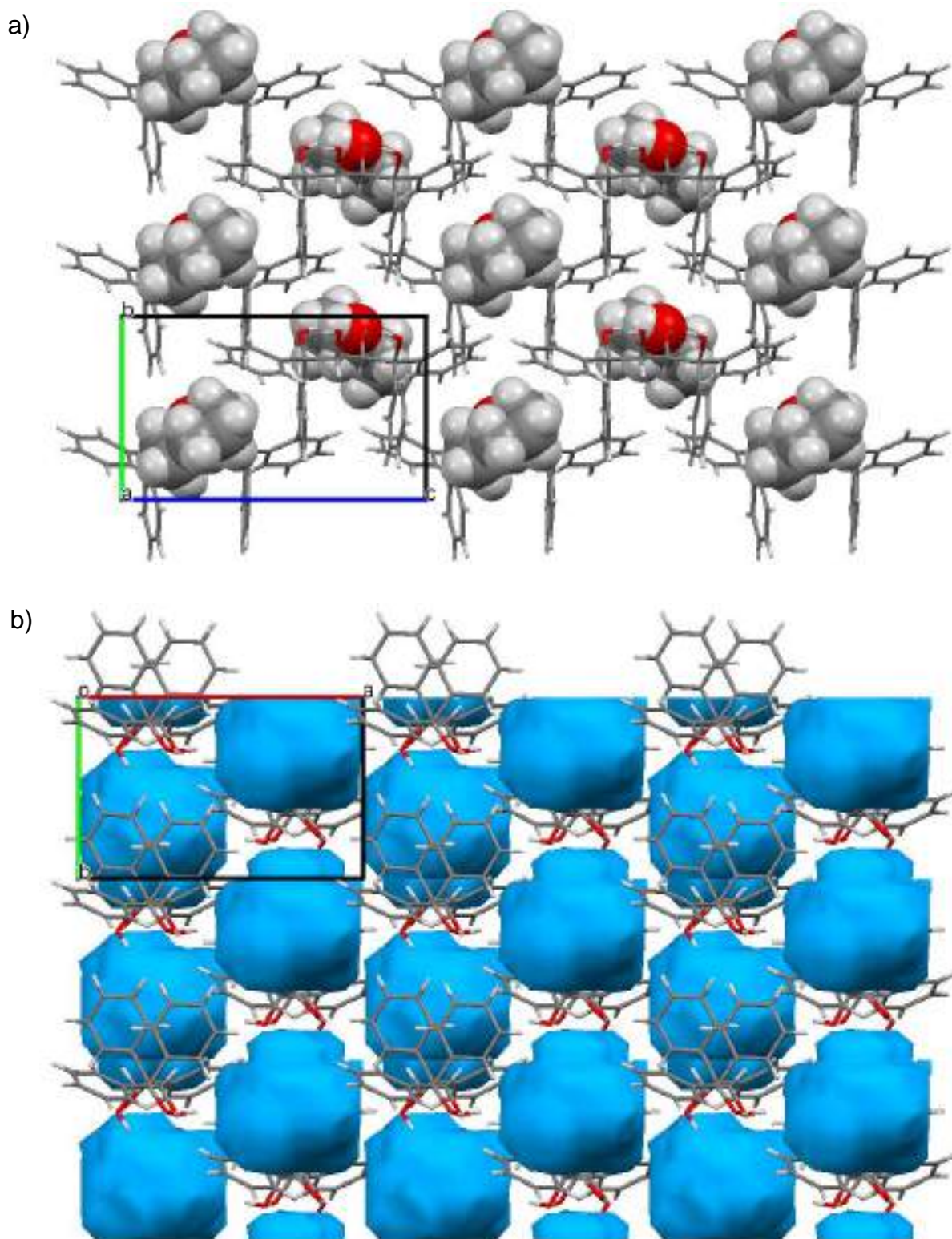
Figure 4: a) Crystal packing of the TET·COL inclusion complex with guests in spacefill form, b) calculated voids (blue) for TET·COL indicating guest accommodation in cavities; (oxygen – red, carbon – grey and hydrogen – light grey)

a)

b)
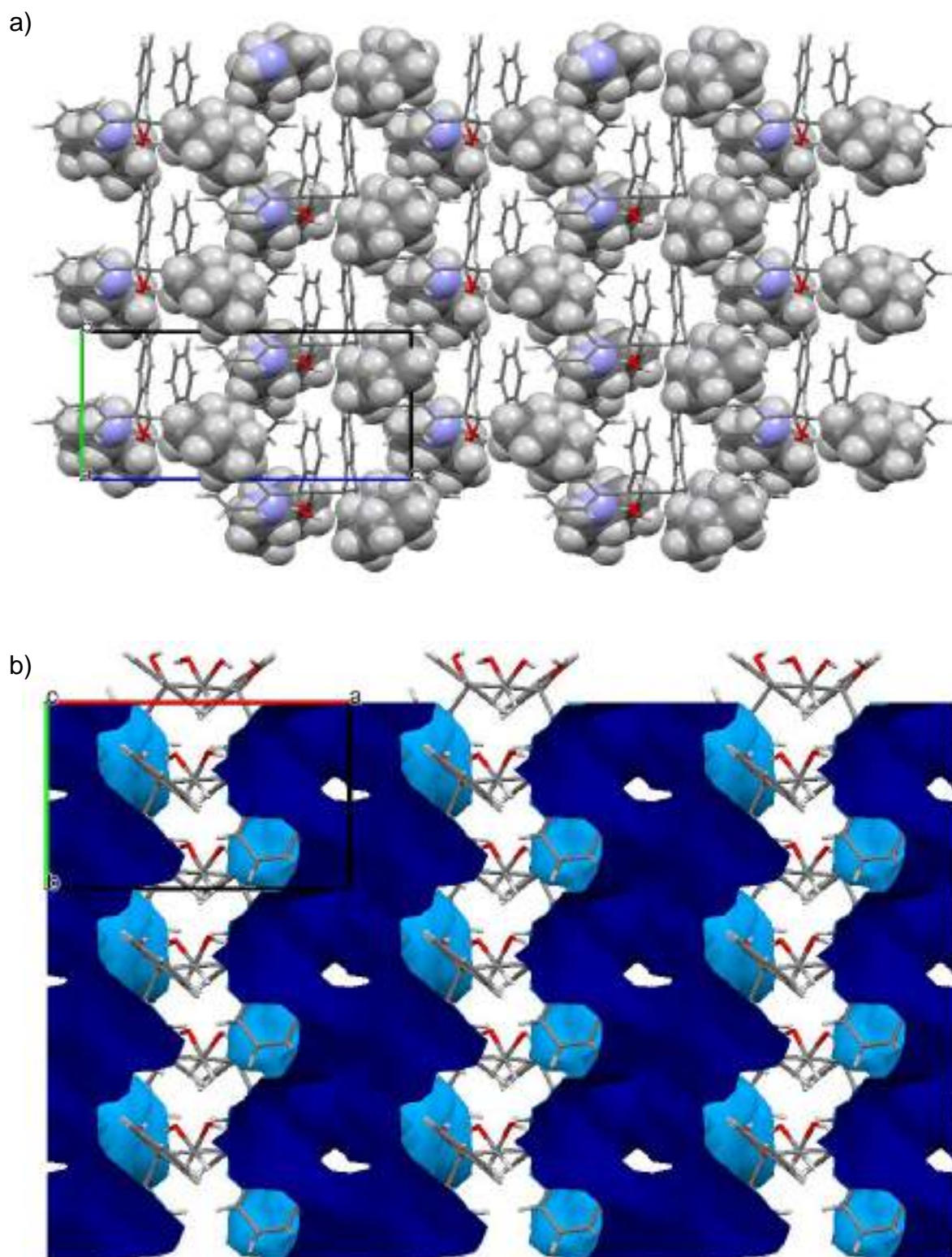
Figure 5: a) Crystal packing of the TET·2CAM inclusion complex with guests in spacefill form, b) calculated voids (blue) for TET·2CAM indicating guest accommodation in channels; (oxygen – red, nitrogen – blue, carbon – grey and hydrogen – light grey)

a)

b)

c)
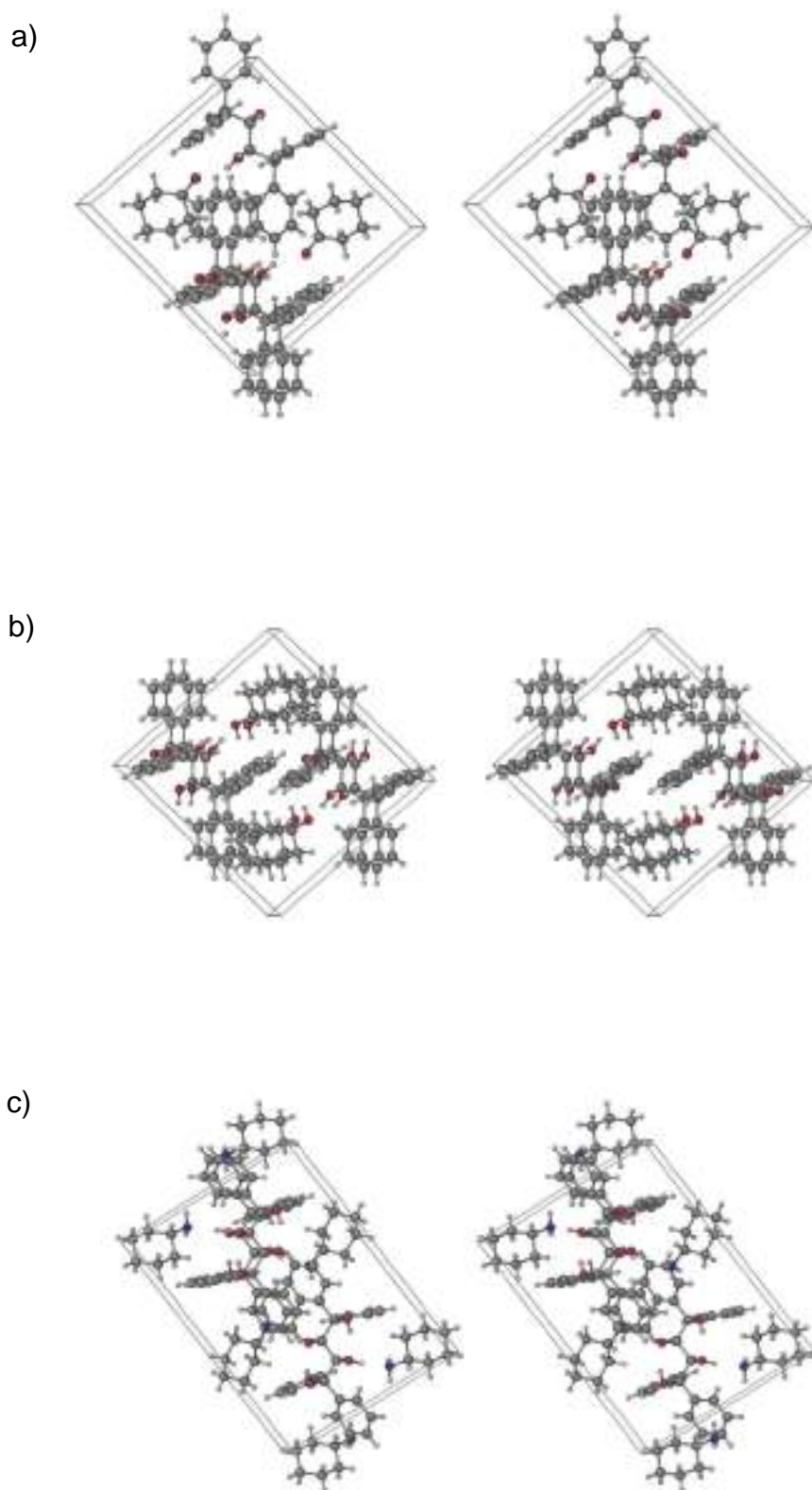
Figure 6: Stereoviews illustrating the unit cells of a) TET·CON b) TET·COL and c) TET·2CAM (the disordered component has been omitted for clarity)

Table 3: Relevant single crystal X-ray crystallographic data for the complexes of TETROL with CON, COL and CAM

	TET·CON	TET·COL	TET·2CAM
Chemical formula	$C_{28}H_{26}O_4\cdot$ $C_6H_{10}O$	$C_{28}H_{26}O_4\cdot$ $C_6H_{12}O$	$C_{28}H_{26}O_4\cdot$ $2(C_6H_{13}N)$
Formula weight	524.63	526.64	624.84
Crystal system	Monoclinic	Monoclinic	Monoclinic
Space group	$P2_1$	$P2_1$	$P2_1$
μ (Mo Kα)/mm^{-1}	0.084	0.083	0.076
a/Å	12.5944(4)	12.7541(3)	12.3859(5)
b/Å	8.1531(2)	8.1884(2)	8.2405(3)
c/Å	13.4570(5)	13.4145(3)	17.1370(7)
α/°	90	90	90
β/°	94.025(2)	94.861(1)	96.305
γ/°	90	90	90
V/Å^3	1378.40(8)	1395.91(6)	1738.53(12)
Z	2	2	2
F (000)	560	564	676
Temp (K)	200	200	200
Restraints	1	1	0.999
Nref	6501	6031	8486
Npar	356	356	427
R1	0.0388	0.0424	0.0473
wR2	0.1043	0.1246	0.1255
S	1.04	1.04	1.05
Θ min, max/°	1.5, 28.3	1.6, 28.4	1.2, 28.3
Tot. data	13345	16674	29351
Unique data	6501	6031	8486
Observed data [I > 2.0σ(I)]	5554	5445	7473
Rint	0.017	0.014	0.017
Diffrn measured fraction Θ full	0.996	0.992	0.999
Min. resd. dens. (e/Å^3)	−0.21	−0.26	−0.34
Max. resd. dens. (e/Å^3)	0.21	0.28	0.48

3.3.1   H-Bonding Interactions Between Host and Guest Species

The host framework is stabilised by a pair of 1,3-intramolecular hydrogen bonds, and each guest held in the crystal by means of (guest)H–O···H–O(host), (guest)C=O···H−O(host) and (guest)N···H−O(host) interactions for TET·COL, TET·CON and TET·2CAM, respectively (Table 4). Oxygen (O) and nitrogen (N) have different van der Waals radii (1.52 and 1.55 Å, respectively), which influences the length of the H-bond formed. To determine which guest experiences the stronger H-bond with TETROL, we compared the O···O and O···N distances formed between the host and guest.[179,180] Therefore, the respective sums of the van der Waals radii for O···O is 3.04 Å [i.e., $\sum$ vdW$_{O+O}$ = 1.52 (O) + 1.52 (O) = 3.04 Å] and 3.07 Å for O···N [i.e., $\sum$ vdW$_{N+O}$ = 1.55 (N) + 1.52 (O) = 3.07 Å].[181,182] The relative strength of the hydrogen bond is then determined by the difference between these sums of the van der Waals radii and the distance observed in the X-ray (Table 5). The larger this difference, the stronger the H-bond.[183] From Table 5, the strength of these H-bonds decrease in the order TET·COL (0.331 Å) > TET·CON (0.324 Å) > TET·2CAM (0.285 and 0.313 Å). Surprisingly, this order is the reverse of the selectivity order observed for TETROL and these three cyclic compounds.

Theoretically, according to Abraham,[182] a level of comparison can be made for the strength of an H-bond donor, where O–H > N–H, and acceptor, with N > O. Since the host is predominantly an H-bond donor,[157] it will preferably form a complex with a strong acceptor such as cyclohexylamine. Furthermore, carbonyl oxygens are more basic and therefore better hydrogen bond acceptors than hydroxyl oxygens.[184,185] These factors, therefore, do correlate with the observed selectivity order of TET for the three guests (CAM > CON > COL), but do not correlate with the calculated H-bond distances and, therefore, strengths. It is also worth noting that the H-bond angles associated with CAM are much closer to linearity (173, 167°) which may be a further factor that favours CAM over CON and COL (Table 4).

Table 4: Analysis of intermolecular hydrogen bonding interactions between TETROL and guests CON, CAM and COL

Guest	Unit cell H:G ratio	Guest[†]	(host)O⋯X(guest)/Å	(host)H⋯X(guest) Å	(host)O–H ⋯X(guest) /°	Symmetry operator
CON	1:1	[1]	2.716(2) X = O	1.93	156	x,y,z
CAM	1:2	[1]	2.785(3) X = N	1.95	173	x,y,z
		[2]	2.757(3) X = N	1.93	167	x,y,z
COL	1:1	[1]	2.709(2) X = O	1.93	155	x,y,z

[†]The unit cells in TET·CON and TET·COL are comprised of one guest, whereas TET·2CAM is comprised of two guests in unique environments. Hence these guests have been labelled CON[1], COL[1], CAM[1] and CAM[2]

Table 5: The calculated hydrogen bond strength for each complex with TETROL

Complex	Theoretical (host)O⋯X(guest)/Å (A)	Experimental (host)O⋯X(guest) /Å (B)	$\Delta_{(A)-(B)}$ / Å
TET·CON	3.04 X = O	2.716(2) X = O	0.324
TET·2CAM	3.07 X = N	2.785(3) X = N	0.285
		2.757(3) X = N	0.313
TET·COL	3.04 X = O	2.709(2) X = O	0.331

3.3.2 Short Ring (π···π) and X–H···π Interactions in the Complexes of CON, CAM and COL with TETROL

Complementing the role of hydrogen bonding are multiple, cooperative (guest)CH···π(host) and (guest)H···C_{Ar}(host) stabilizing interactions (Table 6). The host framework for each complex is also stabilised by (host)π···π(host) interactions in comparable ranges [Table 6, 4.709(2)–5.943(2) Å]. In the crystals of TET·CON and TET·COL, each guest is stabilised by two (guest)C–H···π(host) interactions within similar ranges for the two complexes (Table 6, 2.84–2.98 Å, 145–157°). The TET·2CAM complex is stabilized by three (guest)C–H···π(host) interactions in the range 2.58–2.97 Å with angles ranging between 150–158° (Table 6). The TET·2CAM complex therefore experiences the shortest (guest)C–H···π(host) interaction (Table 6, 2.58 Å, 158°), along with further stabilising short contacts, one (host)C_{Ar}···H–N(guest) (Table 6, 2.85 Å, 106°) contact and one (guest)C–H···C_{Ar}(host) (Table 6, 2.81 Å, 129°) contact. The presence of these additional stabilising interactions coincides with the hosts preference for CAM over CON and COL.

Table 6: Analysis of other significant interactions in complexes of TETROL with guests CON, CAM and COL

Interaction	TET·CON	TET·2CAM	TET·COL
π⋯π (Host⋯Guest)	N/A	N/A	N/A
π⋯π (Host⋯Host)	4.749(1)–5.911(1) (9 contacts)	4.709(2)–5.824(2) (9 contacts)	4.770(1)–5.943(2) (9 contacts)
π⋯π (Guest⋯Guest)	N/A	N/A	N/A
CH⋯π	2.84 Å, 157° (H⋯Cg, C–H⋯Cg) (guest)C–H⋯π(host) 2.98 Å, 145° (H⋯Cg, C–H⋯Cg) (guest)C–H⋯π(host)	2.58 Å, 158° (H⋯Cg, C–H⋯Cg) (guest)C–H⋯π(host) 2.97 Å, 150° (H⋯Cg, C–H⋯Cg) (guest)C–H⋯π(host) 2.74 Å, 150° (H⋯Cg, C–H⋯Cg)[a] (guest)C–H⋯π(host)	2.96 Å, 152° (H⋯Cg, C–H⋯Cg) (guest)C–H⋯π(host) 2.87 Å, 156° (H⋯Cg, C–H⋯Cg) (guest)C–H⋯π(host)
Short contacts	None	2.85 Å, 146° (C⋯H, C–C⋯H)[a] (host)C_{Ar}⋯H–N(guest) 2.81 Å, 129° (C⋯H, C–C⋯H) (guest)C–H⋯C_{Ar}(host)	None

[a]Interaction involving CAM(dis) guest

3.4   Hirshfeld Surface Analysis

Hirshfeld surface analyses were conducted on the TET·CON, TET·2CAM and TET·COL complexes to assist in summarising, quantitatively, the multiple intermolecular interactions present (Figure 7). A summary of the percentage of each interaction type is displayed graphically in Figure 8, while Table 7 provides the actual values obtained from this figure.
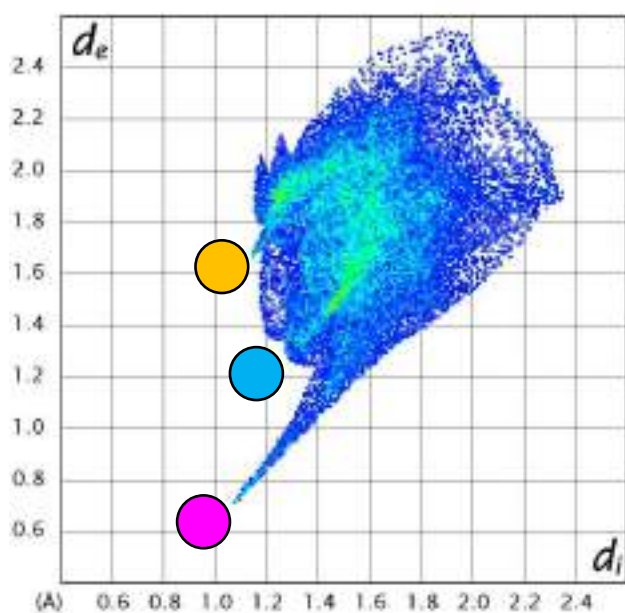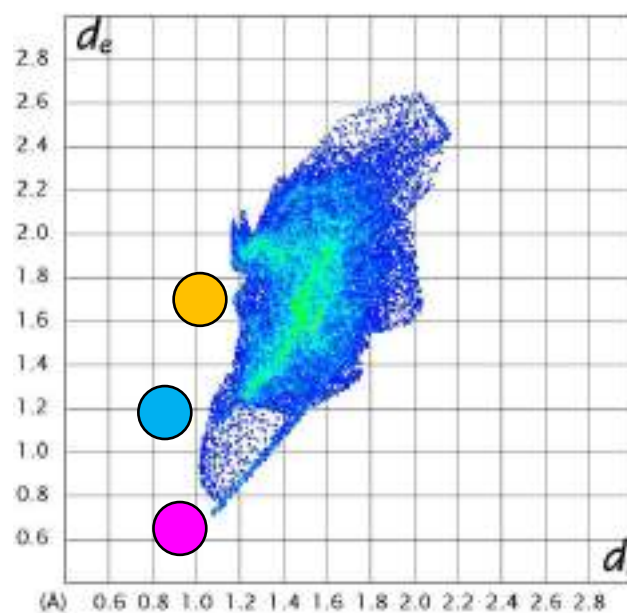
TET·CON

TET·COL
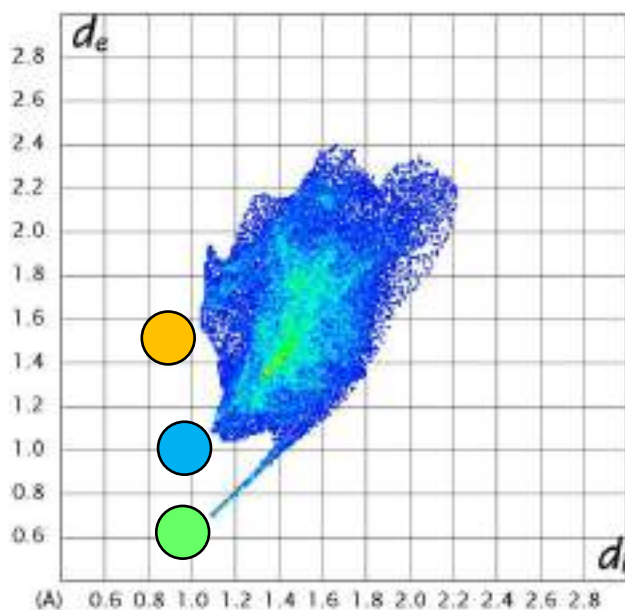
TET·2CAM[1]
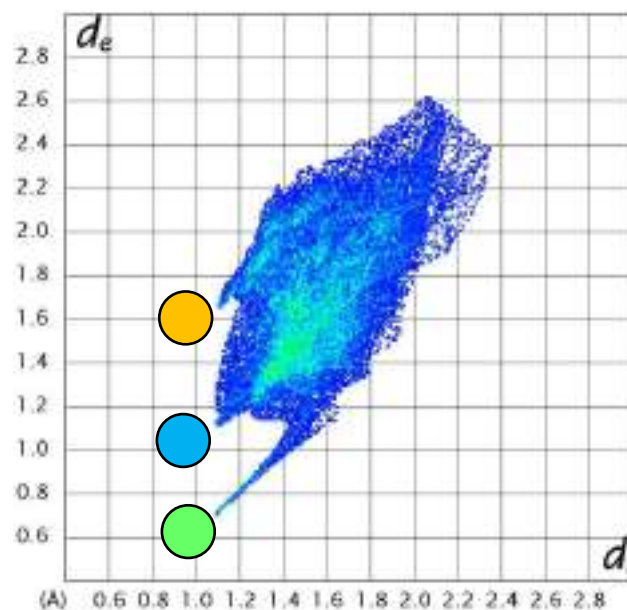
TET·2CAM[2]
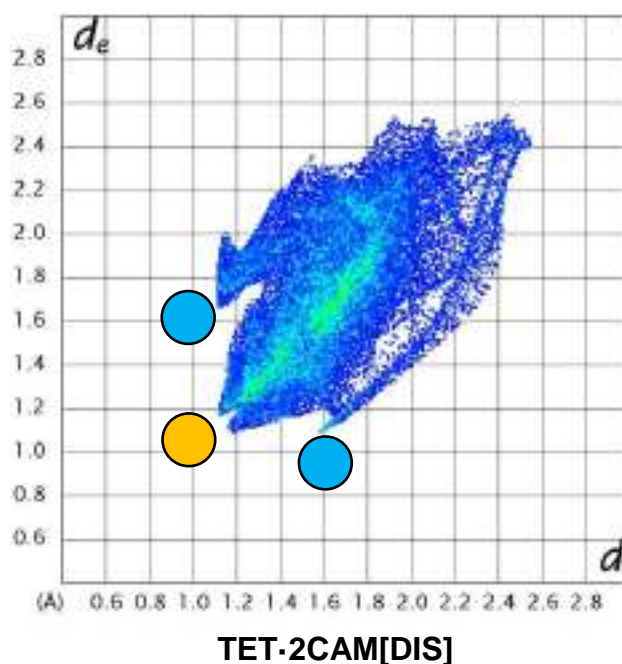
TET·2CAM[DIS]

Figure 7: Hirshfeld fingerprint plots for TET·CON, TET·COL, TET·2CAM[1], TET·2CAM[2] and TET·2CAM[DIS]; The 'spike' and 'wings' observed in the Hirshfeld plots are colour coded and depict N···H (green), O···H (magenta), H···H (blue) and C···H (orange) contacts
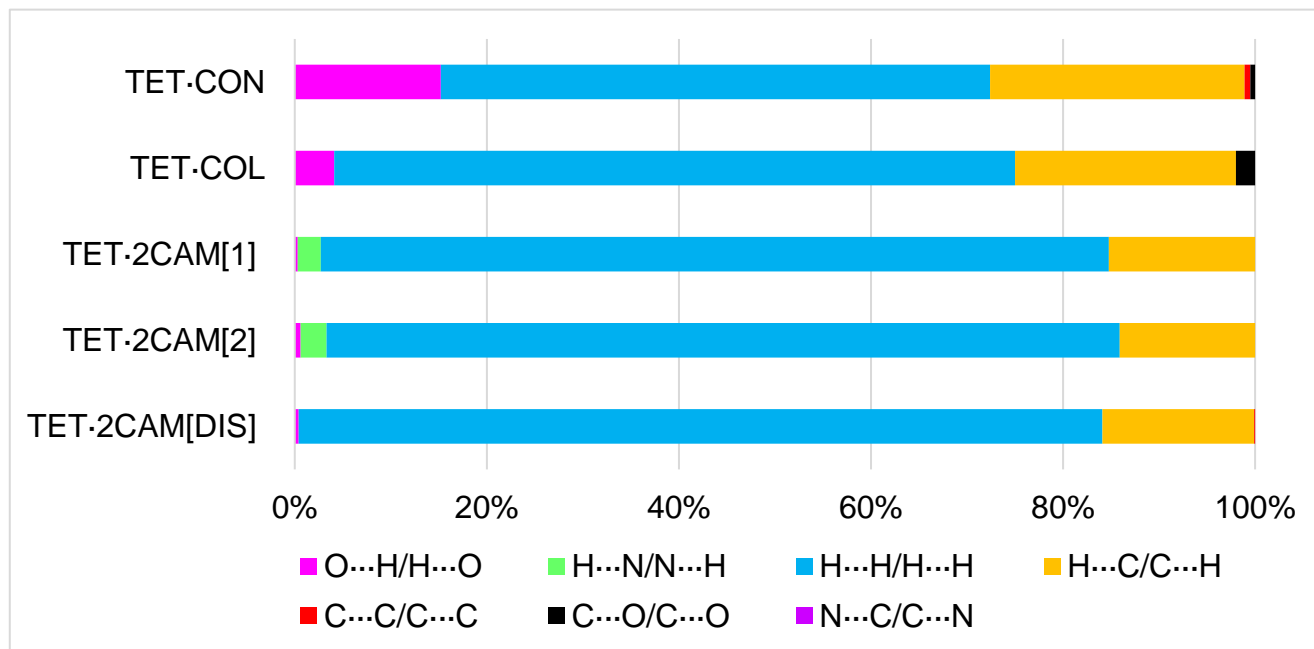
Figure 8: Graphical display showing the percentage intermolecular interactions of each type for the TET·CON, TET·COL, TET·2CAM[1], TET·2CAM[2] and TET·2CAM[DIS] complexes

Table 7: Percentage guest···host/host···guest (G···H/H···G) intermolecular interactions in each inclusion complex of TETROL with CAM, COL and CON

	O···H/ H···O	H···N/ N···H	H···H/ H···H	H···C/ C···H	C···C/ C···C	C···O/ C···O	N···C/ C···N
TET·2CAM[DIS]	0.4	0	83.8	15.8	0.1	0	0
TET·2CAM[2]	0.6	2.7	82.7	14.1	0	0	0
TET·2CAM[1]	0.3	2.4	82.0	15.2	0	0	0
TET·COL	4.1	0	70.9	23	0	2	0
TET·CON	15.2	0	57.2	26.5	0.6	0.5	0

All complexes with TETROL are predominantly stabilised by H···H interactions (57.2–83.8%), with TET·2CAM experiencing the higher number of this type [82.0–83.8% relative to 70.9% (TET·COL) and 57.2% (TET·CON)], in accordance with the hosts preference for CAM. Furthermore, and C···H interactions (14.1–26.5%) are also significant (Figure 8, Table 7), and TET·CON experiences more O···H/H···O interactions (15.2%) in comparison to TET·COL (4.1%) and TET·2CAM (0.3–0.6%).

3.5 Thermal Analyses

Both DSC and TG experiments were carried out on the three inclusion complexes. The traces obtained are provided in Figures 9a–c and a summary of the thermal events in Table 8. Upon heating of TET·CON, a stepwise guest release process ensues (Figure 9a), with an onset temperature (T_{on}) of ~83.3 °C (Table 8). It appears as though the majority of the guest release occurred concomitantly with the melting of the host (Figure 9a, 143.2°C). The expected mass loss for the 1:1 H:G complex was calculated to be 18.7%, which is in reasonable agreement with the actual mass loss observed (Table 8, 17.6%). In comparison to TET·CON, the stepwise guest release process for TET·COL is more complex, with a T_{on} value of 84.5 °C (Figure 9b, Table 8). The observed mass loss (Table 8, 19.0%) is in reasonable agreement with that expected for a 1:1 complex (16.5%). The TET·2CAM complex also follows a convoluted stepwise guest release process, with a T_{on} value of 60.0 °C (Figure 9c, Table 8) and an observed mass loss (Table 8, 26.9%) slightly lower than that expected for a 1:2 complex (31.7%).

The onset temperatures for the guest release events do not correlate with the preference order of TETROL for these guests (CAM > CON > COL), but are in accordance with the H-bond strength order of COL (84.5 °C) > CON (83.3 °C) > CAM (60.0 °C) calculated previously (Table 5)

a)

b)

c)
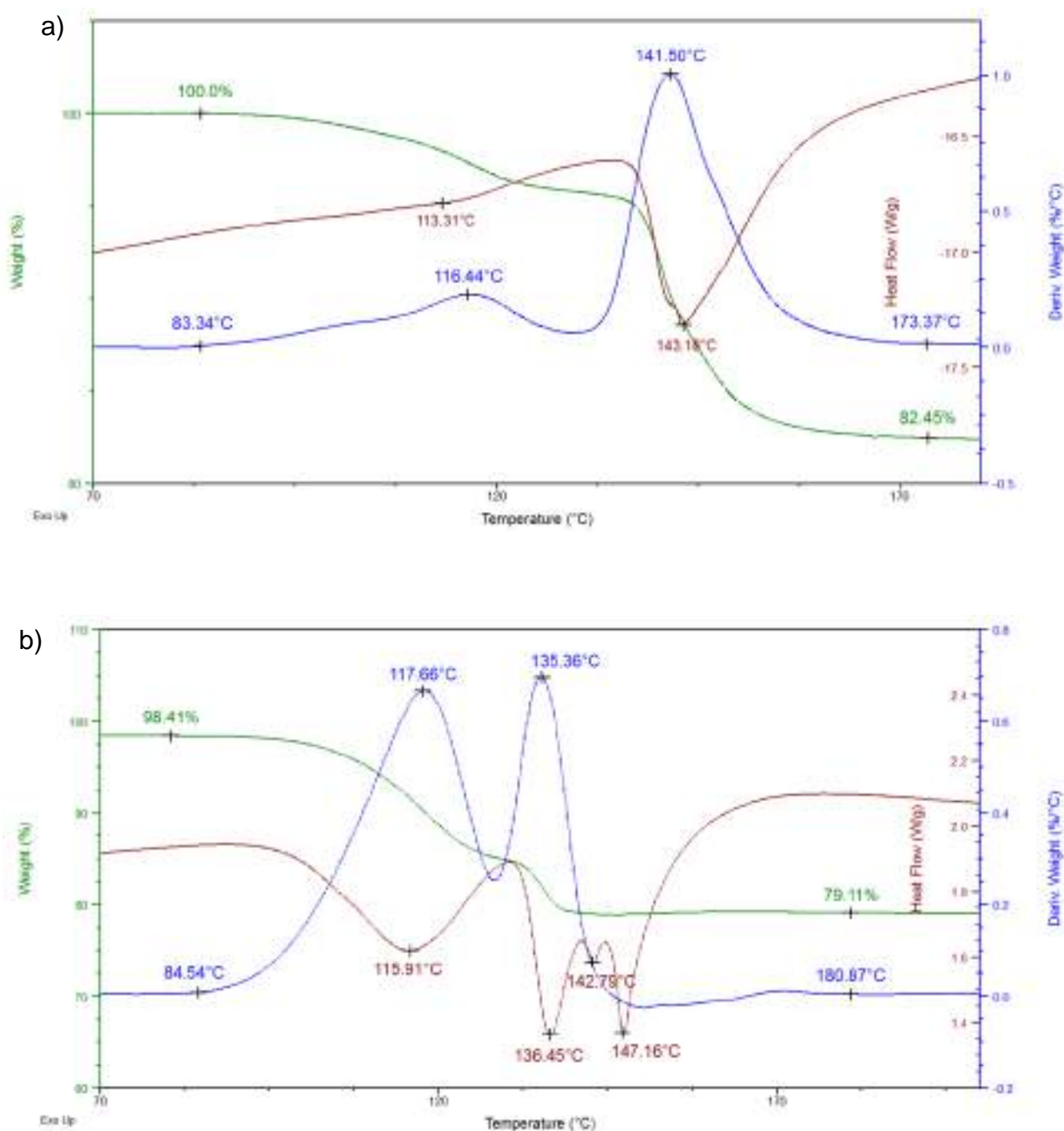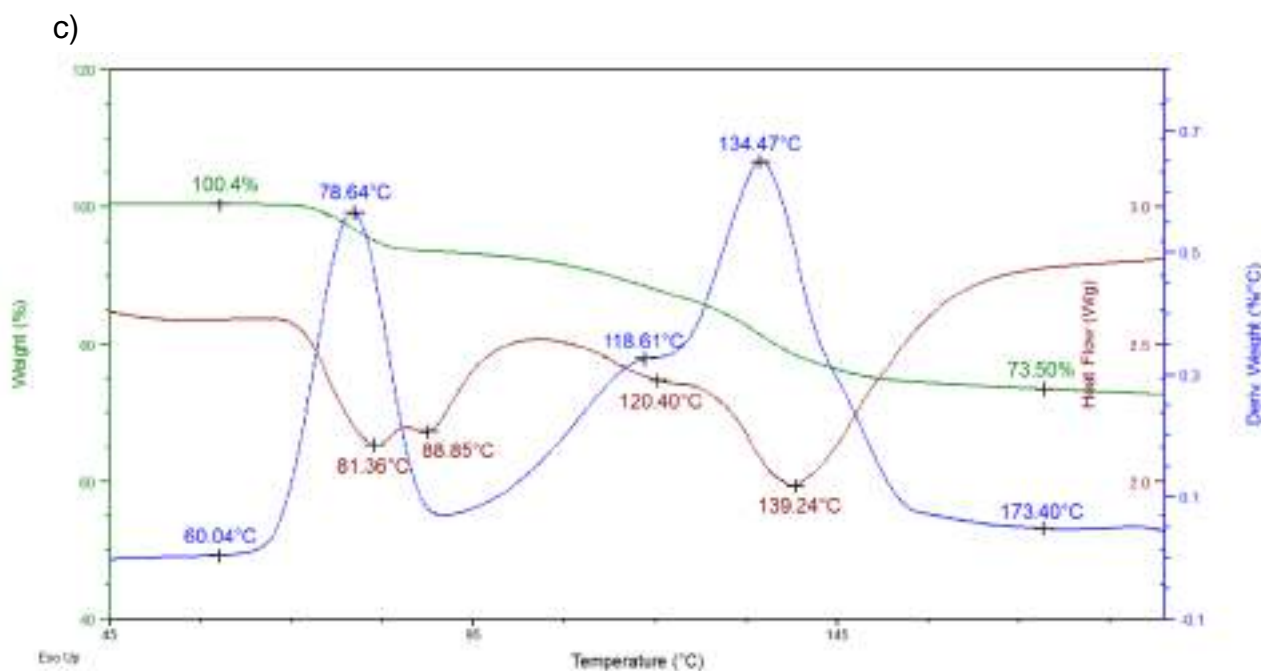
Figure 9: Overlaid traces for the DSC (brown), TG (green) and its derivative (DTG, blue) for the a) TET·CON, b) TET·COL and c) TET·2CAM complexes

Table 8: Thermal data from DSC/TG traces for the TET·CON, TET·COL and TET·2CAM complexes

Guest	T_{on} (°C)	T_p (°C)[a]	T_{end} (°C)[b]	Mass loss % (expected)	Mass loss % (actual)
CON	83.3	116.4 141.5	~113.3 143.2	18.7	17.6
COL	84.5	117.7 135.4	115.9 142.8 147.2	19.0	16.5
CAM	60.0	78.6 ~118.6 134.5	81.4 88.9 ~120.4 139.2	31.7	26.9

[a]Tp values determined from blue DTG traces
[b]Tend were obtained from the brown DSC traces

3.6   Conclusion

TETROL proved to be an efficient host for the inclusion of the three CON, COL and CAM cyclic compounds. This host showed a high selectivity for CAM when recrystallised from mixtures of the three guests, resulting in a selectivity order of CAM (53.0%) > CON (35.3%) > COL (11.7%). Thermal analyses did not provide evidence for the observed selectivity order of the host, but Hirshfeld surface analysis showed that TET·2CAM experienced the highest number of H···H interactions (82.0–83.8%). From SCXRD analyses, it was observed that the TET·2CAM complex experienced the shortest (guest)C–H···π(host) interaction observed (Table 6, 2.58 Å, 158°), and was the only complex to experience further stabilising short contacts in the form of (host)C_{Ar}···H–N(guest) and (guest)C–H···C_{Ar}(host).   Furthermore,   a   H-bonding investigation showed that the CAM guests were stabilized by interactions of this type, where the angles were significantly closer to linearity than in the other two complexes having COL and CON as guests. These observations may therefore explain the preferred inclusion of CAM over CON and COL.

Chapter 4
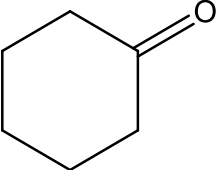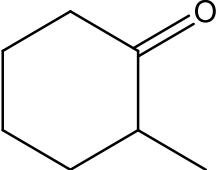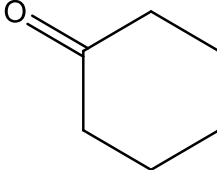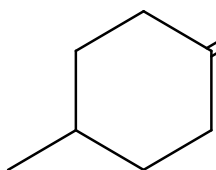
Separation of Cyclohexanone and Its Methyl Isomers

4.1   Introduction

In this investigation, we explore the host properties of TETROL for separating cyclohexanone (CON), 2-methylcyclohexanone (2MCON), 3-methylcyclohexanone (3MCON) and 4-methylcyclohexanone (3MCON) from mixtures (Table 1). As stated previously, CON is an important material in the nylon industry: it is employed for the manufacture of caprolactam, a raw material used in the production of nylon and other synthetic fibres. It is imperative to produce a high percentage yield of pure CON as its purity directly affects the quality of the final product. Distillation is often used in the separation and purification of CON, but constitutes three steps and is therefore uneconomical.[174]

Cyclohexanone and the methylcyclohexanone isomers are synthesised by the catalytic hydrogenation of phenol and cresols, respectively.[186] The methyl isomers are used as intermediates in the flavour, fragrance, and pharmaceutical industry. Methylcyclohexanones have similar boiling points, especially 3MCON (169–170°C) and 4MCON (169–171°C), and therefore cannot easily be separated by distillation processes (Table 1).[187] Previous studies have been conducted on the inclusion ability of TETROL with cyclohexanone and the three isomeric methylcyclohexanones and all were enclathrated when crystals of this host compound were grown from each of these guest solvents; the host:guest ratio was consistently 1:1. Barton *et al* discovered, through SCXRD analysis, that the 3- and 4- methylcyclohexanones were included by TETROL entirely in their energetically unfavourable axial conformations, but that the 2-methyl analogue was enclathrated as the more conventional equatorial conformer.[159,160] In this investigation, we explore the selectivity of TETROL for the four cyclohexanones when this host was recrystallized from various mixtures of these guests.

Table 1: The structure and properties of the four cyclohexanone compounds

	CON	2MCON	3MCON	4MCON
Structure				
Boiling point (°C)	155.6	162–163	169–170	169–171

4.2   Competition Experiments

Competition experiments were conducted and the selectivity of TET for these guests investigated to establish if the host would discriminate between them. In Tables 2 and 3, we summarise data obtained from the recrystallization of TETROL from various equimolar binary, ternary and quaternary combinations of CON, 2MCON, 3MCON and 4MCON. The so-formed crystal inclusions were analysed using proton NMR spectroscopy and GC-MS. The preferred guest species is given in bold red font face.

Table 2: Competition experiments of the host in the presence of equimolar mixtures of the isomeric methylcyclohexanones [a,b]

2MCON	3MCON	4MCON	Guest ratios (%e.s.d.)	Overall H:G ratio
X	X		**88.6**:11.4 (1.4)	1:1
X		X	**94.3**:5.7 (2.0)	1:1
	X	**X**	26.2:**73.8** (0.7)	1:1
X	X	X	**79.2**:13.8:7.0 (4.5) (3.9) (1.0)	1:1

[a]Ratios determined using proton NMR spectroscopy and gas chromatography

[b]Experiments were conducted in triplicate; %e.s.d.'s are provided in parenthesis

From the competition studies between the isomeric methylcyclohexanones, it is clear that 2MCON was significantly preferred in equimolar binary mixtures whenever it was present (Table 2, 88.6 and 94.3%). In the absence of 2MCON, 3MCON was discriminated against in favour of 4MCON (73.8%). However, as can be observed from the equimolar ternary experiment, the presence of 2MCON prompted a selectivity switch where TET displayed a higher selectivity for 3MCON (13.8%) than 4MCON (7.0%). Consequently, the host selectivity for these isomers may be written in the order 2MCON (79.2%) >> 3MCON (13.8%) > 4MCON (7.0%).

Table 3: Competition experiments of the host in the presence of equimolar mixtures of cyclohexanone and the isomeric methylcyclohexanones[a,b]

CON	2MCON	3MCON	4MCON	Guest ratios (%e.s.d.)	Overall H:G ratio
X	X			**83.6** : 16.4 (1.39)	1:1
X		X		**74.7** : 25.3 (1.15)	1:1
X			X	**67.6** : 32.4 (0.87)	1:1
X	X	X		**66.5** : 13.0 : 20.5 (0.58) (0.52) (0.06)	1:1
X	X		X	**61.4** : 9.7 : 28.9 (1.26) (2.30) (1.05)	1:1
X		X	X	**60.2** : 14.6 : 25.2 (1.11) (0.33) (1.40)	1:1
X	X	X	X	**52.1** : 4.6 : 13.3 : 30.0 (0.67) (0.53) (1.14) (2.31)	1:1

[a]Ratios determined using proton NMR spectroscopy and gas chromatography

[b]Experiments were conducted in triplicate; %e.s.d.'s are provided in parenthesis

Table 3 displays the equimolar binary, ternary and quaternary competition studies conducted in the presence of unsubstituted cyclohexanone. In each instance, CON was the preferred guest. From the binary experiments comprising CON and one of each of the methylcyclohexanones, the selectivity decreases in the order 4MCON > 3MCON > 2MCON (32.4, 25.3 and 16.4%, respectively). This is a complete reversal

of the selectivity order observed for the binary experiments in Table 2 and was somewhat surprising. The equimolar quaternary experiment furnished a host selectivity order of CON (52.1%) > 4MCON (30.0%) > 3MCON (13.3%) > 2MCON (4.6%) (Table 3).

Further binary competitions were conducted but varying molar ratios of cyclohexanone and the three methylcyclohexanone compounds were used, and the guest selectivity of TET thus evaluated by means of selectivity profiles for CON/2MCON, CON/3MCON, CON/4MCON, 2MCON/3MCON, 2MCON/4MCON and 3MCON/4MCON combinations (Figures 1a−f, respectively). Analyses were carried out using NMR and GC-MS as before. In each figure, the straight-line plot (red data points) is a theoretical one, representing the case where the host is completely unselective towards both guests and is inserted for ease of comparison with the experimentally-determined data points (blue).

d)

$K_{2MCON:3MCON} = 6.0$

e)
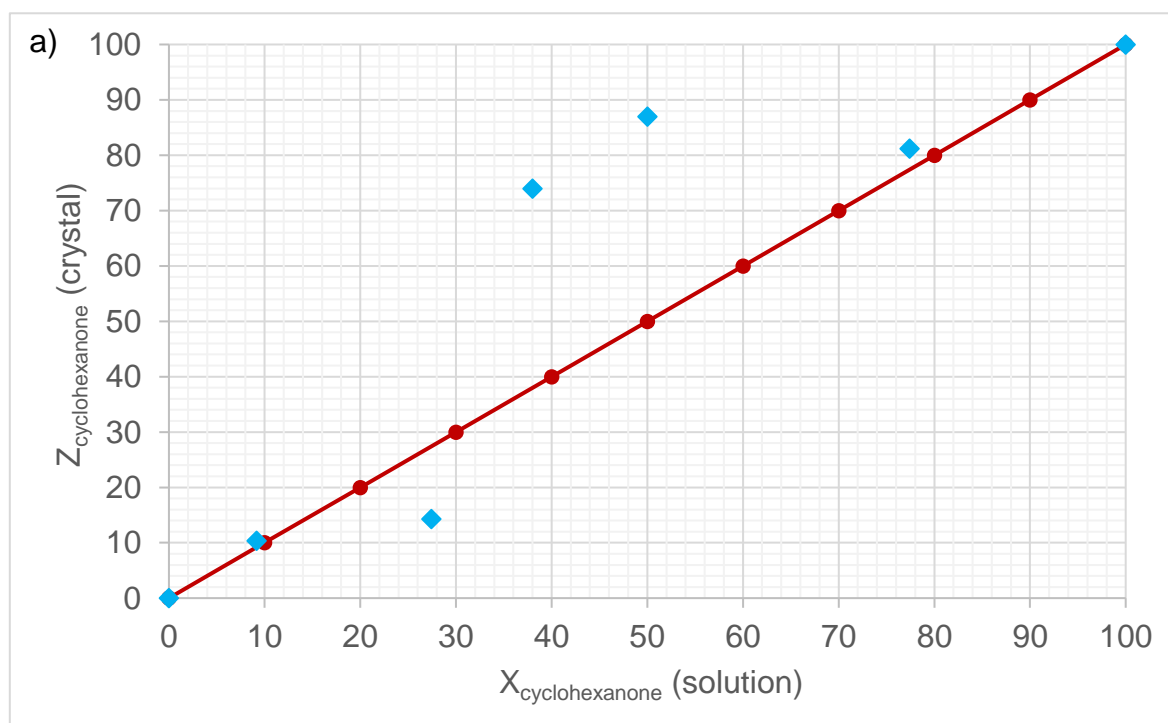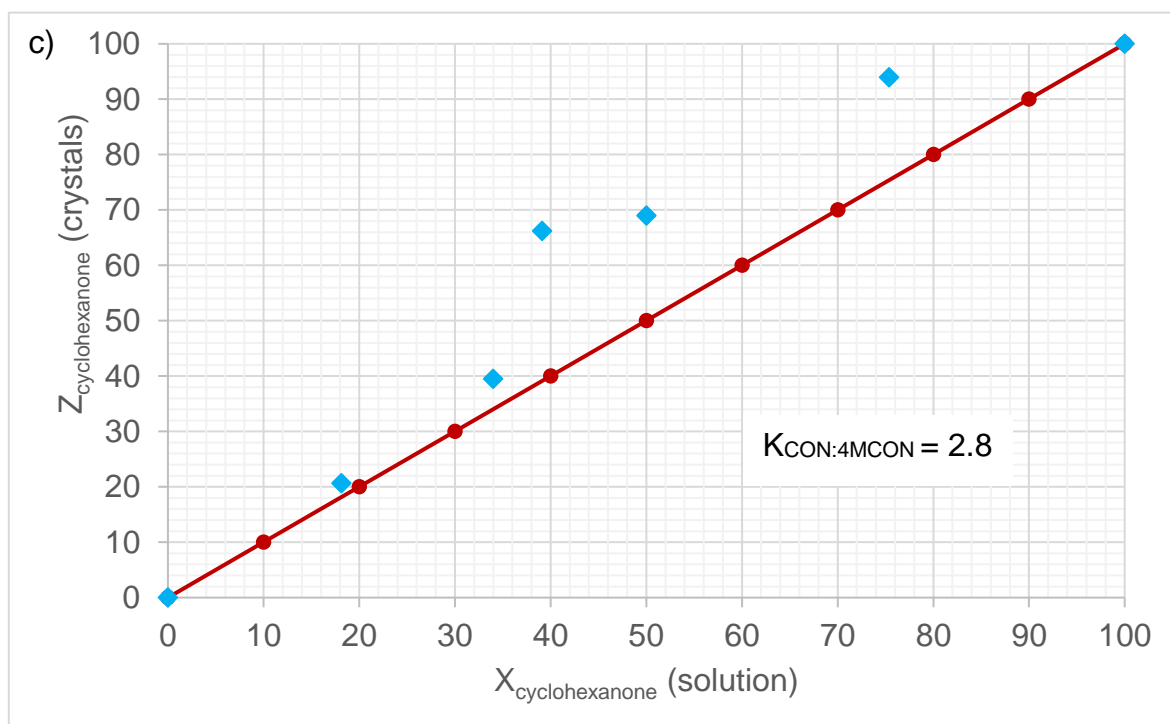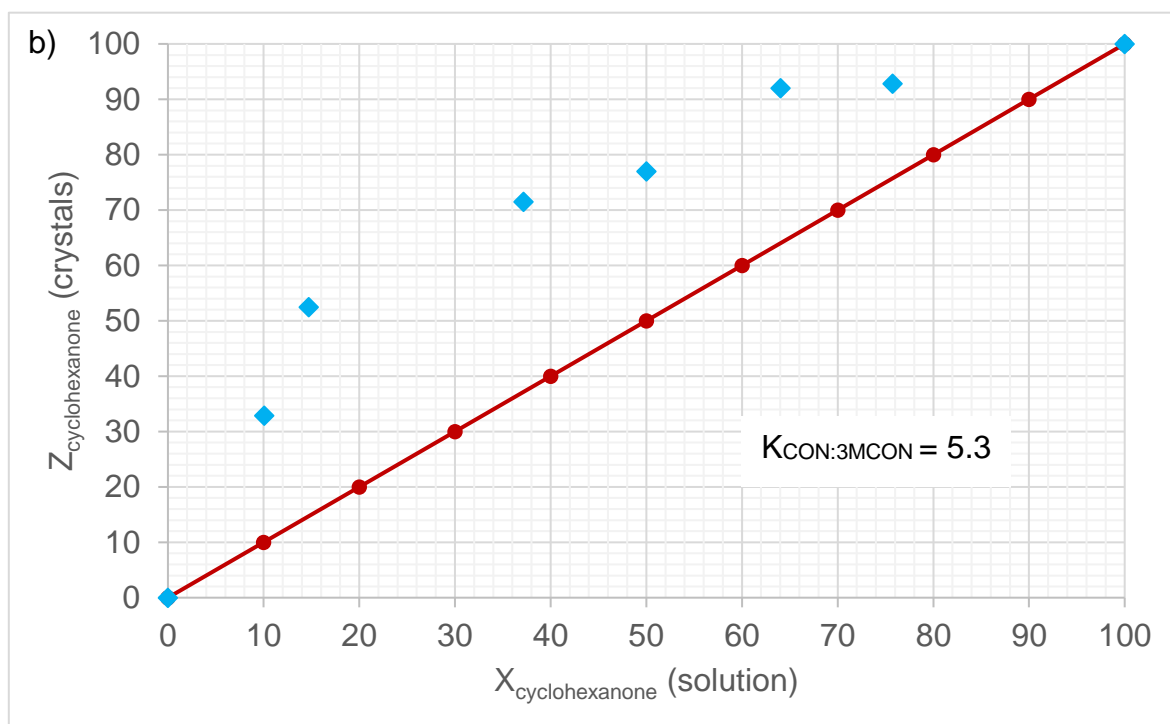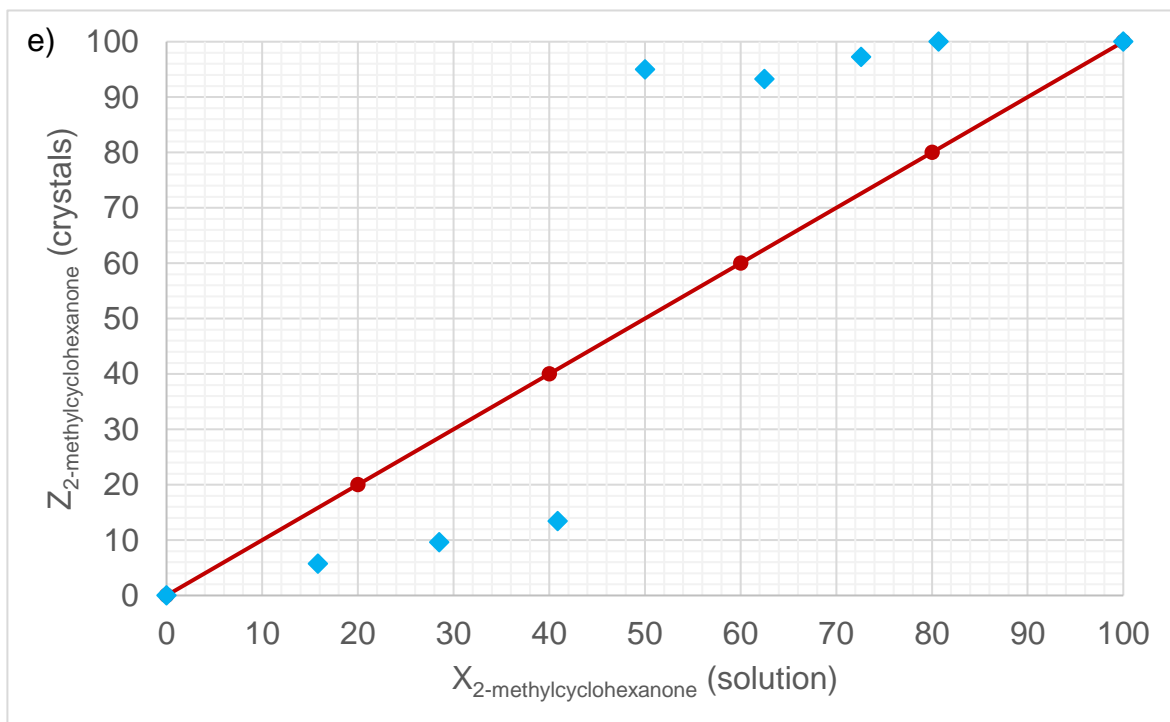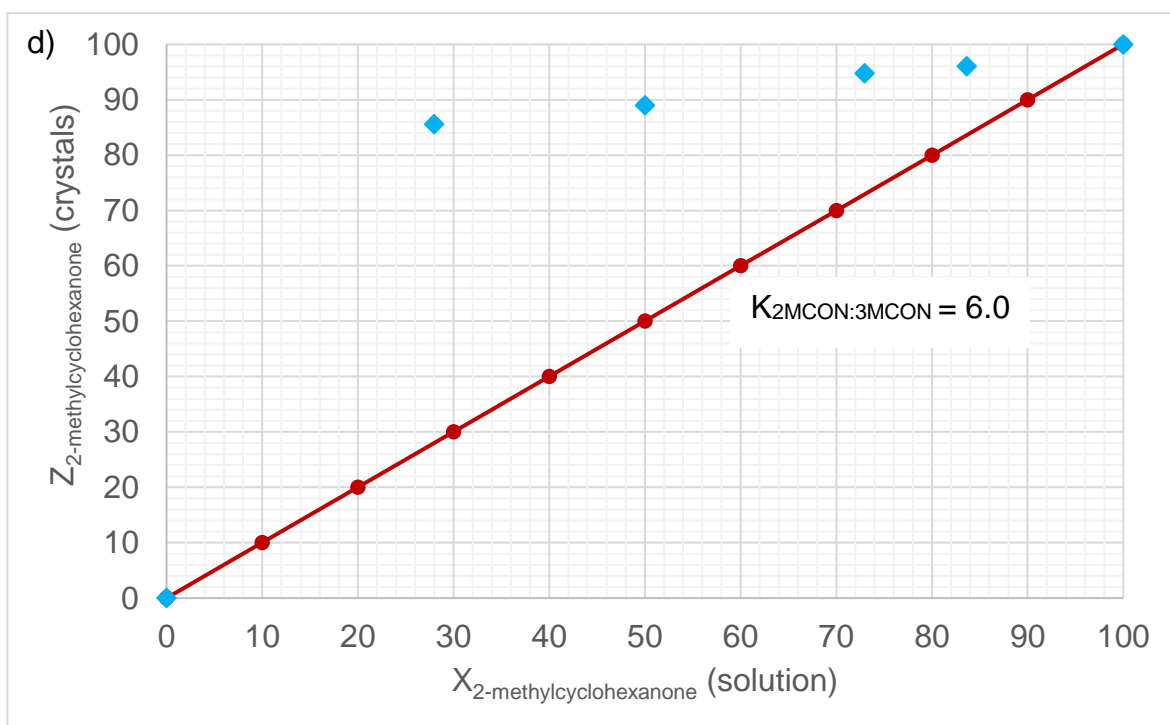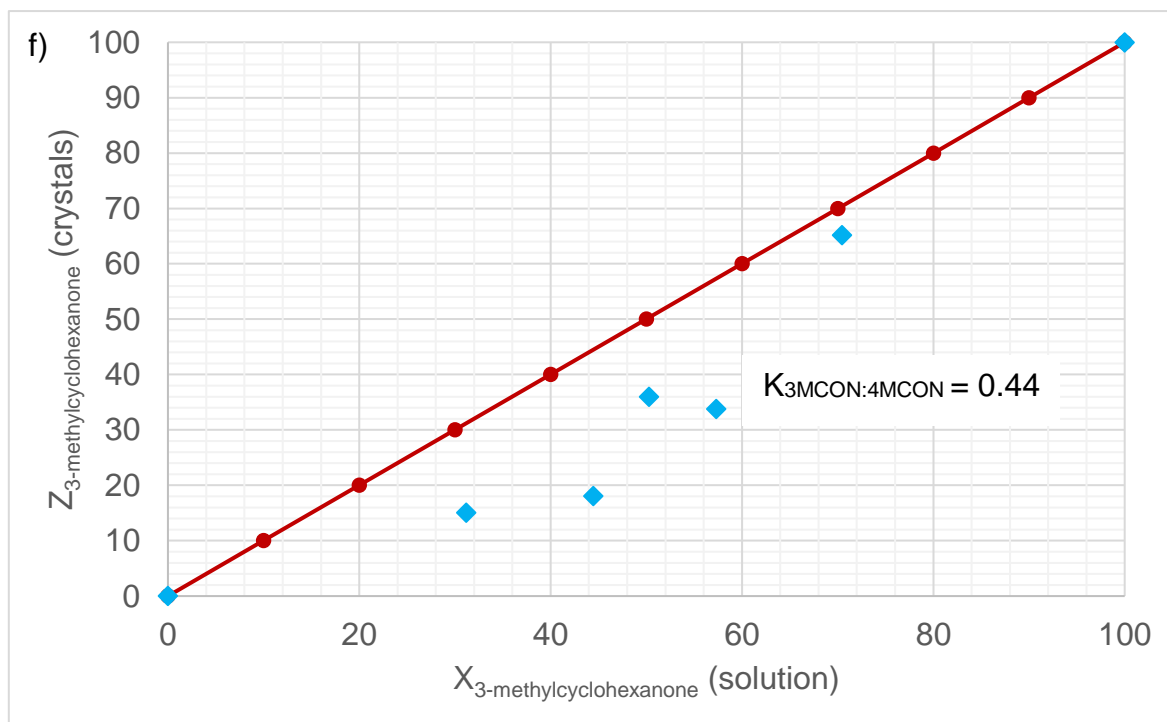
Figure 1: Selectivity curves for a) CON/2MCON, b) CON/3MCON, c) CON/4MCON, d) 2MCON/3MCON, e) 2MCON/4MCON and f) 3MCON/4MCON

The curve obtained for CON/2MCON (Figure 1a) shows the selectivity of the host to be guest-concentration dependent: at low concentrations of CON (up to approximately 10%), no significant host selectivity is observed for either guest. After this point, 2MCON was favoured until a CON concentration of approximately 30% was reached (where the selectivity constant K ≈ 1). Thereafter, CON remains preferred. A selectivity coefficient for this profile is not provided here as the value obtained would be misleading due to the observed host selectivity change with guest concentration change.

For combinations of CON/3MCON (Figure 1b, $K_{CON:3MCON}$ = 5.3) and CON/4MCON (Figure 1c, $K_{CON:4MCON}$ = 2.8), a consistent host preference for CON over 3MCON and 4MCON, respectively, was observed for the entire concentration range investigated. A similar host preference was observed in the 2MCON/3MCON experiment (Figure 1d) where 3MCON was significantly discriminated against in favour of 2MCON. In the presence of 2MCON and 4MCON (Figure 1e), the selectivity of the host was, once more, guest-concentration dependent, where the host selected more of 4MCON at

high concentrations of this isomer while at low concentrations, 2MCON was more prevalent in the crystals. A selectivity coefficient for this profile is not provided as the value obtained would be misleading due to the data oscillation above and below the line of zero selectivity. The selectivity curve for 3MCON/4MCON (Figure 1f) on the other hand, shows a consistent preference for the 4MCON isomer.

4.3 Single Crystal X-ray Diffraction (SCXRD)

The crystal data for the four complexes have been published by our team on a prior occasion, but will undergo further analysis in this study.[159] The crystal structures and refinement parameters are provided in Table 4. Both the TET·CON and TET·3MCON complexes are isostructural and crystallize in the monoclinic crystal system and $P2_1$ space group with Z = 2, while the TET·2MCON (orthorhombic, $P2_12_12_1$, Z = 4) and TET·4MCON (triclinic, $P1$, Z = 1) complexes differ from these and one another. The chiral 2MCON and 3MCON analogues are disordered over two positions [s.o.f. 0.645(6) and 0.778(3), respectively] owing to the presence of the two enantiomers, with the (R)-isomer being favoured in both instances. Furthermore, the guests are accommodated in discrete cavities in each crystal (Figures 2–5). Here we also include data from our previous work for the individual enclathrations of CON, 2MCON, 3MCON and 4MCON for ease of discussion. Figure 6 displays stereoviews of the 3MCON and 4MCON complexes, as well as the H-bonds associated within the crystal packing. The stereoview for the TET·2MCON complex for various reasons could not be provided here. Since the TET·CON complex is isostructural with TET·3MCON, its stereoview is also not given here for the sake of brevity.
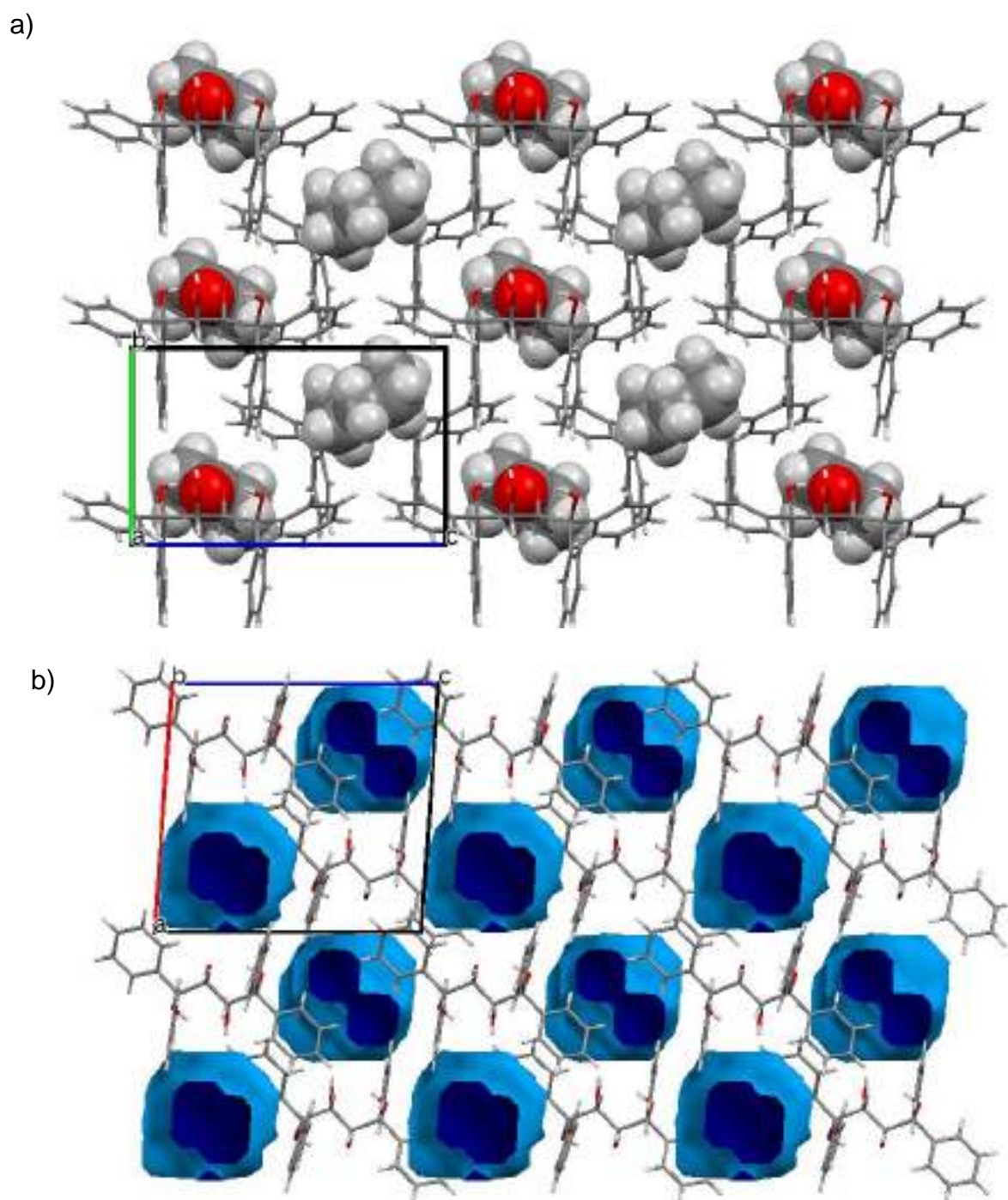
a)

b)

Figure 2: a) Crystal packing of the TET·CON inclusion complex with guest in spacefill form; b) Calculated voids (light blue) for TET ·CON indicating guest accommodation in discrete cavities; (oxygen – red, nitrogen – blue, carbon – grey and hydrogen – light grey)

a)

b)
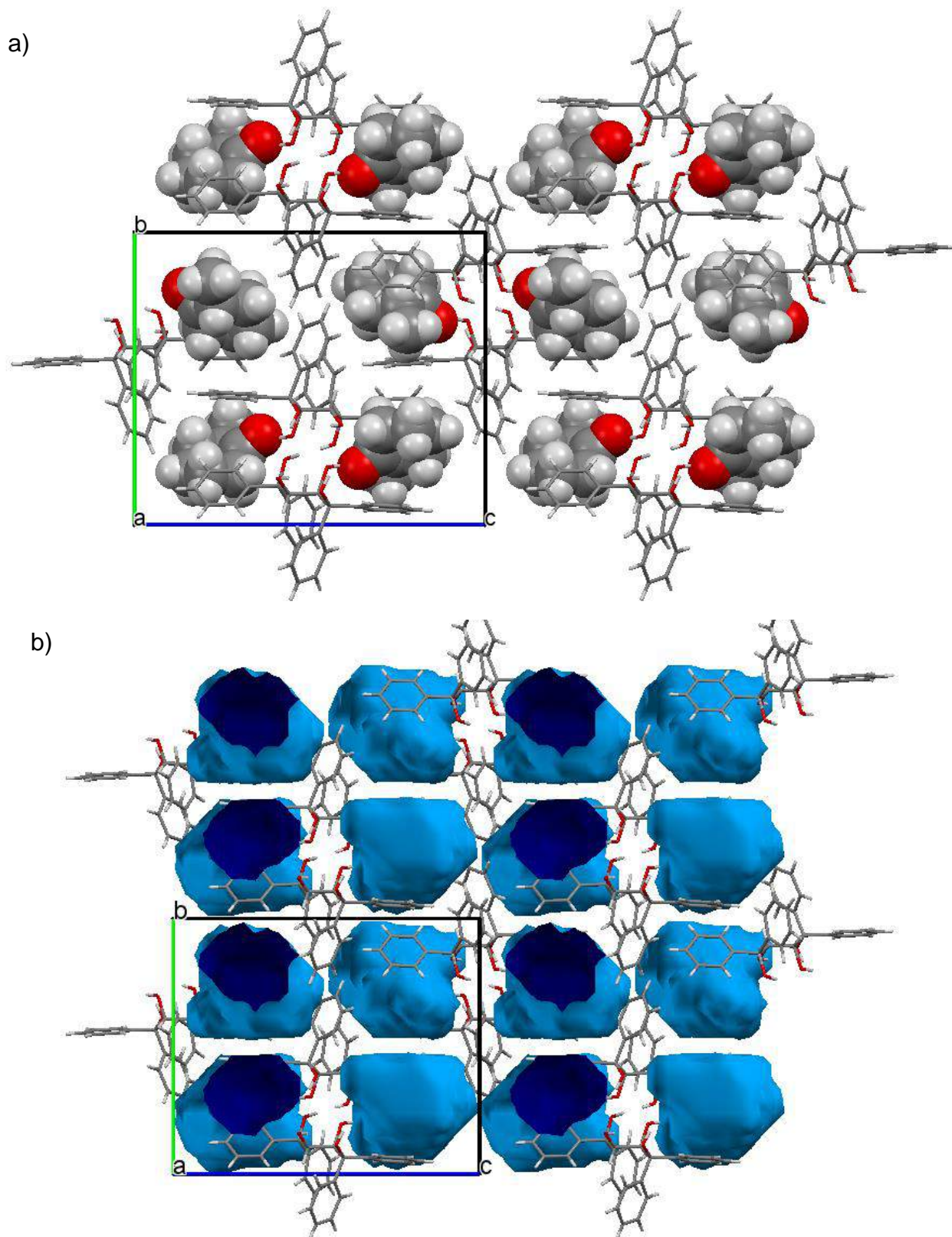
Figure 3: a) Crystal packing of the TET ·2MCON inclusion complex with guest in spacefill form; b) Calculated voids (light blue) for TET ·2MCON indicating guest accommodation in discrete cavities; (oxygen – red, nitrogen – blue, carbon – grey and hydrogen – light grey)

a)

b)
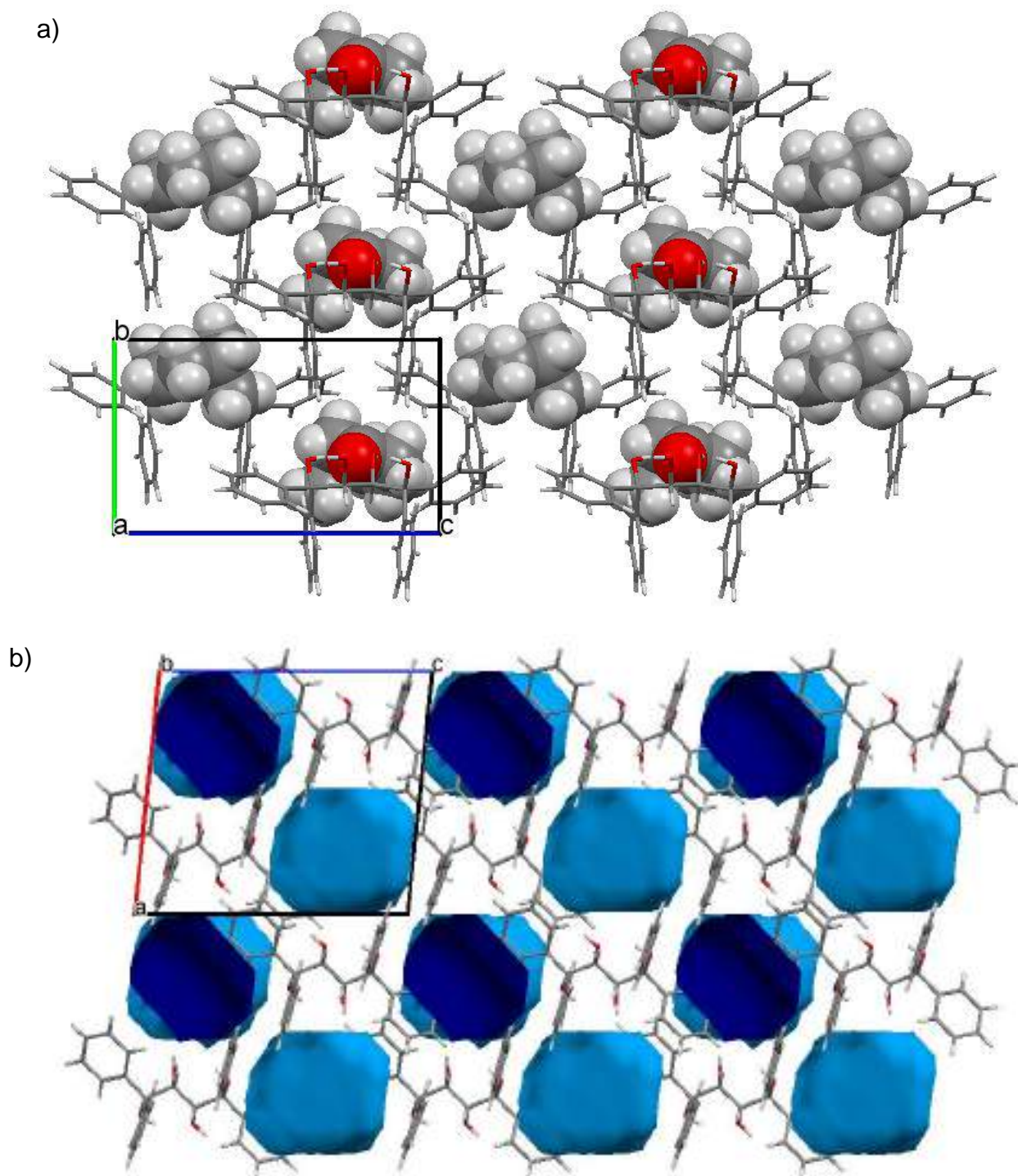
Figure 4: a) Crystal packing of the TET ·3MCON inclusion complex with guest in spacefill form; b) Calculated voids (light blue) for TET ·3MCON indicating guest accommodation in discrete cavities; (oxygen – red, nitrogen – blue, carbon – grey and hydrogen – light grey)

a)

b)
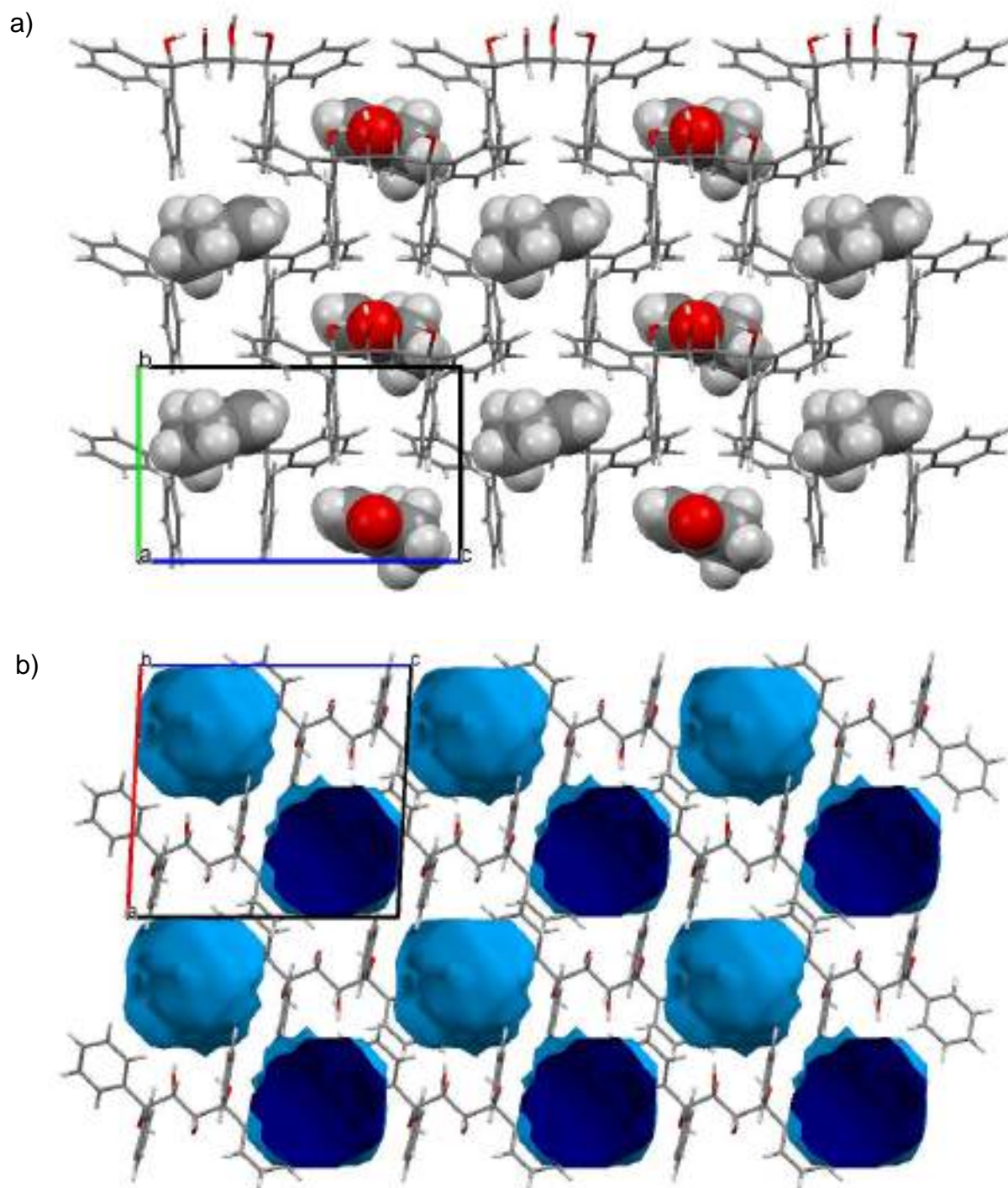
Figure 5: a) Crystal packing of the TET ·4MCON inclusion complex with guest in spacefill form; b) Calculated voids (light blue) for TET ·4MCON indicating guest accommodation in discrete cavities; (oxygen – red, nitrogen – blue, carbon – grey and hydrogen – light grey)

93

Table 4: Relevant single crystal X-ray crystallographic data for the complexes of TETROL with CON, 2MCON, 3MCON and 4MCON

	TET·CON	TET·2MCON	TET·3MCON	TET·4MCON
Chemical formula	$C_{28}H_{26}O_4 \cdot C_6H_{10}O$	$C_{28}H_{26}O_4 \cdot C_7H_{12}O$	$C_{28}H_{26}O_4 \cdot C_7H_{12}O$	$C_{28}H_{26}O_4 \cdot C_7H_{12}O$
Formula weight	524.63	538.65	538.65	538.65
Crystal system	Monoclinic	Orthorhombic	Monoclinic	Triclinic
Space group	$P2_1$	$P2_12_12_1$	$P2_1$	$P1$
μ (Mo Kα)/mm^{-1}	0.084	0.082	0.083	0.084
a/Å	12.5944(4)	10.3843(3)	12.4493(6)	8.181(2)
b/Å	8.1531(2)	15.2193(3)	8.2368(4)	9.952(3)
c/Å	13.4570(5)	18.2734(4)	13.9466(7)	10.163(3)
α/°	90	90	90	79.296(6)
β/°	94.025(2)	90	95.843(2)	68.813(5)
γ/°	90	90	90	65.825(5)
V/Å^3	1378.40(8)	2887.96(12)	1422.69(12)	703.2(3)
Z	2	4	2	1
F (000)	560	1152	576	288
Temp (K)	200	200	200	173
Restraints	1	0	9	3
Nref	6501	6716	6823	9403
Npar	356	440	399	366
R1	0.0388	0.0335	0.0459	0.0515
wR2	0.1045	0.0862	0.1354	0.1338
S	1.04	1.03	1.04	0.94
Θ min, max/°	1.5, 28.3	1.7, 28.3	2.1, 28.3	2.2, 27.1
Tot. data	13345	15292	26618	9415
Unique data	6501	6716	6823	9403
Observed data [I > 2.0σ(I)]	5556	6013	6031	5729
Rint	0.017	0.012	0.014	0.000
Diffrn measured fraction Θ full	0.996	0.999	0.996	0.952
Min. resd. dens. (e/Å^3)	−0.21	−0.17	−0.27	−0.25
Max. resd. dens. (e/Å^3)	0.21	0.22	0.28	0.26

a)

b)
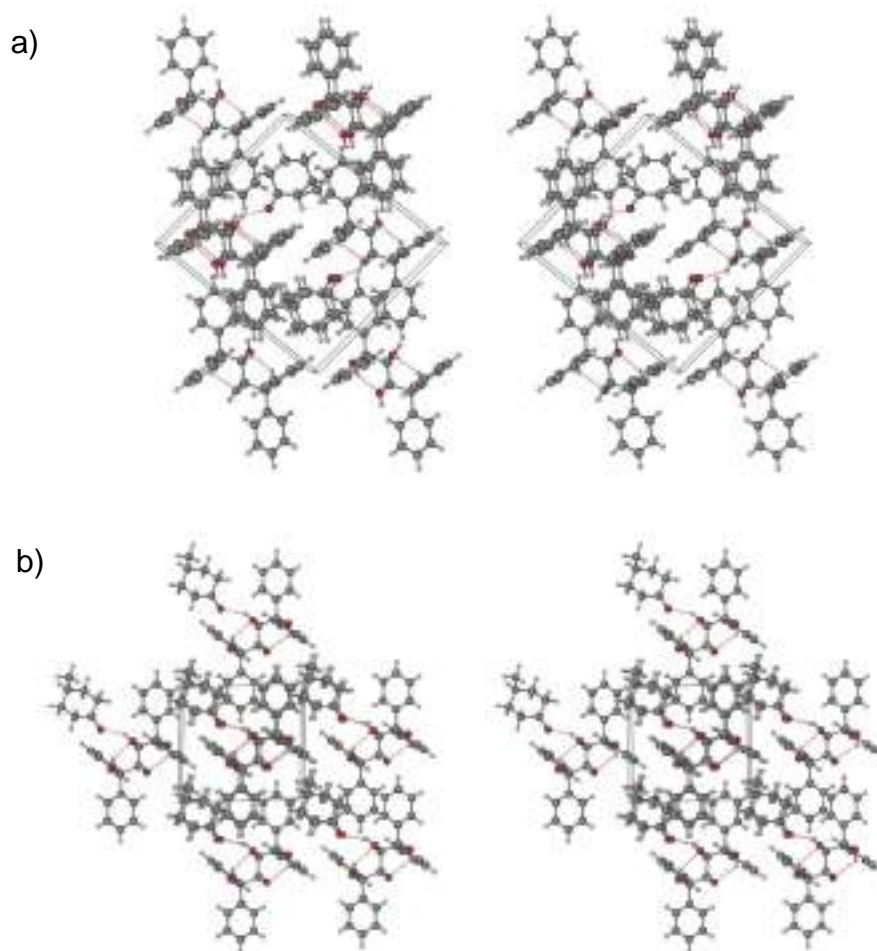
Figure 6: Stereoviews illustrating the crystal packing of a) TET·3MCON and b) TET·4MCON

4.3.1   H-Bonding Interactions Between Host and Guest Species

The host geometry is stabilised by means of 1,3-intramolecular hydrogen bonds, and each guest held in the crystal by mode of (guest)C=O···H−O(host) hydrogen bonds involving only the secondary host hydroxyl groups (Table 5) (note that both enantiomers of chiral compounds 2MCON and 3MCON experience hydrogen bonding, and hence two values are provided for each of these in the table). The guest experiencing the shortest contact of this type is one of the enantiomers of 3MCON [2.621(2)], but an angle of 141° would weaken this interaction somewhat. The other enantiomer has a much longer H-bond with the host than all the other guests [3.125(8), 152°]. CON, 2MCON and 4MCON are involved in H-bonds with the host of comparable strength [2.705(6)–2.716(2), 152–167°].

Table 5: Analysis of intermolecular hydrogen bonding interactions between TET and guests CON, 2MCON, 3MCON and 4MCON

Guest	Unit cell H:G ratio	Guest[†]	(host)O···O(guest) /Å	(host)H···O(guest) /Å	(host)O–H···O(guest) /°	Symmetry operator
CON	1:1	[1]	2.716(2)	1.93	156	x,y,z
2MCON	1:1	[1] [2]	2.716(2) 2.705(6)	1.89 1.88	167 167	x,y,z x,y,z
3MCON	1:1	[1] [2]	2.621(2) 3.125(8)	1.91 2.36	141 152	x,y,z x,y,z
4MCON	1:1	[1]	2.713(4)	1.94	152	x,y,z x,y,z

[†]The unit cells of the TET·2MCON and TET·3MCON complexes each compromise a disordered guest, representing the two enantiomers, labelled [1] and [2]

4.3.2 Short Ring (π···π) and X–H···π Interactions Between Host and Guest Species

The host framework for each complex is further stabilised by (host)π···π(host) interactions with comparable ranges [Table 6, 4.749(1)–5.934(3) Å]. Accompanying these interactions are a multitude of cooperative (guest)C–H···π(host) contacts.

In the crystal of TET·2MCON, stabilization of the guest is mediated by four (guest)C–H···π(host) interactions in the range 2.73–2.90 Å with angles ranging between 143–164° (Table 6). The TET·CON and TET·4MCON complexes are respectively stabilised by two (guest)C–H···π(guest) interactions within the range 2.66–2.98 Å with angles 137–159°. The TET·3MCON complex involves four similar (guest)C–H···π(host) interactions (2.75–2.91 Å, 142–156°) and a noticeably shorter interaction of this type (2.49 Å, 140°) (Table 6). This data does not support the preferential inclusion of CON over the three methylcyclohexanone isomers and therefore does not explain the selectivity order of TETROL for these four cyclohexanone guests.

Table 6: Analysis of the significant interactions between TETROL and guests CON, 2MCON, 3MCON and 4MCON

Interaction	CON	2MCON	3MCON	4MCON
π···π (Host···Guest)	N/A	N/A	N/A	N/A
π···π (Host···Host)	4.749(1)–5.911(1) (9 contacts)	4.784(1)–5.594(1) (7 contacts)	4.760(1)–5.927(1) (9 contacts)	4.805(3)–5.934(3) (8 contacts)
π···π (Guest···Guest)	N/A	N/A	N/A	N/A
CH···π	2.84 Å, 157° (H···Cg, C–H···Cg) (guest)C–H···π(host) 2.98 Å, 145° (H···Cg, C–H···Cg) (guest)C–H···π(host)	2.90 Å, 143° (H···Cg, C–H···Cg) (guest)Me–C–H···π(host) 2.73 Å, 150° (H···Cg, C–H···Cg) (guest)C–H···π(host) 2.76 Å, 147° (H···Cg, C–H···Cg) (guest)C–H···π(host) 2.84 Å, 164° (H···Cg, C–H···Cg)[a] (guest)Me–H···π(host)	2.87 Å, 153° (H···Cg, C–H···Cg) (guest)Me–C–H···π(host) 2.83 Å, 151° (H···Cg, C–H···Cg)[a] (guest)C–H···π(host) 2.75 Å, 142° (H···Cg, C–H···Cg)[a] (guest)C–H···π(host) 2.49 Å, 140° (H···Cg, C–H···Cg)[a] (guest)C–H···π(host) 2.91 Å, 156° (H···Cg, C–H···Cg)[a] (guest)C–H···π(host)	2.66 Å, 159° (H···Cg, C–H···Cg) (guest)C–H···π(host) 2.96 Å, 137° (H···Cg, C–H···Cg) (guest)C–H···π(host)
Short contacts	None	None	None	None

[a]Interaction involving disordered components

4.3.3 SCXRD Analysis of a Mixed Complex Containing CON and 4MCON

We subsequently grew crystals of TETROL from an equimolar mixture of CON and 4MCON. Suitable crystals were analysed using SCXRD and the selected crystal was determined to have a s.o.f. for the major component (CON) of 0.723, and the minor component 0.277 (4MCON), which is in reasonable agreement with the GC-MS experiment discussed previously (Table 3). This CON:4MCON ratio was confirmed to be a bulk property by ^{1}H-NMR analyses, showing a CON:4MCON ratio of 71:29, which correlates with the SCXRD result. Furthermore, this bulk property was also confirmed from the correlating powder patterns computed from the single crystal .cif file for the mixed complex and that obtained experimentally (Figure 7). This proved that the crystal of the mixed complex selected for SCXRD represented the bulk, and that these crystals constituted a single, pure phase rather than two phases, as alluded to by both GC-MS and ^{1}H-NMR experiments. Figure 8 shows a stereoview of the host and guests' orientations in the unit cell. It is clear that both guests occupy the same site within the crystal and that their orientations are identical, with each cyclohexyl ring carbon atom exactly overlapping, appearing as though only 4MCON is present (Figures 8 and 9). The reasons for the axial orientation of the methyl-substituted guest has been reported previously.[160] This conformation is stabilized by means of two (guest)C−H···π(host) and four (guest)H···C_{Ar} interactions. Of these interactions, the methyl group experienced two interactions of the (guest)Me–H···C_{Ar} type, which is also the case in this study, despite the different packing systems (2.86 and 2.77 Å, 152 and 153°, respectively). This explains the maintenance of the axial orientation of this alkyl group in the mixed complex as well. The guests are retained in this crystal by (host)O−H···O(guest) H-bonding, measuring 2.711(3) Å with angles of 150°.
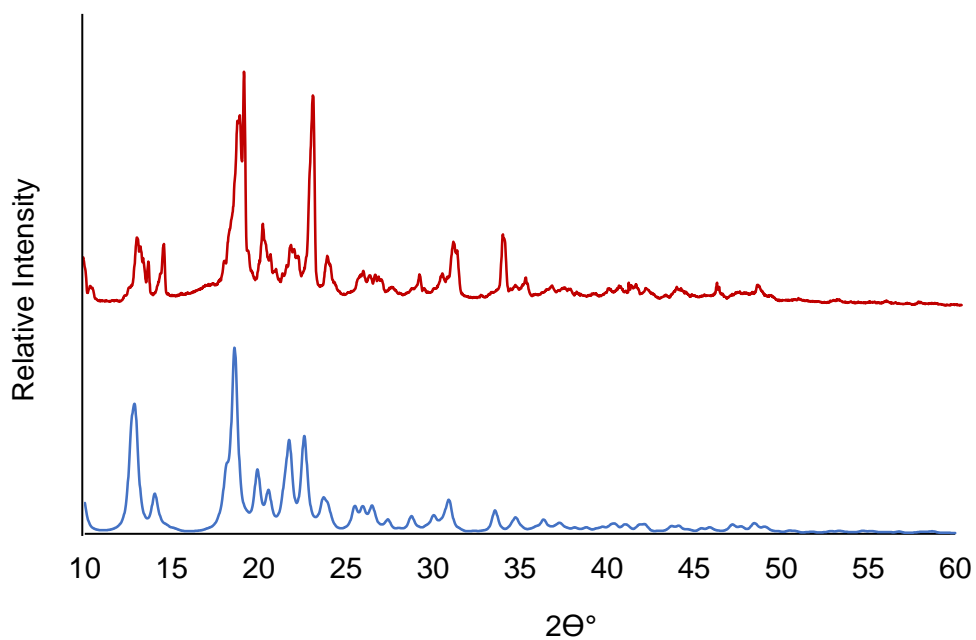
Figure 7: Overlay of the powder diffraction (PXRD) patterns generated from the single crystal .cif file (blue) and that obtained experimentally for the mixed clathrate (red); peaks show close correlation with one another, alluding to a pure, single phase
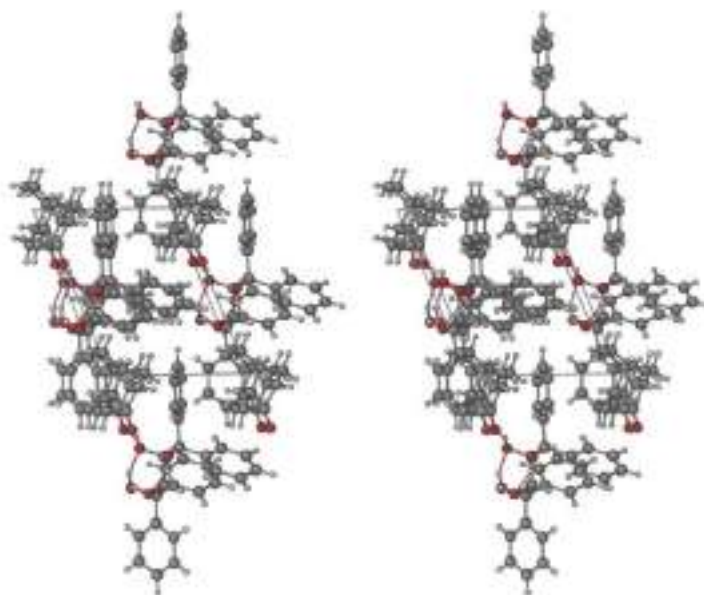
Figure 8: Stereoview illustrating the host and guests' orientations in the unit cells of the CON:4MCON mixed complex
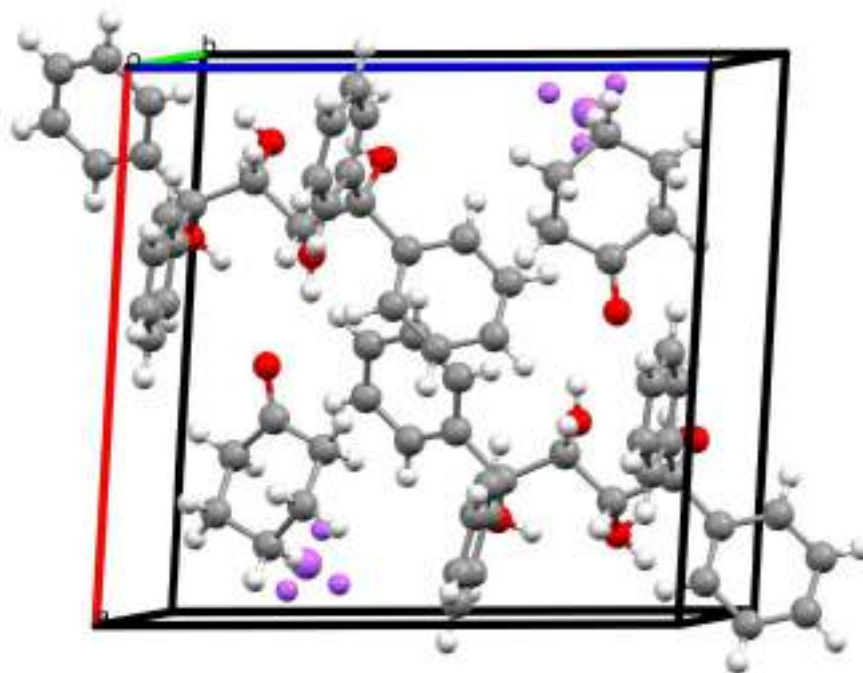
Figure 9: The unit cell of the TET·CON·4MCON complex showing both guests occupying the same site within the crystal, with each cyclohexyl ring carbon atom exactly overlapping; the methyl group of 4MCON is highlighted in purple

Crystal data and refinement parameters for TET·CON, TET·4MCON and the mixed complex are listed in Table 7. Upon close analysis of these data, it is observed that the TET·CON and TET·(0.72)CON·(0.28)4MCON complexes are isostructural, with very similar unit cell dimensions, crystallizing in the monoclinic crystal system and $P2_1$ space group. However, the TET·4MCON complex has a different packing (triclinic, $P1$, Table 7). As observed from the competition experiments, the CON guest is overwhelmingly favoured by TET. It is therefore consequently possible that the host compound is encouraged to crystallize in the crystal system of the preferred CON guest despite the presence of 4MCON. The presence of CON therefore steers the host packing towards the monoclinic crystal system ($P2_1$), possibly being favoured for the mixed complex as the preferred guest is then able to experience a larger number of stabilizing O···H/H···O interactions (see later, Figure 11, Table 8). This possibly explains the change in the host selectivity for the alkylcycohexanones whenever CON is present, since its presence affects the crystal packing that the host selects during crystallization.

Table 7: Relevant single crystal X-ray crystallographic data for the complexes of TETROL with CON, 2MCON, 3MCON and 4MCON

	TET·CON	TET·4MCON	TET·CON(0.72)·4MCON(0.28)
Chemical formula	$C_{28}H_{26}O_4$·$C_6H_{10}O$	$C_{28}H_{26}O_4$·$C_7H_{12}O$	$C_{28}H_{26}O_4$·$C_{6.28}H_{10.55}O$
Formula weight	524.63	538.65	528.52
Crystal system	Monoclinic	Triclinic	Monoclinic
Space group	$P2_1$	$P1$	$P2_1$
μ (Mo Kα)/mm^{-1}	0.084	0.084	0.083
a/Å	12.5944(4)	8.181(2)	12.6617(6)
b/Å	8.1531(2)	9.952(3)	8.1716(4)
c/Å	13.4570(5)	10.163(3)	13.4898(7)
α/°	90	79.296(6)	90
β/°	94.025(2)	68.813(5)	93.883(2)
γ/°	90	65.825(5)	90
V/Å^3	1378.40(8)	703.2(3)	1392.54(12)
Z	2	1	2
F (000)	560	288	565
Temp (K)	200	173	200
Restraints	1	3	1
Nref	6501	9403	6643
Npar	356	366	366
R1	0.0388	0.0515	0.0440
wR2	0.1045	0.1338	0.1232
S	1.04	0.94	1.03
Θ min, max/°	1.5, 28.3	2.2, 27.1	1.5, 28.3
Tot. data	13345	9415	377634
Unique data	6501	9403	6643
Observed data [I > 2.0σ(I)]	5556	5729	5452
Rint	0.017	0.000	0.022
Diffrn measured fraction Θ full	0.996	0.952	1.000
Min. resd. dens. (e/Å^3)	−0.21	−0.25	−0.23
Max. resd. dens. (e/Å^3)	0.22	0.26	0.37

4.4   Hirshfeld Surface Analysis

To visualise the multiple intermolecular host–guest interactions observed in the host packing structures (Figure 2–5), we considered Hirshfeld surface analyses for the TET·CON, TET·2MCON, TET·3MCON and TET·4MCON complexes. The fingerprint plots are provided in Figure 10, while a summary of the percentage of each interaction type is displayed graphically in Figure 11. Table 8 provides the actual values obtained from this figure.
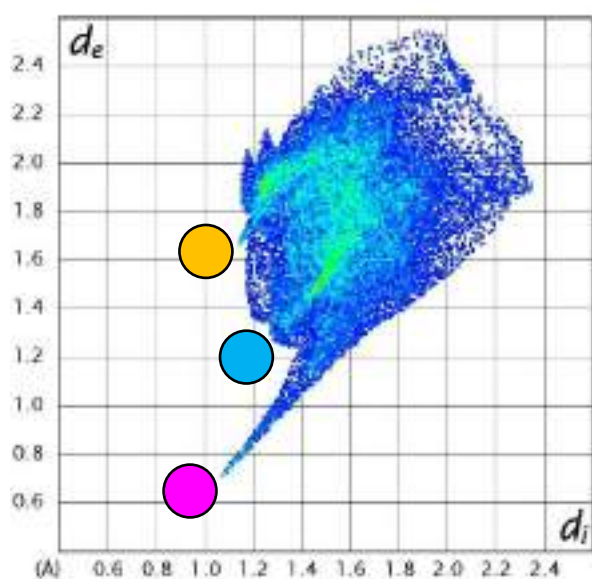
TET·CON

TET·2MCON [1]
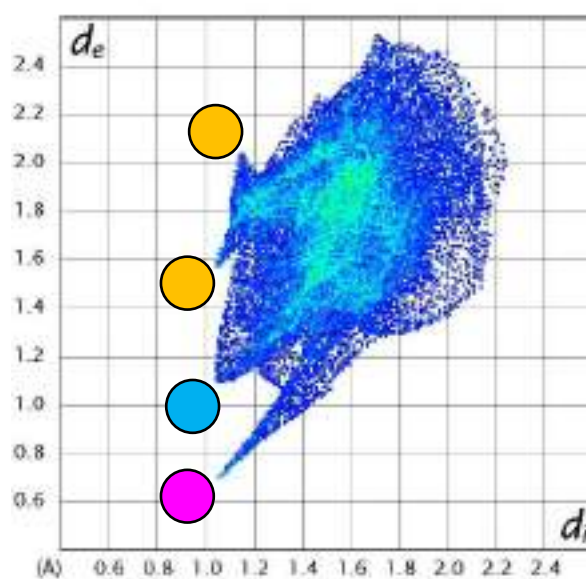
TET·2MCON [2]
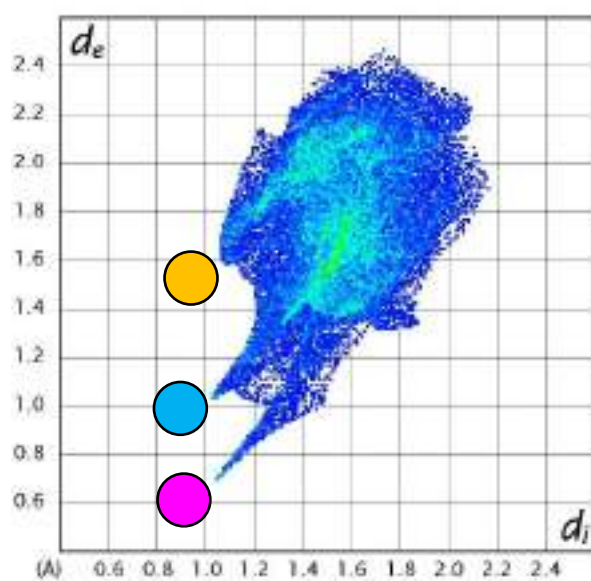
TET·3MCON [1]
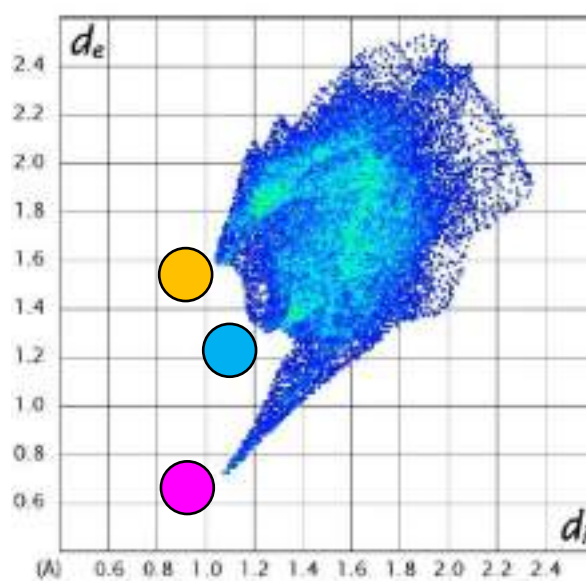
TET·3MCON [2]   **TET·4MCON**
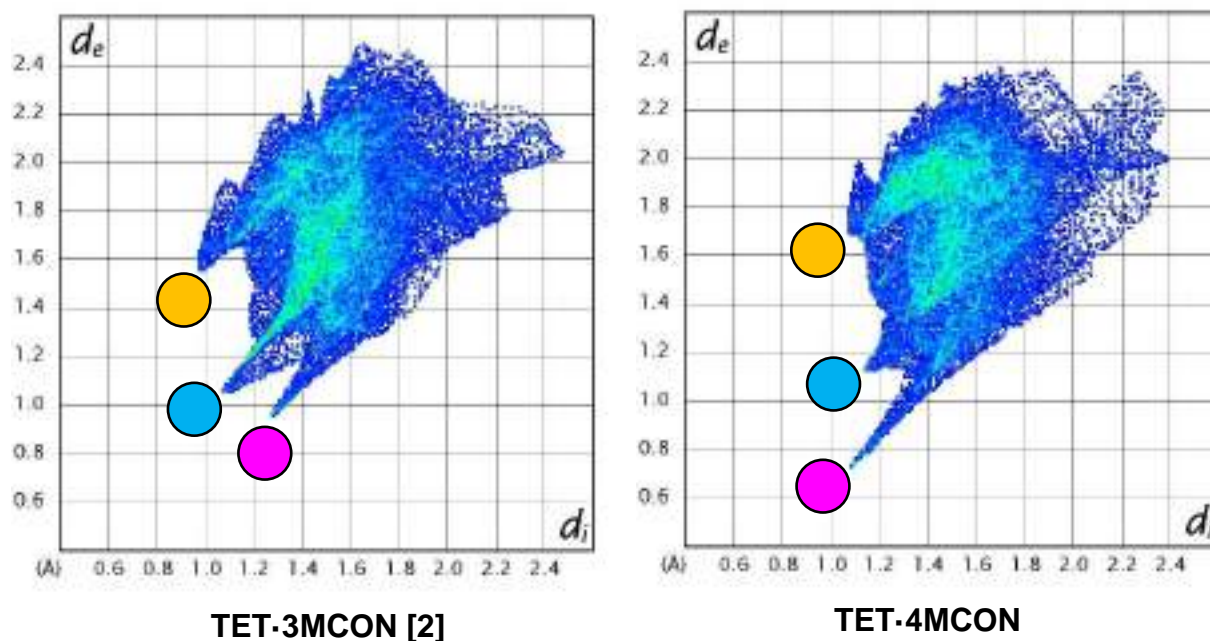
Figure 10: Hirshfeld fingerprint plots for TET·CON, TET·2MCON[1], TET·2MCON[2], TET·3MCON[1], TET·3MCON[2] and TET·4MCON ; The 'spike' and 'wings' observed in the Hirshfeld plots are colour coded and depict O···H (magenta), H···H (blue) and C···H (orange) contacts
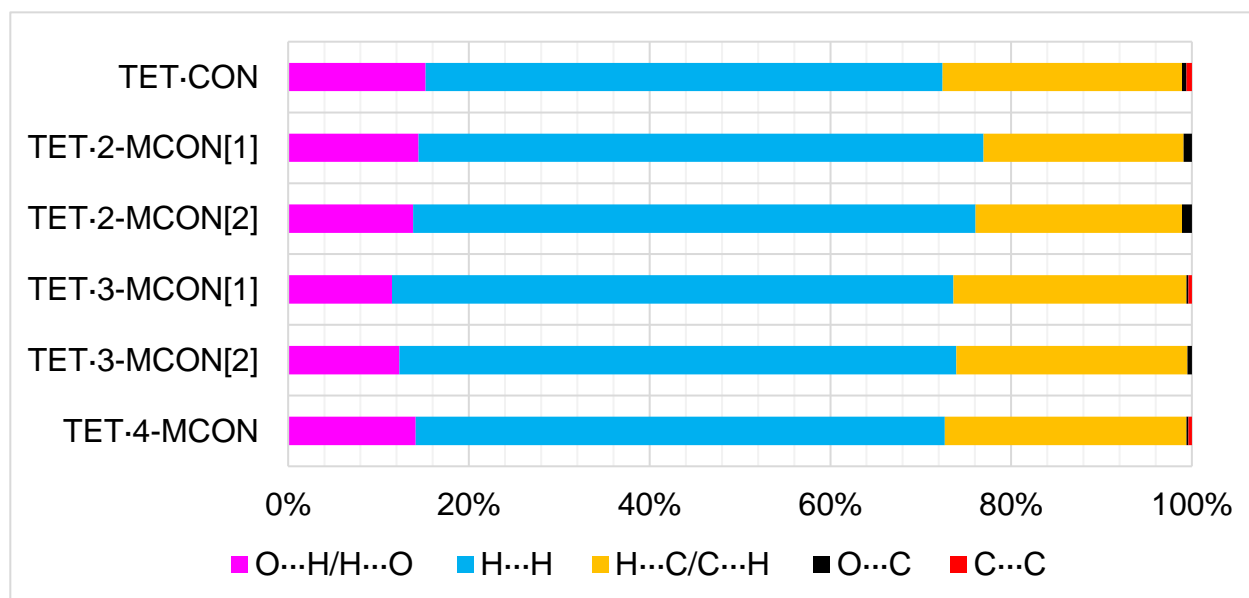
Figure 11: Graphical display showing the percentage intermolecular interactions of each type for the TET·CON, TET·2MCON[1], TET·2MCON[2], TET·3MCON[1], TET·3MCON[2] and TET·4MCON complexes

Table 8: Percentage intermolecular interactions in each inclusion complex (G···H/H···G)

	O···H/H···O	H···H	H···C/C···H	O···C [a]	C···C	O···O
TET·4-MCON	14.1	58.5	26.7	0.2	0.4	0
TET·3-MCON[2]	12.3	61.7	25.6	0.5	0	0
TET·3-MCON[1]	11.5	62.1	25.8	0.2	0.4	0
TET·2-MCON[2]	13.8	62.2	22.8	1.1	0	0.1
TET·2-MCON[1]	14.4	62.4	22.1	0.9	0	0.1
TET·CON	15.2	57.2	26.5	0.5	0.6	0

[a]Only guest···host interactions were observed

All complexes with TETROL are predominantly stabilised by H···H (57.2–62.4%) and C···H (22.1–26.7%) interactions (Figure 11, Table 8). It is observed that the TET·CON experiences significantly more O···H/H···O interactions (15.2% compared with the second most prevalent occurring in TET·2-MCON, 14.4%) and a high amount of H···C/C···H interactions (26.5% compared with the most prevalent occurring in TET·4MCON, 26.7%). These results correlate with the observed preference of TETROL for CON, and possibly allude to the importance of these interaction types in the crystals.

We removed each of the guests in turn from the TET·(0.72)CON·(0.28)4MCON mixed complex for the respective Hirshfeld surface determinations, and the 2D fingerprint plots were recalculated (Figures 12a and b). Unsurprisingly, Figure 12a is very similar to the TET·CON fingerprint plot in Figure 10: it is expected that the CON guest molecules in the mixed complex experience similar host−guest intermolecular interaction types compared with those in the pure TET·CON complex, owing to the identical packing mode in each of these complexes. Alternatively, the fingerprint plot for 4MCON (Figure 12b) in the mixed complex differs from that for TET·4MCON (Figure 10) indicating that the packing modes in the two complexes are not the same, as expected since the presence of cyclohexanone encourages TET to pack in the same mode as for the favoured guest species, CON. A summary of the percentage of each interaction type is displayed graphically in Figure 13, while Table 9 provides the actual values obtained from this figure.

a)

b)
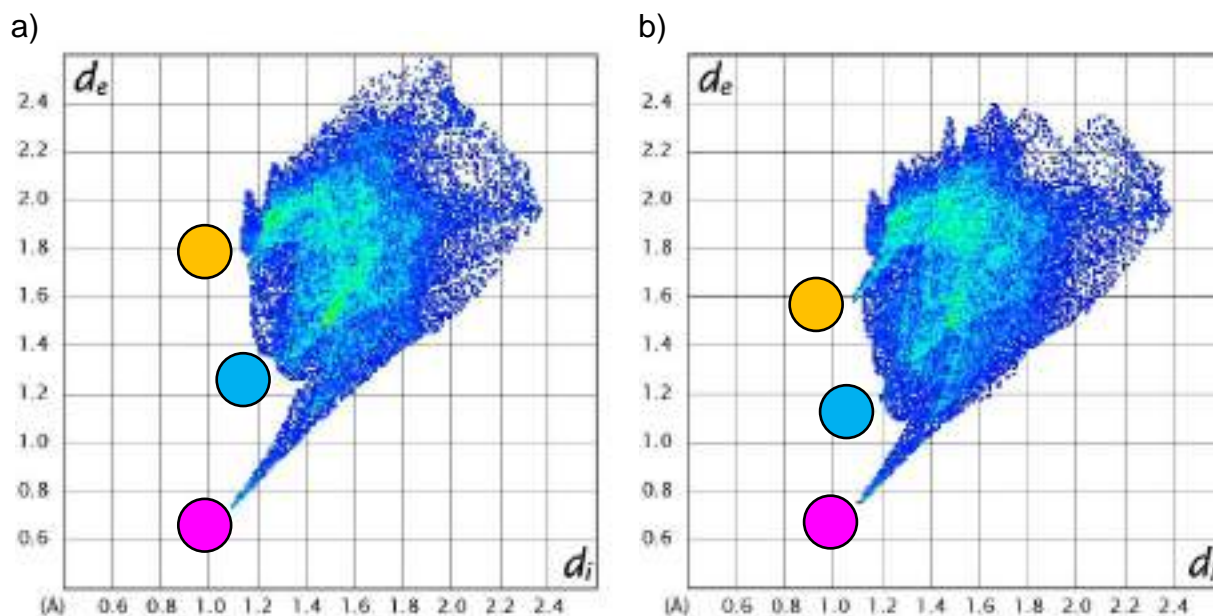
Figure 12. Hirshfeld fingerprint plots obtained after hypothetical removal of a) 4MCON and b) CON from the TET·(0.72)CON·(0.28)4MCON mixed complex
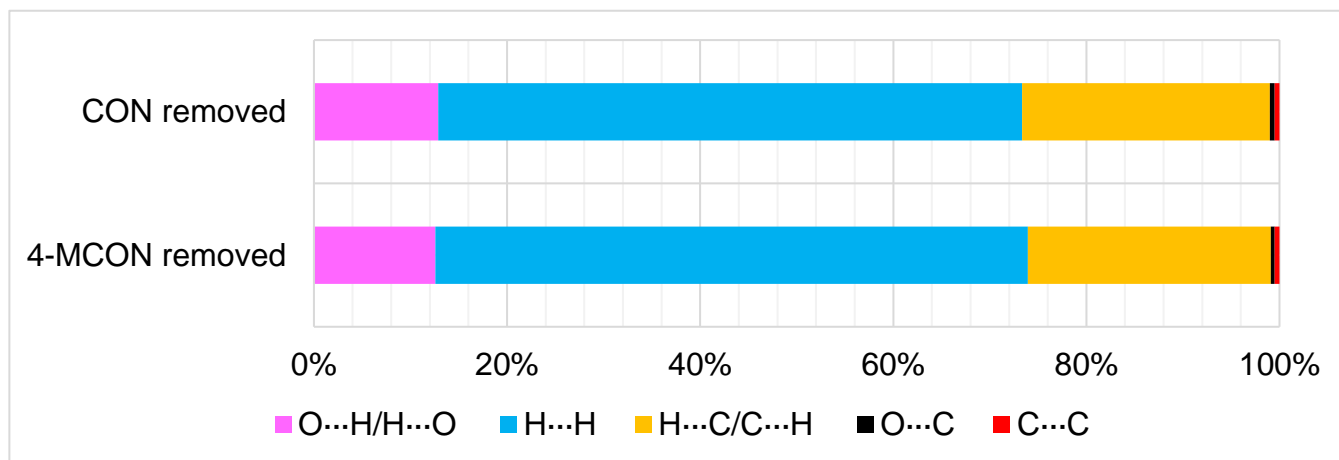
Figure 13: Graphical display showing the percentage intermolecular interactions of each type for the TET·(0.72)CON·(0.28)4MCON complex after removal of each guest in turn from the surface calculation

Table 9: Percentage intermolecular interactions (G···H/H···G) in the TET·(0.72)CON·(0.28)4MCON after removal of each guest in turn

	O···H/H···O	H···H	H···C/C···H	O···C/C···O	C···C/C···C
CON removed	12.9	60.5	25.7	0.5	0.5
4MCON removed	12.6	61.4	25.2	0.4	0.5

Both guests in the mixed complex therefore experience identical interaction types with comparable quantities.

4.5   Thermal Analyses

DSC and TG experiments for the four complexes, along with the traces obtained, have been reported previously.[159] Figure 14 is an overlay of the four TG traces associated with the heating process, thereby representing the guest loss. It is clear from these traces that CON (red curve) is held more tightly in the crystal, relative to the other three guests (green, magenta, and blue), due to the higher temperature associated with the release of this guest. This observation is supported by the increased number of stabilizing O···H/H···O host–guest interactions experienced in the TET·CON complex.
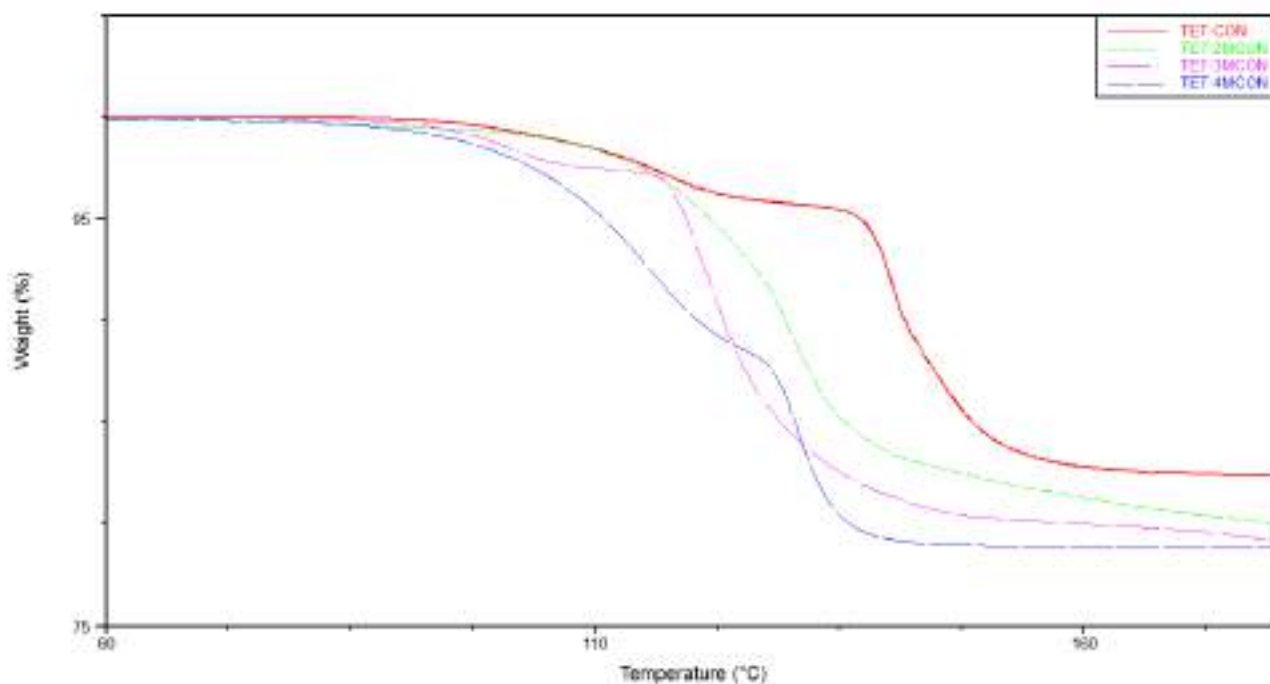
Figure 14: An overlay of the TG traces obtained for complexes of TET with CON, 2MCON, 3MCON and 4MCON

106

4.6   Conclusion

Competition experiments demonstrated that the selectivity order of TETROL for the three isomeric methylcyclohexanones was reversed in the presence of cyclohexanone [Table 3, CON (52%) > 4MCON (30%) > 3MCON (13%) > 2MCON (5%)] compared with when this guest was absent [Table 2, 2MCON (79%) >> 3MCON (14%) > 3MCON (7%)]. It was proposed that the overwhelming preference of TETROL for CON over all the alkylcyclohexanones effected this host behaviour change whenever this guest was present. SCXRD analysis indicated that the mode of packing for the mixed complex, TET·(0.72)CON·(0.28)4MCON, was isostructural with the pure TET·CON complex. It was therefore suggested that the presence of cyclohexanone encouraged the host to pack in the same mode as for the favoured CON guest species. Hirshfeld analyses showed this host packing to be energetically favourable since cyclohexanone experiences a high number of stabilizing O···H/H···O interactions in the crystal . Thermogravimetric analyses further confirmed the observation that cyclohexanone is much more tightly bound in the crystal than the other guests, and hence the host's consistent preference for it.

Chapter 5
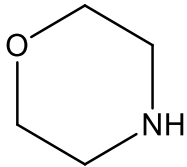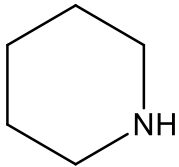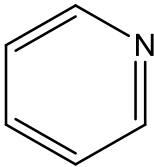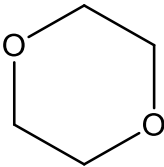
The Selectivity of TETROL for Four Selected Heterocyclic Compounds

5.1   Introduction

A heterocyclic compound may be defined as a ring compound that contains one or more heteroatoms such as nitrogen, oxygen or sulfur.[188] At this point, we will briefly introduce the four heterocycles relevant to this specific study. Pyridine is produced either from the processing of coal tar or by direct synthesis. Apart from this compound's extensive use as a solvent, it also has applications in the production of agricultural chemicals and pharmaceuticals.[189] Most importantly, pyridine is used in the catalytic hydrogenation production of piperidine. Piperidine has wide applications as a solvent, an intermediate in organic synthesis, the manufacture of pharmaceuticals, a catalyst in silicone esters and as a curing agent for rubber and epoxy resins.[190] There are various methods for the production of morpholine, with the most prevalent including the catalytic amination of diglycol under hydrogen pressure. Applications of this compound involve its use as an intermediate in the production of pharmaceuticals, crop protection, dyes, optical brighteners and its conversion to vulcanization accelerators or sulfur donors.[191] 1,4-Dioxane is synthesised by the acid-catalyzed conversion of diethylene glycol through dehydration and ring closure.[189] This compound has very many applications as a solvent, along with being a stabilizer for chlorinated solvents and printing inks, an agent in textile processing, agrochemicals and pharmaceuticals, and also in the manufacture of detergents.[192]

In this investigation, we explore the selectivity of TETROL for these four heterocyclic compounds, morpholine (MOR), piperidine (PIP), pyridine (PYR) and dioxane (DIO) (Table 1). These compounds were all enclathrated when crystals of this host compound were grown from each of these guest solvents, forming TET·MOR, TET·2PIP, TET·2PYR, TET·2DIO complexes, as viewed in Table 1 together with the boiling points of the pure guests. This investigation is purely of academic interest at this point.

Table 1: The structure and properties of the four heterocyclic compounds

	MOR	PIP	PYR	DIO
Structure				
Host (H):guest (G) ratio	1:1	1:2	1:2	1:2
Boiling point (°C)	129	106	115.6	101

5.2 Competition Experiments

Since each guest was enclathrated individually, competition experiments were conducted, and the selectivity of TET for these guests investigated to establish if the host would discriminate between them. In Table 2, we summarize data obtained from the recrystallization of TET from various equimolar binary, ternary and quaternary combinations of MOR, PIP, PYR and DIO. The so-formed crystal inclusions were analysed using proton NMR spectroscopy and GC-MS. As usual, the preferred guest species is given in bold red font face.

From Table 2, it is clear that MOR was the preferred guest in all equimolar competition experiments whenever it was present. MOR/PIP, MOR/PYR and MOR/DIO binary experiments showed the selective inclusion of morpholine with molar ratios of 78.9, 95.1 and 93.5%, respectively. In the absence of MOR, PIP was consistently selected for, as observed in the PIP/PYR and PIP/DIO experiments (89.8 and 97.4%). PYR was preferred when both MOR and PIP were absent (PYR/DIO, 98.9%). Equimolar ternary experiments involving MOR, once more, showed the host's preference for this guest (MOR/PIP/PYR, MOR/PYR/DIO and MOR/PIP/DIO experiments afforded crystals with 89.2, 93.6 and 76.5% of MOR, respectively) while in its absence, PIP was once more selected (PIP/PYR/DIO, 87.3%). Finally, the equimolar quaternary experiment showed the host to have a selectivity order of MOR (75.3%) > PIP (18.2%) > PYR (5.3%) > DIO (1.2%) for these guests. The overall H:G ratio remained 1:1 for all of the competition experiments involving MOR, and 1:2 for all other mixtures (Table 2).

Table 2: Competition experiments using host TETROL and various equimolar mixtures of the guests MOR, PIP, PYR and DIO[a,b]

Morpholine	Piperidine	Pyridine	Dioxane	Guest ratios (%e.s.d.)	Overall H:G ratio
X	X			**78.9**:21.1 (0.9)	1:1
X		X		**95.1**:4.9 (0.7)	1:1
X			X	**93.5**:6.5 (1.0)	1:1
	X	X		**89.8**:10.2 (1.2)	1:2
	X		X	**97.4**:2.6 (0.2)	1:2
		X	X	**98.9**:1.1 (0.1)	1:2
X	X	X		**89.2**:10.6:0.2 (0.8)	1:1
X		X	X	**93.6**:4.8:1.6 (1.1)	1:1
X	X		X	**76.5**:23.5:0 (0.5)	1:1
	X	X	X	**87.3**:11.6:1.1 (1.4)	1:2
X	X	X	X	**75.3**:18.2:5.3:1.2 (1.6)	1:1

[a]Ratios determined using proton NMR spectroscopy and gas chromatography

[b]Experiments were conducted in triplicate; %e.s.d.'s are provided in parentheses

Binary competitions were then carried out where the molar ratios of the four heterocyclic compounds were varied beyond equimolar, and the guest selectivity of TET thus evaluated by means of selectivity profiles for MOR/PIP, MOR/PYR, MOR/DIO, PIP/PYR, PIP/DIO and PYR/DIO combinations (Figures 1a−f, respectively). Analyses were carried out using NMR and GC-MS as before. In each figure, the straight-line plot (red data points) is a theoretical one, representing the case

where the host is completely unselective towards both guests, and is inserted for ease of comparison with the experimentally-determined data points (blue).

a) $K_{MOR:PIP} = 0.39$

b) $K_{MOR:PYR} = 10.5$

c)

$K_{MOR:DIO} = 4708.2$

d)

$K_{PIP:PYR} = 16.4$

e) $K_{PIP:DIO} = 232.33$

f) $K_{PYR:DIO} = 20.0$
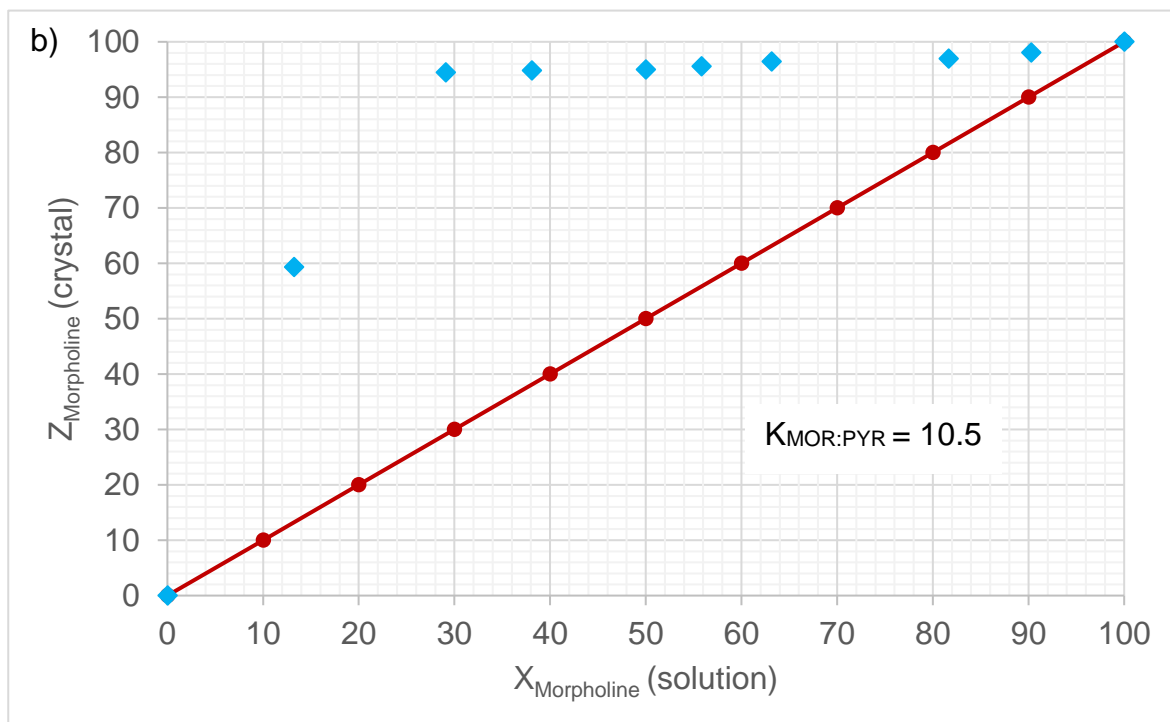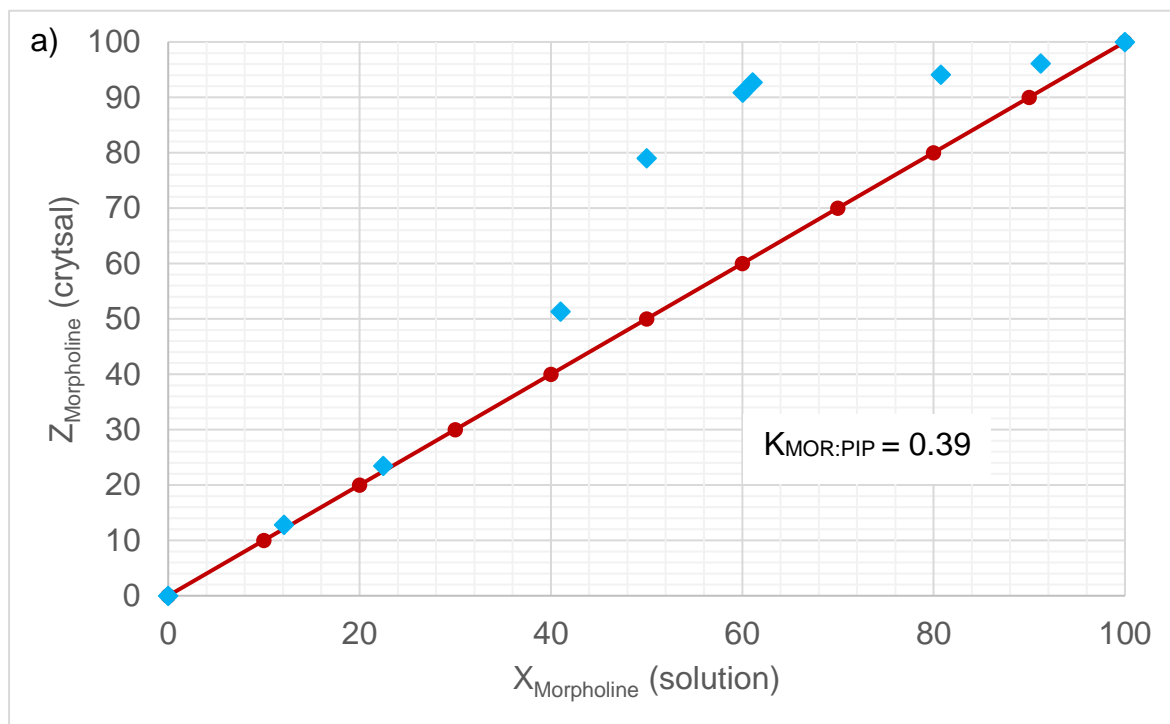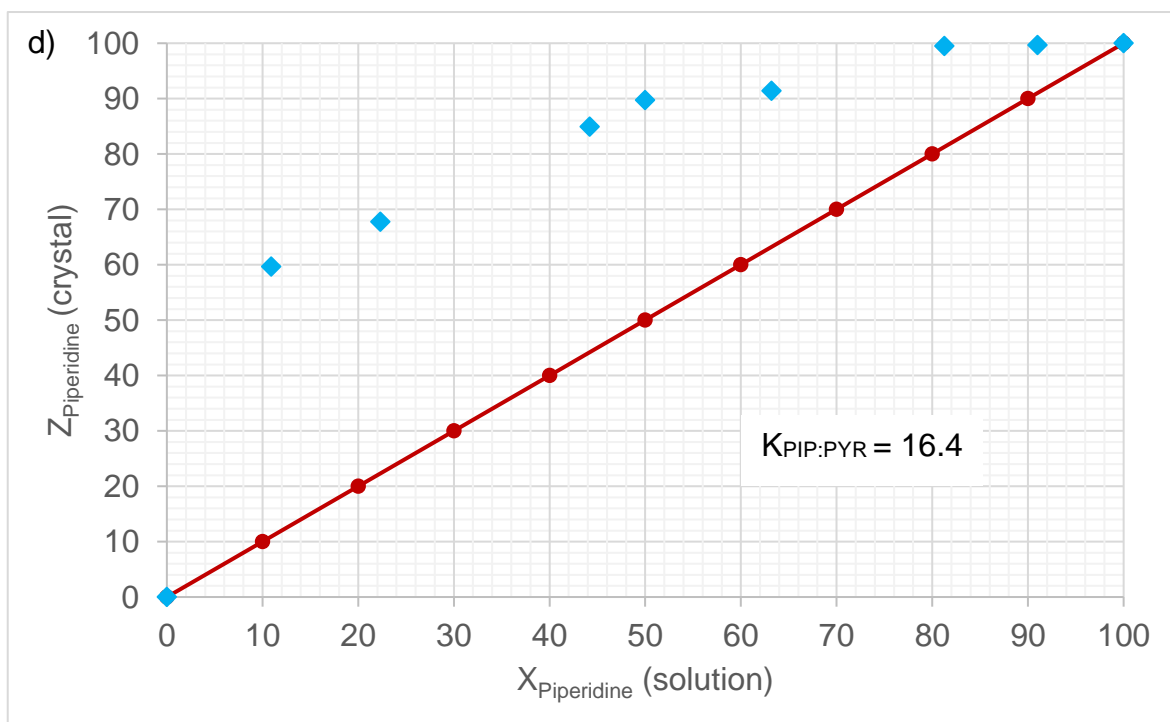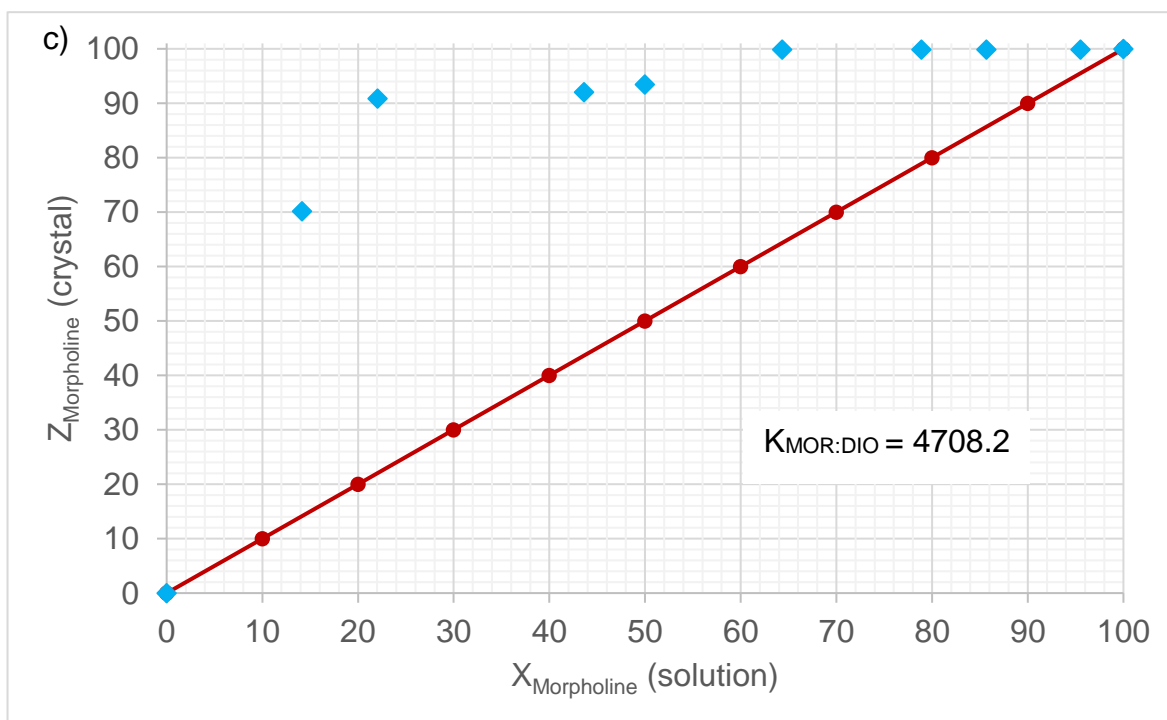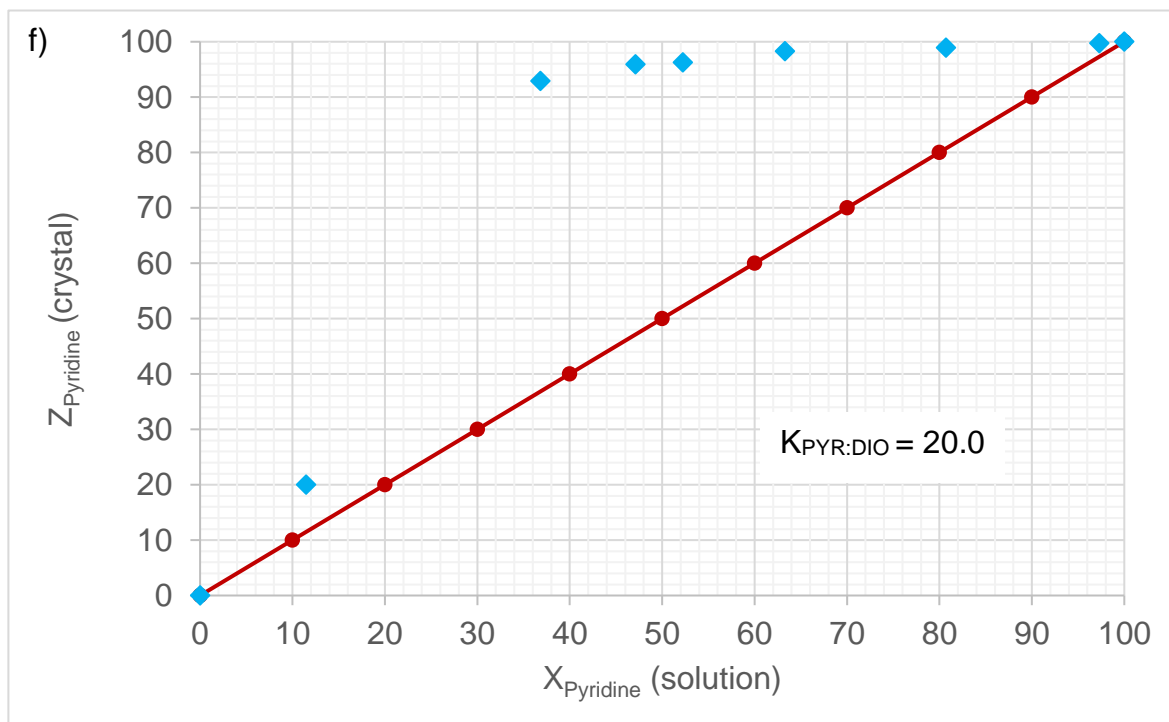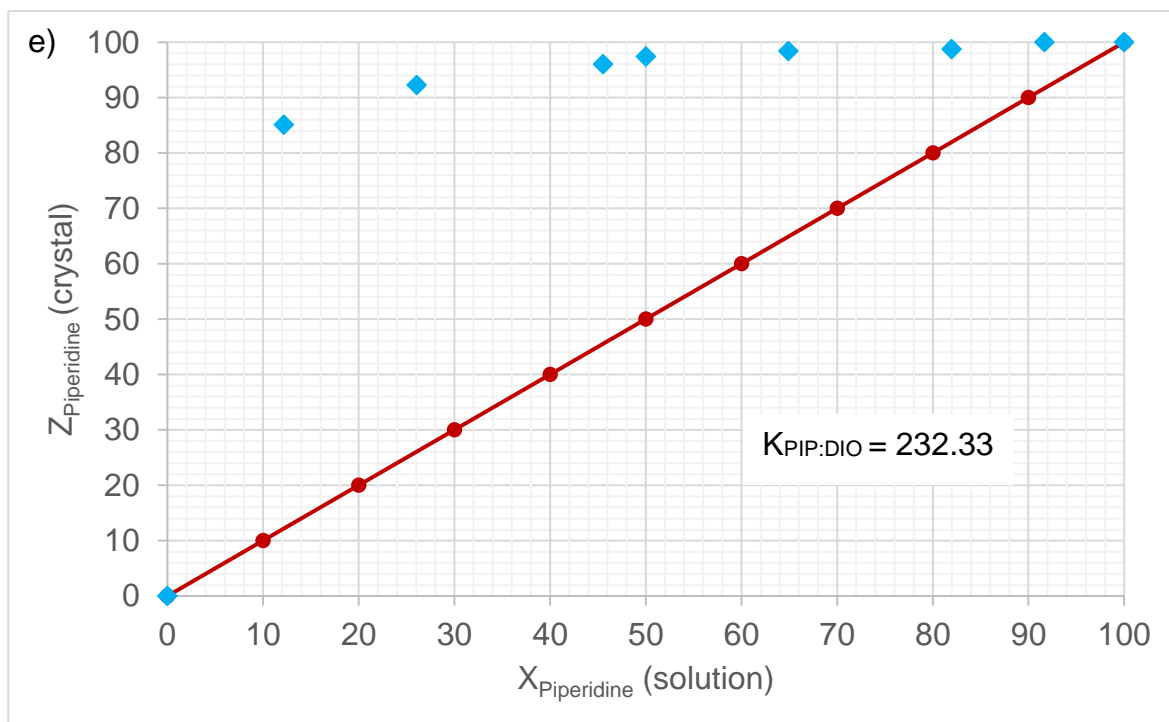
Figure 1: Selectivity curves for a) MOR/PIP, b) MOR/PYR, c) MOR/DIO, d) PIP/PYR, e) PIP/DIO and f) PYR/DIO

According to these experimental results, low guest selectivity was observed for TET when recrystallized from mixtures containing MOR and PIP, since the selectivity coefficient was determined to be 0.39 (in favour of MOR) (Figure 1a). The selectivity of the host was also guest-concentration dependent: at low concentrations of MOR (up to approximately 22%), no significant host selectivity was observed for either guest. The host showed complete selectivity towards MOR soon after this point (~22.5%). For combinations of MOR/PYR (Figure 1b, $K_{MOR:PYR}$ = 10.5) and MOR/DIO (Figure 1c, $K_{MOR:DIO}$ = 4708.2), a consistent host preference for MOR over PYR and DIO, respectively, was observed for the entire concentration range investigated. It is notable that DIO is significantly discriminated against in the latter experiment. A similar host preference was obtained in the PIP/PYR and PIP/DIO selectivity studies (Figures 1d and e) where both PYR and DIO were discriminated against in favour of PIP. This consistent host preference was also observed in the PYR/DIO experiment, where PYR was clearly favoured over DIO when X_{PYR} > 10% (Figure 1f). Evidently, in the presence of DIO, the host continuously favours the other three heterocyclic guests.

We extended these selectivity experiments to incorporate the ternary guest mixtures observed in Table 2. The results are shown in the ternary plots in Figures 2 and 3, where each apex represents the pure components. In each figure, points A to G represent the seven mother liquor combinations of the three heterocyclic compounds from which the complex crystallised. The percentage composition of the enclathrated guests are shown as points A' to G'. Here we focused on the MOR/PYR/DIO (Figure 2) and MOR/PIP/PYR (Figure 3) ternary mixture experiments and, once more, the results observed from the earlier equimolar competition experiments (Table 2) are reinforced here, where the majority of the complexes were enriched in MOR. This result is clearly displayed in Figure 2b where the red-shaded area represents the mother liquor and the blue-shaded area the percentage of the guests in the crystals: the crystals were all significantly morpholine-enriched. Similar results were obtained for the MOR/PIP/PYR experiments (point D', blue cross, appears to be an outlier).

a)
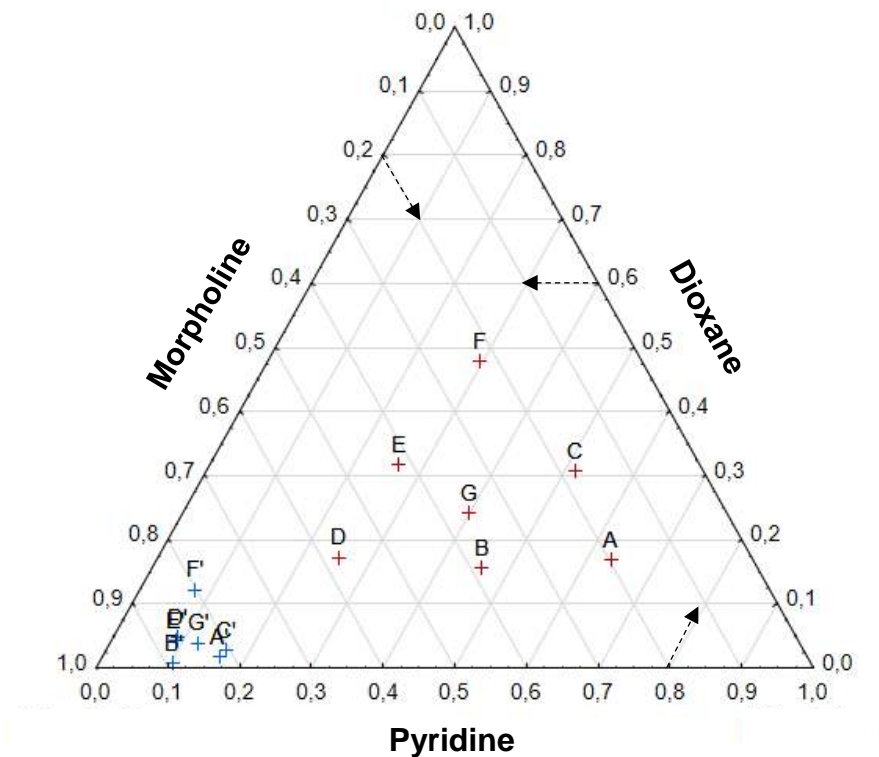
b)
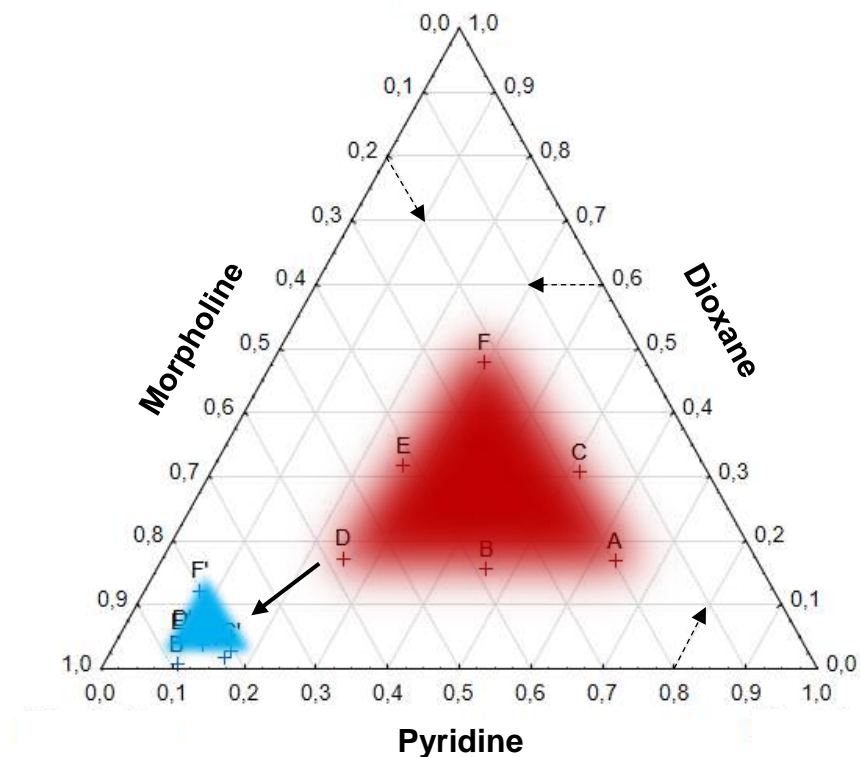
Figure 2: a) Graphical display for the MOR/PYR/DIO ternary experiment; A to G (red crosses) – seven initial mother liquor mixtures of MOR/PYR/DIO with differing guest percentages; A' to G'(blue crosses) – percentage of guests in the crystal; b) Visualization of the preferential guest inclusion of MOR
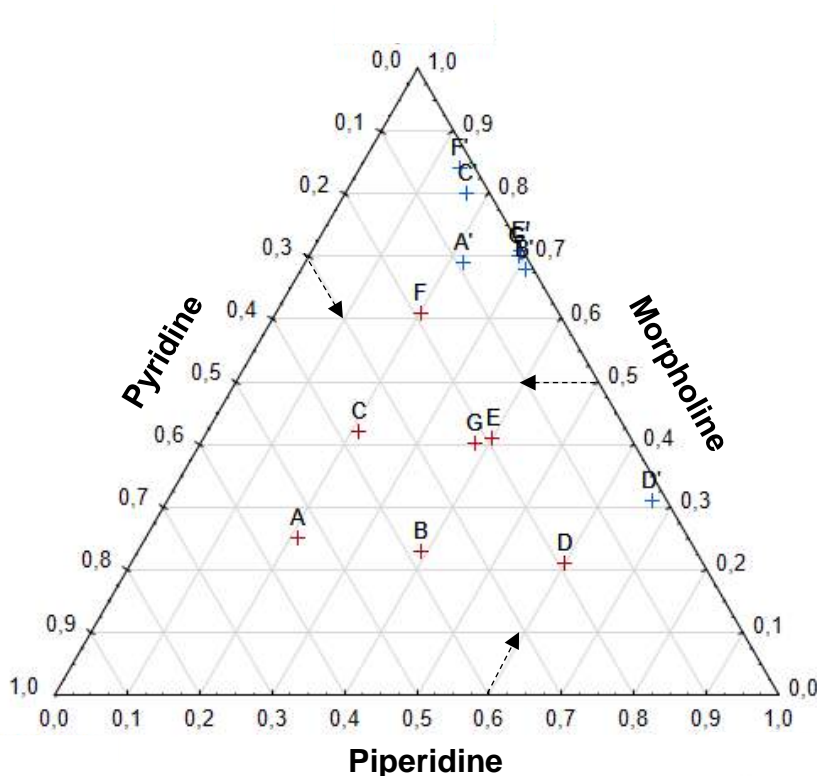
Figure 3: Graphical display for the MOR/PIP/PYR ternary experiment; A to G (red crosses) – seven initial mother liquor mixtures of MOR/PIP/PYR with differing guest percentages; A' to G'(blue crosees) – percentage of guests in the crystal

5.3   Single Crystal X-ray Diffraction (SCXRD)

SCXRD experiments were carried out on suitable crystals of the four successfully-formed complexes. The crystal structures and refinement parameters are provided in Table 3. Both TET·MOR and TET·2PYR crystallize in the triclinic crystal system and $P1$ space group with $Z = 1$, while the TET·2PIP (monoclinic, $I2$, $Z = 4$) and TET·2DIO (orthorhombic, $P2_12_12_1$, $Z = 4$) complexes differ from these and one another (Table 3).

The guest accommodation type was analysed using the Mercury CSD 3.5.1 software package and the guests omitted from the packing calculation, and the remaining voids displayed (Figures 4–7). The crystal packing of TET·MOR and TET·2DIO are characterized by guests situated in cavities (Figures 4 and 5), while the TET·2PYR and TET·2PIP complexes have the guests occupying constricted and reasonably open channels, respectively (Figure 6 and 7).

116

a)

b)
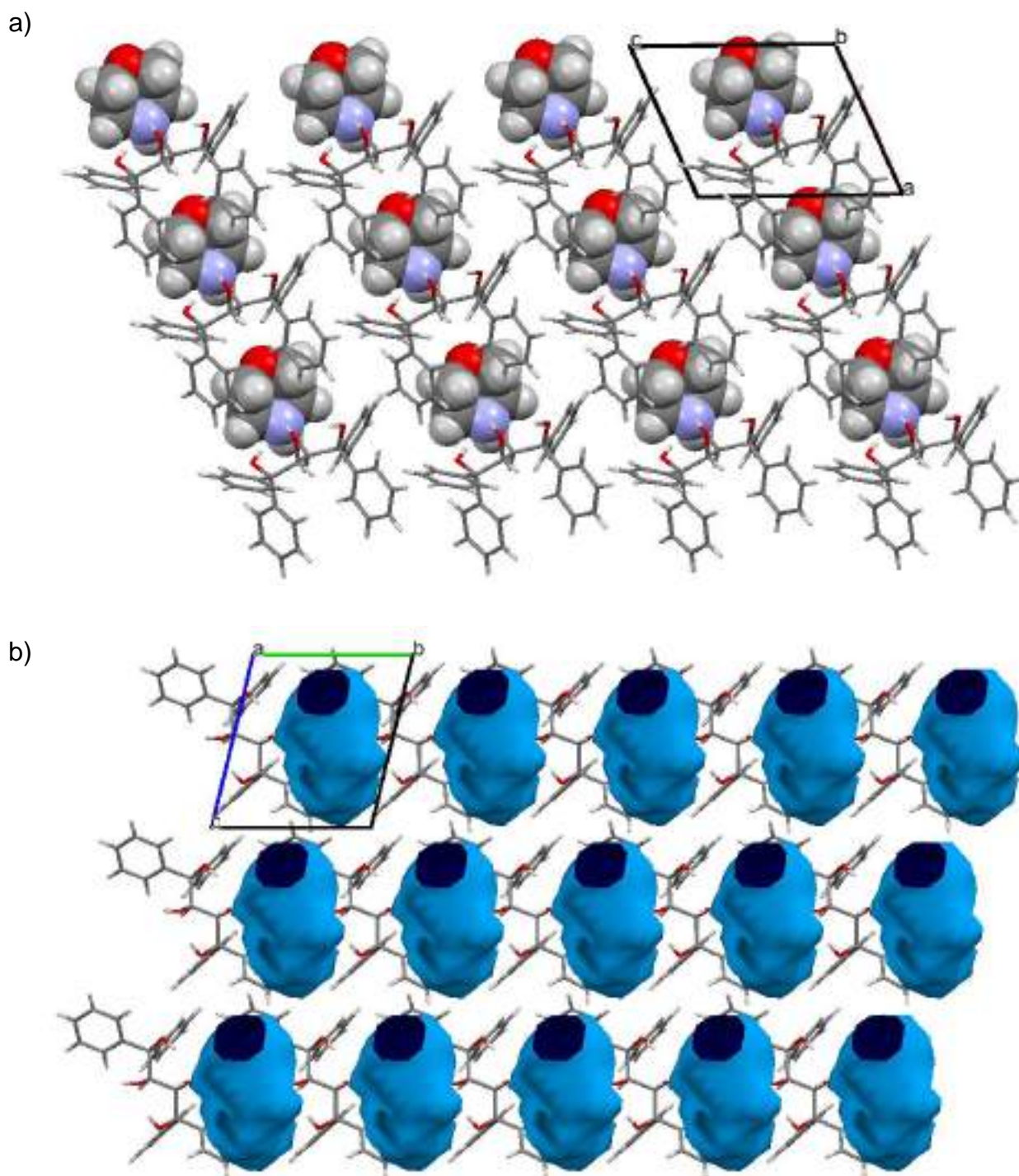
Figure 4: a) Crystal packing of the TET·MOR inclusion complex with guests in spacefill form; b) Calculated voids (light blue) for TET·MOR indicating guest accommodation in discrete cavities; (oxygen – red, nitrogen – blue, carbon – grey and hydrogen – light grey)

a)

b)
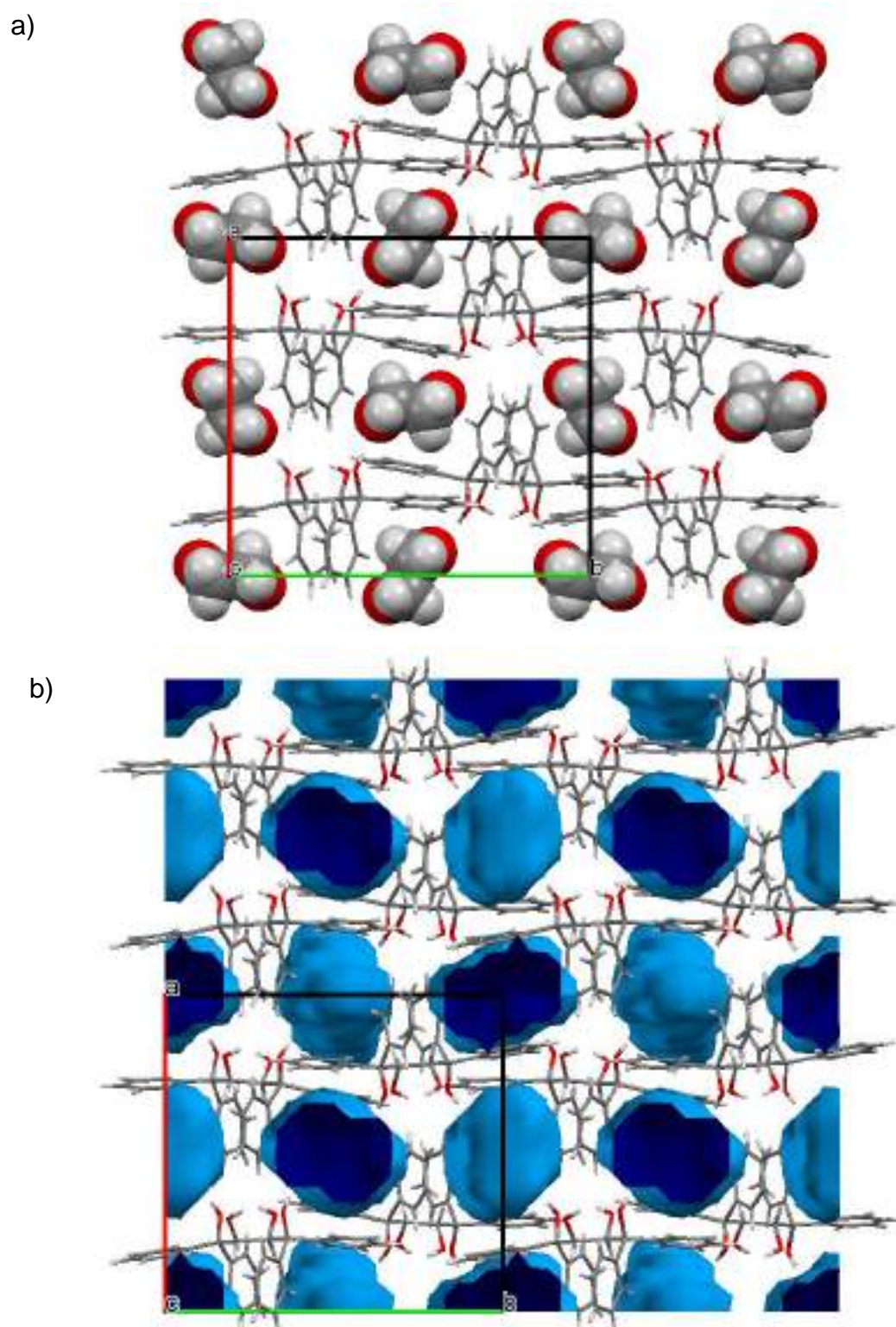
Figure 5: a) Crystal packing of the TET·2DIO inclusion complex with guests in spacefill form; b) Calculated voids (light blue) for TET·2DIO indicating guest accommodation in discrete cavities; (oxygen – red, nitrogen – blue, carbon – grey and hydrogen – light grey)

a)
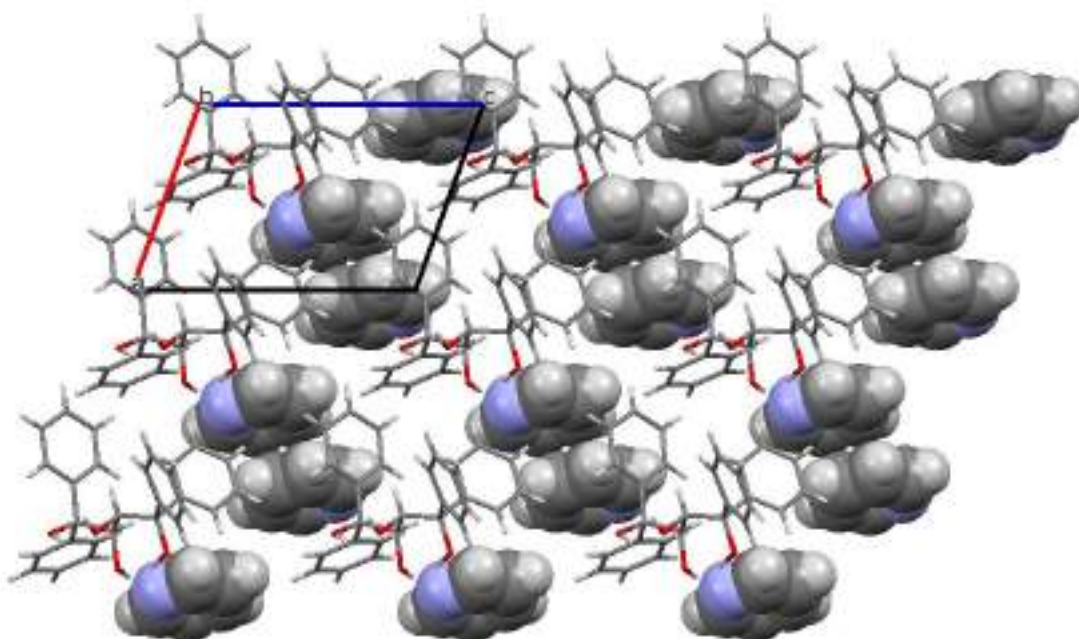
b)
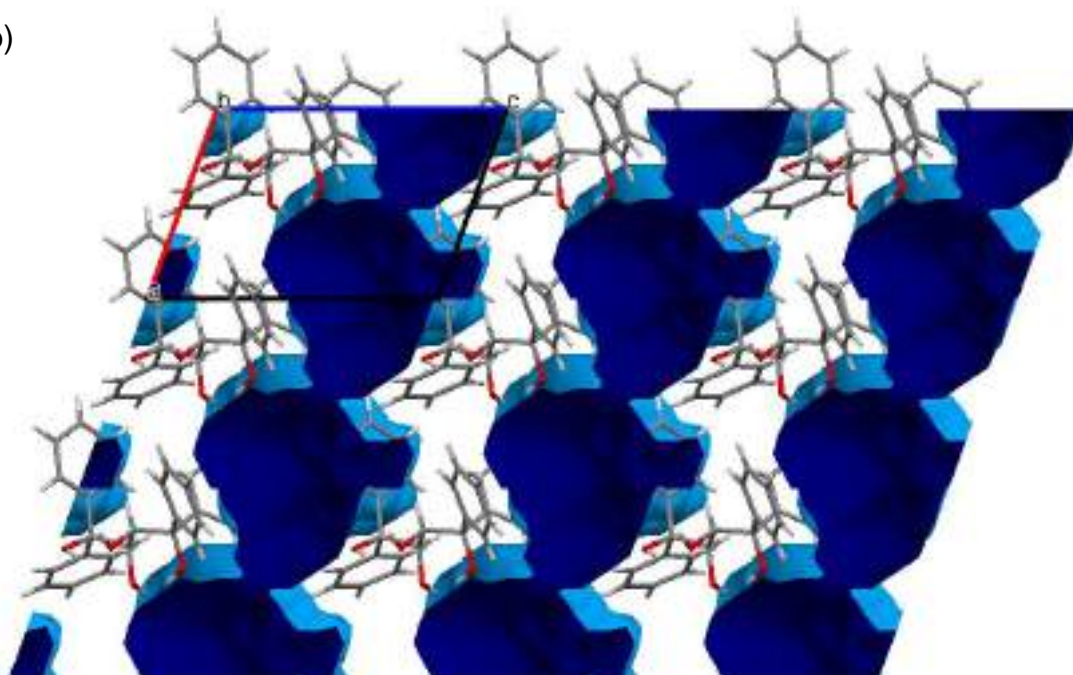
Figure 6: a) Crystal packing of the TET·2PYR inclusion complex with guests in spacefill form; b) Calculated voids (light blue) for TET·2PYR indicating guest accommodation in highly restricted channels; (oxygen – red, nitrogen – blue, carbon – grey and hydrogen – light grey)

a)

b)
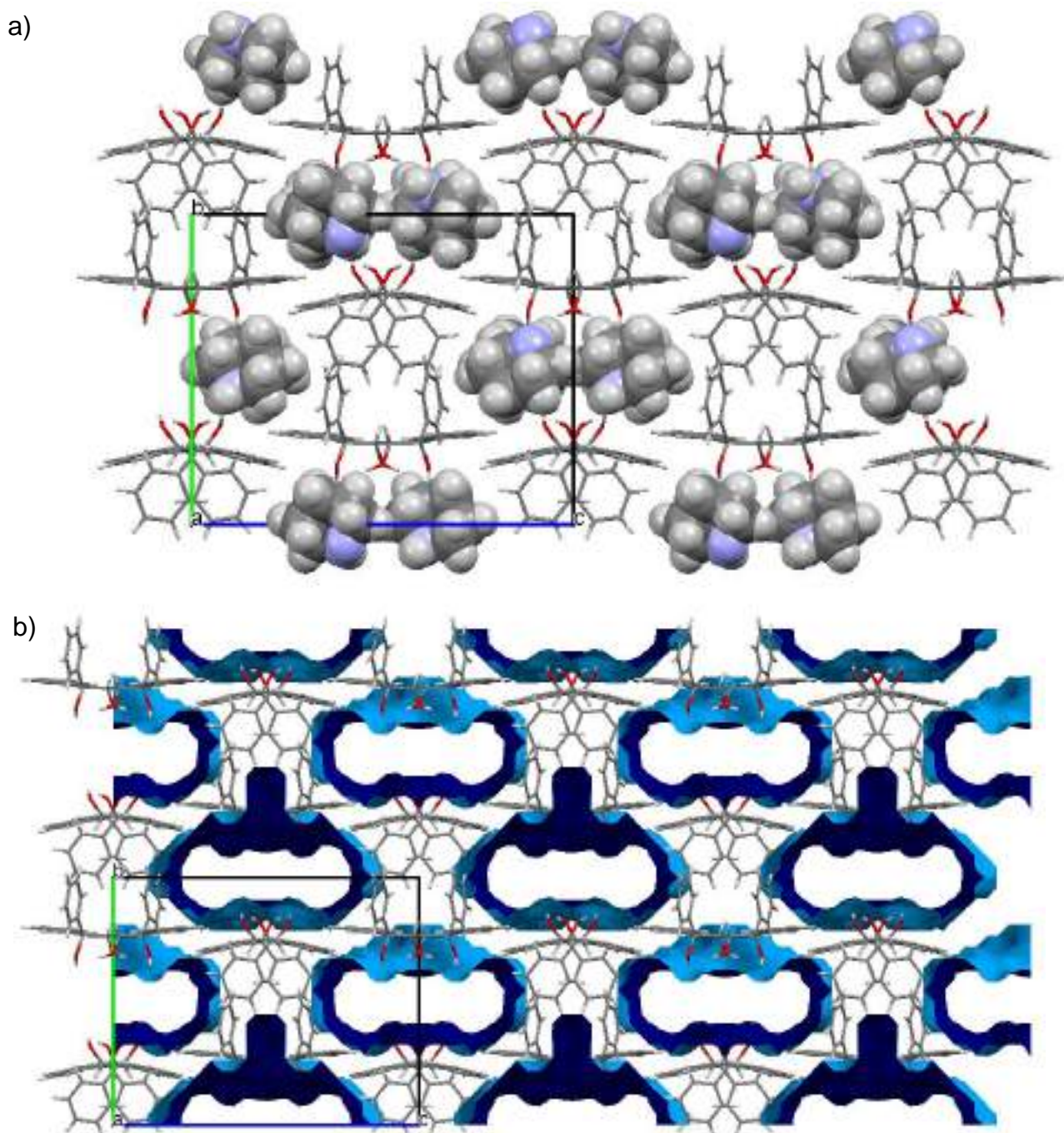
Figure 7: a) Crystal packing of the TET·2PIP inclusion complex with guests in spacefill form; b) Calculated voids (light blue) for TET·2PIP indicating guest accommodation in reasonably open channels; for both host molecules, half the molecule is symmetry-generated from the other half (around a two-fold proper rotational axis) and hence the presence of two hosts and two guests in the unit cell; (oxygen – red, nitrogen – blue, carbon – grey and hydrogen – light grey)

Table 3: Relevant single crystal X-ray crystallographic data for the complexes of TET with MOR, PIP, PYR and DIO

	TET·MOR	TET·2PIP	TET·2PYR	TET·2DIO
Chemical formula	$C_{28}H_{26}O_4$· C_4H_9NO	$C_{28}H_{26}O_4$· $2(C_5H_{11}N)$	$C_{28}H_{26}O_4$· $2(C_5H_5N)$	$C_{28}H_{26}O_4$· $2(C_4H_8O_2)$
Formula weight	513.61	596.78	584.69	514.59
Crystal system	Triclinic	Monoclinic	Triclinic	Orthorhombic
Space group	$P1$	$I2$	$P1$	$P2_12_12_1$
μ (Mo Kα)/mm^{-1}	0.086	0.074	0.083	0.083
a/Å	8.2222(3)	11.1907(8)	8.2430(2)	14.993(5)
b/Å	8.6821(3)	15.7825(11)	9.7660(2)	16.008(7)
c/Å	10.3388(4)	19.8092(13)	10.8739(3)	11.709(5)
α/°	100.217(2)	90	90.663(1)	90
β/°	111.765(2)	100.839(4)	108.101(1)	90
γ/°	96.176(2)	90	113.368(2)	90
V/Å^3	662.32(4)	3436.2(4)	754.62(3)	2810(2)
Z	1	4	1	4
F (000)	274	1288	310	1096
Temp (K)	200	200	150	200
Restraints	3	1	1	0
Nref	6262	8102	3732	7019
Npar	352	409	405	347
R1	0.0362	0.0387	0.0336	0.0414
wR2	0.0963	0.1036	0.0908	0.1025
S	1.04	1.02	1.04	1.02
Θ min, max/°	2.4, 28.4	1.7, 28.3	2.3, 28.4	1.7, 28.4
Tot. data	22 557	28393	38700	23317
Unique data	6262	8102	3732	7019
Observed data [I > 2.0σ(I)]	5790	7075	3666	5768
Rint	0.022	0.016	0.016	0.025
Diffrn measured fraction Θ full	0.992	1	0.992	1
Min. resd. dens. (e/Å^3)	−0.18	−0.16	−0.26	−0.20
Max. resd. dens. (e/Å^3)	0.23	0.23	0.29	0.22

5.3.1 H-Bonding Interactions Between Host and Guest Species

The host's geometry is stabilised by a pair of 1,3-intramolecular hydrogen bonds, and each guest is held in the crystal either by means of (guest)C−O···H−O(host) or (guest)C−N···H−O(host) hydrogen bonds involving only the secondary host hydroxyl groups. Once more, to determine which guest experiences the strongest H-bond with TETROL, we compared the O···O and O···N distances formed between the host and guest (Table 4).[179,180] From Table 5, the strength of these H-bonds decrease in the order TET·MOR (0.360 Å) > TET·2PIP (0.350 and 0.314 Å) > TET·2PYR (0.328 and 0.316 Å) > TET·2DIO (0.311 and 0.249 Å). This order is in direct accordance with the selectivity order observed from the competition experiments between TETROL and the four heterocyclic compounds, and here alludes to the importance of guest H-bonding to the host during these competition experiments.

Table 4: Analysis of intermolecular hydrogen bonding interactions between TET and guests MOR, PIP, PYR and DIO

Guest	Unit cell H:G ratio	Guest[†]	(host)O··· X(guest) /Å	(host)H··· X(guest) /Å	(host)O–H ···X(guest) /˚	Symmetry operator
MOR	1:1	MOR[1]	2.710(3) X=N	1.92	157	x,–1+y,z
PIP	1:2	PIP[1]	2.720(2) X=N	1.88	175	x,y,z
		PIP[2]	2.756(2) X=N	1.94	165	x,y,z
PYR	1:2	PYR[1]	2.754(2) X=N	1.94	167	x,y,z
		PYR[2]	2.742(2) X=N	1.93	165	x,y,z
DIO	1:2	DIO[1]	2.729(2) X=O	1.92	162	x,y,z
		DIO[2]	2.791(2) X=O	1.98	162	x,y,z

[†]The TET·MOR complex is comprised of one guest in an unique environment whereas TET·2PIP, TET·2PYR and TET·2DIO are each comprised of two guests in unique environments. Hence these guests have been labelled MOR[1], PIP[1], PIP[2], PYR[1], PYR[2], DIO[1] and DIO[2]

Table 5: The calculated hydrogen bond strength for the guest in each complex with TETROL

Complex	Theoretical (host)O···X(guest)/Å (A)	Experimental (host)O···X(guest) /Å (B)	$\Delta_{(A)-(B)}$ / Å
TET·MOR	3.07 X = N	2.710(3) X=N	0.360
TET·2PIP	3.07 X = N	2.720(2) X=N	0.350
		2.756(2) X=N	0.314
TET·2PYR	3.07 X = N	2.754(2) X=N	0.316
		2.742(2) X=N	0.328
TET·2DIO	3.04 X = O	2.729(2) X=O	0.311
		2.791(2) X=O	0.249

5.3.2 Short Ring (π···π) and X–H···π Interactions Between Host and Guest Species

Each crystal complex with TET experiences (host)π···π(host) interactions in the range 4.713–5.989 Å (Table 6). Complementing the anchoring role of the (host)O−H···N(guest) and (host)O−H···O(guest) hydrogen bonds are the presence of multiple, cooperative (guest)CH···π(host) and (guest)π···π(host) stabilizing interactions (in the case of PYR). Both pyridine guests in the TET·2PYR complex are stabilised by (host)π···π(guest) interactions [Table 5, 3.670(2)–5.9314(1) Å (10)] and accompanying these interactions are also (guest)π···π(guest) contacts [Table 6, 3.620(2) Å] where the pyridine guest molecules are situated in a sandwich configuration with their dipoles aligned anti-parallel to one another (Figure 8). This pyridine dimer configuration has been computed by Hohenstein and Sherrill[190] to be a favourable electrostatic interaction between two pyridine molecules. The other complexes do not experience these inclusions with the host due to their non-aromatic nature.
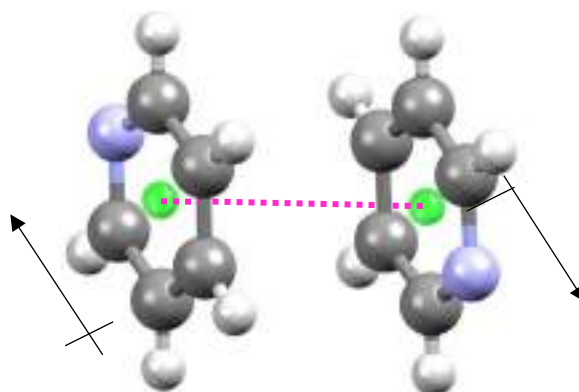
Figure 8: Stabilising (guest)π···π(guest) interaction (pink dotted line) between two pyridine guest molecules situated in a sandwich configuration with their dipoles positioned anti-parallel to one another

In the crystal of TET·2PYR, stabilization of the guest is mediated by two (guest)*m*-ArH···π(host) interactions (Table 6, 2.70, 2.98 Å and 152, 142°, respectively) and one (host)C–H···π(guest) interaction (Table 6, 2.99 Å 133°). Further stabilization occurs due to two short contacts of the type (guest)C–H···C_{Ar}(host) (Table 6, 2.80 and 2.88 Å, with angles of 152 and 166°) as well as one (host)*m*-ArH···H–C(guest) interaction (Table 6, 2.27 Å, 178°). It was noted that pyridine experiences guest–guest stabilization through a (guest)C_{Ar}···C_{Ar}(guest) (3.38 Å) short contact. The TET·MOR complex experiences a (guest)C–H···π(host) interaction and (host)*o*-ArH···O(guest) short contact (2.66 and 2.66 Å, with angles of 147 and 131°, respectively). No C–H···π interactions were observed for complexes containing PIP and DIO, but the TET·2DIO complex is stabilized by a (host)C–H···O(host) short contact of 2.60Å with an angle of 139°. These data were incapable of supporting the selectivity order of TETROL for these guests.

Table 6: Short ring-interactions (π···π) for the complexes of 1 with MOR, PIP, PYR and DIO

Interaction	TET·MOR	TET·2PIP	TET·2PYR	TET·2DIO
π···π (Host···Guest)	–	–	3.670(2)–5.9314(1) (10 contacts)	–
π···π (Host···Host)	4.728(2)–5.989(2) (10 contacts)	4.7702(1)–5.821(2) (10 contacts)	4.713(2)–5.8800(1) (9 contacts)	4.795(3)–5.936(3) (8 contacts)
π···π (Guest···Guest)	–	–	3.620(2) (1 contact)	–
CH···π	2.66 Å, 147° (H···Cg, C–H···Cg) (guest)C–H···π(host)	–	2.99 Å, 133° (H···Cg, C–H···Cg) (host)C–H···π(guest) 2.98 Å, 142° (H···Cg, C–H···Cg) (guest)*m*-ArH···π(host) 2.70 Å, 151° (H···Cg, C–H···Cg) (guest) *m*-ArH···π(host)	–
Short contacts	2.66 Å, 131° (H···Cg, C–H···Cg) (host)o-ArH···O(guest)	–	2.88 Å, 166° (H···Cg, C–H···Cg) (guest)C–H···C_{Ar}(host) 2.80 Å, 152° (H···Cg, C–H···Cg) (guest)C–H···C_{Ar}(host) 2.27 Å, 178° (H···Cg, C–H···Cg) (host)*m*-ArH···H–C(guest) 3.38 Å, (H···Cg, C–H···Cg) (guest)C_{Ar}···C_{Ar}(guest)	2.60 Å, 139° (H···Cg, C–H···Cg) (host)C–H···O(host)

5.4   Hirshfeld Surface Analysis

Hirshfeld surface analyses were conducted on the TET·MOR, TET·2PIP, TET·2PYR and TET·2DIO complexes to assist in summarising, quantitatively, the multiple intermolecular interactions present (Figure 9). A summary of the percentage of each interaction type is displayed graphically in Figure 10, while Table 7 provides the actual values obtained from this figure.

1·MOR

1·PIP [1]

1·PIP [2]

1·PYR [1]

1·PYR [2]

1·DIO [1]

1·DIO [2]
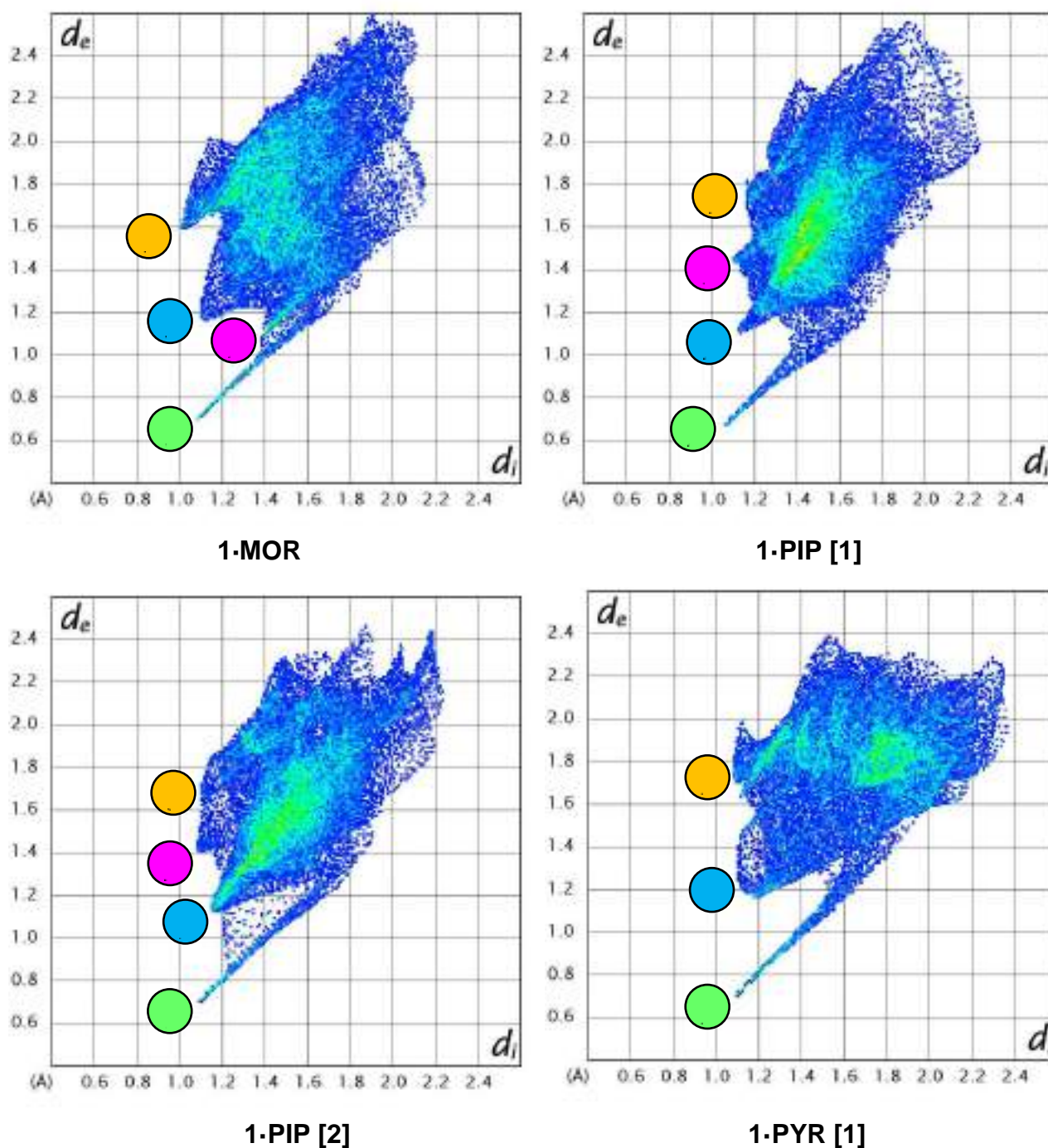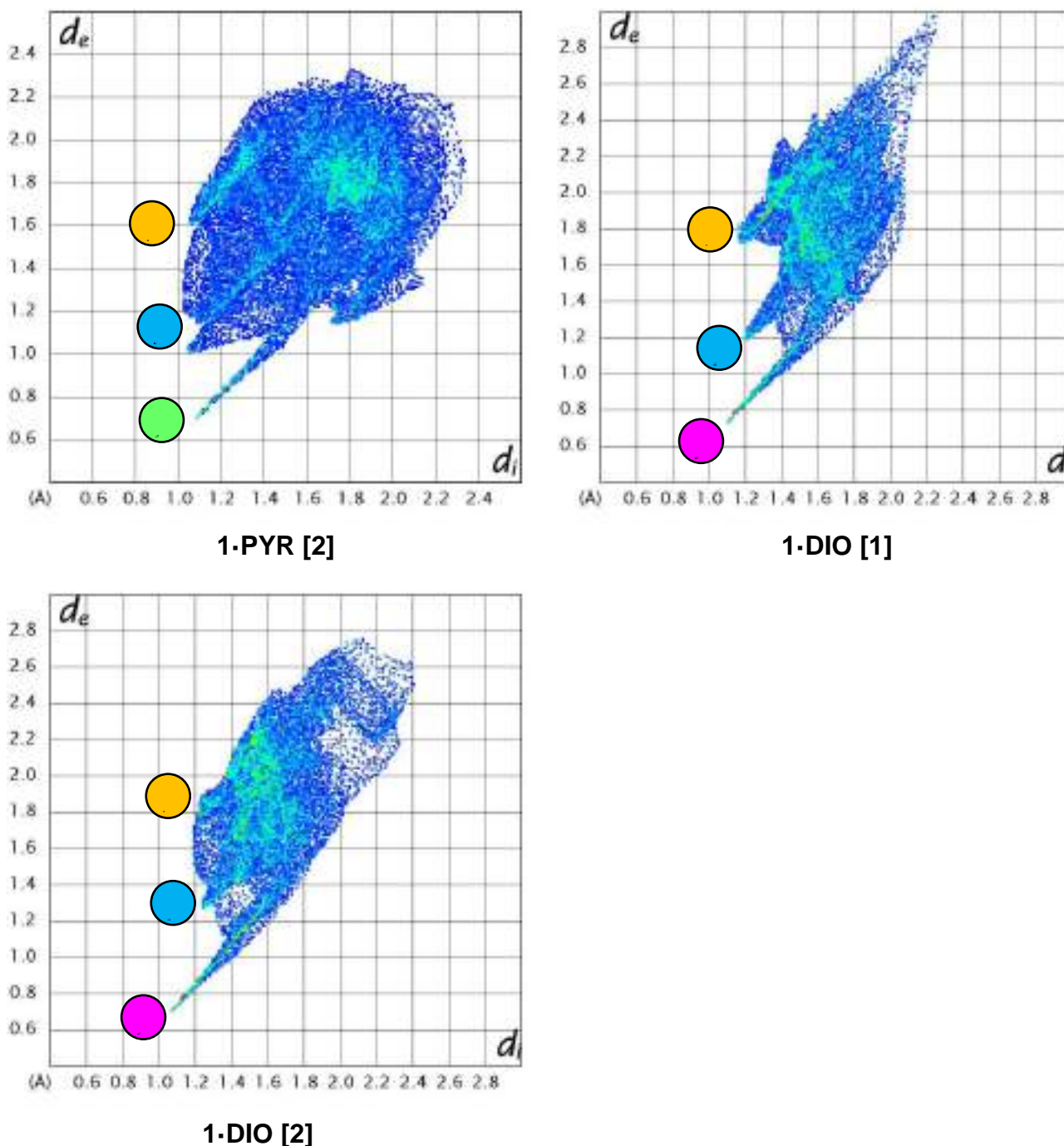
Figure 9: Hirshfeld fingerprint plots for TET·MOR, TET·2PIP[1], TET·2PIP[2], TET·2PYR[1], TET·2PYR[2], TET·2DIO[1] and TET·2DIO[2]; The 'spike' and 'wings' observed in the Hirshfeld plots are colour coded and represent N⋯H (green), O⋯H (magenta), H⋯H (blue) and C⋯H (orange) contacts

The 'spike' and 'wings' observed in the Hirshfeld plots are colour-coded and represent N⋯H (green), O⋯H (magenta), H⋯H (blue) and C⋯H (orange) contacts, respectively. The predominant interactions in each structure are due to the H⋯H close

contacts (Figure 10). It is interesting to note that TET·2PIP has the highest percentage of H···H contacts (84.8, 85.1%) but the lowest percentage of C···H contacts (7.6, 9.7%). Overall, a possible explanation for the observed selectivity for MOR is not obvious from these analyses. MOR does not display any significant number of favourable interactions in comparison with the other complexes. We therefore decided to analyse the four complexes using thermal analysis.
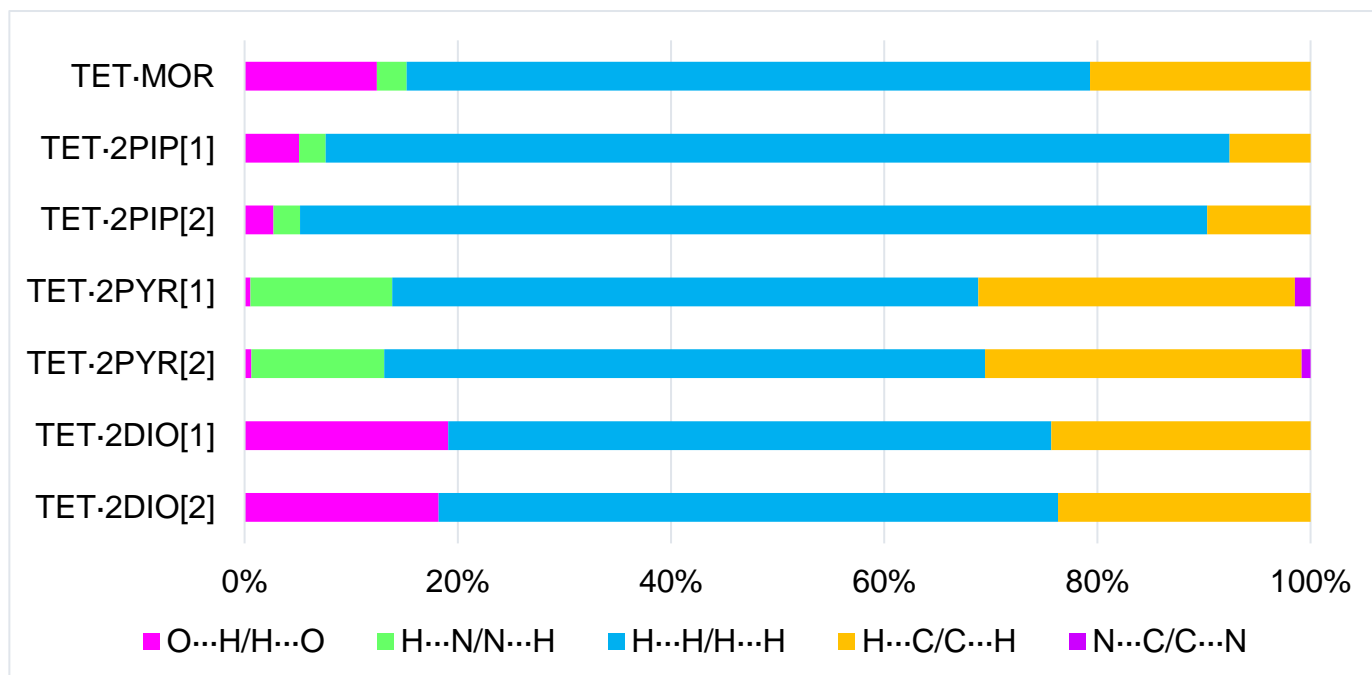
Figure 10: Graphical display showing the percentage intermolecular interactions of each type for the TET·MOR, TET·2PIP, TET·2PYR and TET·2DIO

Table 7: Percentage intermolecular interactions in each inclusion complex (G···H/H···G)

	O···H/H···O	H···N/N···H	H···H/H···H	H···C/C···H	N···C/C···N
1·MOR	12.4	2.8	64.1	20.7	0.0
1·PIP [1]	5.1	2.5	84.8	7.6	0.0
1·PIP [2]	2.7	2.5	85.1	9.7	0.0
1·PYR [1]	0.5	11.8	48.9	26.4	1.3
1·PYR [2]	0.6	11.7	53.0	27.9	0,8
1·DIO [1]	19.1	0.0	56.5	24.3	0.0
1·DIO [2]	18.2	0.0	58.1	23.7	0.0

5.5   Thermal Analyses

Both DSC and TG experiments were carried out on the four inclusion complexes. The traces obtained are given in Figures 11a−d. Upon heating of TET·MOR, a stepwise guest release process ensues (Figure 11a), with an onset temperature (T_{on}) of ~75.4 °C (Table 8). The expected mass loss for the 1:1 H:G complex was calculated to be 17.0%, which is in close agreement with the actual mass loss observed (Table 8, 16.8%). In comparison to TET·MOR, the guest release process for TET·2PIP is somewhat more complex, with a T_{on} of 73.8 °C (Figure 11b), and it appears as though both the guest release and host melt processes occur concomitantly. The observed mass loss (16.5%, Table 8) is not in agreement with that expected for a 1:2 complex (28.5%) and we currently cannot provide an explanation for this observation. Another complex guest release occurs for the TET·2PYR complex, with all the guest released prior to the melting of the host (Figure 11c, 148.3 °C). T_{on} was estimated to be 48.2 °C for this complex, and the loss expected (27.1%) is in agreement with that obtained (25.8%). For the TET·2DIO complex, no visible host melt is observed once more, and the expected mass loss was calculated to be 29.2%, somewhat higher than the actual mass loss observed (Table 8, ~22.4%). T_{on} for this complex could not be identified here due to the fact that the guest is lost from the host crystal at the outset of the experiment (TG), alluding to a guest that is not tightly bound in the crystal, which is in accordance with the observation that TETROL consistently discriminates against DIO in competition experiments.

The fact that the onset temperature for guest release is higher in TET·MOR (75.4 °C) compared with TET·2PIP (73.8°C), TET·2PYR (48.2 °C) and TET·DIO is indicative of the fact that MOR is more tightly bound in the complex. Furthermore, the onset temperatures for the guest release processes correlate exactly with and explains the preference order of TETROL for these guests (MOR > PIP > PYR > DIO).

a)

b)
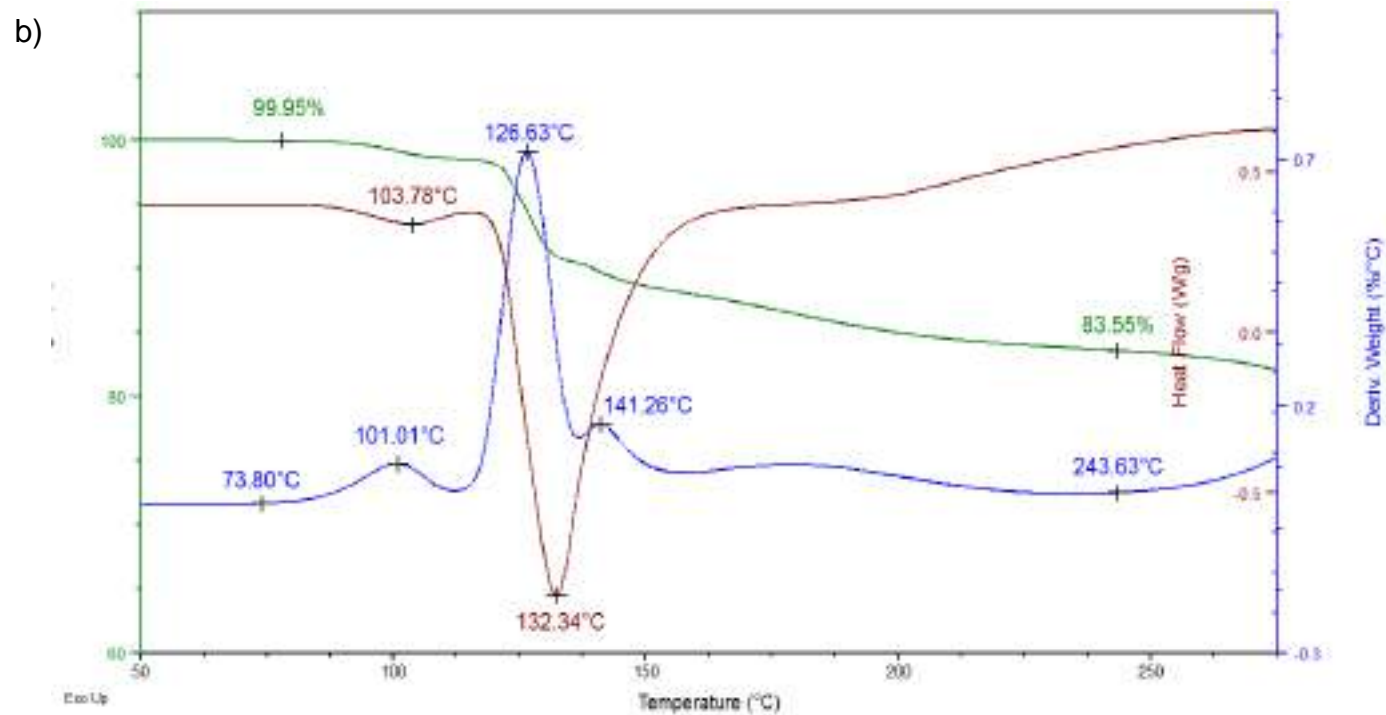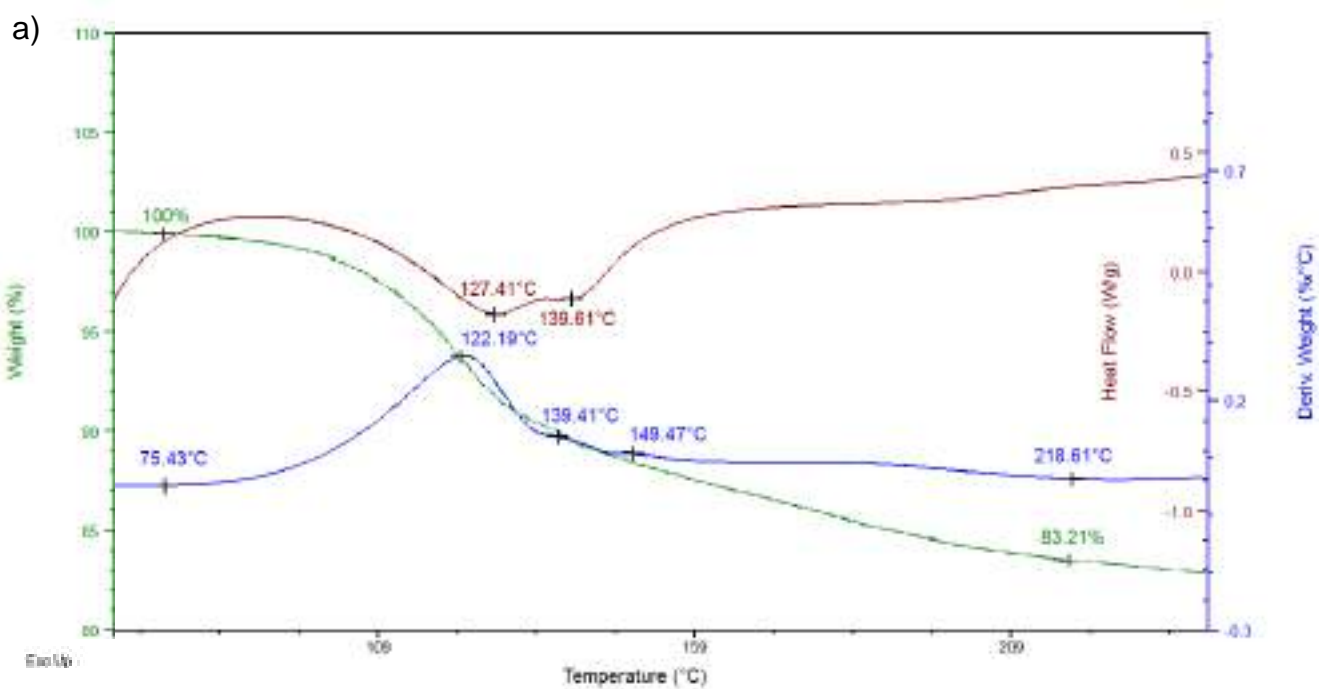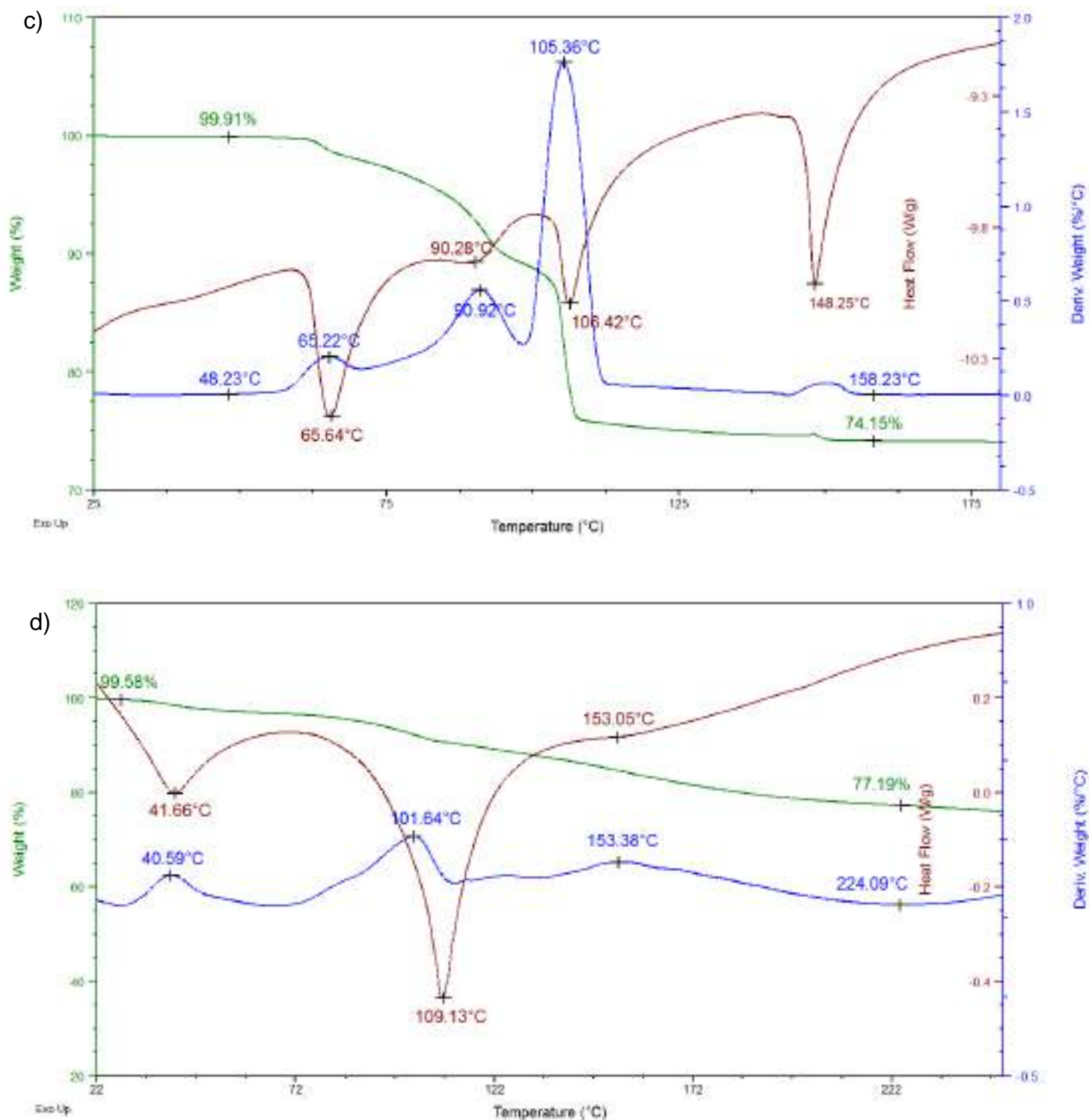
Figure 11: Overlaid traces for the DSC (brown), TG (green) and its derivative (DTG, blue) for the a) TET·MOR, b) TET·2PIP, c) TET·2PYR and d) TET·2DIO complexes

Table 8: Thermal data from DSC/TG traces for of TET·MOR, TET·2PIP, TET·2PYR and TET·2DIO

Guest	T_{on} (°C)	T_p (°C)[a]	T_{end} (°C)[b]	Mass loss % (expected)	Mass loss % (actual)
MOR	75.4	122.2 ~139.4 ~149.5	127.4 ~139.6	17.0	16.8
PIP	73.8	101.0 126.6 141.3	~103.8 132.3	28.5	16.5
PYR	48.2	65.2 90.9 105.4	65.6 ~90.3 106.4 148.3	27.1	25.8
DIO	[c]	40.6 101.6 ~153.4	41.7 109.1 ~153.1	29.2	~22.4[c]

[a]T_p values determined from blue DTG traces
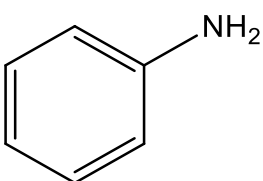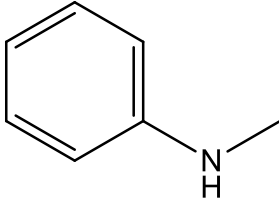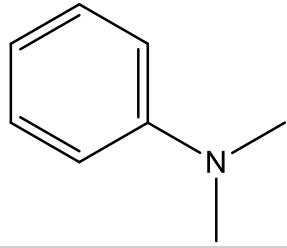
[b]T_{end} were obtained from the brown DSC traces

[c]Guest release occurred from the onset of the experiment, and T_{on} could thus not be identified; the actual mass loss is thus also just an estimation

5.6   Conclusion

The compound TETROL proved to be an effective host for the complexation of morpholine, piperidine, pyridine and dioxane. TETROL showed high selectivity for MOR when recrystallised from mixtures of all four compounds, and a host selectivity order of MOR > PIP > PYR > DIO was obtained. As evidence, SCXRD analysis showed that the TET·MOR complex experienced the strongest host–guest H-bond interaction, while Hirshfeld surface analyses were not useful in this regard. Thermogravimetric analyses confirmed that MOR was more tightly bound in the crystal compared to the other three guests, and T_{on} values correlated exactly with the host's selectivity order.

Chapter 6

Separation of Aniline and Its *N*-Methylated Derivatives

6.1   Introduction

The following investigation explored the separation of the nitrogen-methylated homologues of aniline (ANI), *N*-methylaniline (NMA) and *N,N*-dimethylaniline (NNMA). Aniline and *N*-alkylated aniline derivatives are valuable intermediates for the synthesis of many important industrial chemicals such as dyes, rubbers, pharmaceuticals and agrochemicals, but these processes often require a high degree of purity for these compounds.[191] The industrial synthesis of the *N*-alkylated derivatives from aniline using suitable alkylating agents such as methanol usually produces mixtures of *N*-methylaniline, *N,N*-dimethylaniline and the starting aniline (Scheme 1).[192,193]

aniline   *N*-methylaniline   *N,N*-dimethylaniline

Scheme 1: Methylation of aniline in the presence of methanol producing a mixture of *N*-methylaniline and *N,N*-dimethylaniline

Isolating these amines with high purity is not simple due to the small differences in their boiling points (Table 1). Ordinary separation methods such as simple or fractional distillations are therefore usually impractical. We therefore investigated the plausibility of using TET to separate mixtures of aniline and its nitrogen-methylated derivatives by means of host-guest chemistry. TET enclathrated ANI and NMA forming 2TET·3ANI and 2TET·4NMA complexes, as viewed in Table 1, but did not form an inclusion compound with NNMA, as was observed using proton NMR spectroscopy.

Table 1: The structure and properties of aniline and its nitrogen-methylated homologues

	ANI	NMA	NNMA
Structure			
Host (H):guest (G) ratio	2:3	2:4	—[a]
Boiling point (°C)	184.1	195.7	193.5

[a]Inclusion complex did not form

6.2   Competition Experiments

Considering that the ANI and NMA guests were enclathrated individually, competition experiments were conducted and the selectivity of TET for these guests investigated to establish if the host would discriminate between them. Table 2 summarises the results obtained when TETROL was recrystallized from various equimolar binary and ternary combinations of ANI, NMA and NNMA. The so-formed crystals were analysed using proton NMR spectroscopy and GC-MS. The preferred guest species is given in bold red font face.

Table 2: Competition experiments using TET and various equimolar mixtures of the guests[a,b]

ANI	NMA	NNMA	Guest ratios (%e.s.d.)	Overall H:G ratio
X	X		**68.3** : 31.7 (0.3)	2:3
X		X	**95.1** : 4.9 (0.7)	2:3
	X	X	—[c]	
X	X	X	**67.3** : 28.5 : 4.2 (0.6) (0.6)(0.1)	2:3

[a]Ratios determined using proton NMR spectroscopy and gas chromatography

[b]Experiments were conducted in triplicate; %e.s.d.'s are provided in parentheses

[c]Crystallization failed to occur

From Table 2, it is clear that ANI was the preferred guest in all equimolar competition experiments whenever it was present. In fact, in the absence of ANI, crystallization failed to occur. Binary experiments showed the preference for the three aniline guests to decrease in the order ANI > NMA > NNMA. The equimolar ternary experiment correlated exactly with this order: ANI (67.3%) > NMA (28.5%) > NNMA (4.2%).

Binary competitions were then carried out where the molar ratios of the three aniline compounds were varied beyond equimolar, and the guest selectivity of TET thus evaluated by means of selectivity profiles for ANI/NMA and ANI/NNMA combinations (Figures 1a and b, respectively). Note that, due to the failure to form crystals from NMA/NNMA combinations, a selectivity profile could not be constructed here. Analyses were carried out using NMR and GC-MS as before. In each figure, the straight-line plot (red data points) is a theoretical one, representing the case where the host is completely unselective towards both guests, and is inserted for ease of comparison with the experimentally-determined data points (blue).

a) $K_{ANI:NMA} = 1.93$

$Z_{Aniline}$ (crystal) vs $X_{Aniline}$ (solution)
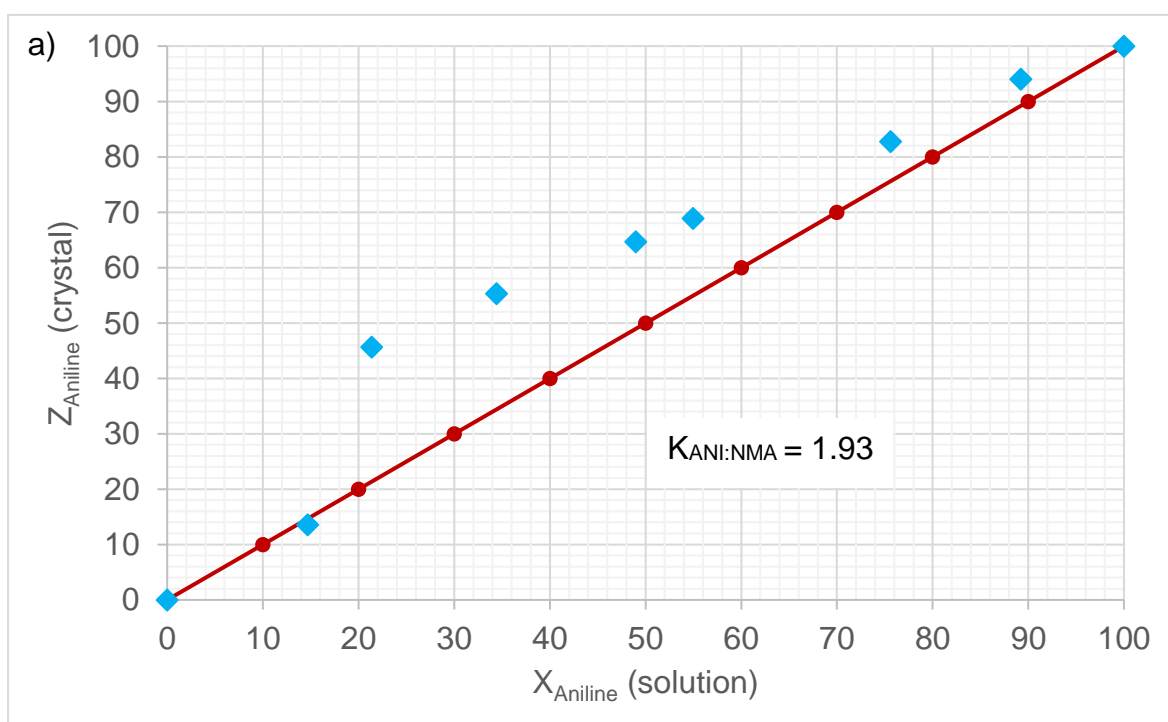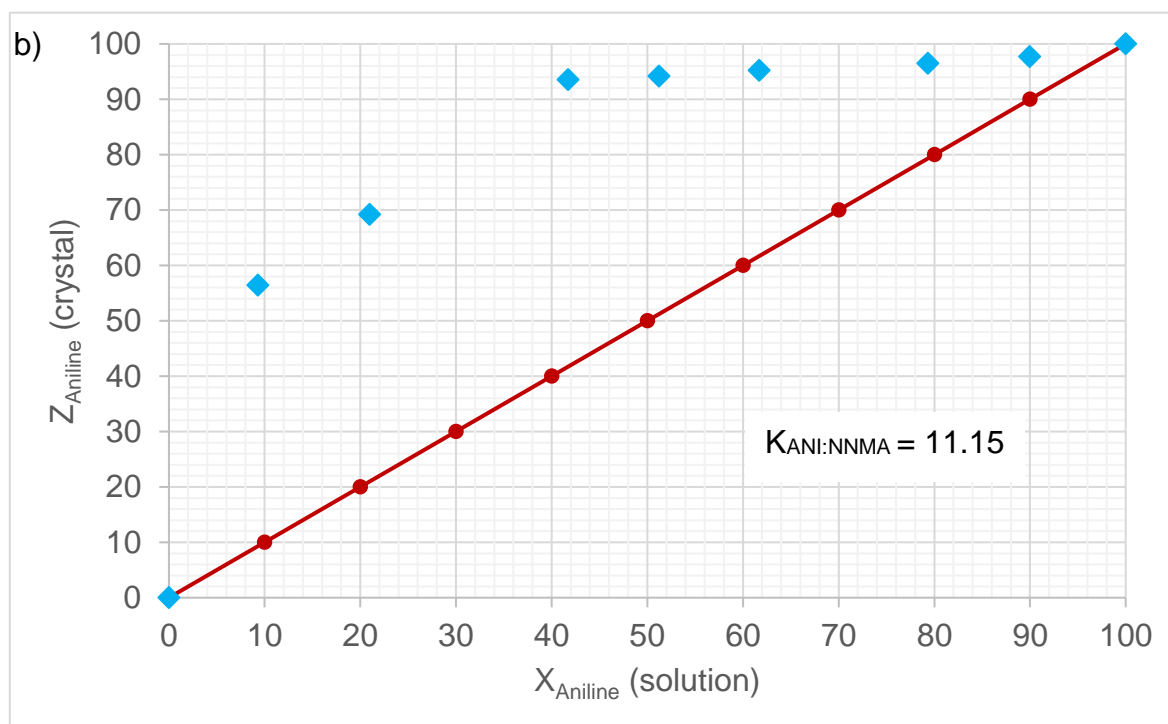
Figure 1: Selectivity curves for a) ANI/NMA and b) ANI/NNMA

According to these experimental results, there was moderate guest selectivity between ANI and NMA, and the guest selectivity coefficient of TET was determined to be 1.93 in favour of ANI. This is demonstrated by the data points obtained for all ANI/NMA combinations assessed (Figure 1a). However, the selectivity of the host was guest-concentration dependent: at low concentrations of ANI (approximately 14.7%), no significant host selectivity was observed for either guest. After this point, ANI is preferred consistently. For combinations of ANI/NNMA, $K_{ANI:NMMA} = 11.5$, and Figure 1b shows a consistent host preference for ANI over NNMA for the entire concentration range.

6.3   Single Crystal X-ray Diffraction (SCXRD)

SCXRD experiments were carried out on suitable crystals of the two successfully-formed complexes. The crystal structures and refinement parameters for 2TET·3ANI and 2TET·4NMA are provided in Table 3. The complex of TET with aniline crystallizes in the orthorhombic crystal system and $P2_12_12_1$ space group with Z = 4. The TET and *N*-methylaniline complex crystallizes in the triclinic crystal system and $P1$ space group

with Z = 2. The guests were omitted from the packing calculation, and the remaining voids displayed (Figures 2 and 3). The 2TET·3ANI complex has the guests accommodated in zig-zagging channels (Figure 2), while the guests in the 2TET·4NMA complex occupy more linear channels in the crystal (Figure 3).

Table 3: Relevant single crystal X-ray crystallographic data for the complexes of TET with ANI and NMA

	2TET·3ANI	2TET·4NMA
Chemical formula	$2(C_{28}H_{26}O_4)\cdot2(C_6H_7N)$, $C_6H_5N^a$	$2C_{28}H_{26}O_4\cdot$ $4(C_7H_9N)$
Formula weight	1130.34	640.79
Crystal system	Orthorhombic	Triclinic
Space group	$P2_12_12_1$	P_1
μ (Mo Kα)/mm^{-1}	0.080	0.078
a/Å	17.3680(9)	11.5756(6)
b/Å	17.5435(9)	13.1533(7)
c/Å	20.0346(10)	13.6373(6)
α/°	90	62.163(2)
β/°	90	89.734(2)
γ/°	90	74.043(2)
V/Å^3	6104.5(5)	1746.56(16)
Z	4	2
F (000)	2400	684
Temp (K)	200	200
Restraints	6	3
Nref	15216	16209
Npar	758	893
R1	0.0401	0.0338
wR2	0.1135	0.0788
S	1.04	1.02
Ө min, max/°	1.5, 28.3	1.7, 28.3
Tot. data	147780	62431
Unique data	15216	16209
Observed data [I > 2.0σ(I)]	12442	14356
Rint	0.023	0.020
Diffrn measured fraction Ө full	1.000	1.000
Min. resd. dens. (e/Å^3)	−0.32	−0.17
Max. resd. dens. (e/Å^3)	0.40	0.22

^{a}Hydrogen atoms could not be placed during SCXRD structural refinement of crystal structure

a)

b)
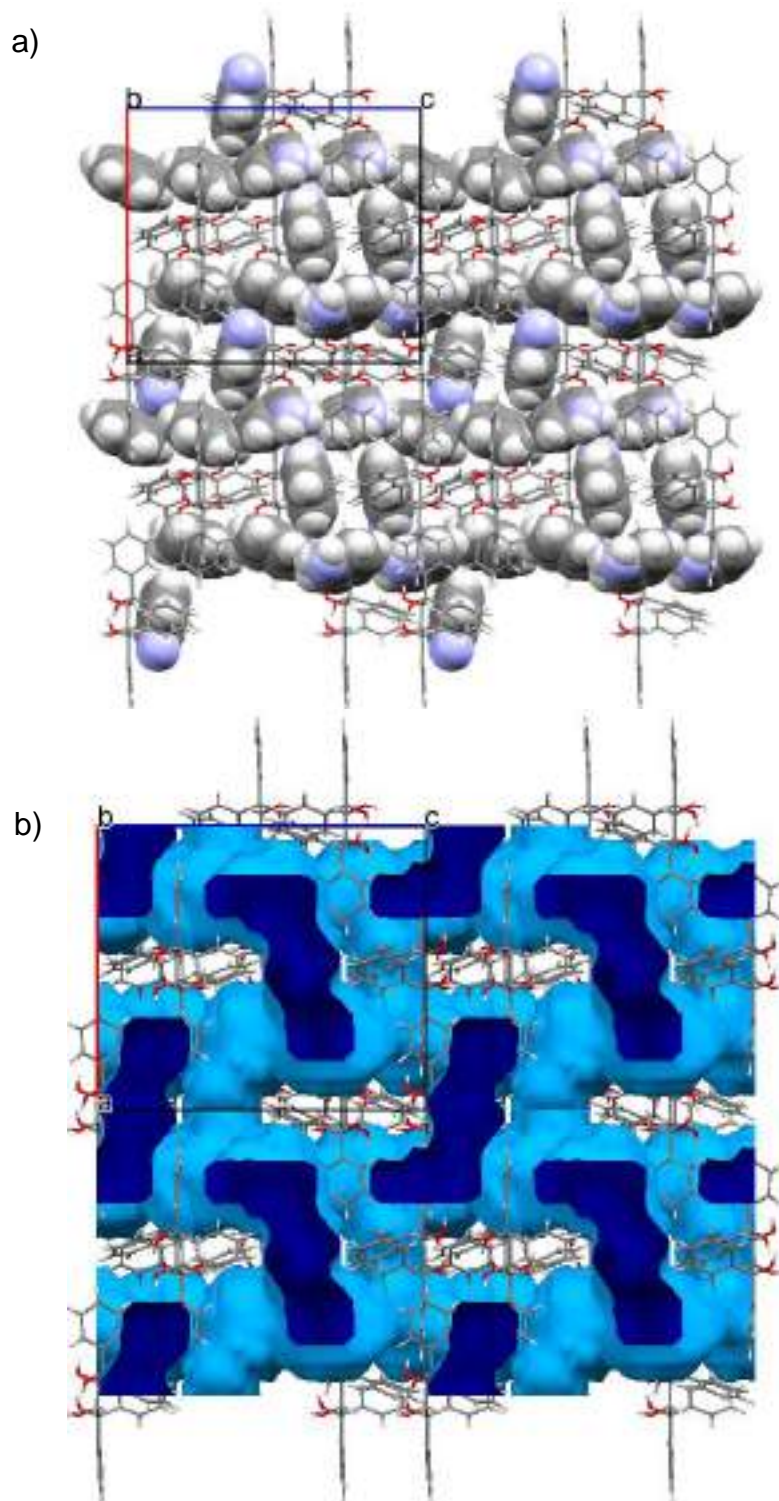
Figure 2: a) Crystal packing of 2TET·3ANI inclusion complex with guest in spacefill form; b) Calculated voids (dark blue) for 2TET·3ANI indicating guest accommodation in zig-zagging channels; oxygen – red, nitrogen – blue, carbon – grey and hydrogen – light grey

a)

b)
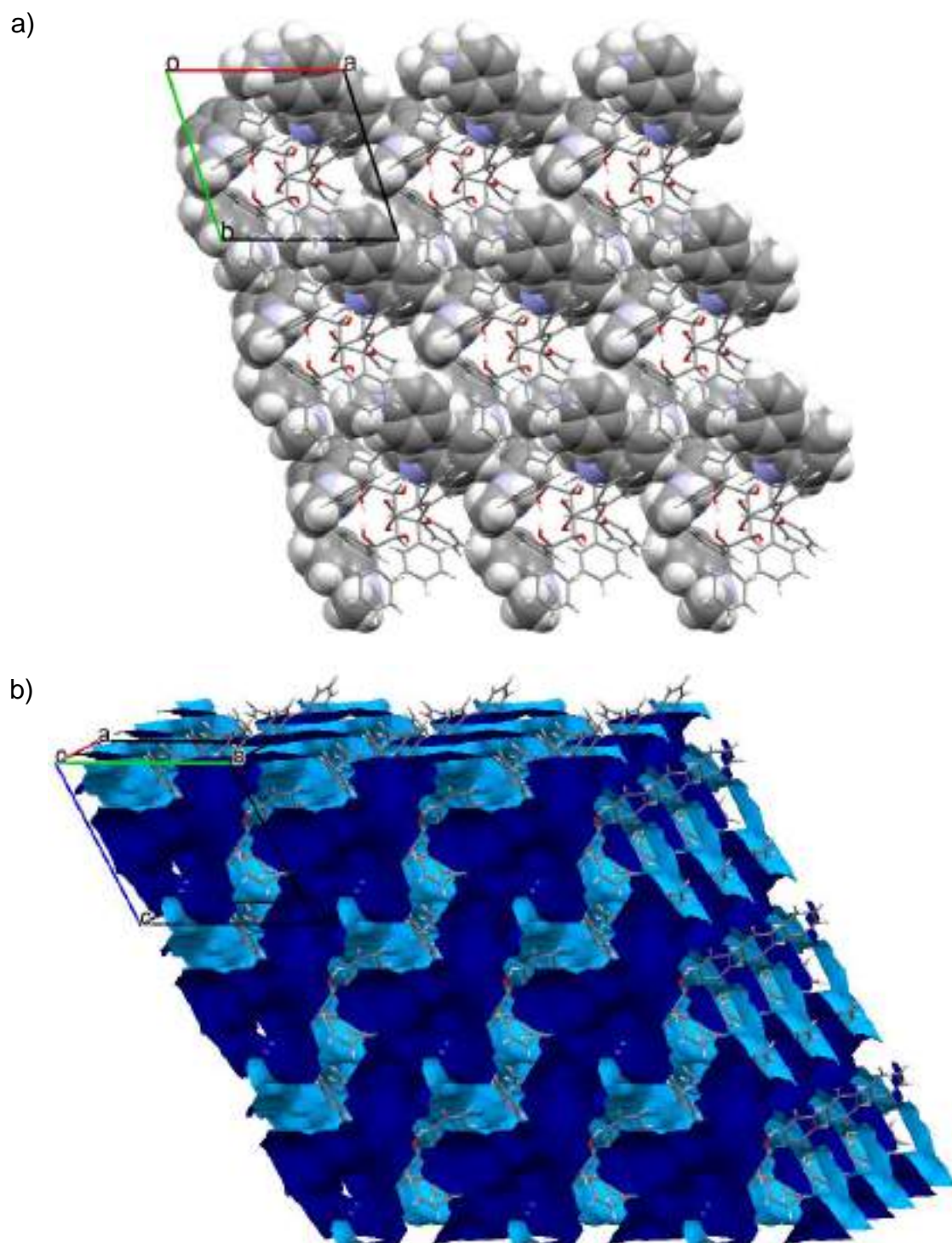
Figure 3: a) Crystal packing of 2TET·4NMA inclusion complex with guest in spacefill form, b) calculated voids (dark blue) for 2TET·4NMA indicating guest accommodation in near-linear channels; oxygen – red, nitrogen – blue, carbon – grey and hydrogen – light grey

6.3.1 H–Bonding Interactions Between Host and Guest Species

The data for the H-bonding interactions between host and guest species are summarized in Table 4. The majority of the guests experience one (host)O−H⋯N(guest) interaction involving a secondary hydroxyl group of the host. These hydrogen bond distances [2.738(2)–2.763(3) Å] are comparable in both complexes, with the strongest occurring in the 2TET·4NMA complex [2.738(2) Å, 154°]. The host is known to predominantly function as a hydrogen-bond donor,[157] but it functions as both a hydrogen-bond donor and acceptor within the complex containing NMA (Figure 4).

Table 4: Analysis of intermolecular hydrogen bonding interactions between TET and guests ANI and NMA

Guest	Unit cell H:G ratio	Guest	(host)O⋯X(guest)[a] /Å	(host)H⋯X(guest) /Å	(host)O–H⋯X(guest) /°	Symmetry operator
ANI	2:3	ANI [1]	2.763(3)	1.94	167	x,y,z
		ANI [2]	2.746(3)	1.93	165	x,y,z
NMA	2:4	NMA [1]	3.019(2)	2.24	152	x,y,z
		NMA [2]	2.738(2)	1.96	154	x,y,z
		NMA [2]	3.097(2)	2.32	156	x,y,z
		NMA [3]	2.738(2)	1.97	151	x,y,z
		NMA [3]	3.098(2)	2.25	165	x,y,z

[a]X = N for all instances
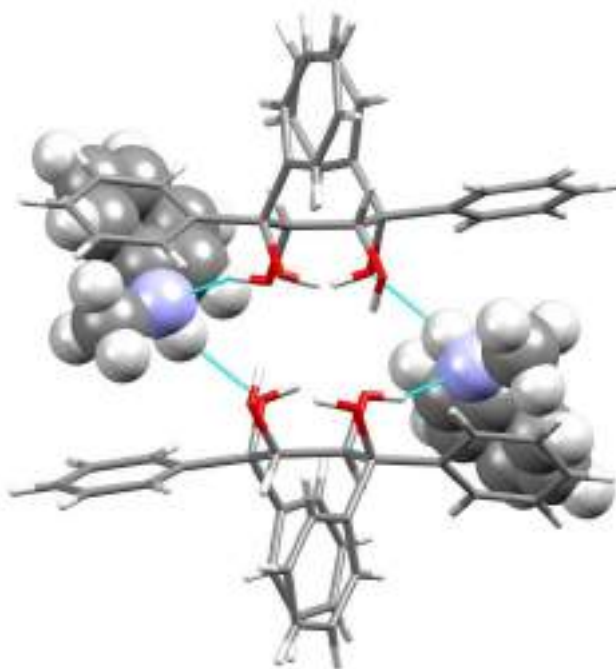
Figure 4: TETROL exhibits bifunctionality as a hydrogen-bond donor and acceptor with NMA [2] and [3] (Table 4)

6.3.2 Short Ring (π···π) and X–H···π Interactions Between Host and Guest Species

In Table 5, we observe a multitude of π···π and X–H···π interactions for both 2TET·3ANI and 2TET·4NMA complexes. The host framework for each complex is stabilised by multiple and comparable (host)π···π(host) [4.680(2)–5.9547(1)], (host)π···π(guest) [4.860(2)–5.923(2)] and (guest)π···π(guest) [5.278(2)–5.766(2)] interactions. Additionally, both complexes experience comparable interactions of the types (host)C–H···π(guest) (2.78–2.97 Å, 151–160°) and (guest)C–H···π(host) (2.80–2.99 Å, 132–150°). In the crystal of 2TET·3ANI, the aniline guests are further stabilised by (guest)N–H···π(host) interactions in the range 2.61–2.75 Å, with angles ranging between 131–177°. These guests experience additional short contacts of the type (host)*m*-ArH···N–H(guest) (2.69 Å, 153°) and (guest)N–H···C_{Ar}(host) (2.86 Å, 151°). The 2TET·4NMA complex experiences a multitude of (guest)NMe–H···π(host) interactions in the range 2.74–2.97 Å, with angles ranging between 109–142°, along with a (host)*m*-ArH···N(guest) short contact of 2.74 Å with an angle of 133°. It is noted that the ANI guest experiences the shortest short contacts between the two complexes

(2.69 Å, 153°), alluding to the preference of TETROL for this guest compared with NMA.

Table 5: Significant host–guest interactions for the complexes of TET with ANI and NMA

Interaction	2TET·3ANI	2TET·4NMA
π···π (Host···Guest)	4.903(2)–5.835(2) (24 contacts)	4.860(2)–5.923(2) (22 contacts)
π···π (Host···Host)	4.680(2)–5.945(2) (18 contacts)	4.7029(1)–5.9547(1) (15 contacts)
π···π (Guest···Guest)	5.341(2)–5.524(2) (4 contacts)	5.278(2) and 5.766(2) (2 contacts)
CH···π	2.90 Å, 153° (H···Cg, C–H···Cg) (host)*m*-ArH···π(guest)	2.92 Å, 160° (H···Cg, C–H···Cg) (host)*m*-ArH···π(host)
	2.88 Å, 151° (H···Cg, C–H···Cg) (host)*m*-ArH···π(guest)	2.78 Å, 157° (H···Cg, C–H···Cg) (host)*m*-ArH···π(host)
	2.97 Å, 156° (H···Cg, C–H···Cg) (host)*m*-ArH···π(guest)	2.80 Å, 150° (H···Cg, C–H···Cg) (guest)*p*-ArH···π(host)
	2.94 Å, 137° (H···Cg, C–H···Cg) (guest)*m*-ArH···π(host)	2.99 Å, 132° (H···Cg, C–H···Cg) (guest)*m*-ArH···π(host)
	2.73 Å, 173° (H···Cg, N–H···Cg) (guest)N–H···π(host)	2.97 Å, 113° (H···Cg, C–H···Cg) (guest)NMe–H···π(host)
	2.61 Å, 139° (H···Cg, N–H···Cg) (guest)N–H···π(host)	2.81 Å, 142° (H···Cg, C–H···Cg) (guest)NMe–H···π(host)
	2.73 Å, 131° (H···Cg, N–H···Cg) (guest)N–H···π(host)	2.96 Å, 109° (H···Cg, C–H···Cg) (guest)NMe–H···π(host)

	2.75 Å, 177° (H···Cg, N–H···Cg) (guest)N–H···π(host)	2.74 Å, 135° (H···Cg, C–H···Cg) (guest)NMe–H···π(host)
		2.86 Å, 134° (H···Cg, C–H···Cg) (guest)NMe–H···π(guest)
		2.93 Å, 113° (H···Cg, C–H···Cg) (guest)NMe–H···π(guest)
Short contacts	2.69 Å, 153° (H···N, C–H···N) (host)*m*-ArH ···N–H(guest) 2.86 Å, 151° (H···C, H···C–C) (guest)N–H···C$_{Ar}$(host)	2.74 Å, 133° (H···N, C–H···N) (host)*m*-ArH···N(guest)

6.4   Hirshfeld Surface Analysis

Due to the sheer number of interactions in these complexes, it is difficult to know which are more significant. We therefore carried out Hirshfeld surface analyses. The 'spikes' and 'wings' observed on the Hirshfeld plots are colour-coded and depict $N \cdots H$ (green), $O \cdots H$ (magenta), $H \cdots H$ (blue) and $C \cdots H$ (orange) contacts. The fingerprint plots for the 2TET·3ANI complex (Figures 5a–d) exhibit three distinct areas representing $N \cdots H$, $H \cdots H$ and $C \cdots H$ interactions {the Hirshfeld surface for the disordered component of the ANI guest was generated and displayed here (ANI[dis])}. The fingerprint plots for aniline molecules [1] and [2] are similar, with large spikes depicting short $N \cdots H$ interactions. The fingerprint plots for the 2TET·4NMA complex (Figures 5e–h) differ from these with the presence of additional spikes representing the $O \cdots H$ interactions.
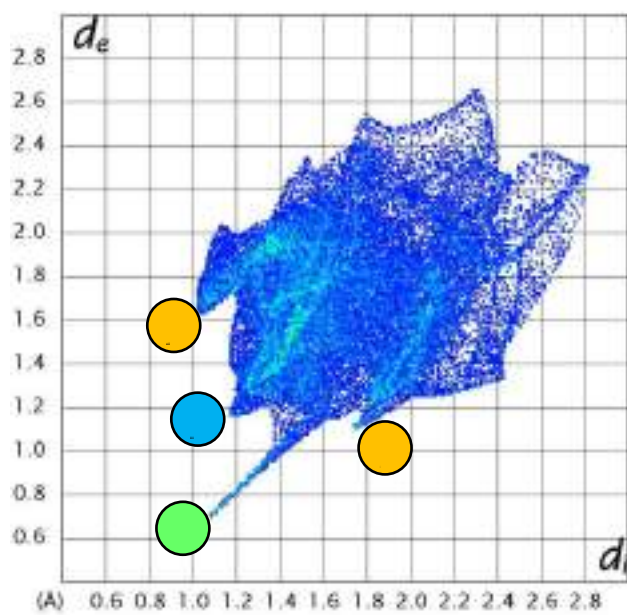
TET·ANI [1]
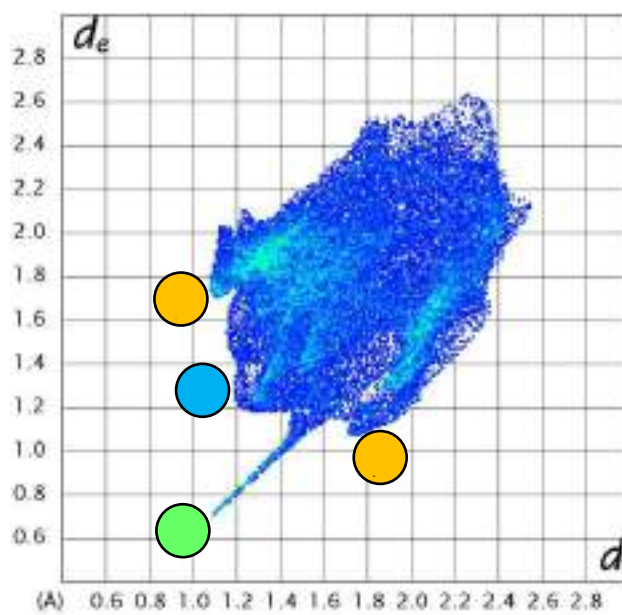
TET·ANI [2]
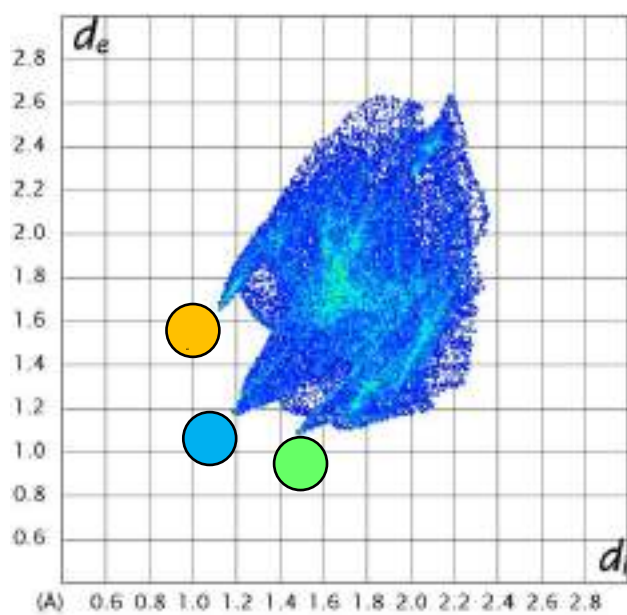
TET·ANI [3]
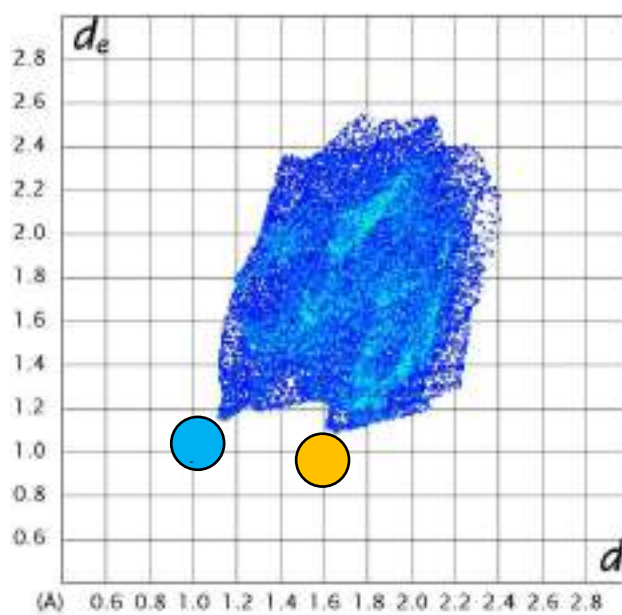
TET·ANI [dis]
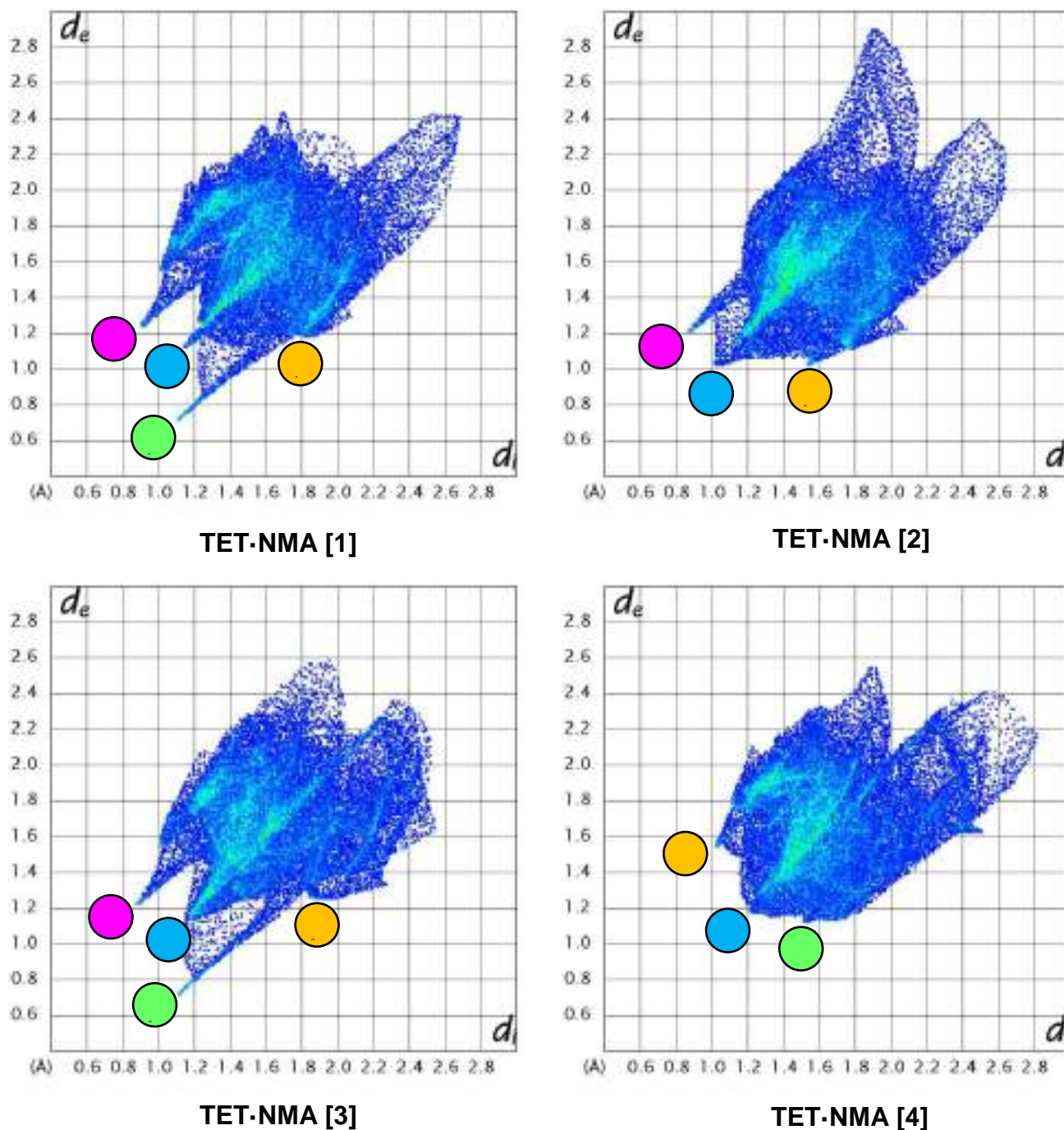
Figure 5: Hirshfeld fingerprint plots for the 2TET·3ANI (guests [1–3] and [dis] – disordered guest) and 2TET·4NMA (guests [1-4]) complexes

Figure 6 compares the percentage of the intermolecular interactions (G⋯H/H⋯G) present in each complex graphically while Table 6 lists these values numerically. The predominant interactions in each structure are H⋯H close contacts (Figure 6). The 2TET·3ANI complex has a significantly higher percentage of N⋯H contacts (3.2–

14.9%) compared with 2TET·4NMA (1.7–2.8%, Table 6), which correlates with the selectivity order of the host as obtained from competition experiments (ANI > NMA) (Table 2), and possibly suggests that this interaction type is more important for the stabilization of these complexes. Furthermore, only in the 2TET·3ANI complex are C⋯N interactions observed. All other interactions are comparable in the two complexes.
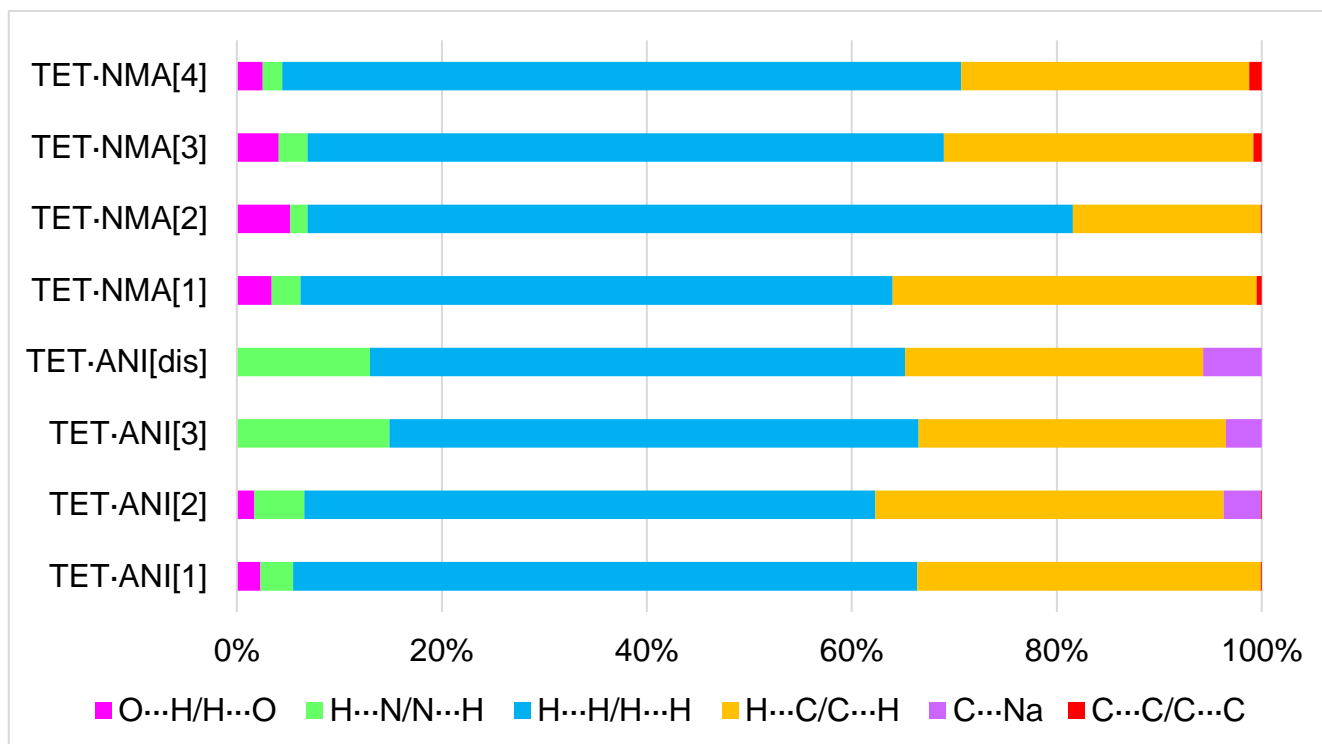
Figure 6: Graphical display showing the percentage intermolecular interactions of each type for a) 2TET·3ANI and b) 2TET·4NMA

Table 6: Percentage intermolecular interactions in each inclusion complex (G···H/H···G)

Complex	O···H/H···O	H···N/N···H	H···H/H···H	H···C/C···H	C···N [a]	C···C/C···C
TET·ANI[1]	2.3	3.2	60.9	33.5	0.0	0.1
TET·ANI[2]	1.7	4.9	55.7	34.0	3.6	0.1
TET·ANI[3]	0.0	14.9	51.7	30.0	3.5	0.0
TET·ANI[dis]	0.0	13.0	52.2	29.1	5.7	0.0
TET·NMA[1]	3.4	2.8	57.6	35.4	0.0	0.5
TET·NMA[2]	5.2	1.7	74.6	18.3	0.0	0.1
TET·NMA[3]	4.1	2.8	62.1	30.2	0.0	0.8
TET·NMA[4]	2.5	1.9	66.0	28.0	0.0	1.2

[a]Only guest···host interactions were observed

6.5   Thermal Analyses

Thermal experiments (DSC and TG) were carried out on the two inclusion complexes. The traces obtained are given in Figures 7a and b. Upon heating 2TET·3ANI, a complex guest release process ensues, with the majority of the guest released prior to the melting of the host (Figure 7a, 149.6 °C). The guest release onset temperature, T_{on}, was estimated to be 70.9 °C (Table 7). The expected mass loss for the 2:3 H:G complex was calculated to be 24.7%, which is in close agreement with the actual mass loss observed (25.3%, Table 7). The endotherm peaking at 144.1 °C, prior to the melting of the host, is possibly due to a phase change occurring within the crystal as no mass loss is associated with this endotherm. In comparison to 2TET·3ANI, the guest release process for 2TET·4NMA is less complex, with a T_{on} of 41.4 °C (Figure 7b). The observed mass loss (32.6%, Table 7) is, once more, in close agreement with that expected for this complex (33.4%).

The fact that the onset temperature for guest release is significantly higher in 2TET·3ANI (70.9 °C) compared with 2TET·4NMA (41.4 °C) alludes to the guest being more tightly bound in the crystal in the former complex, and correlates directly with the host selectivity order.

a)

b)
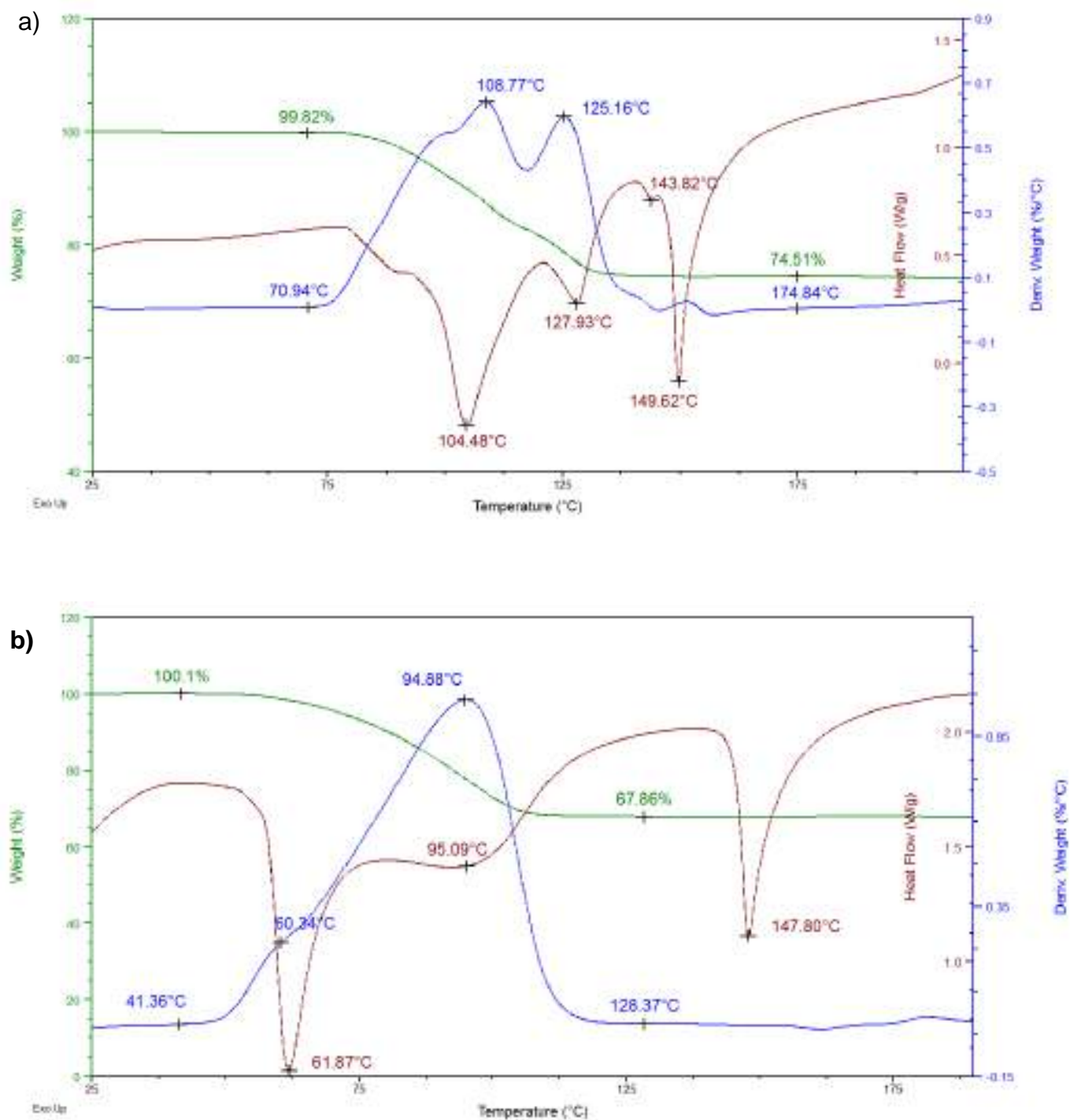
Figure 7: a) Overlaid traces of the DSC (brown), TG (green) and its derivative (DTG, blue) for the a) 2TET·3ANI and d) 2TET·4NMA complexes

Table 7: Thermal data from DSC/TG traces for 2TET·3ANI and 2TET·4NMA[a,b]

Guest	T_{on} (°C)	T_p (°C)	T_{end} (°C)	Mass loss % (expected)	Mass loss % (actual)
ANI	70.9	108.8 125.2	104.5 127.9 143.8 149.6	24.7	25.3
NMA	41.4	~60.3 94.9	61.9 ~95.1 147.8	33.4	32.2

[a]T_p values determined from blue DTG traces

[b]T_{end} were obtained from the brown DSC traces

Figure 8 is an overlay of the two TG traces that were obtained showing the mass loss associated with this heating process, and therefore represents the guest loss (and, later, host decomposition). It is clear from these plots that ANI (green curve) is held more tightly in the crystal relative to NMA (blue curve). [This was also observed by the higher temperatures associated with the release of the ANI guest (70.9 °C), as discussed previously]. It is probable that the increased number of stabilizing N···H interactions experienced by this host-guest complex is responsible for this observation.
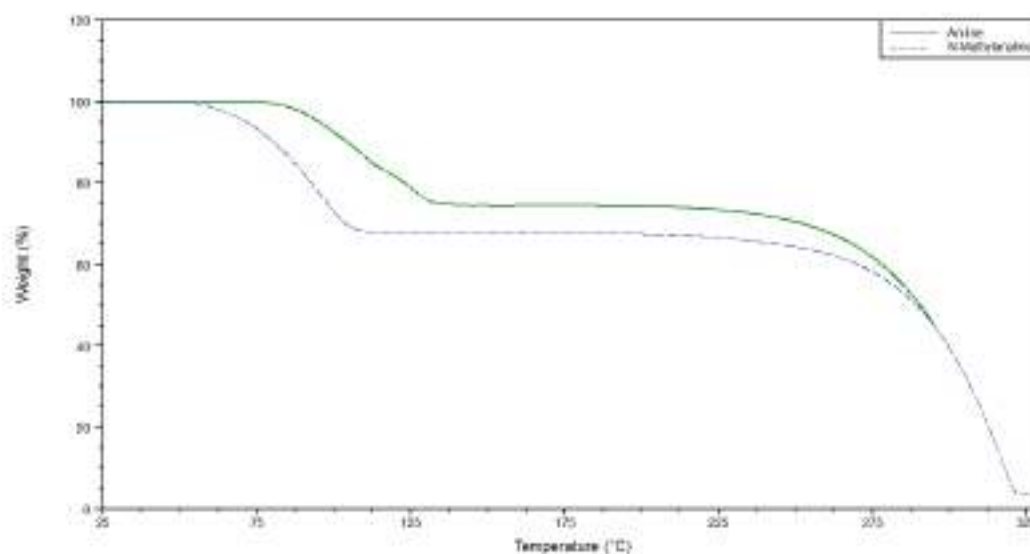
Figure 8: An overlay of the TG traces obtained for complexes of TET with ANI (green) and NMA (blue)

6.6   Conclusion

The compound, TETROL, proved to be an effective host for the complexation of aniline and *N*-methylaniline, but did not include NNMA. TETROL showed high selectivity for aniline when recrystallised from mixtures of all three compounds, and a host selectivity order of aniline > *N*-dimethylaniline > *N,N*-dimethylaniline was obtained. As evidence, Hirshfeld analysis proved that the 2TET·3ANI complex experienced a higher degree of stabilising N···H/H···N contacts in comparison to 2TET·4NMA. SCXRD analyses proved that this complex experiences the shortest short contact (2.69 Å, 153°), coinciding with thermogravimetric analyses confirming that aniline was more tightly bound in the crystal than NMA. This correlated with the host's selectivity order, as did the higher T_{on} value for 2TET·3ANI (70.9 °C) relative to 2TET·4NMA (41.4 °C).

Chapter 7
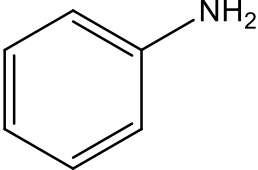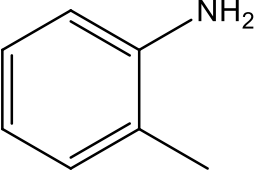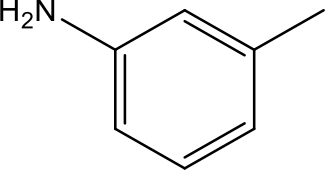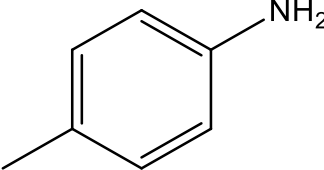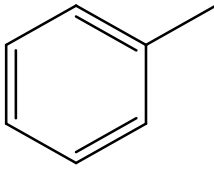
The Selectivity of TETROL for Aniline, Toluene and the Selected Toluidine Isomers

7.1 Introduction

The toluidine isomers *o*-, *m*- and *p*-toluidine, are predominantly used as solvents, chemical intermediates and for the production of antioxidants, agricultural, pharmaceutical and rubber chemicals.[194] All three isomers are aryl amines that are structurally similar to aniline except that a methyl group is substituted onto the benzene ring. Similarly, these isomers are also related to toluene except that an amino group is present on the benzene ring. For these reasons, aniline and toluene were added as guests in the selectivity study of TETROL with the toluidines.

The separation of the individual toluidine isomers involves both physical and chemical methods that require extensive equipment, profound processing requirements, and numerous repetitive treatment steps that produce, at most, poor yields of slightly pure products.[194] Since the three toluidine isomers have effectively the same boiling points, fractional distillation is obviously unsatisfactory as a means of purifying the mixture. In this investigation, we explore the selectivity of TETROL for toluene (TOLU), aniline (ANI) and its three methylaniline isomers (*o*-TOLU, *m*-TOLU and *p*-TOLU) (Table 1). Of the five compounds, three were enclathrated when crystals of this host compound were grown from each of these guest solvents forming 2TET·3ANI, 2TET·3*m*-TOLU and 2TET·3*p*-TOLU inclusion complexes, as viewed in Table 1, together with the boiling points of the pure guests. Toluene and *o*-TOLU did not form complexes with this host material.

Table 1: The structure and properties of aniline, the toluidine isomers and toluene

	ANI	*o*-TOLU	*m*-TOLU	*p*-TOLU	TOLU
Structure					
Host (H): Guest (G) ratio	2:3	—[a]	2:3	2:3	—[a]
Boiling point (°C)	184.1	200	203	200	110.6

[a] Inclusion complex did not form

7.2 Competition Experiments

Competition experiments were conducted with these five guests to establish the selectivity of the host and whether it would discriminate between them. In Tables 2–4, we summarize the data obtained from the recrystallization of TET from various equimolar binary, ternary, quaternary and quinary combinations of ANI, *o*-TOLU, *m*-TOLU, *p*-TOLU and TOLU. Due to the number of guests present, we have grouped the experiments as ANI and the toluidines (Table 2), TOLU and the toluidines (Table 3) and all five guests species together (Table 4) for the sake of clarity. The so-formed crystals were analysed using proton NMR spectroscopy and GC-MS. The preferred guest species is given in bold red font face.

Table 2: Competition experiments using TET and various equimolar mixtures of ANI and the three toluidine isomers[a,b]

ANI	*o*-TOLU	*m*-TOLU	*p*-TOLU	Inclusion ratio (%)	Host: Guest ratio
X	X			**73.3**:26.7 (0.2)	2:3
X		X		**68.7**:31.3 (0.1)	2:3
X			**X**	42.6:**57.4** (0.3)	2:3
	X	X		−*c*	2:3
	X		**X**	16.5:**83.5** (0.3)	2:3
		X	**X**	29.9:**70.1** (0.4)	2:3
X	X	X		**47.4**:18.5:34.1 (0.2)(0.4)(0.6)	2:3
X	X		**X**	27.2:18.1:**54.7** (0.4)(0.6)(1.0)	2:3
X		X	**X**	26.9:26.7:**46.4** (0.0)(1.3)(1.3)	2:3
	X	X	**X**	14.2:27.3:**58.5** (0.1)(0.6)(0.7)	2:3
X	X	X	**X**	24.6:13.2:19.9:**42.3** (0.9)(0.0)(2.4)(1.5)	2:3

[a]Ratios determined using proton NMR spectroscopy and gas chromatography

[b]Experiments were conducted in triplicate; %e.s.d.'s are provided in parentheses

[c]Crystallization failed to occur

In Table 2 are the results obtained when ANI and the toluidine isomers were made to compete. In this table, it is clear that *p*-TOLU was the preferred guest in all equimolar competition experiments whenever it was present. The binary experiments of ANI/*p*-TOLU, *o*-TOLU/*p*-TOLU and *m*-TOLU/*p*-TOLU showed the selective inclusion of *p*-TOLU with molar ratios of 57.4%, 83.5% and 70.1%, respectively. In the absence of *p*-TOLU, the second preferred guest was ANI as observed in the ANI/*o*-TOLU and ANI/*m*-TOLU experiments (73.3% and 68.7%, respectively). A binary experiment conducted in the absence of these preferred guests (*p*-TOLU and ANI) failed to yield any crystals (*o*-TOLU/*m*-TOLU). Equimolar ternary experiments involving *p*-TOLU, once more, showed TET's preference for this guest (ANI/*o*-TOLU/*p*-TOLU, ANI/*m*-TOLU/*p*-TOLU and *o*-TOLU/*m*-TOLU/*p*-TOLU experiments afforded crystals with 54.7%, 46.4% and 58.5% *p*-TOLU, respectively) while, in its absence, ANI was, once more, selected (ANI/*o*-TOLU/*m*-TOLU, 47.4). Finally, the equimolar quaternary experiment showed the host to have a selectivity order of *p*-TOLU (42.3%) > ANI (24.6%) > *m*-TOLU (19.9%) > *o*-TOLU (13.2%) for these guests.

Table 3: Competition experiments using TET and various equimolar mixtures of TOLU and the three toluidine isomers[a,b]

o-TOLU	*m*-TOLU	*p*-TOLU	TOLU	Inclusion ratio (%)	Host: Guest ratio
X			X	–[c]	2:3
	X		X	**100.0**:0.0 (0.0)	2:3
		X	X	**86.7**:13.3 (2.2)	2:3
X	X		X	–[c]	2:3
X		**X**	X	18.7:**80.6**:0.7 (2.3)(1.6)(0.7)	2:3
	X	**X**	X	30.7:**67.5**:1.8 (1.0)(0.8)(1.8)	2:3
X	X	**X**	X	13.3:30.1:**56.6**:0.0 (0.4)(1.2)(0.8)(0.0)	2:3

[a]Ratios determined using proton NMR spectroscopy and gas chromatography

[b]Experiments were conducted in triplicate; %e.s.d.'s are provided in parentheses

[c]Crystallization failed to occur

When TOLU was made to compete with the toluidine isomers (Table 3), the same selectivity order for the toluidine isomers was observed as in Table 2 (*p*-TOLU > *m*-TOLU > *o*-TOLU). The host did not include *o*-TOLU nor TOLU in single solvent experiments, and it has been established in our laboratories time and time again that if an attempt is made to recrystallize the host from a mixture of guests it has no affinity for, crystallization normally fails. This was the case for the *o*-TOLU/TOLU and *o*-TOLU/*m*-TOLU/TOLU solvent systems. Toluene was also discriminated against in favour of the *meta*- and *para*- toluidine isomers using *m*-TOLU/TOLU and *p*-TOLU/TOLU experiments, affording crystals with 100% and 86.7% of this guest, respectively. Equimolar ternary experiments proved the host's preference for *p*-TOLU (*o*-TOLU/*p*-TOLU/TOLU and *m*-TOLU/*p*-TOLU/TOLU mixtures afforded crystals with molar ratios of 80.6% and 67.5% of *p*-TOLU, respectively). The equimolar quaternary experiment showed the host to have a selectivity order of *p*-TOLU (56.6%) > *m*-TOLU (30.1%) > *o*-TOLU (13.3%) > TOLU (0.0%) for these guests.

Table 4: Competition experiments using host and various equimolar mixtures of ANI, TOLU and the three toluidine isomers[a,b]

ANI	*o*-TOLU	*m*-TOLU	*p*-TOLU	TOLU	Inclusion ratio (%)	Host: Guest ratio
X				X	**70.6**:29.4 (4.9)	2:3
X	X			X	–[c]	2:3
X		X		X	**56.5**:37.0:6.5 (2.2)(2.4)(0.2)	2:3
X			**X**	X	33.6:**63.7**:2.7 (2.8)(5.5)(2.7)	2:3
X	X	X		X	**46.6**:20.7:32.7:0.0 (0.9)(2.4)(1.4)(0)	2:3
X	X		**X**	X	34.3:13.4:**46.8**:5.5 (0.3)(0.9)(0.3)(1.5)	2:3
X		X	**X**	X	26.9:24.4:**45.5**:3.3 (1.0)(0.1)(0.6)(1.7)	2:3
X	X	X	**X**	X	24.6:12.2:18.7:**42.8**:1.8 (1.0)(0.0)(1.4)(0.2)(0.7)	2:3

[a]Ratios determined using proton NMR spectroscopy and gas chromatography

[b]Experiments were conducted in triplicate; %e.s.d.'s are provided in parentheses

[c]Crystallization failed to occur

Finally, we analysed the selectivity of the host in the presence of all five guests in equimolar binary, ternary, quaternary and quinary competition mixtures (Table 4). It was not surprising that TET remained selective for *p*-TOLU whenever it was present in equimolar ternary and quaternary experiments (ANI/*p*-TOLU/TOLU, ANI/*o*-TOLU/*p*-TOLU/TOLU and ANI/*m*-TOLU/*p*-TOLU/TOLU mixtures with molar ratios of 63.7%, 46.8% and 45.5% for this guest, respectively). When *p*-toluidine was excluded from these experiments, the next preferred guest remained ANI as observed in the ANI/TOLU, ANI/*m*-TOLU/TOLU and ANI/*o*-TOLU/m-TOLU/TOLU experiments (70.6%, 56.5% and 46.6%, respectively). The quinary competition mixture showed the hosts selectivity order to correlate exactly with data from Tables 2 and 3 [*p*-TOLU (42.8%) > ANI (24.6%) > *m*-TOLU (18.7%) > *o*-TOLU (12.2%) > TOLU (1.8%)]. Note that the solvent system ANI/*o*-TOLU/TOLU, comprising two solvents that are usually discriminated against (*o*-TOLU and TOLU), failed to crystallise.

Due to the host being usually unable to form crystallization compounds from mixtures containing TOLU and *o*-TOLU, most binary competitions involving these two guests proved experimentally challenging with respect to obtaining the required data for selectivity curves. We therefore focused rather on the selectivity profiles for ANI/*m*-TOLU, ANI/*p*-TOLU, *p*-TOLU/*m*-TOLU and *p*-TOLU/*o*-TOLU binary competition experiments (Figures 1a–d). Analyses were carried out using strictly GC-MS methods, due to proton ^{1}H-NMR signals of the toluidine isomers overlapping.

According to Figure 1a (for the mixture of ANI/*m*-TOLU), the host was unselective at low concentrations of ANI (< 4%) and then showed selectivity towards ANI soon after this point for the remainder of the concentration range investigated (Figure 1a, $K_{ANI:m\text{-}TOLU}$ = 2.1). Furthermore, the host showed little to no selectivity in the binary competition using ANI/*p*-TOLU ($K_{ANI:p\text{-}TOLU}$ = 1.0, Figure 1b). This is readily observed by the experimentally-determined blue data points which are situated close to the red data line representing a case where the host is completely unselective towards both guests. This result was not entirely surprising given the data in Table 2, where the host showed some ambivalence towards the two guests in the equimolar binary experiment (ANI/*p*-TOL 42.6%:57.4%). For the binary mixture of *p*-TOLU/*m*-TOLU, the host showed reasonable selectivity for *p*-TOLU at very low concentrations of this guest (at ~9.3% *p*-TOLU in the mother liquor, the crystals already contained 28.4% *p*-TOLU)

until a concentration of 90.4%, whereafter the host displayed no selectivity for either guest (Figure 1c, $K_{p\text{-TOLU}:m\text{-TOLU}} = 1.9$). The highest selectivity coefficient obtained was for the *p*-TOLU/*o*-TOLU experiment (Figure 1d, $K_{p\text{-TOLU}:o\text{-TOLU}} = 10.0$) where the host displayed high selectivity for *p*-TOLU over the entire concentration range.
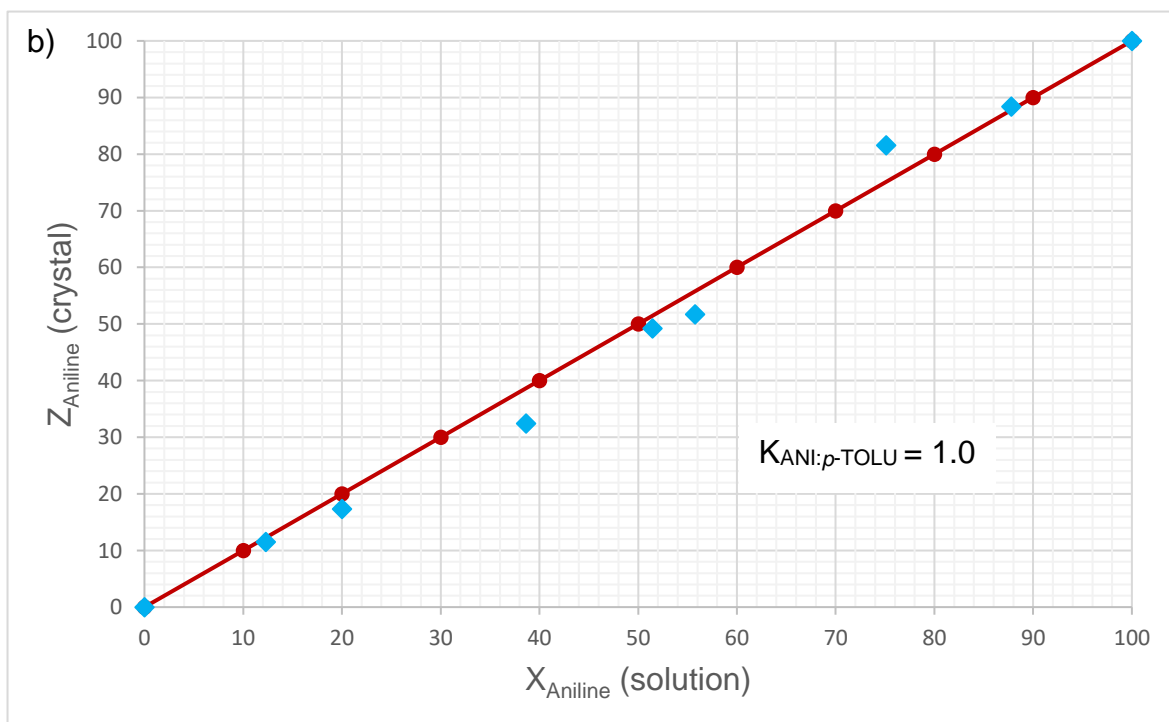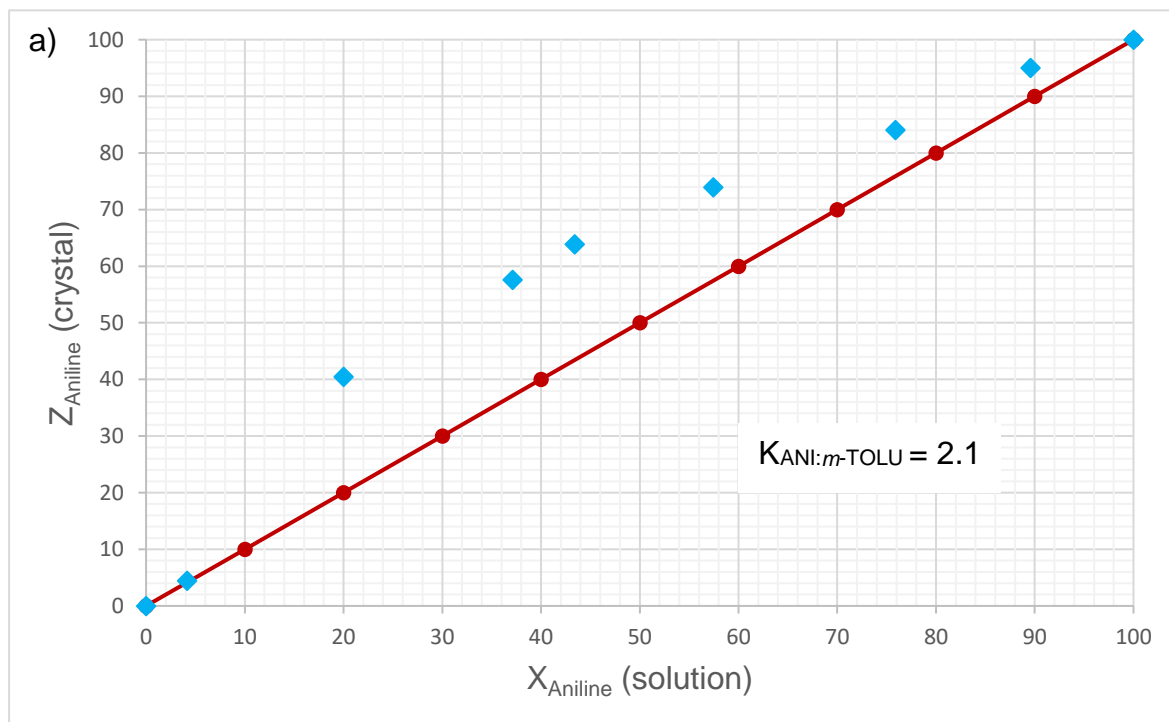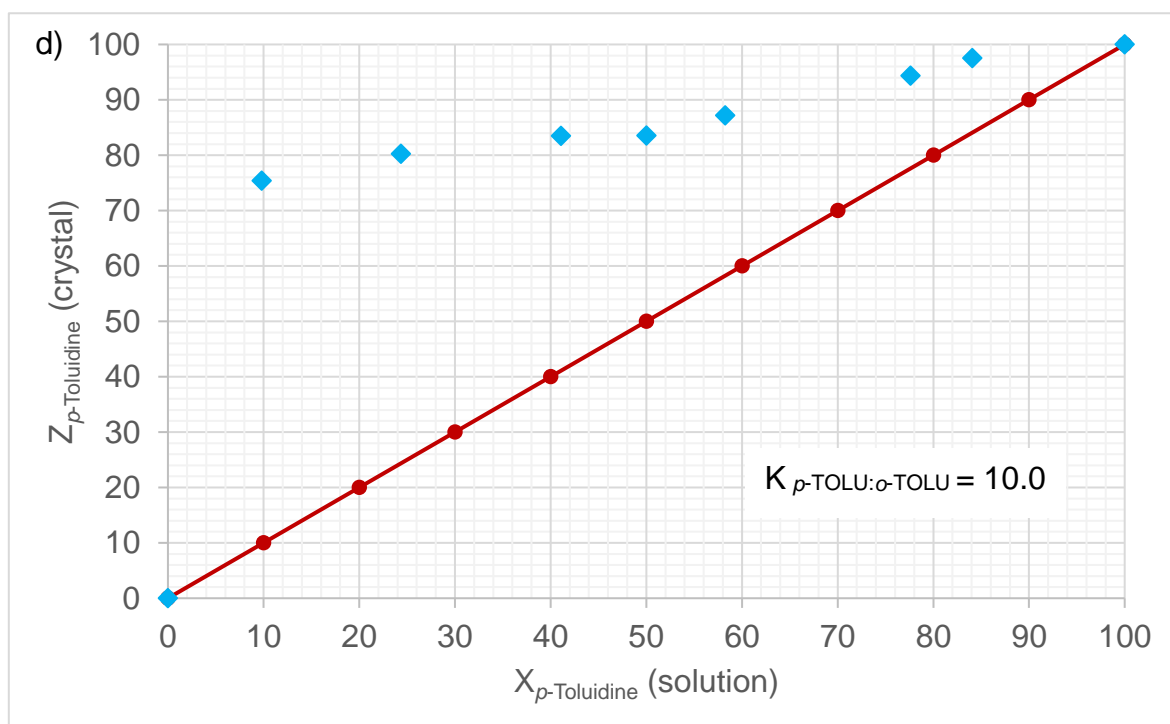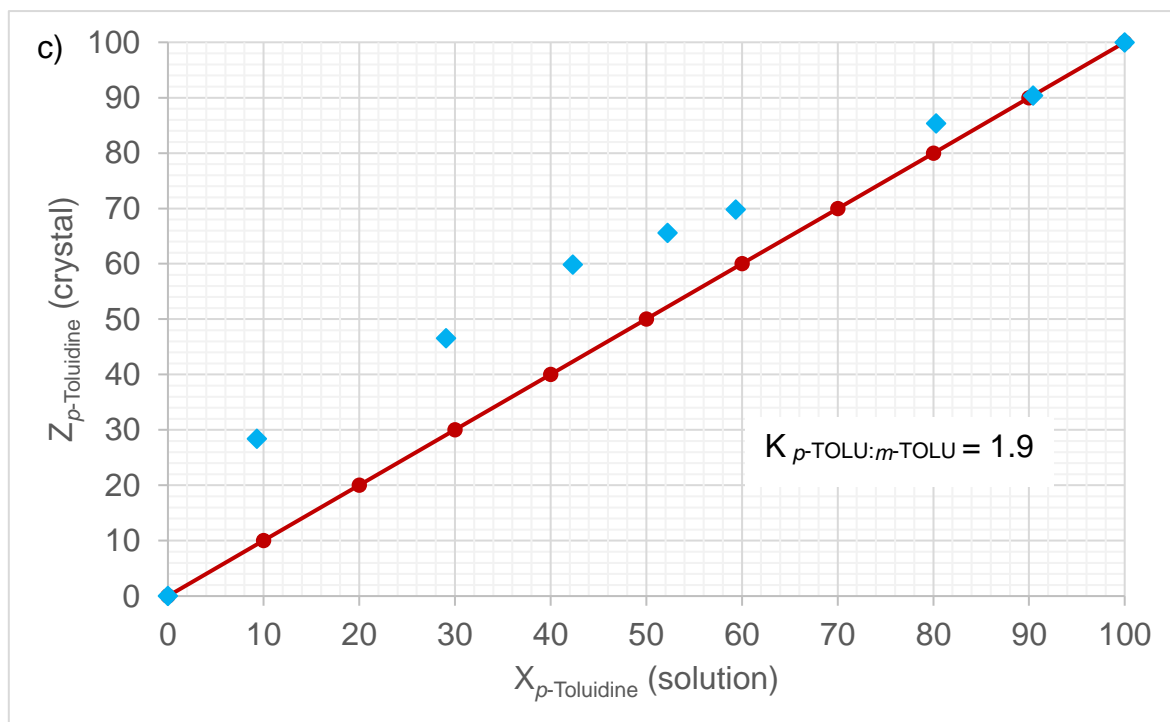
Figure 1: Selectivity curves for a) ANI/*m*-TOLU, b) ANI/*p*-TOLU, c) *p*-TOLU/*m*-TOLU and d) *p*-TOLU/*o*-TOLU

7.3   Single Crystal X-ray Diffraction (SCXRD)

SCXRD experiments were carried out on suitable crystals of the successfully-formed 2TET·3*m*-TOLU and 2TET·3*p*-TOLU complexes. The 2TET·3ANI complex was discussed in a previous chapter but the SCXRD data will be re-presented here for ease of comparison. Crystal data and refinement parameters are listed in Table 5 for the two toluidine complexes with TETROL. The 2TET·3*m*-TOLU complex crystallizes in the triclinic crystal system and $P1$ space group with Z = 1 while the 2TET·3*p*-TOLU crystallizes in the orthorhombic crystal system and $P2_12_12_1$ space group with Z = 4.

The respective packing diagrams for each complex are displayed in Figures 2 and 3. In both cases, the toluidine guest molecules were found to occupy restricted channels within their respective host frameworks. Figures 4a and b are stereoviews to observe the host-guest packing more clearly.

a)

b)
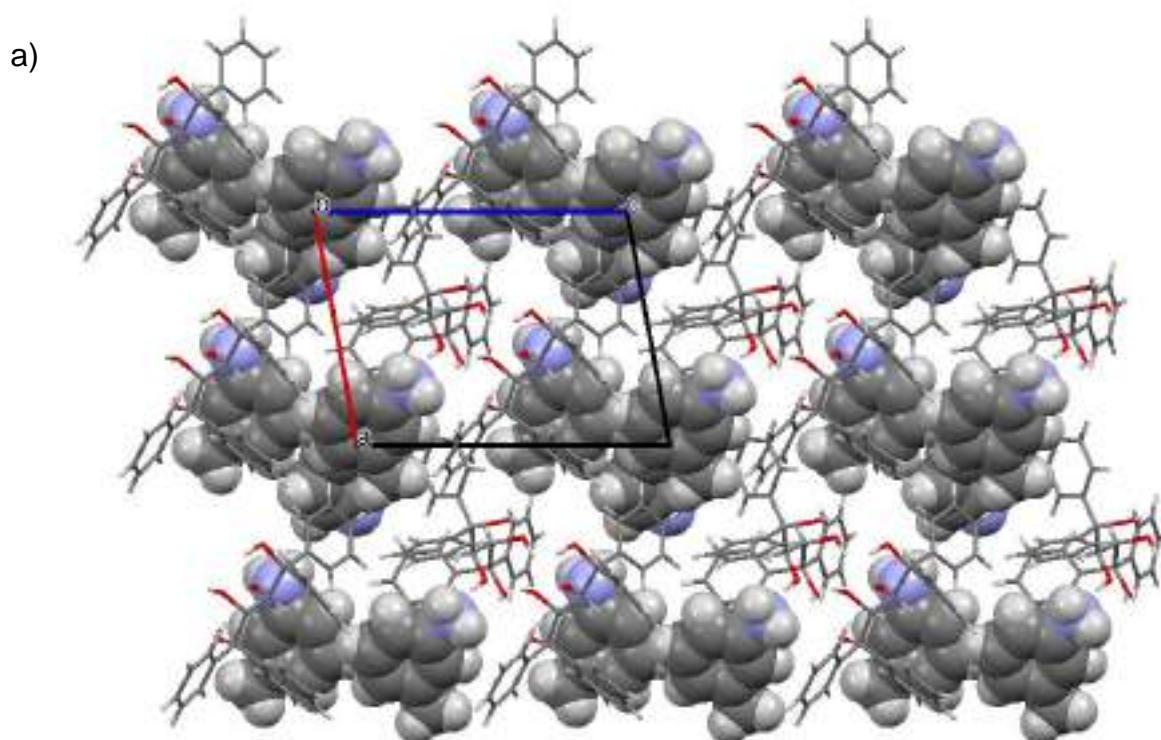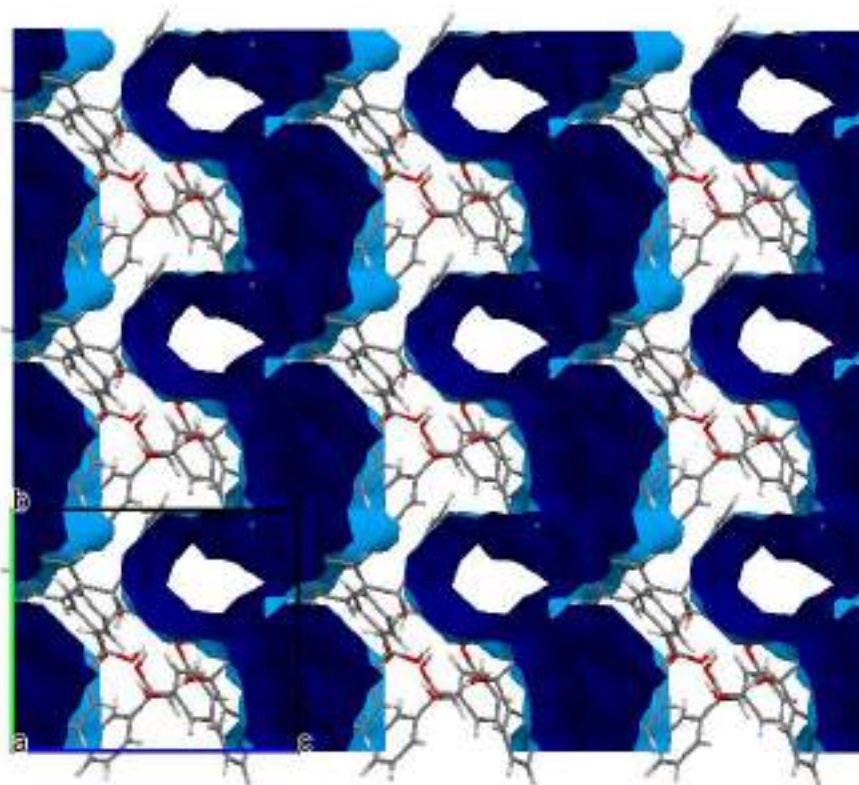
Figure 2: a) Crystal packing of the 2TET·3*m*-TOLU inclusion complex with guests in spacefill form; b) Calculated voids (blue) for 2TET·3*m*-TOLU indicating guest accommodation in channels; Oxygen – red, nitrogen – blue, carbon – grey and hydrogen – light grey

a)

b)
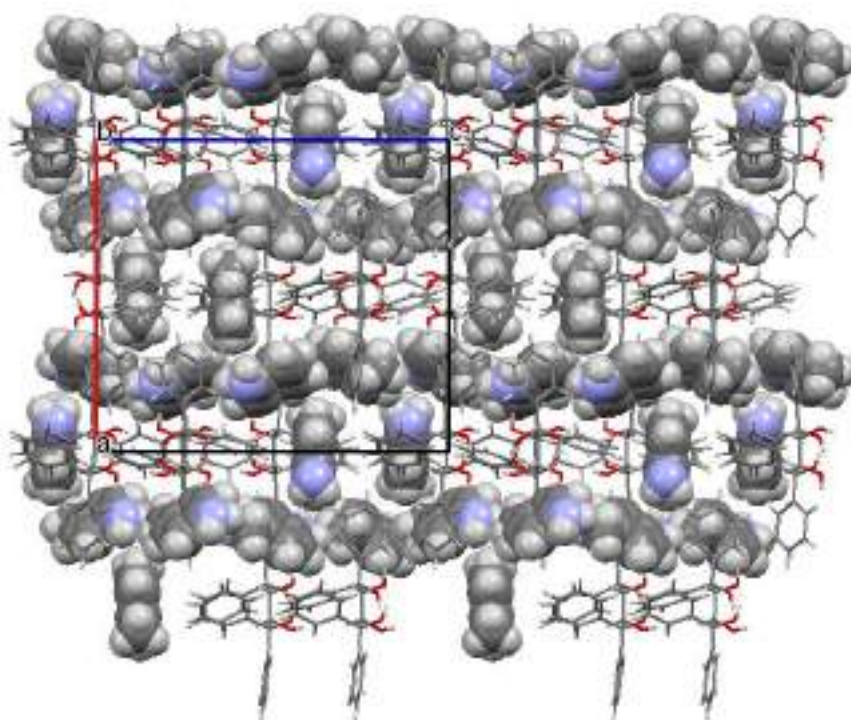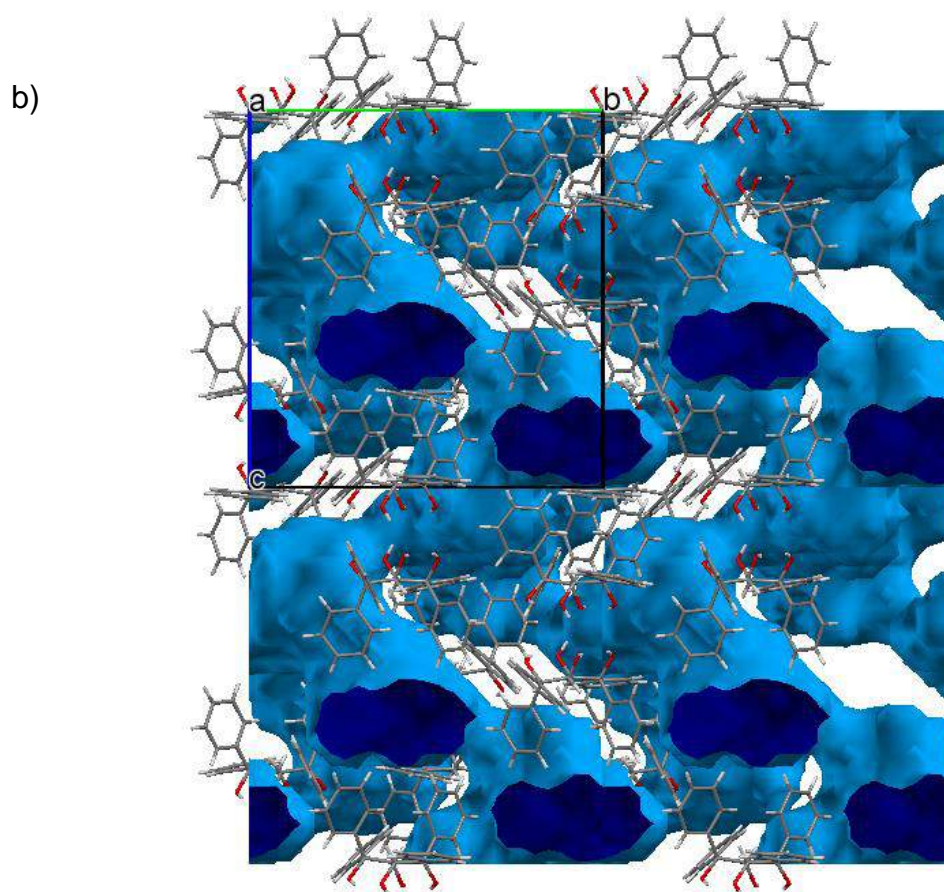
Figure 3: a) Crystal packing of the 2TET·3*p*-TOLU inclusion complex with guests in spacefill form; b) Calculated voids (blue) for 2TET·3*p*-TOLU indicating guest accommodation in highly restricted channels; Oxygen – red, nitrogen – blue, carbon – grey and hydrogen – light grey

a)

b)
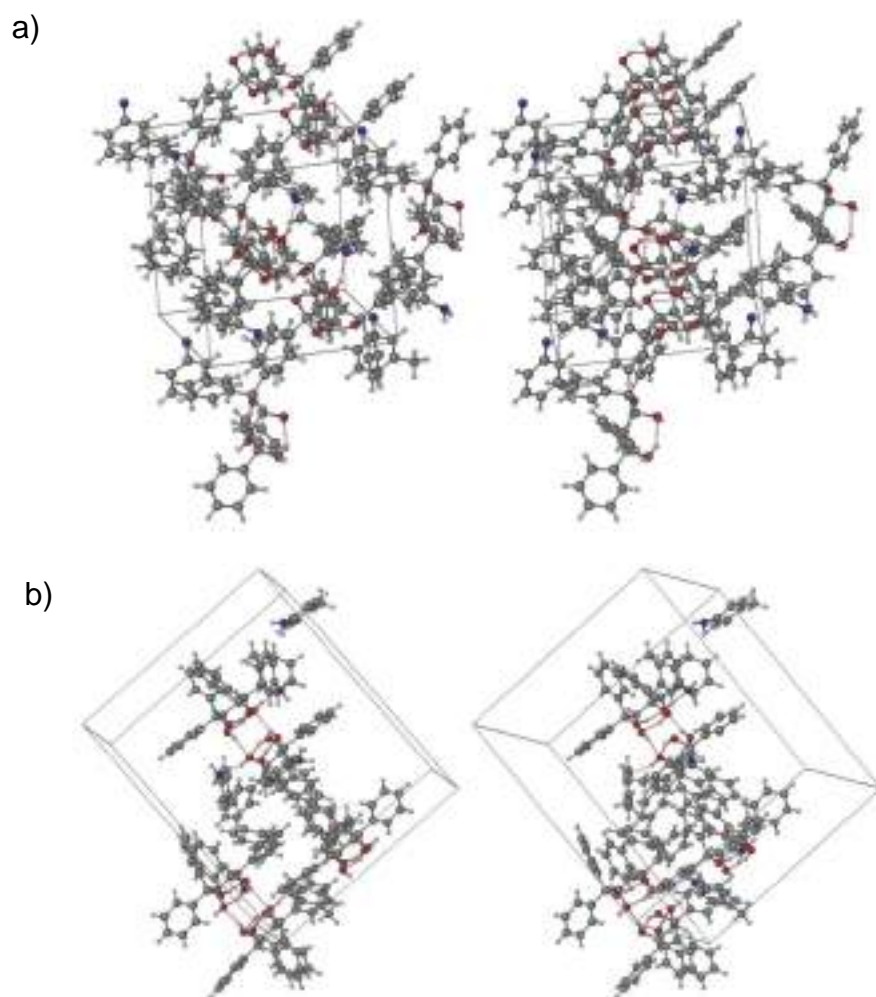
Figure 4: Stereoviews illustrating the crystal packing of a) 2TET·3 *m*-TOLU and b) 2TET·3 *p*-TOLU

Table 5: Relevant single crystal X-ray crystallographic data for the complexes of TETROL with *m*-TOLU and *p*-TOLU

	2TET·3*m*-TOLU	2TET·3*p*-TOLU
Chemical formula	$2(C_{28}H_{26}O_4)\cdot$ $2(C_7H_9N),C_7H_7N^a$	$2(C_{28}H_{26}O_4)\cdot$ $3(C_7H_9N)$
Formula weight	1172.42	1174.43
Crystal system	Triclinic	Orthorhombic
Space group	P_1	$P2_12_12_1$
μ (Mo Kα)/mm^{-1}	0.078	0.078
a/Å	10.7717(4)	17.4913(5)
b/Å	11.8825(5)	18.5146(5)
c/Å	13.4957(6)	19.8236(6)
α/°	86.693(2)	90
β/°	79.059(2)	90
γ/°	71.473(2)	90
V/Å^3	1608.08(12)	6419.8(3)
Z	1	4
F (000)	624	2504
Temp (K)	200	200
Restraints	1	1
Nref	14904	15966
Npar	808	819
R1	0.0405	0.0411
wR2	0.1087	0.1032
S	1.02	1.02
Θ min, max/°	1.8, 28.3	1.6, 28.3
Tot. data	56 880	116349
Unique data	14904	15966
Observed data [I > 2.0σ(I)]	12943	12034
Rint	0.020	0.027
Diffrn measured fraction Θ full	1.000	1.000
Min. resd. dens. (e/Å^3)	−0.21	−0.22
Max. resd. dens. (e/Å^3)	0.28	0.20

^{a}Hydrogen atoms could not be located during SCXRD structural refinement of the crystal structure

7.3.1 H-Bonding Interactions Between Host and Guest Species

The host's geometry is stabilised by a pair of 1,3-intramolecular hydrogen bonds, and each guest is held in the crystal by means of (guest)C−N···H−O(host) hydrogen bonds involving only the secondary host hydroxyl groups, but only two of the three guests within each complex experience this interaction type. Accordingly, two unique hydrogen-bonded host−guest O···N distances are quantified for each complex, and all are comparable [Table 6, 2.710(2)−2.771(3) Å] with angles ranging between 159−

167°. The strongest hydrogen bond is between the host and *p*-TOLU guest [Table 6, 2.710(2), 165°], and the weakest H-bond interaction was observed for the complex containing *m*-TOLU [Table 6, 2.771(3), 160°] in accordance with the host selectivity order for these two guests. Table 6 also contains these data for the ANI complex for ease of comparison. Two of these three guests also experience H-bonding of similar strength [Table 6, 2.746(3), 2.763(3), 165 and 167°].

Table 6: Analysis of intermolecular hydrogen bonding interactions between TET and guests ANI, *m*-TOLU and *p*-TOLU

Guest	Unit cell H:G ratio	Guest†	(host)O···X(guest) /Å	(host)H···X(guest) /Å	(host)O–H···X(guest) /°	Symmetry operator
ANI	2:3	ANI [1]	2.763(3) X = N	1.94	167	x,y,z
		ANI [2]	2.746(3) X = N	1.93	165	x,y,z
m-TOLU	2:3	*m*-TOLU [1]	2.722(3) X = N	1.90	165	x,y,z
		m-TOLU [2]	2.771(3) X = N	1.97	160	x,y,z
p-TOLU	2:3	*p*-TOLU [1]	2.732(3) X = N	1.93	159	x,y,z
		p-TOLU [2]	2.710(2) X = N	1.89	165	x,y,z

†The unit cell in each complex is comprised of three guests in unique environments. Two of these guests experience H-bonding and have been labelled ANI[1], ANI[2], *m*-TOLU[1], *m*-TOLU[2], *p*-TOLU[1] and *p*-TOLU[2]

7.3.2 Short Ring (π···π) and X–H···π Interactions Between Host and Guest Species

The host framework in each of the complexes, 2TET·3*m*-TOLU and 2TET·3*p*-TOLU is stabilised by (host)π···π(host) interactions with comparable ranges (Table 7, 4.667(2)–5.945(2) Å). Additionally, stabilising (host)π···π(guest) and (guest)π···π(guest) interactions occur for these complexes in the ranges 4.735(2)–5.889(2) Å and 4.702(2)– 5.945(2) Å, respectively (Table 7). Accompanying these are cooperative (host)C–H···π(guest), (guest)C–H···π(guest) and (guest)N–H···π(host) interactions.

In the crystal of 2TET·3ANI, stabilization of the guest is mediated by three (host)*m*-ArH···π(guest) interactions (Table 7, 2.90–2.97 Å, 151–156°) and one (guest)*m*-ArH···π(host) interaction (Table 7, 2.94 Å 137°). Further stabilization occurs from two short contacts of the type (host)*m*-ArH···N–H(guest) and (guest)N–H···C$_{Ar}$(host) (Table 7, 2.86 and 2.69 Å, with angles 151 and 153°, respectively). The TET·3*m*-TOLU complex is stabilised by one (host)*m*-ArH···π(guest) and one (guest)Me–H···π(host) interaction within similar ranges (Table 7, 2.88–2.95 Å, 122–162°). Accompanying these interactions is a short (guest)*o*-ArH···C$_{Ar}$(host) contact (Table 7, 2.83 Å, 141°). The 2TET·3*p*-TOLU complex is stabilized by two (host)*m*-ArH···π(guest) interactions (Table 7, 2.94 and 2.91 Å, 167 and 160°, respectively), along with four short contacts of the type (host)*m*-ArH···H–Me(guest) (2.28 Å, 151°), (guest)C$_{Ar}$···O–H(host) (2.71 Å, 155°), (host)*m*-ArH···C$_{Ar}$(guest) (2.84 Å, 135°) and (guest)Me–H···C$_{Ar}$(guest) (2.88 Å, 122°). It is noted that this complex experiences a higher degree of short contact interactions, as well as the shortest short interaction of all complexes investigated (2.28 Å). The 2TET·3ANI and 2TET·3*p*-TOLU complexes both exhibit more interactions of the type (guest)N–H···π(host) and (host)π···π(guest) in comparison to TET·*m*-TOLU. These data provide an explanation for the selectivity of TETROL for *p*-TOLU and ANI above *m*-TOLU, which coincides with the selectivity order of TETROL (*p*-TOLU > ANI > *m*-TOLU).

Table 7: Significant host–guest interactions for the complexes of TET with ANI, *m*-TOLU and *p*-TOLU

Interaction	2TET·3ANI	2TET·3*m*-TOLU	2TET·3*p*-TOLU
π···π (Host···Guest)	4.903(2)–5.835(2) (24 contacts)	4.735(2)–5.889(2) (15 contacts)	4.940(1)–5.880(2) (22 contacts)
π···π (Host···Host)	4.680(2)–5.945(2) (18 contacts)	4.667(2)–5.846(2) (17 contacts)	4.670(1)–5.908(2) (16 contacts)
π···π (Guest···Guest)	5.341(2)–5.524(2) (4 contacts)	4.702(2) and 5.945(2) (2 contacts)	5.025(2) and 5.402(2) (2 contacts)
XH···π	2.90 Å, 153° (H···Cg, C–H···Cg) (host)*m*-ArH···π(guest) 2.88 Å, 151° (H···Cg, C–H···Cg) (host)*m*-ArH···π(guest) 2.97 Å, 156° (H···Cg, C–H···Cg) (host)*m*-ArH···π(guest) 2.94 Å, 137° (H···Cg, C–H···Cg) (guest)*m*-ArH···π(host) 2.73 Å, 173° (H···Cg, N–H···Cg) (guest)N–H···π(host) 2.61 Å, 139° (H···Cg, N–H···Cg) (guest)N–H···π(host) 2.73 Å, 131° (H···Cg, N–H···Cg) (guest)N–H···π(host)	2.95 Å, 162° (H···Cg, C–H···Cg) (host)*m*-ArH···π(guest) 2.88 Å, 122° (H···Cg, C–H···Cg) (guest)Me–H···π(host) 2.95 Å, 163° (H···Cg, N–H···Cg) (guest)N–H···π(host) 2.54 Å, 138° (H···Cg, N–H···Cg) (guest)N–H···π(host)	2.94 Å, 167° (H···Cg, C–H···Cg) (host)*m*-ArH···π(guest) 2.91 Å, 160° (H···Cg, C–H···Cg) (host)*m*-ArH···π(guest) 2.79 Å, 169° (H···Cg, N–H···Cg) (guest)N–H···π(host) 2.65 Å, 131° (H···Cg, N–H···Cg) (guest)N–H···π(host) 2.79 Å, 169° (H···Cg, N–H···Cg) (guest)N–H···π(host)

	2.75 Å, 177° (H···Cg, N–H···Cg) (guest)N–H···π(host)		

			2.28 Å, 151° (H···H, H···H–C) (host)*m*-ArH···H–Me(guest)
Short contacts	2.69 Å, 153° (H···N, C–H···N) (host)*m*-ArH ···N–H(guest) 2.86 Å, 151° (H···C, H···C–C) (guest)N–H···C$_{Ar}$(host)	2.83 Å, 141° (H···C, H···C–C) (guest)*o*-ArH···C$_{Ar}$(host)	2.71 Å, 155° (C···H, C···H–O) (guest)C$_{Ar}$···O–H(host) 2.84 Å, 135° (H···C, H···C–C) (host)*m*-ArH···C$_{Ar}$(guest) 2.88 Å, 122° (H···C, C···C–C) (guest)Me–H···C$_{Ar}$(guest)

7.3.3 SCXRD Analyses of Three Mixed Complexes

From the equimolar competition experiments performed, the host displayed little preference for TOLU whenever this guest was present. However, in the equimolar ANI/TOLU mixture, TOLU was included with a molar ratio of 29.4% (Table 4). We subsequently analysed the crystal obtained from this ANI/TOLU experiment in order to observe the partial inclusion of TOLU by TET, as this host does not form an inclusion with this guest during single solvent experiments. Also, we analysed the 2TET·2ANI·*o*-TOLU mixed complex in the same way. [In the binary competition experiment, ANI was favoured (73.3%)]. Crystal data and refinement parameters are listed in Table 8 for these two mixed complexes with TETROL. It is clear from this data that the two mixed complexes are isostructural with the 2TET·3ANI complex (also in Table 8), crystallizing in the orthorhombic crystal system and $P2_12_12_1$ space group with Z = 4. Figures 5a–c display the crystal packing of 2TET·3ANI, 2TET·2ANI·TOLU and 2TET·2ANI·*o*-TOLU, respectively. Two of the three ANI guests are stabilised within the host framework by H-bond interactions (Table 6, ANI[1] and ANI[2] and Figure 5a magenta). The third ANI guest (Figure 5a, orange) is not stabilized via H-bonding but rather that of (host)π···π(guest) [5.422(3) Å], (guest)π···π(guest) [5.410(3) and 5.429(3) Å], (guest)π···π(host) [5.056(3)–5.813(3) (5) Å], and (host)*m*-ArH···π(guest) (2.88 and 2.97 Å, with angles 151 and 156°,respectively) interactions. Upon recrystallisation of the host from an ANI/TOLU mixture, the third aniline guest is replaced by a toluene molecule (Figure 5b, green) that experiences comparable (host)π···π(guest) [5.402(2) and 5.450(2) Å], (guest)π···π(guest) [5.381(3) and 5.550(3) Å], (guest)π···π(host) [5.143(3)–5.682(3) (4) Å], (host)*m*-ArH···π(guest) (2.92 Å, 155°) interactions, as well as the additional stabilising (host)C–H···C_{Ar}(guest) (2.86 Å, 133°) short contact. A similar phenomenon was noted when the host was recrystallised from the ANI/*o*-TOLU mixture. Once again, the *o*-TOLU guest (Figure 5c, yellow) replaced the position of ANI[3]. The *o*-TOLU guest (Figure 5c, yellow) is stabilized by means of (host)π···π(guest) [5.303(2) and 5.445(2) Å], (guest)π···π(guest) [5.265(3) and 5.648(3) Å], (guest)π···π(host) [5.371(3)–5.552(3) (4) Å], and (host)*p*-ArH···C–H(guest) (1.93 Å, 153°) interactions. The ANI[3], TOLU and *o*-TOLU guests were hypothetically removed from their respective mixed complexes and the guest accommodation type computed and the remaining voids

displayed (Figures 6a–c). It is clear that all three guests are accommodated in identical cavities. Figures 7a and b display the stereoviews calculated for the 2TET·2ANI·TOLU and 2TET·2ANI·*o*-TOLU mixed complexes, with the former being a rather eventful stereoview.

a)

b)

c)
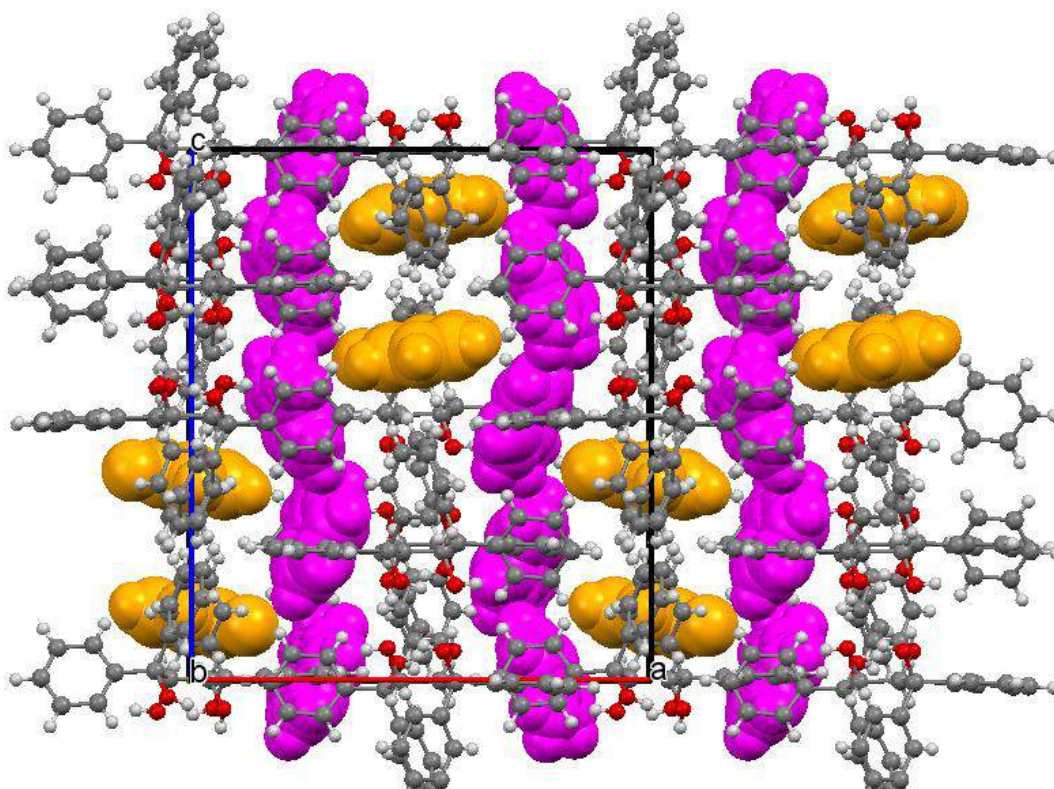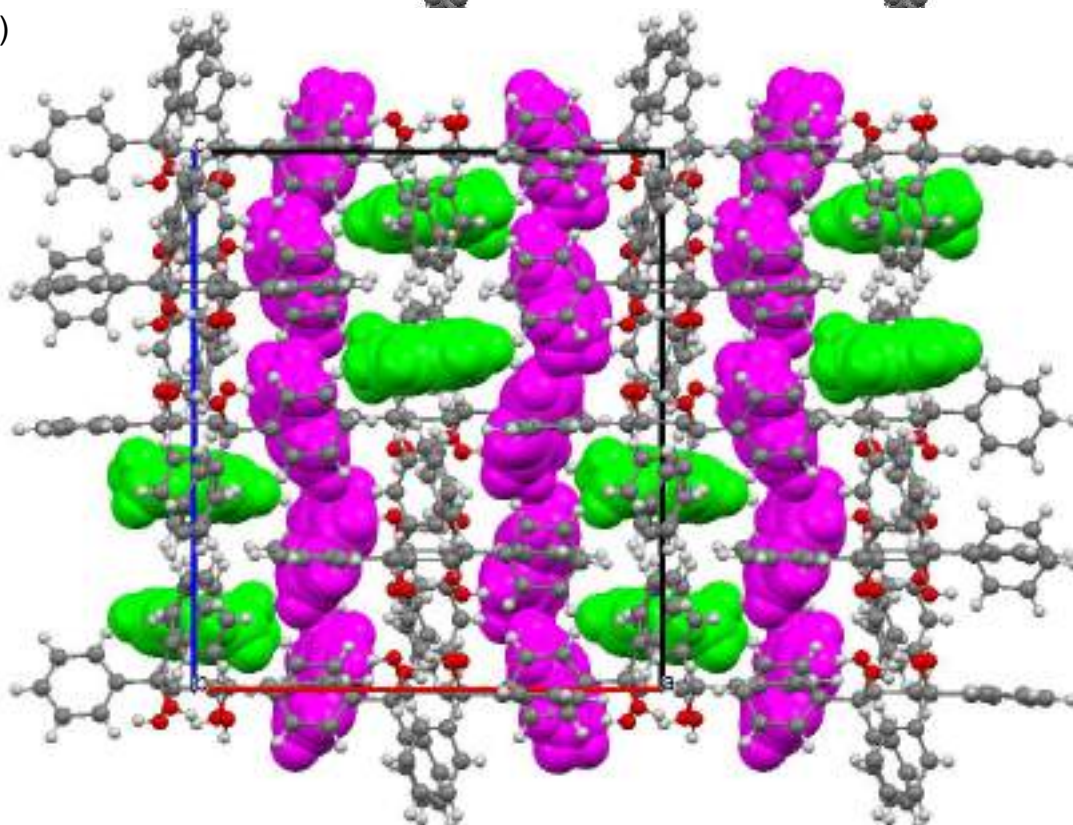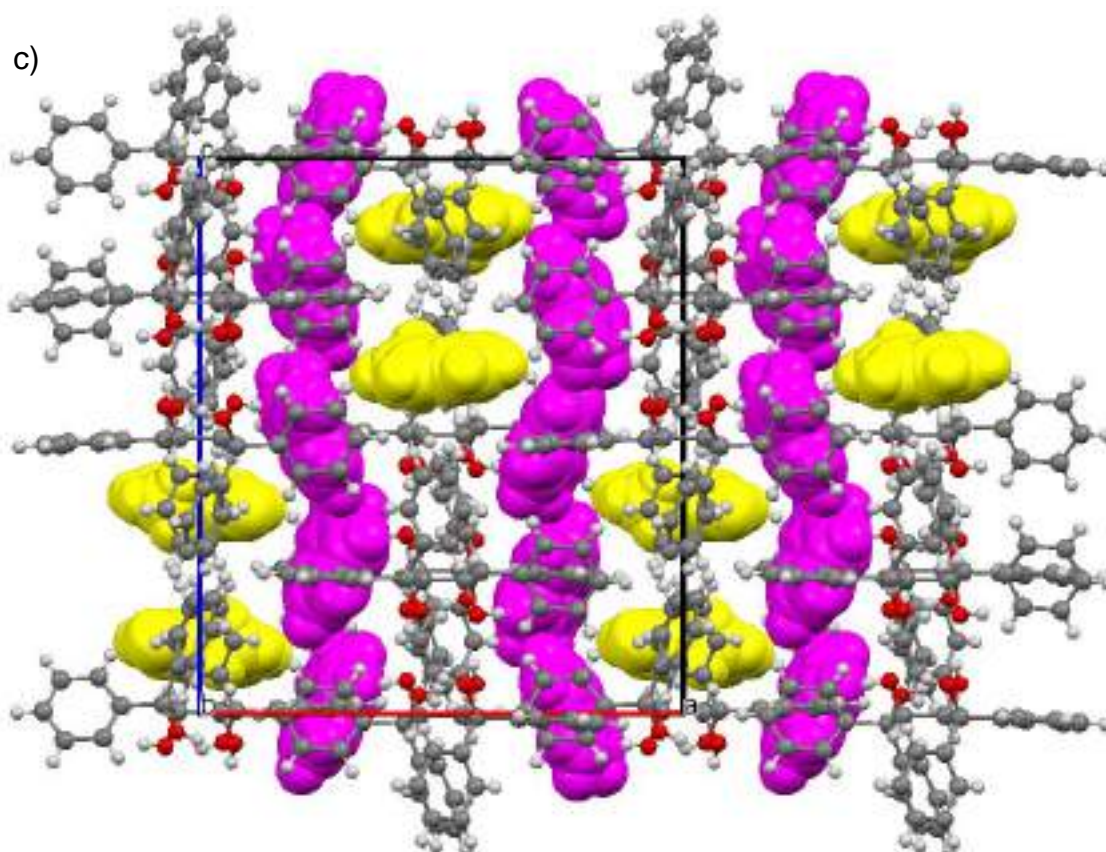
Figure 5: Crystal packing of a) 2TET·3ANI, b) 2TET·2ANI·TOLU and c) 2TET·2ANI·*o*-TOLU; host and guest shown in 'ball and stick' and spacefilling form, respectively; oxygen (red), nitrogen (blue), carbon (grey), hydrogen (light grey), H-bonded ANI molecules (magenta), ANI[3] molecule (orange), TOLU (green) and *o*-TOLU (yellow)
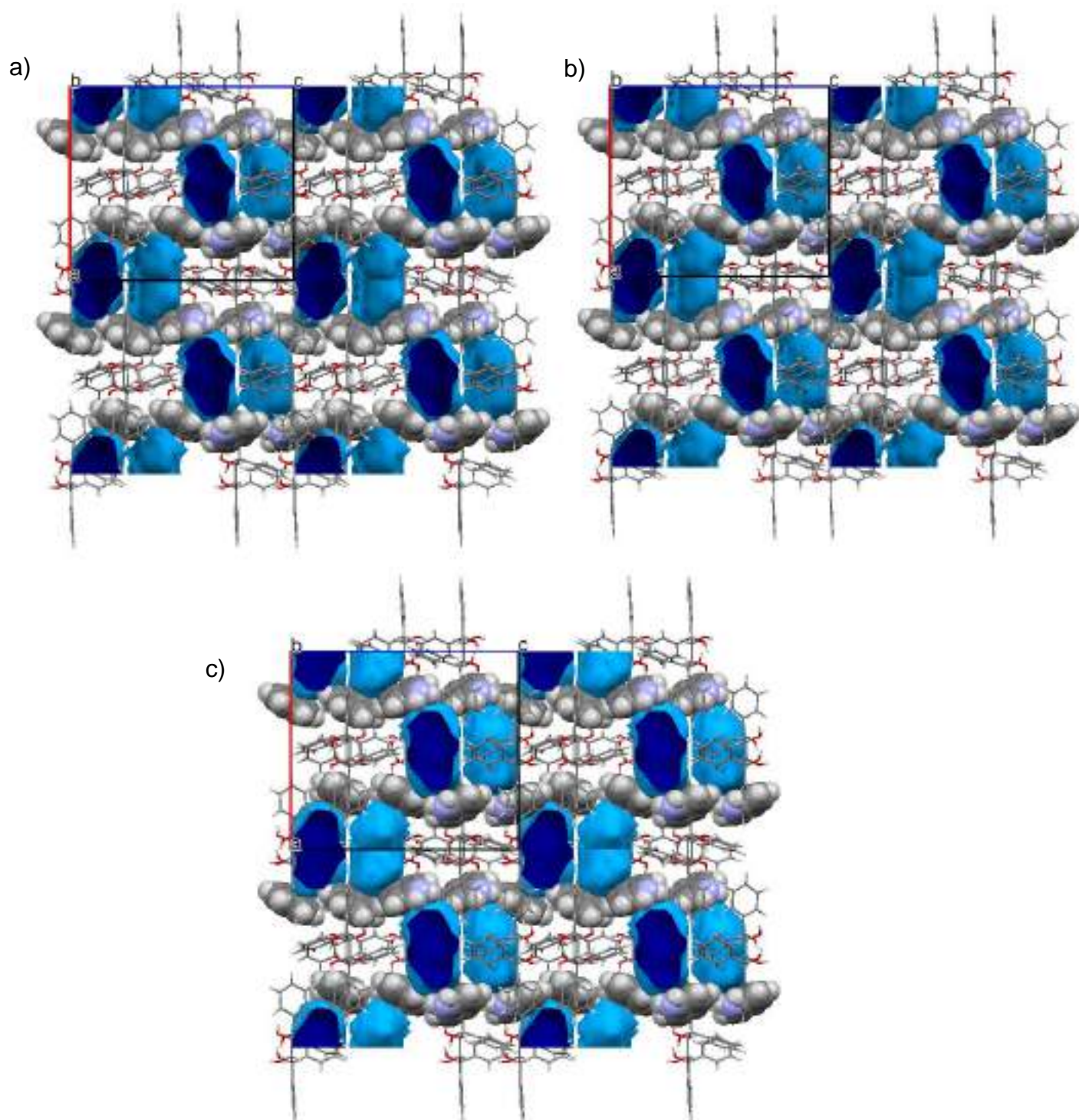
Figure 6: calculated voids (blue) for a) 2TET·3ANI with the third aniline guest removed, b) 2TET·2ANI·TOLU with toluene removed, and c) 2TET·2ANI· *o*-TOLU with *o*-toluidine removed, indicating identical guest accommodation in discrete cavities for these removed guests; oxygen (red), nitrogen (blue), carbon (grey), hydrogen (light grey)
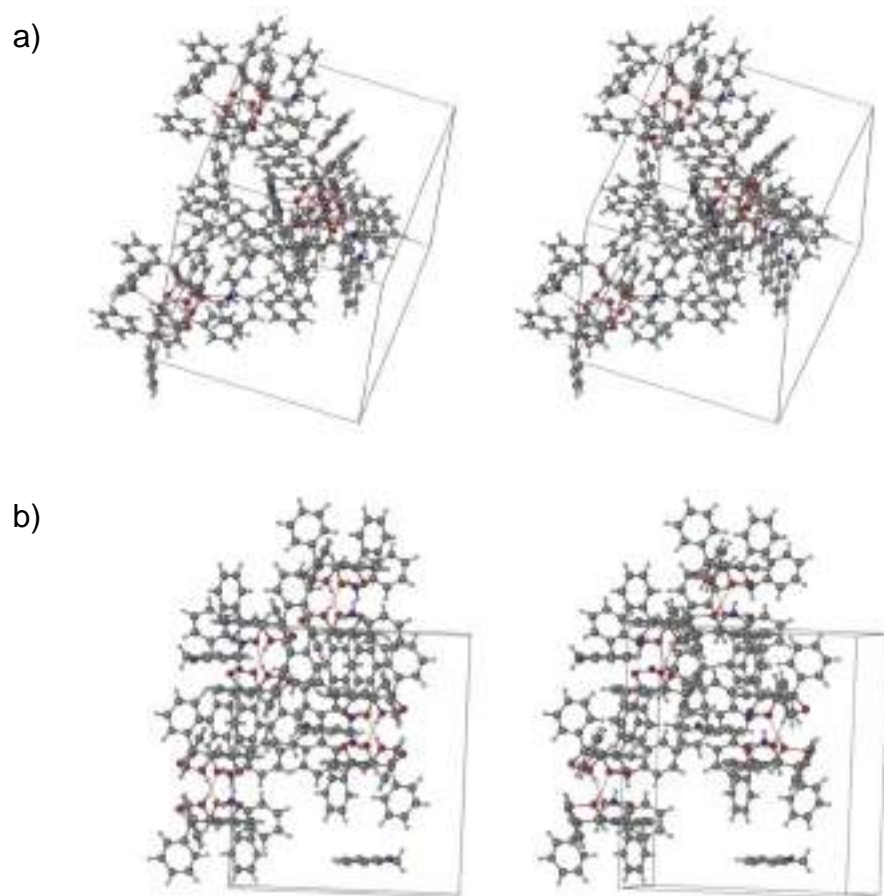
Figure 7: Stereoviews illustrating the unit cells of a) 2TET·2ANI·TOLU and b) 2TET·2ANI·*o*-TOLU

Table 8: Relevant single crystal X-ray crystallographic data for 2TET·3ANI and the 2TET·2ANI·TOLU and 2TET·2ANI· *o*-TOLU mixed complexes

	2TET·3ANI	2TET·2ANI·TOLU	2TET·2ANI· *o*-TOLU
Chemical formula	$2(C_{28}H_{26}O_4)\cdot$ $2(C_6H_7N)\cdot C_6H_5N^a$	$2(C_{28}H_{26}O_4)\cdot$ $2(C_6H_7N)\cdot C_7H_8$	$2(C_{28}H_{26}O_4)\cdot0.551(C_7H_7N)\cdot$ $2(C_6H_7N)\cdot0.449(C_6H_5N)^a$
Formula weight	1130.34	1131.36	1138.07
Crystal system	Orthorhombic	Orthorhombic	Orthorhombic
Space group	$P2_12_12_1$	$P2_12_12_1$	$P2_12_12_1$
μ (Mo Kα)/mm^{-1}	0.080	0.079	0.079
a/Å	17.3680(9)	17.4047(5)	17.4315(6)
b/Å	17.5435(9)	17.5573(5)	17.6733(6)
c/Å	20.0346(10)	20.0344(6)	20.0258(7)
α/°	90	90	90
β/°	90	90	90
γ/°	90	90	90
V/Å^3	6104.5(5)	6122.1(3)	6169.4(4)
Z	4	4	4
F (000)	2400	2408	2418
Temp (K)	200	200	200
Restraints	6	6	6
Nref	15216	15291	15382
Npar	758	758	761
R1	0.0401	0.0397	0.0442
wR2	0.1135	0.1053	0.1266
S	1.04	1.02	1.03
Θ min, max/°	1.5, 28.3	1.5, 28.4	1.5, 28.3
Tot. data	147780	89513	118328
Unique data	15216	15291	15382
Observed data [I > 2.0σ(I)]	12442	11924	12216
Rint	0.023	0.025	0.023
Diffrn measured fraction Θ full	1.000	1.000	1.000
Min. resd. dens. (e/Å^3)	−0.32	−0.23	−0.32
Max. resd. dens. (e/Å^3)	0.40	0.28	0.43

[a]Hydrogen atoms could not be located during SCXRD structural refinement of the crystal structure

Similarities were observed between the 2TET·3ANI and 2TET·3*p*-TOLU complexes from competition experiments and SCXRD analyses (Table 2, 42.6:57.4 ANI:*p*-TOLU and Table 7). We are aware that *p*-TOLU is a symmetrical molecule and that TETROL would perhaps have a similar crystal packing with this guest as with ANI, also symmetrical. We subsequently grew host crystals from an equimolar mixture of ANI and *p*-TOLU. The suitable crystals were analysed using SCXRD and s.o.f values determined for each of the guest pairs included (Figure 8, A–C). (Note that both ANI and *p*-TOLU were able to occupy each of the three sites in the host crystal.) For A, an s.o.f of 0.713 was determined for the major component (*p*-TOLU) and 0.287 for the minor component (ANI). Surprisingly, for the second H-bonded guest pair (Figure 8, B), the major component was ANI (79.5%) and the minor component *p*-TOLU (20.5%). The major component for C was *p*-TOLU (83.1%) and the minor component ANI (16.9%). From this complex, the overall ANI:*p*-TOLU ratio was determined to be 41.7:58.3. These results are in excellent agreement with the GC-MS experiment discussed previously (Table 2, 42.6:57.4). From Figure 8, it is clear that both guests occupy the same site within the crystal and that their orientations are identical, with each aniline ring exactly overlapping, appearing as though only *p*-TOLU is present. Figure 9 shows a stereoview of the host and guest orientations in the unit cell. The guests are retained in this crystal by means of two (host)O−H⋯N(guest) H-bonds measuring 2.722(4) and 2.747(4) Å, with angles of 165 and 161°, respectively. Additionally, the guests are stabilised by one (guest)N−H⋯π(host) (2.72–2.87 Å, 132–170°), two (host)C−H⋯π(guest) (2.89 and 2.96 Å, 156 and 166°, respectively) and two (host)*m*Ar–H⋯H–Me(guest) (2.24 and 1.99 Å, 133 and 131°, respectively) interactions. Crystal data and refinement parameters for this complex are listed in Table 9, and this crystal is clearly isostructural with 2TET·3ANI, crystallizing in the orthorhombic crystal system and $P2_12_12_1$ space group with Z = 4.
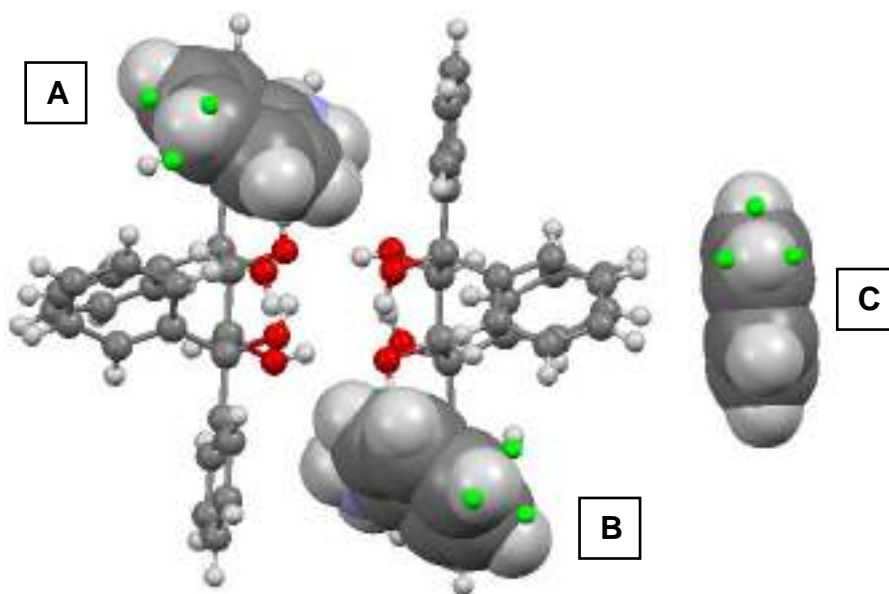
Figure 8: Unit cell of for the ANI·*p*-TOLU mixed complex; oxygen (red), nitrogen (blue), carbon (grey), hydrogen (light grey) and *p*-TOLU methyl hydrogens (green)
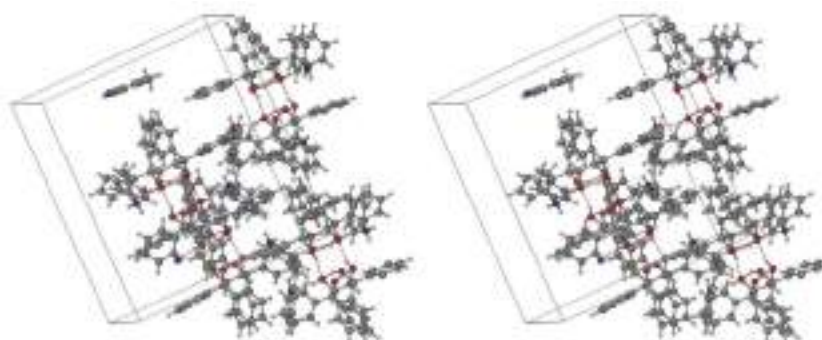
Figure 9: Stereoview illustrating the unit cell for the ANI·*p*-TOLU mixed complex; oxygen (red), nitrogen (blue), carbon (grey) and hydrogen (light grey)

Table 9: Relevant single crystal X-ray crystallographic data for the complexes of TETROL with 3ANI and *p*-TOLU, and the TET/ANI/*p*-TOLU mixed complex

	2TET·3ANI	2TET·3*p*-TOLU	TET/ANI/*p*-TOLU
Chemical formula	$2(C_{28}H_{26}O_4)\cdot$ $2(C_6H_7N)\cdot C_6H_5N^a$	$2(C_{28}H_{26}O_4)\cdot$ $3(C_7H_9N)$	$2(C_{28}H_{26}O_4)\cdot C_{6.71}H_{8.43}N\cdot$ $C_{6.21}H_{7.41}N\cdot C_{6.83}H_{6.66}N$
Formula weight	1130.34	1174.43	1154.87
Crystal system	Orthorhombic	Orthorhombic	Orthorhombic
Space group	$P2_12_12_1$	$P2_12_12_1$	$P2_12_12_1$
μ (Mo Kα)/mm^{-1}	0.080	0.078	0.078
a/Å	17.3680(9)	17.4913(5)	17.5536(8)
b/Å	17.5435(9)	18.5146(5)	18.1591(8)
c/Å	20.0346(10)	19.8236(6)	19.7729(8)
α/°	90	90	90
β/°	90	90	90
γ/°	90	90	90
V/Å^3	6104.5(5)	6419.8(3)	6302.9(5)
Z	4	4	4
F (000)	2400	2504	2456
Temp (K)	200	200	200
Restraints	6	1	1
Nref	15216	15966	15680
Npar	758	819	809
R1	0.0401	0.0411	0.0489
wR2	0.1135	0.1032	0.1293
S	1.04	1.02	1.01
Θ min, max/°	1.5, 28.3	1.6, 28.3	1.9, 28.3
Tot. data	147780	116349	75228
Unique data	15216	15966	15680
Observed data [I > 2.0σ(I)]	12442	12034	10243
Rint	0.023	0.027	0.033
Diffrn measured fraction Θ full	1.000	1.000	1.000
Min. resd. dens. (e/Å^3)	−0.32	−0.22	−0.19
Max. resd. dens. (e/Å^3)	0.40	0.20	0.29

^{a}Hydrogen atoms could not be located during SCXRD structural refinement of the crystal structure

7.4 Hirshfeld Surface Analysis

Hirshfeld surface analyses were conducted on the 2TET·3*m*-TOLU and 2TET·3*p*-TOLU complexes to summarise the multiple intermolecular interactions present (Figure 10). A summary of the percentage of each interaction type is displayed graphically in Figure 11, while Table 10 provides the actual values obtained from this figure. For comparison purposes, we have included the Hirshfeld analysis data for the 2TET·3ANI complex (Figure 11 and Table 10).

It is important to note that the third ANI and *m*-TOLU guests appear to experience a greater number of H⋯N/N⋯H contacts due to these guests being disordered and undefined from SCXRD analysis as a result of not being held in position by H-bonds (Table 10). The 2TET·3*m*-TOLU [3] and 2TET·3ANI [3] complexes will, therefore, be omitted from this discussion. From Figure 11, it is clear that all complexes with TETROL are predominantly stabilised by H⋯H (51.7–69.3%) and C⋯H (23.4–37.2%) contacts (Table 10). The 2TET·3*p*-TOLU[2] experiences a greater percentage of O⋯H/H⋯O interactions (Table 10, 3.9%), while the 2TET·3*m*-TOLU[1] has a greater number of H⋯N/N⋯H interactions (Table 7, 6.0%). Consequently, these analyses do not provide evidence for the host's selectivity order for these guests.
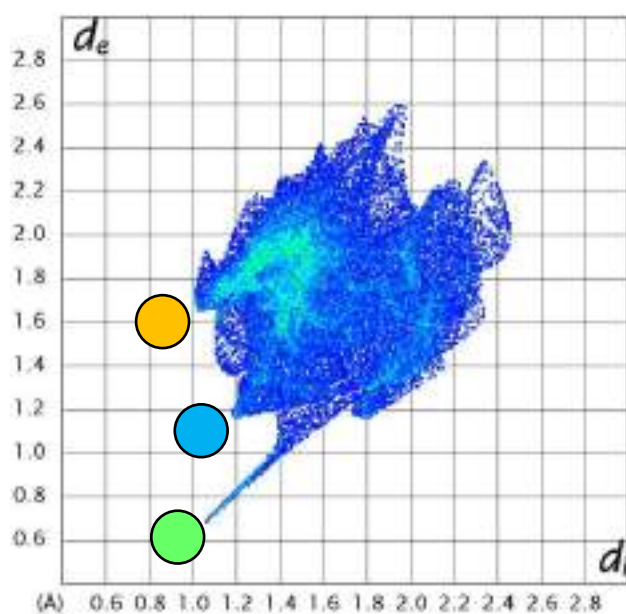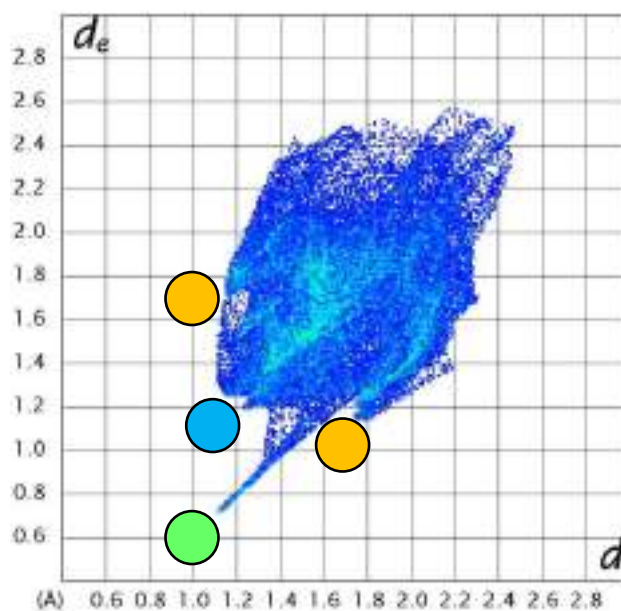
2TET·3*m*-TOLU [1]   **2TET·3*m*-TOLU [2]**
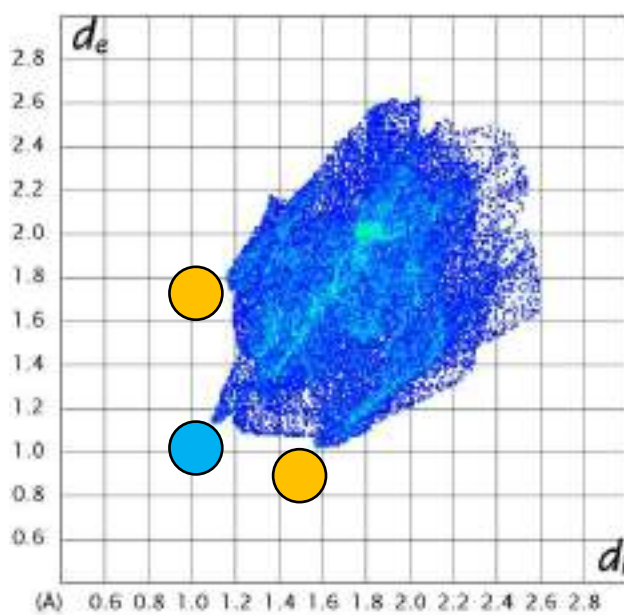
2TET·3*m*-TOLU [3]
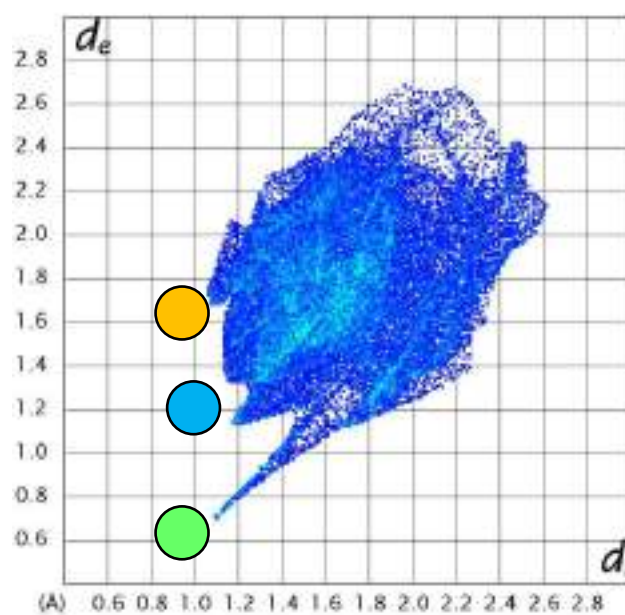
2TET·3*p*-TOLU [1]
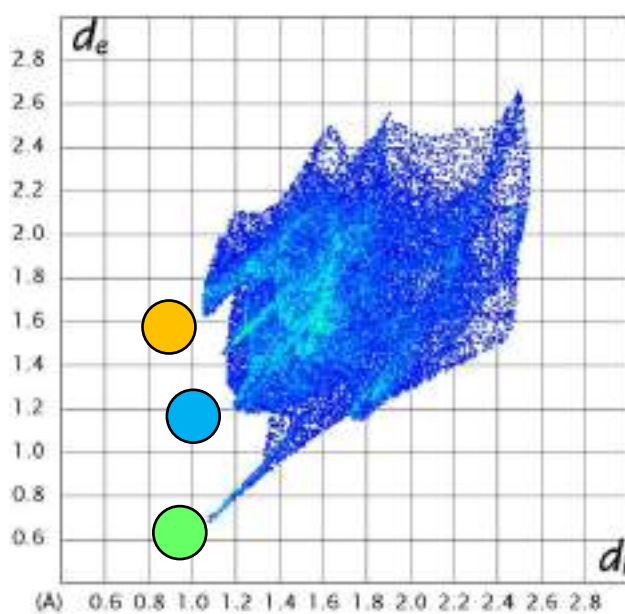
2TET·3*p*-TOLU [2]
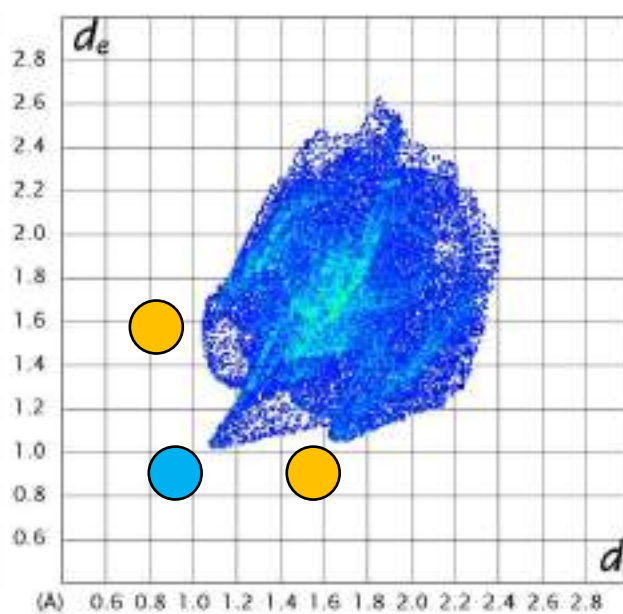
2TET·3*p*-TOLU [3]

Figure 10: Hirshfeld fingerprint plots for 2TET·3*m*-TOLU and 2TET·3*p*-TOLU crystal structures; the 'spike' and 'wings' observed in the Hirshfeld plots are colour coded and depict N···H (green), H···H (blue) and C···H (orange) contacts
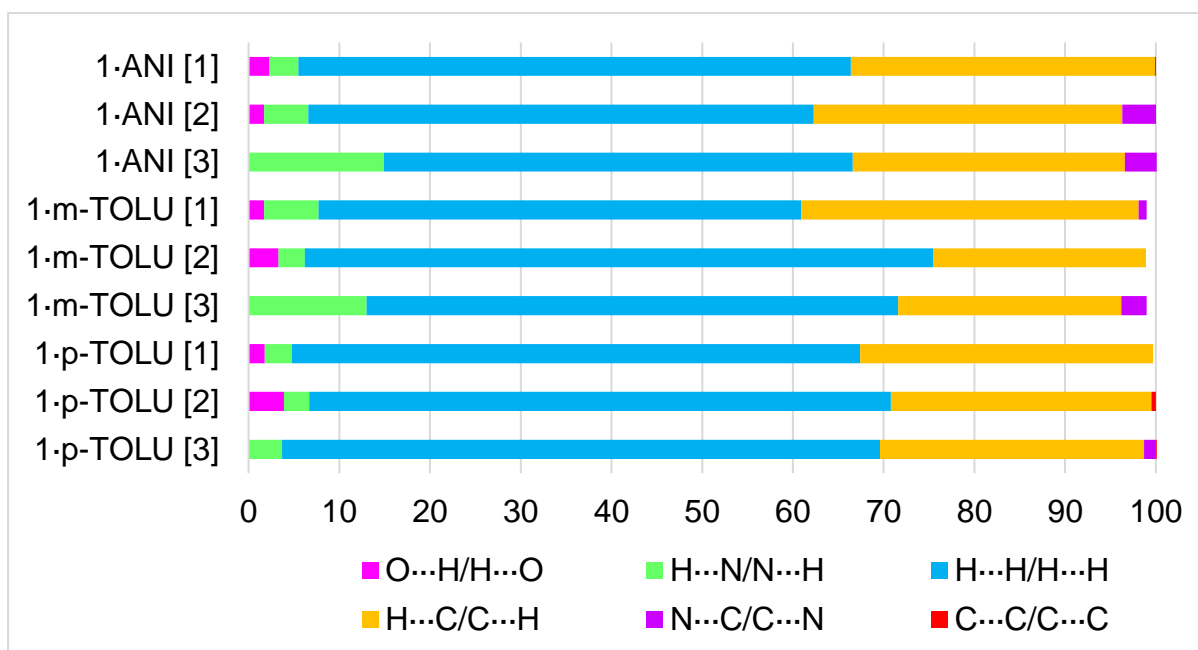
Figure 11: Graphical display showing the percentage intermolecular forces of each type for 2TET·3ANI, 2TET·3*m*-TOLU and 2TET·3*p*-TOLU complexes

Table 10: Percentage intermolecular interactions in each inclusion complex (G···H/H···G)

	O···H/ H···O	H···N/ N···H	H···H/ H···H	H···C/ C···H	N···C/ C···N	C···C/ C···C
2TET·3ANI [1]	2.3	3.2	60.9	33.5	0	0.1
2TET·3ANI [2]	1.7	4.9	55.7	34	3.6	0.1
2TET·3ANI [3]a	0	14.9	51.7	30	3.5	0
2TET·3*m*-TOLU [1]	1.7	6	53.2	37.2	0.9	0
2TET·3*m*-TOLU [2]	3.3	2.9	69.3	23.4	0	0
2TET·3*m*-TOLU [3]ª	0	13	58.6	24.6	2.8	0
2TET·3*p*-TOLU [1]	1.8	3	62.6	32.3	0	0
2TET·3*p*-TOLU [2]	3.9	2.8	64.1	28.7	0	0.5
2TET·3*p*-TOLU [3]	0	3.7	65.9	29.1	1.3	0.1

ªInteractions experienced by disordered guest component

7.5   Thermal Analyses

Both DSC and TG experiments were carried out on the four inclusion complexes and the traces obtained are provided in Figures 12a and b. Upon heating of 2TET·3*m*-TOLU, a stepwise guest release process ensues (Figure 12a), with an onset temperature (T_{on}) of ~56.4 °C (Table 11). The majority of the guest is released prior to the melting of the host (Figure 12a, 145.2 °C). The expected mass loss for the 2:3 H:G complex was calculated to be 27.4%, which is in agreement with the actual mass loss observed (Table 11, 27.1%). In comparison to 2TET·3*m*-TOLU, the guest release process for 2TET·3*p*-TOLU is less complex, with a T_{on} value of 73.8 °C (Figure 12b), and it appears as though both the guest release and host melt processes occur concomitantly. The observed mass loss (Table 11, 27.5%) is in agreement with that expected for a 2:3 complex (27.4%).

Furthermore, the onset temperatures for the guest release processes correlate exactly with and explain the preference order of TETROL for these guests (*p*-TOLU > ANI > *m*-TOLU). The higher onset temperature for *p*-TOLU alludes to the guest being more tightly bound in the crystal of the formed complex.

a)

b)
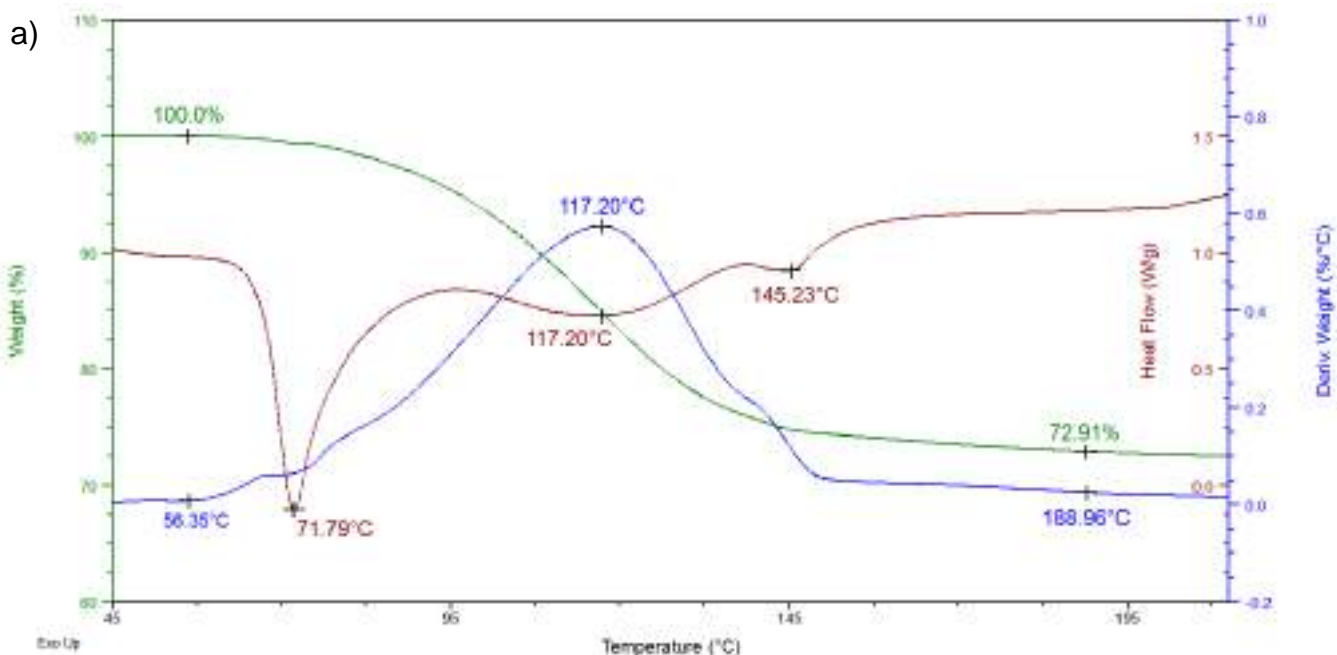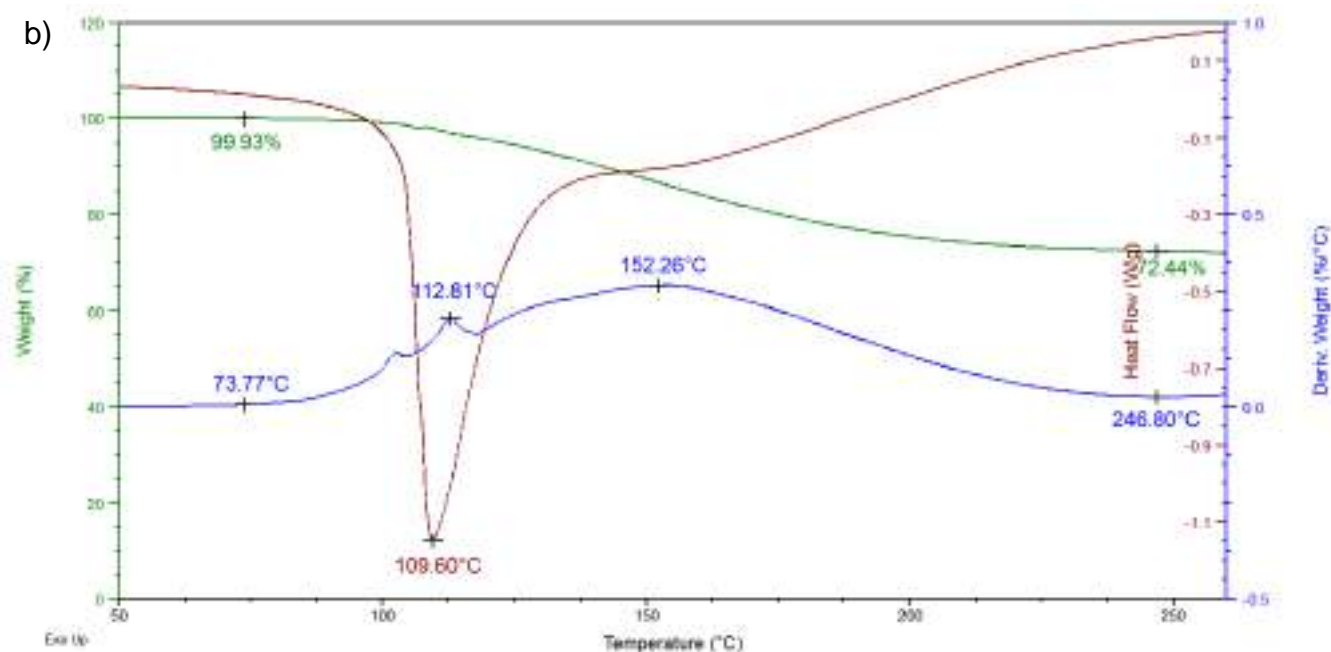
Figure 12: Overlaid traces for the DSC (brown), TG (green) and its derivative (DTG, blue) for the a) 2TET·3*p*-TOLU and b) 2TET·3*m*-TOLU complexes

Table 11: Thermal data from DSC/TG traces for of 2TET·3*p*-TOLU and 2TET·3*m*-TOLU

Guest	T_{on} (°C)	T_p (°C)[a]	T_{end} (°C)[b]	Mass loss % (expected)	Mass loss % (actual)
ANI[c]	70.9	~98.8 108.8 125.2	~89.8 104.5 127.9	24.7	25.3
m-TOLU	56.4	117.2	71.79 ~117.2 ~145.2	27.4	27.1
p-TOLU	73.8	112.8 ~152.3	109.6	27.4	27.5

[a]T_p values determined from blue DTG traces
[b]T_{end} were obtained from the brown DSC traces
[c]Thermal data included for ease of comparison

7.6   Conclusion

The host, TETROL, showed selectivity towards the toluidine isomers, *o*-TOLU, *m*-TOLU and *p*-TOLU. This host showed high selectivity for *p*-TOLU when recrystallised from mixtures of the three isomers, and also in the presence of ANI and TOLU, resulting in a selectivity order of *p*-TOLU > ANI > *m*-TOLU > *o*-TOLU > TOLU. As evidence, SCXRD analysis showed that the 2TET·3*p*-TOLU complex experienced the strongest host-guest H-bond interactions [Table 6, 2.710(2), 165°] and the shortest stabilising short contact (Table 7, 2.28 Å, 151°). Hirshfeld surface analyses were not useful in this regard. Thermogravimetric analyses confirmed that *p*-TOLU was more tightly bound in the crystal compared to the other two guests (ANI and *m*-TOLU), and T_{on} values correlated exactly with the host selectivity order.

Chapter 8

The Selectivity of TETROL for Four Selected Cyclic and Aromatic Compounds

8.1   Introduction

Pure cyclohexanol is produced by the hydrogenation of phenol using an appropriate catalytic system such as nickel on silica or alumina (Scheme 1). The yield of cyclohexanol is almost quantitative and is separated from the reaction by condensation.[195] However, due to low experimental costs, cyclohexanol is currently produced from cyclohexane.[196] Phenol, in turn, is obtained from coal tar or petroleum, and is industrially important in the manufacture of a variety of compounds such as drugs, dyes and phenolic resins.[197] In general, phenol is commonly used as a disinfectant for toilets, stables, cesspools, floors and drains, and can be found in germicidal paints, slimicides and glue.[198]
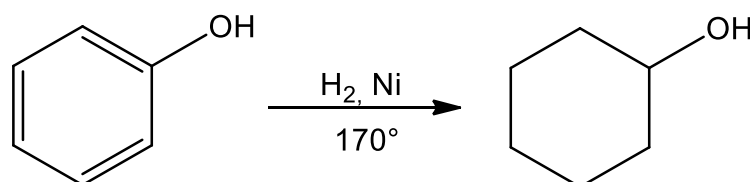
Scheme 1: Catalytic hydrogenation of phenol for the synthesis of cyclohexanol

As previously stated in Chapter 3, cyclohexylamine can be produced by the catalytic hydrogenation of aniline (Scheme 2).[175] The great difficulties associated with this reaction, at an industrial level, is in finding optimal conditions to separate pure cyclohexylamine product from unreacted aniline starting material.[199] The primary source of aniline is the catalytic hydrogenation of nitrobenzene, producing cyclohexylamine and dicyclohexylamine as by-products (Scheme 3).[200] This reaction has been intensely studied by researchers to ultimately produce one product.[200–202]
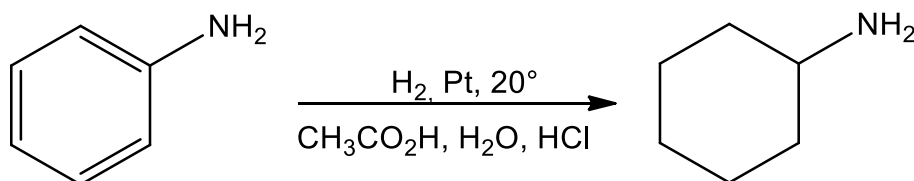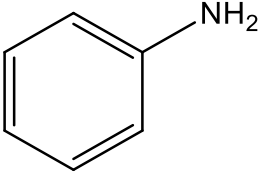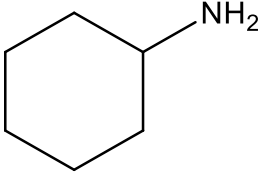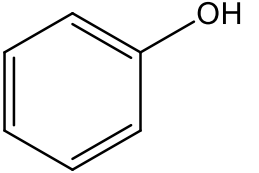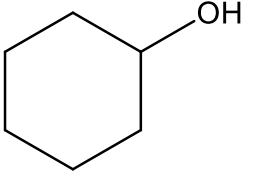
Scheme 2: Catalytic hydrogenation of aniline for the synthesis of cyclohexylamine
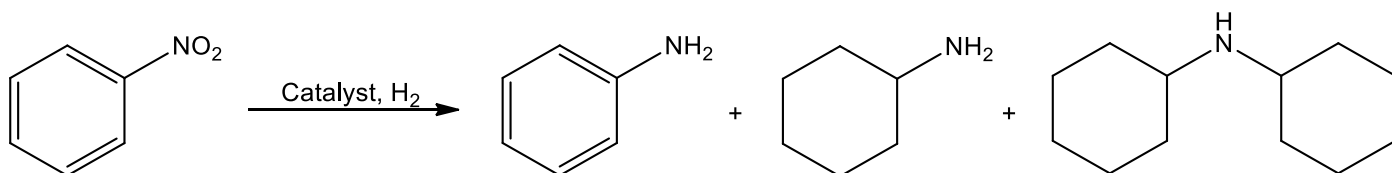
Scheme 3: Catalytic hydrogenation of nitrobenzene for the synthesis of aniline, with cyclohexylamine and dicyclohexylamine as by-products

In this investigation, we analyse the ability of TETROL to separate cyclohexanol from phenol and cyclohexylamine from aniline, as well as from mixtures of one another. Additionally, it is interesting to determine whether the host's inclusion preference can, once more, be characterized by amine versus hydroxyl hydrogen-bond donor guests. The four guests species were all enclathrated when crystals of this host compound were grown from each of them forming 2TET·3ANI, TET·2CAM, TET·PHO and TET·COL complexes, as provided in Table 1, together with the boiling points of the pure guests.

Table 1: The structure and properties of the four aromatic and non-aromatic cyclic amine and hydroxyl compounds

	Aniline	Cyclohexylamine	Phenol	Cyclohexanol
Structure				
Host (H): guest (G) ratio	2:3	1:2	1:1	1:1
Boiling point (°C)	184.1	134	181.7	161.8

8.2 Competition Experiments

Since each guest was enclathrated individually, competition studies were conducted to determine the selectivity of TETROL for these guests. In Table 2, we summarize the data from recrystallization experiments of TETROL from various equimolar binary, ternary and quaternary combinations of ANI, CAM, PHO and COL. The so-formed crystal inclusions were analysed using NMR spectroscopy and GC-MS. The preferred guest species is given in bold red font face.

From Table 2, CAM was the preferred guest species whenever it was present in binary mixtures (ANI/CAM, CAM/PHO and CAM/COL, with molar ratios of 75.2%, 65.6% and 93.5%, respectively). In the absence of CAM, ANI was selected for, as observed from the ANI/PHO and ANI/COL experiments (85.3% and 94.0%). When CAM and ANI were excluded from these experiments, COL was favoured (COL/PHO, 78.2%). Ternary equimolar experiments, however, yielded surprising results. All experiments involving ANI showed this guest to now be the preferred guest for TETROL, and not CAM (ANI/CAM/PHO, ANI/PHO/COL and ANI/CAM/PHO experiments afforded crystals with 53.3%, 83.9% and 56.6% ANI, respectively) but, in its absence, CAM was then selected for (CAM/PHO/COL, 92.9%). Equimolar quaternary experiments yielded a host selectivity order of ANI (57.5%) > CAM (37.8%) > COL (3.5%) > PHO (1.3%) for these guests.

Table 2: Competition experiments using host and various equimolar mixtures of ANI, CAM, PHO and COL[a,b]

ANI	CAM	PHO	COL	Guest ratios (%e.s.d.s)	Overall H:G ratio
X	**X**			24.8:**75.2** (0.6)	2:3
X		X		**85.3**:14.7 (0.6)	2:3
X			X	**94.0**:6.0 (0.3)	2:3
	X	X		**65.6**:34.4 (0.7)	1:2
	X		X	**93.5**:6.5 (0.9)	1:2
		X	**X**	21.8:**78.2** (0.2)	1:1
X	X	X		**53.3**:44.2:2.5 (0.5)(0.8)(0.3)	2:3
X		X	X	**83.9**:4.4:11.7 (1.3)(0.6)(0.7)	2:3
X	X		X	**56.6**:40.6:2.7 (0.2)(0.6)(0.7)	2:3
	X	X	X	**92.9**:2.6:4.5 (1.9)(1.5)(0.4)	1:2
X	X	X	X	**57.5**:37.7:1.3:3.5 (0.3)(0.7)(0.7)(0.3)	2:3

[a]Ratios determined using proton NMR spectroscopy and gas chromatography

[b]Experiments were conducted in triplicate; %e.s.d.'s are provided in parentheses

The binary experiments were further extended beyond equimolar in the form of selectivity profiles for the ANI/CAM, ANI/PHO, ANI/COL, CAM/PHO, CAM/COL and PHO/COL experiments (Figures 1a–f) with changing guest ratios. Analyses were carried out using proton NMR and GC-MS methods as before.

a)

$Z_{Cyclohexylamine}$ (crystal)

$X_{Cyclohexylamine}$ (solution)

$K_{CAM:ANI} = 75.0$

b)

$Z_{Cyclohexylamine}$ (crystal)

$X_{Cyclohexylamine}$ (solution)

$K_{CAM:COL} = 249.0$

c)

$K_{CAM:PHO} = 3.2$

X-axis: $Z_{Cyclohexylamine}$ (solution)
Y-axis: $Z_{Cyclohexylamine}$ (crystal)

d)

$K_{ANI:PHO} = 6.0$

X-axis: $X_{Aniline}$ (solution)
Y-axis: $Z_{Aniline}$ (crystal)

e)

f)

$K_{COL:PHO} = 46.6$
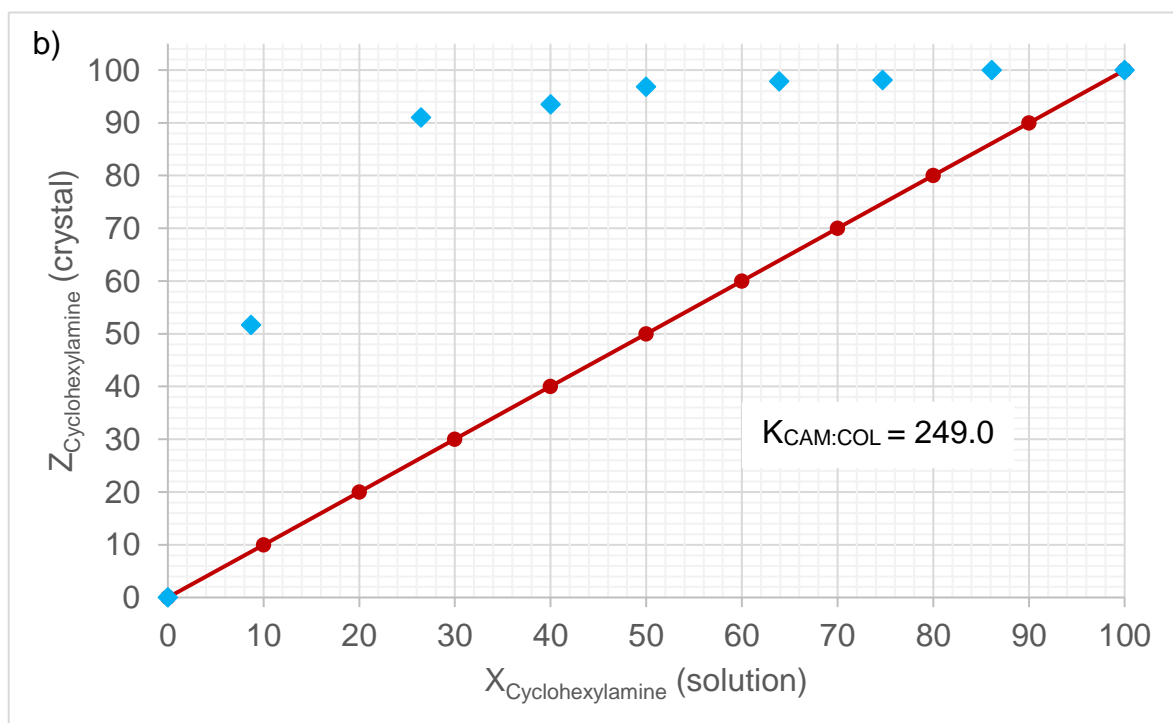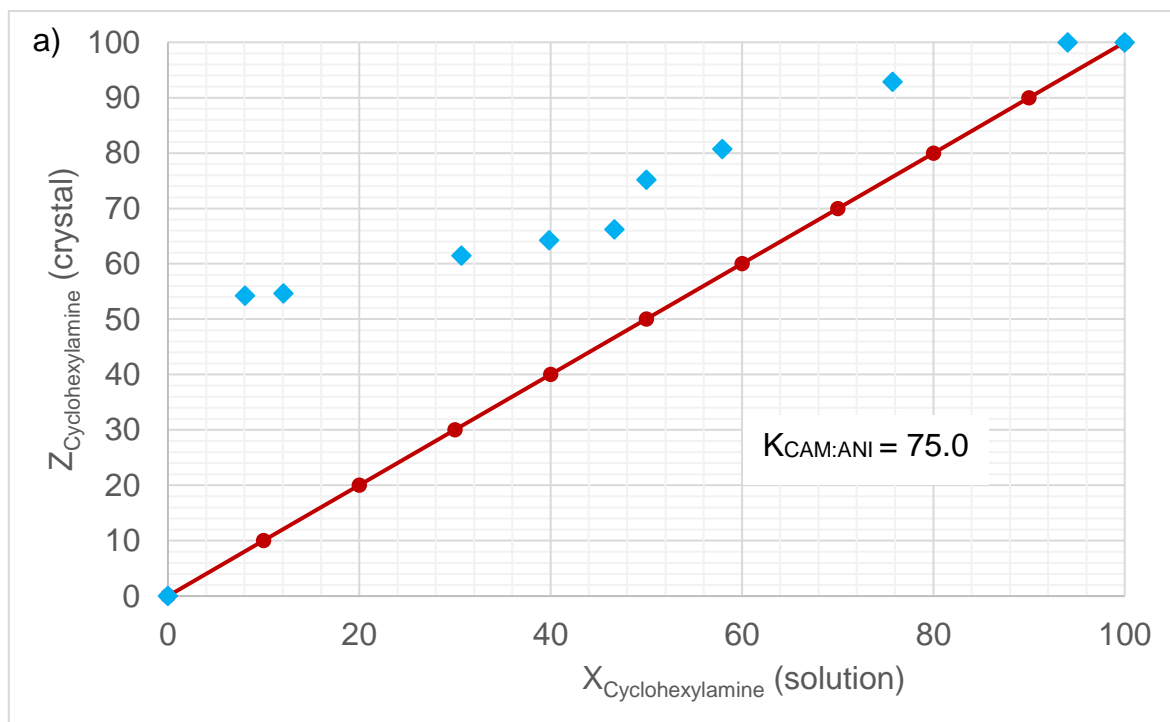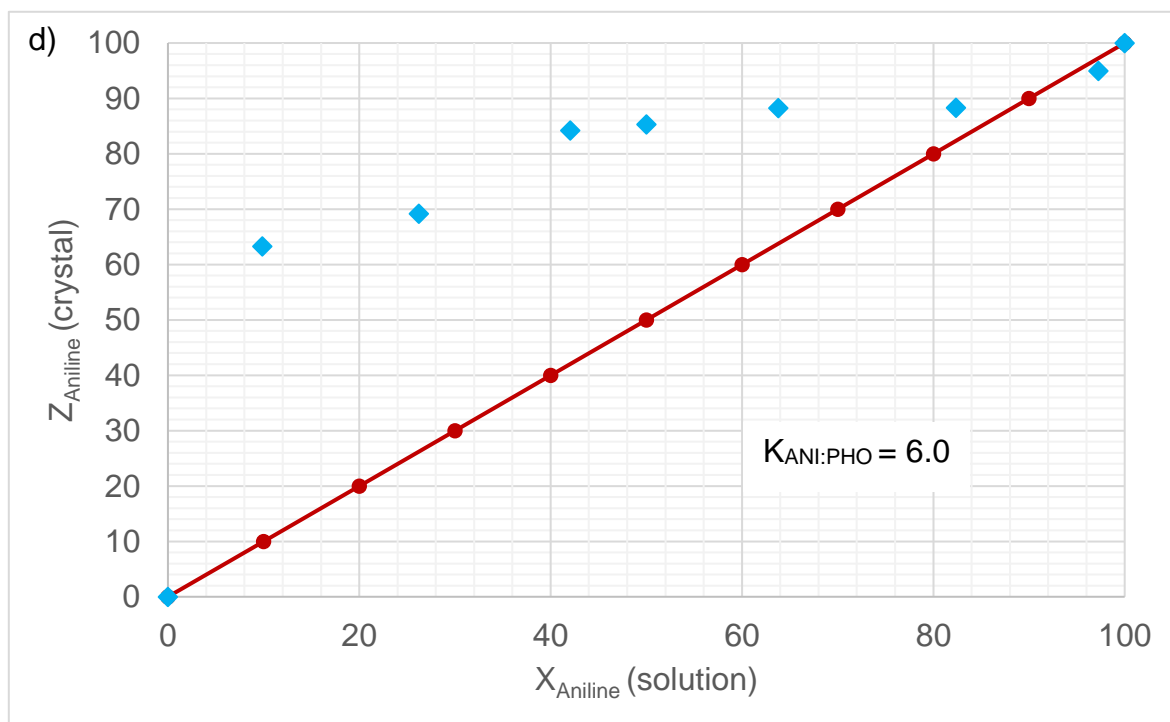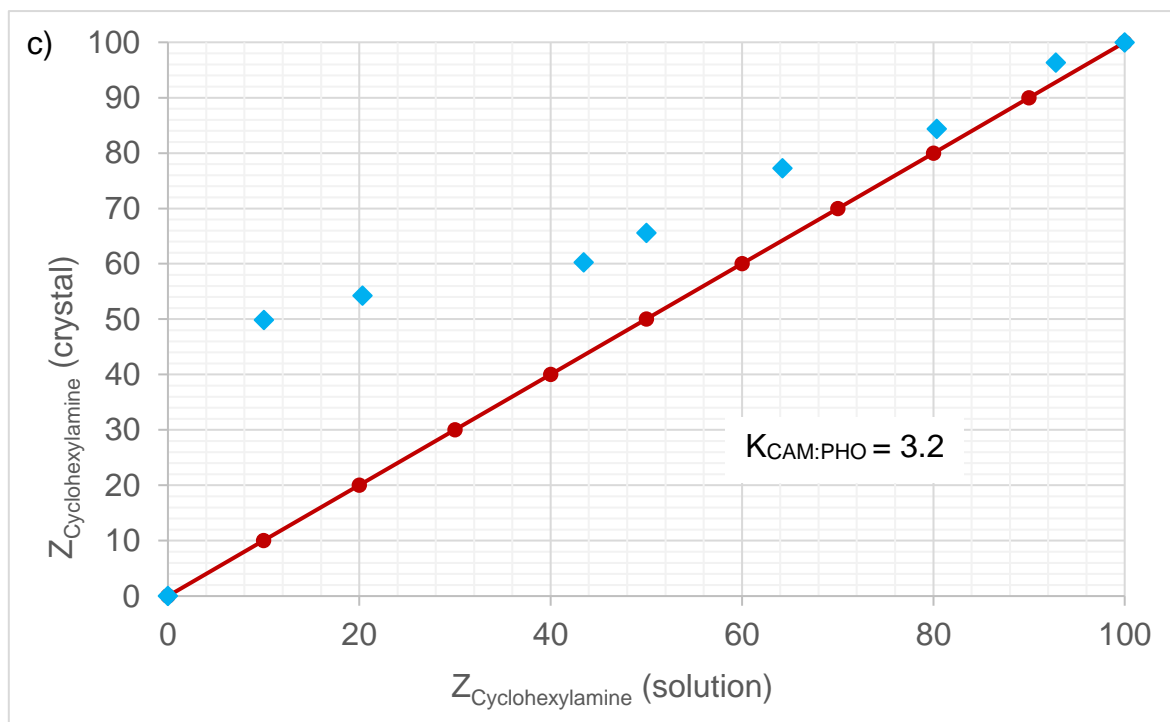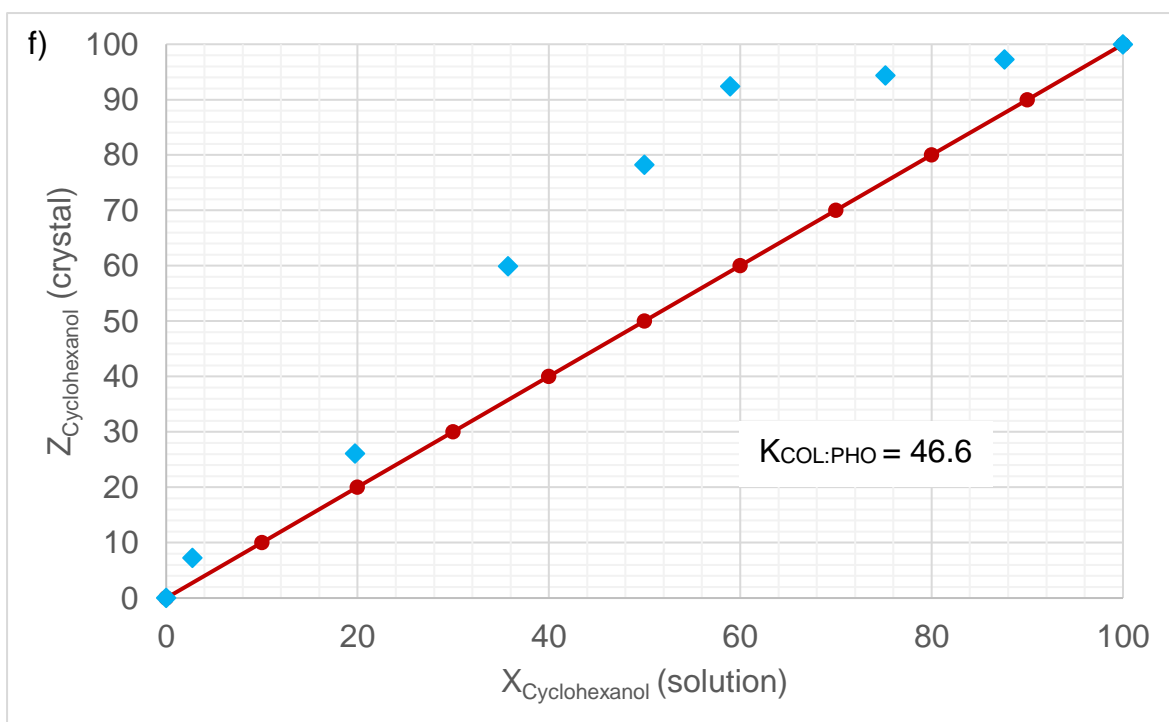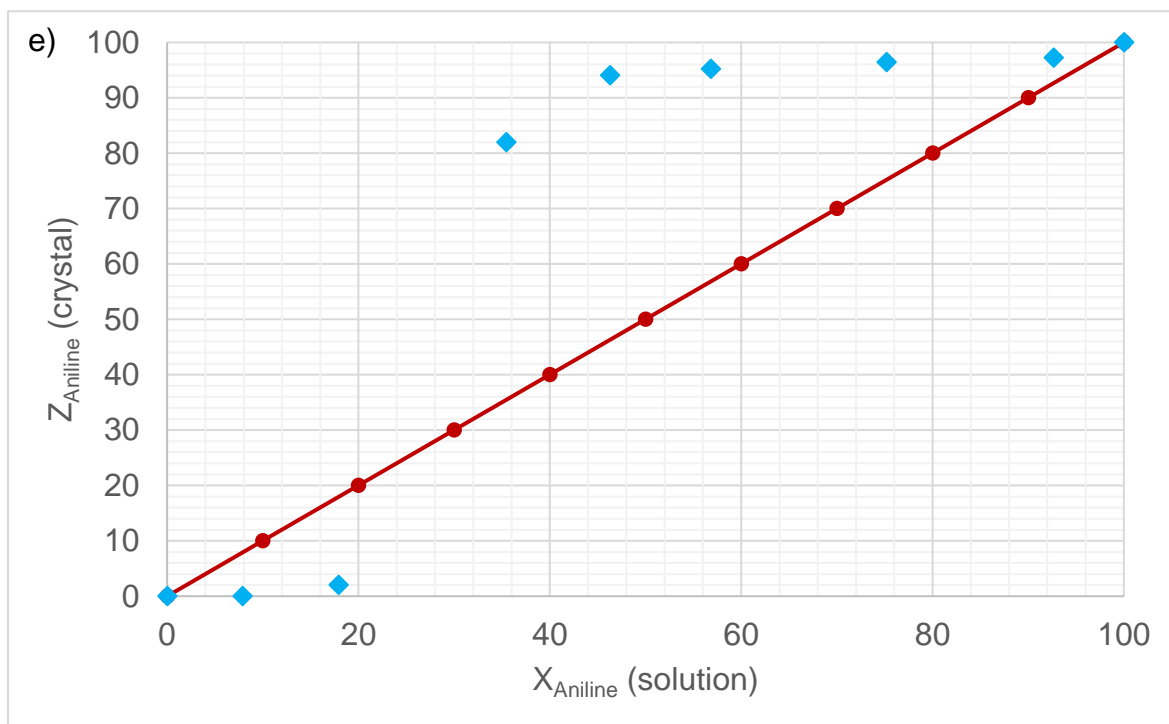
Figure 1. Selectivity curves for a) CAM/ANI, b) CAM/COL, c) CAM/PHO, d) ANI/PHO, e) ANI/COL and f) COL/PHO

Figure 1a (for the mixture of CAM/ANI) shows the selectivity of the host to be in favour of CAM over the entire concentration range investigated ($K_{CAM:ANI}$ = 75.0). This same selectivity was observed in Figures 1b and 1c where CAM was, once more, favoured by the host in the CAM/COL and CAM/PHO binary experiments ($K_{CAM:COL}$ = 249.0 and $K_{CAM:PHO}$ = 3.2, respectively). It must noted that the CAM/COL competition experiment was investigated in a previous chapter (Chapter 3). High selectivity was observed in the ANI/PHO mixture, where ANI was favoured over the entire concentration range, affording $K_{ANI:PHO}$ = 6.0 (Figure 1d). According to Figure 1e (for the mixture of ANI/COL), the selectivity of the host was guest-concentration dependent; at low concentrations of ANI, the host was selective for COL. Soon after, the host changed and showed selectivity towards ANI for the remainder of the concentration range investigated. A selectivity coefficient for this profile is not provided here as the value obtained would be misleading due to the host selectivity change with guest concentration change. For the binary mixture of COL/PHO, the host showed reasonable selectivity for COL over the entire concentration range investigated ($K_{COL:PHO}$ = 46.6, Figure 1f).

8.3   Single Crystal X-ray Diffraction (SCXRD)

SCXRD analyses on the 2TET·3ANI, TET·2CAM and TET·COL complexes have been analysed in previous chapters (Chapters 3, 6 and 7), but will be discussed here again, as appropriate. These analyses could not be conducted on the TET·PHO complex due to poor crystal quality. For revision, both the TET·2CAM and TET·COL complexes crystallize in the monoclinic crystal system and $P2_1$ space group with Z = 2, while the 2TET·3ANI complex crystallizes in the orthorhombic crystal system and $P2_12_12_1$ space group with Z = 4 (Table 3). The crystal packing of TET·COL is characterized by guests situated in cavities (Figure 2a). Alternatively, the TET·2CAM and 2TET·3ANI complexes have their guests occupying channels (Figures 2b and c, respectively).

Table 3: Relevant single crystal X-ray crystallographic data for the complexes of TETROL with CAM, ANI and COL

	TET·2CAM	2TET·3ANI	TET·COL
Chemical formula	$C_{28}H_{26}O_4$· $2(C_6H_{13}N)$	$2(C_{28}H_{26}O_4)$· $2(C_6H_7N)$, $C_6H_5N^a$	$C_{28}H_{26}O_4$· $C_6H_{12}O$
Formula weight	624.84	1130.34	526.64
Crystal system	Monoclinic	Orthorhombic	Monoclinic
Space group	$P2_1$	$P2_12_12_1$	$P2_1$
μ (Mo Kα)/mm^{-1}	0.076	0.080	0.083
a/Å	12.3859(5)	17.3680(9)	12.7541(3)
b/Å	8.2405(3)	17.5435(9)	8.1884(2)
c/Å	17.1370(7)	20.0346(10)	13.4145(3)
α/°	90	90	90
β/°	96.305	90	94.861(1)
γ/°	90	90	90
V/Å^3	1738.53(12)	6104.5(5)	1395.91(6)
Z	19	4	2
F (000)	676	2400	564
Temp (K)	200	200	200
Restraints	0.999		1
Nref	8486	15216	6031
Npar	427	758	356
R1	0.0473	0.0401	0.0424
wR2	0.1255	0.1135	0.1246
S	1.05	1.04	1.04
Θ min, max/°	1.2, 28.3	1.5, 28.3	1.6, 28.4
Tot. data	29351	147780	16674
Unique data	8486	15216	6031
Observed data [I > 2.0σ(I)]	7473	12442	5445
Rint	0.017	0.023	0.014
Diffrn measured fraction Θ full	0.999	1.000	0.992
Min. resd. dens. (e/Å^3)	−0.34	−0.32	−0.26
Max. resd. dens. (e/Å^3)	0.48	0.40	0.28

[a]Hydrogen atoms could not be located during SCXRD structural refinement of the crystal structure
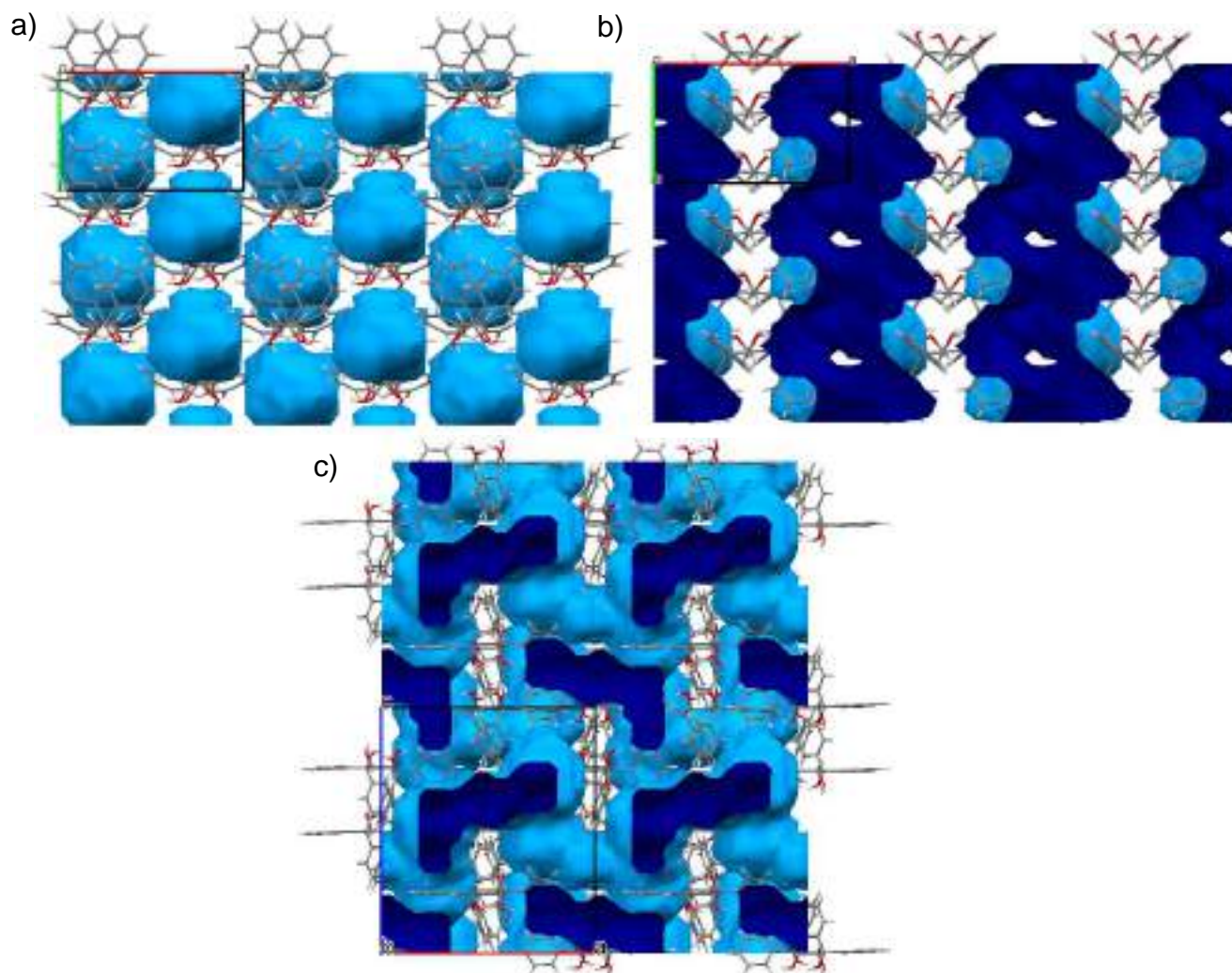
Figure 2: Calculated voids (blue) for a) TET·2COL (guest accommodation in cavities), b) TET·2CAM (guest accommodation in channels) and c) 2TET·3ANI (guest accommodation in convoluted channels); (oxygen – red, carbon – grey, and hydrogen – light grey)

8.3.1 H-Bonding Interactions Between Host and Guest Species

The host framework is stabilised by a pair of 1,3-intramolecular hydrogen bonds, and each guest held in the crystal by means of (host)O–H···O(guest) (as in the case for TET·COL) and (host)O−H···N(guest) interactions (as in the case for TET·2CAM and 2TET·3ANI) (Table 4). Once more, we compared the O···O and O···N distances formed between the host and guest species, and calculated the relative strengths of the hydrogen bonds formed (Table 5).[177,178] The H-bond strengths calculated in Table 5 for TET·COL (0.331 Å), TET·2CAM (0.285 and 0.313 Å) and 2TET·3ANI (0.307 and

0.324 Å) are not in correlation with the selectivity order observed for TETROL with these guests. We refer once more to Abraham,[180] making note that the host is predominantly an H-bond donor[157] and will preferably form a complex with strong acceptors (strong bases) such as aniline and cyclohexylamine. It is worth mentioning that aniline is a weaker base than cyclohexylamine due to lone pair delocalization into the aromatic ring system. This factor correlates with the observed selectivity of TET for CAM over ANI from the binary mixture of these two guests (Table 2), but does not correlate with the overall guest selectivity of TETROL, which favours ANI over CAM whenever these two guests are in the presence of COL or PHO. It is also worth noting that the H-bond angles associated with CAM and ANI are much closer to linearity [(173 and 167°) and (167 and 165°), respectively] which may be a further factor that favours these two amines over COL (155°, Table 4).

Table 4: Analysis of intermolecular hydrogen bonding interactions between TET and guests ANI, CAM and COL

Guest	Unit cell H:G ratio	Guest[†]	(host)O⋯ X(guest) /Å	(host)H⋯ X(guest) /Å	(host)O–H ⋯X(guest) /˚	Symmetry operator
ANI	2:3	ANI [1]	2.763(3) X = N	1.94	167	x,y,z
		ANI [2]	2.746(3) X = N	1.93	165	x,y,z
CAM	1:2	CAM [1]	2.785(3) X = N	1.95	173	x,y,z
		CAM [2]	2.757(3) X = N	1.93	167	x,y,z
COL	1:1	COL[1]	2.709(2) X = O	1.93	155	x,y,z

[†]The unit cell in TET·COL is comprised of only one guest, whereas 2TET·3ANI and TET·2CAM are comprised of three and two guests in unique environments, respectively (but only two ANI guests experience hydrogen bonding). Hence these guests have been labelled ANI[1], ANI[2], CAM[1] and CAM[2]

Table 5: The calculated host–guest hydrogen bond strengths for each complex with TETROL

Complex	Theoretical (host)O⋯X(guest)/Å (A)	Experimental (host)O⋯X(guest) /Å (B)	$\Delta_{(A) - (B)}$ / Å
2TET·3ANI	3.07 X = N	2.763(3) X = N	0.307
		2.746(3) X = N	0.324
TET·2CAM	3.07 X = N	2.785(3) X = N	0.285
		2.757(3) X = N	0.313
TET·COL	3.04 X = O	2.709(2) X = O	0.331

8.3.2 Short Ring (π⋯π) and X–H⋯π Interactions Between Host and Guest Species

The host framework for each complex is stabilised by (host)π⋯π(host) interactions with comparable ranges [Table 6, 4.709(2)–5.945(2) Å]. The 2TET·3ANI complex experiences additional host–guest, guest–host and guest–guest π⋯π interactions in the ranges 4.903(2)–5.835(2)Å, 4.970(2)–5.810(3)Å and 5.341(2)–5.524(2)Å, respectively (Table 6). Each host-guest complex employs stabilising C–H⋯π interactions, but 2TET·3ANI experiences additional N–H⋯π interactions in the range 2.61–2.75Å with angles between 139–177° (Table 6). This complex is further stabilised by a very short contact of the type (host)*m*-ArH ⋯N–H(guest) (Table 6, 2.69 Å, 153°) as well as by a (guest)N–H⋯C_{Ar}(host) (Table 6, 2.86 Å, 151°) short contact. The TET·2CAM complex also experiences interactions of this type, one (host)C_{Ar}⋯H–N(guest) (Table 6, 2.85 Å, 106°) contact and one (guest)C–H⋯C_{Ar}(host) (Table 6, 2.81 Å, 129°) contact; however, the 2TET·3ANI complex experiences a shorter contact in comparison to TET·2CAM (2.69 Å versus 2.81–2.85 Å), thus providing an explanation for the selectivity of TETROL for this guest.

Table 6: Analysis of other significant interactions between TETROL and guests CON, CAM and COL

Interaction	2TET·3ANI	TET·2CAM	TET·COL
π···π (Host···Guest)	4.903(2)–5.835(2) (11 contacts)	N/A	N/A
π···π (Guest···Host)	4.970(2)–5.810(3) (13 contacts)	N/A	N/A
π···π (Host···Host)	4.680(2)–5.945(2) (18 contacts)	4.709(2)–5.824(2) (9 contacts)	4.770(1)–5.943(2) (9 contacts)
π···π (Guest···Guest)	5.341(2)–5.524(2) (4 contacts)	N/A	N/A
CH···π	2.90 Å, 153° (H···Cg, C–H···Cg)[a] (host)*m*-ArH···π(guest) 2.88 Å, 151° (H···Cg, C–H···Cg)[a] (host)*m*-ArH···π(guest) 2.97 Å, 156° (H···Cg, C–H···Cg)[b] (host)*m*-ArH···π(guest) 2.94 Å, 137° (H···Cg, C–H···Cg)[c] (guest)*m*-ArH···π(host) 2.73 Å, 173° (H···Cg, N–H···Cg)[d] (guest)N–H···π(host) 2.61 Å, 139° (H···Cg, N–H···Cg)[d] (guest)N–H···π(host)	2.58 Å, 158° (H···Cg, C–H···Cg) (guest)C–H···π(host) 2.97 Å, 150° (H···Cg, C–H···Cg) (guest)C–H···π(host) 2.74 Å, 150° (H···Cg, C–H···Cg)[e] (guest)C–H···π(host)	2.96 Å, 152° (H···Cg, C–H···Cg) (guest)C–H···π(host) 2.87 Å, 156° (H···Cg, C–H···Cg) (guest)C–H···π(host)

	2.73 Å, 131° (H···Cg, N–H···Cg)^c (guest)N–H···π(host) 2.75 Å, 177° (H···Cg, N–H···Cg)^c (guest)N–H···π(host)		
Short contacts	2.69 Å, 153° (H···N, C–H···N)^b (host)*m*-ArH ···N–H(guest) 2.86 Å, 151° (H···C, H···C–C)^b (guest)N–H···C$_{Ar}$(host)	2.85 Å, 146° (C···H, C–C···H)^e (host)C$_{Ar}$···H–N(guest) 2.81 Å, 129° (C···H, C–C···H) (guest)C–H···C$_{Ar}$(host)	None

^{a}Interaction involving ANI[dis] guest

^{b}Interaction involving ANI[3] guest

^{c}Interaction involving ANI[2] guest

^{d}Interaction involving ANI[1] guest

^{e}Interaction involving CAM[dis] guest

8.3.3 SCXRD Analysis of a Mixed Complex

The ANI and CAM binary competition mixture afforded 24.8 and 75.2% guest inclusion, respectively (Table 2). It was of interest to analyse the crystal obtained from this experiment, as it alluded to an almost perfect ratio of 25% ANI and 75% CAM. The experiment afforded a 2TET·2CAM·ANI inclusion complex crystallizing in the monoclinic crystal system and $P2_1$ space group with Z = 2, but was not isostructural with either the TET·2CAM or 2TET·3ANI single solvent inclusions (Table 7). Figure 3 displays the calculated voids when ANI and CAM were independently removed from the crystal packing of the mixed complex; the removal of ANI showed this guest to occupy isolated cavities (Figure 3a), while the removal of CAM showed these guests residing in larger cavities (Figure 3b) (unlike the channel occupancy in TET·2CAM, Figure 5a, Chapter 3). Overall removal of both ANI and CAM resulted in the appearance of convoluted channels in the crystal (Figure 3c).
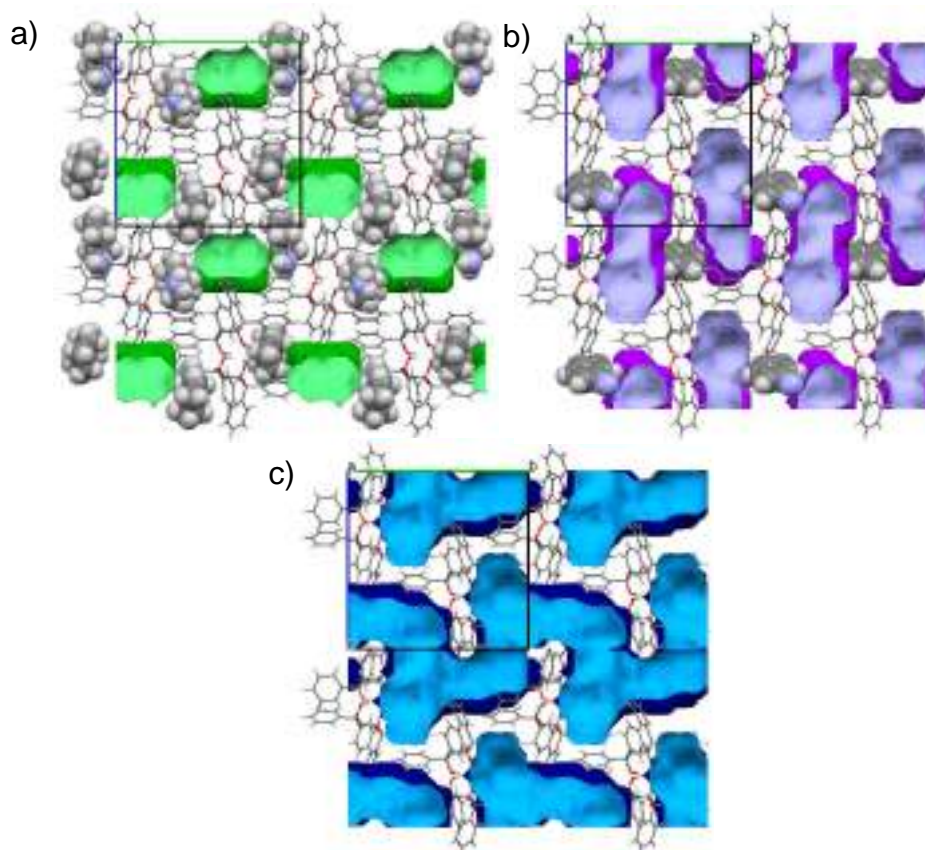
Figure 3: The calculated voids for the removal, in turn, of a) ANI, b) CAM and c) ANI and CAM; oxygen – red, nitrogen – blue, carbon – grey and hydrogen – light grey

Table 7: Relevant single crystal X-ray crystallographic data for the 2TET·2CAM·ANI complex (TET·2CAM and 2TET·3ANI included here for ease of comparison)

	TET·2CAM	2TET·3ANI	2TET·2CAM·ANI
Chemical formula	$C_{28}H_{26}O_4$·$2(C_6H_{13}N)$	$2(C_{28}H_{26}O_4)$·$2(C_6H_7N)$, C_6H_5N[a]	$2(C_{28}H_{26}O_4)$·$2(C_6H_{13}N)$·C_6H_5N[a]
Formula weight	624.84	1130.34	1142.43
Crystal system	Monoclinic	Orthorhombic	Monoclinic
Space group	$P2_1$	$P2_12_12_1$	$P2_1$
μ (Mo Kα)/mm⁻¹	0.076	0.080	0.079
a/Å	12.3859(5)	17.3680(9)	10.3129(5)
b/Å	8.2405(3)	17.5435(9)	17.3864(8)
c/Å	17.1370(7)	20.0346(10)	17.2872(9)
α/°	90	90	90
β/°	96.305	90	91.198(2)
γ/°	90	90	90
V/Å³	1738.53(12)	6104.5(5)	3099.0(3)
Z	19	4	2
F (000)	676	2400	1224
Temp (K)	200	200	200
Restraints	0.999		1
Nref	8486	15216	15230
Npar	427	758	800
R1	0.0473	0.0401	0.0383
wR2	0.1255	0.1135	0.0997
S	1.05	1.04	1.03
Θ min, max/°	1.2, 28.3	1.5, 28.3	1.7, 28.3
Tot. data	29351	147780	66761
Unique data	8486	15216	15230
Observed data [I > 2.0σ(I)]	7473	12442	13242
Rint	0.017	0.023	0.019
Diffrn measured fraction Θ full	0.999	1.000	0.992
Min. resd. dens. (e/Å³)	−0.34	−0.32	−0.21
Max. resd. dens. (e/Å³)	0.48	0.40	0.25

[a]Hydrogen atoms could not be located during SCXRD structural refinement of the crystal structure

Upon SCXRD analysis of this mixed complex, it is noted that only the two CAM guest species experience H-bonding to TETROL [Table 8, 2.683(3) and 2.693(3) Å, 167 and 167°, respectively]. Each guest in the 2TET·2CAM·ANI complex is stabilised by host–guest and, host–host π⋯π interactions [Table 9, 5.429(2)–5.430(2) and 4.6207(1)–5.9519(1), respectively]. However, only the ANI guest is involved in guest–host π⋯π interactions in the range 5.108(2)–5.601(2) (Table 9). This guest is trapped in the host framework by two (host)*m*-ArH⋯π(guest) (2.91 and 2.94 Å, with angles of 153 and 164°, respectively) and one (host)*m*-ArH⋯C$_{Ar}$(guest) (2.80 Å, 140°) interactions (Table 9). Additionally, as observed in Figure 4 [labelled a)], the ANI guest is further stabilised by a (guest)C–H⋯H–C(guest) (Table 9, 2.28 Å, 158°) interaction with CAM due to their close proximity in the crystal.

Table 8: Analysis of intermolecular hydrogen bonding interactions occurring in the 2TET·2CAM·ANI complex

Guest	(host)O⋯ X(guest) /Å	(host)H⋯ X(guest) /Å	(host)O–H ⋯X(guest) /˚	Symmetry operator
CAM [1]	2.683(3) X = N	1.86	167	x,y,z
CAM [2]	2.693(3) X = N	1.87	167	x,y,z

Table 9: Analysis of other significant interactions in the 2TET·2CAM·ANI complex

Interaction	2TET·2CAM·ANI
π···π (Host···Guest)	5.429(2)–5.430(2) (4 contacts)
π···π (Guest···Host)	5.108(2)–5.601(2)[a] (8 contacts)
π···π (Host···Host)	4.6207(1)–5.9519(1) (17 contacts)
π···π (Guest···Guest)	–
XH···π	2.91 Å, 153° (H···Cg, C–H···Cg)[a] (host)*m*-ArH···π(guest)
	2.94 Å, 164° (H···Cg, C–H···Cg)[a] (host)*m*-ArH···π(guest)
	2.65 Å, 136° (H···Cg, N–H···Cg)[b] (guest)N–H···π(host)
	2.92 Å, 171° (H···Cg, N–H···Cg)[c] (guest)N–H···π(host)
	2.58 Å, 140° (H···Cg, N–H···Cg)[c] (guest)N–H···π(host)
Short contacts	2.80 Å, 140° (H···C, H···C–C)[a] (host)*m*-ArH···C_{Ar}(guest)
	2.86 Å, 161° (H···C, H···C–C)[c] (guest)N–H···C_{Ar}(host)
	2.28 Å, 158° (H···H, H···H–C)[d] (guest)C–H···H–C(guest)

[a]Interaction with the ANI guest

[b]Interaction with CAM[1]

[c]Interaction with CAM[2]

[d]Interaction between ANI and CAM
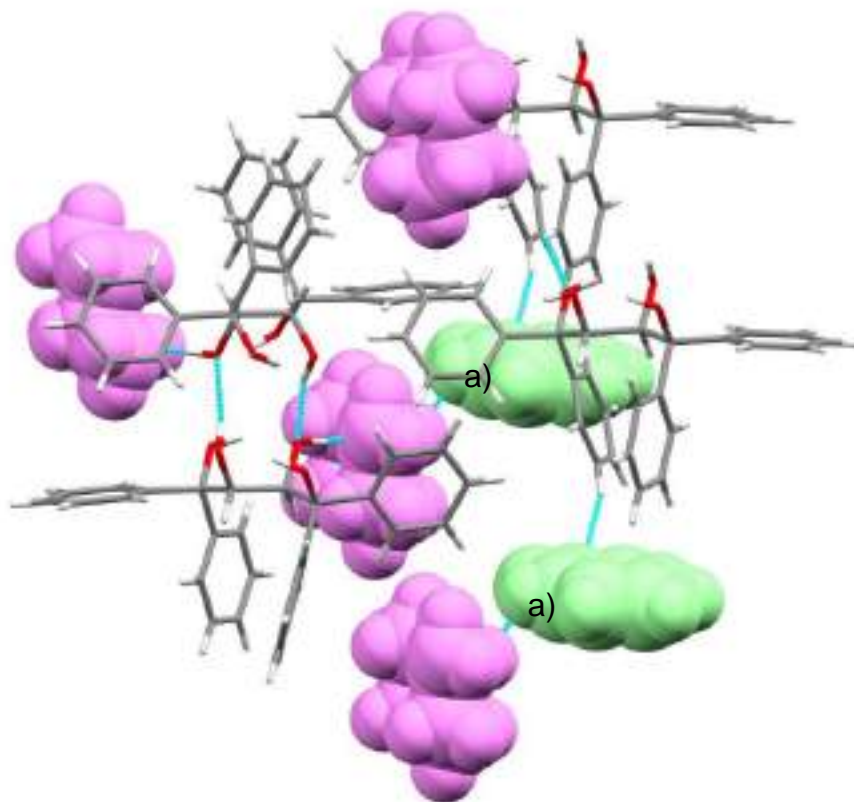
Figure 4: Partial crystal packing of the 2TET·2CAM·ANI complex showing intermolecular H-bonding and other significant interactions; a) (guest)C–H···H–C(guest); CAM – purple and ANI – green; oxygen – red, carbon – grey and hydrogen – light grey

8.4   Hirshfeld Surface Analysis

The Hirshfeld surface analyses for 2TET·3ANI, TET·2CAM and TET·COL have been discussed in previous chapters, but will be re-presented here for the sake of comparison. A summary of the percentage of each interaction type is displayed in Table 10. It is important to note that the third ANI guest is disordered over the nitrogen functional group, and the amine hydrogens could not be defined in the SCXRD analysis. This in turn may afford a misleading Hirshfeld interaction percentage of the type H···N/N···H and we have therefore disregarded this percentage here for the 2TET·3ANI[3] complex.

All complexes with TETROL are predominantly stabilised by H···H interactions (55.7–83.8%), with TET·2CAM experiencing a higher percentage of this interaction [82.0–

83.8% relative to 70.9% (TET·COL), and 55.7 and 60.9% (2TET·3ANI)]. Furthermore, 2TET·3ANI experiences more N···H/H···N interactions (Table 10, 3.2 and 4.9%) in comparison to TET·COL (0%) and TET·2CAM (0–2.7%). This is in accordance with TETROL's preference for ANI over CAM and CON (Table 2).

Table 10: Percentage intermolecular interactions in each inclusion complex (G···H/H···G)

	O···H/ H···O	H···N/ N···H	H···H/ H···H	H···C/ C···H	C···C/ C···C	C···O/ C···O	N···C/ C···N
2TET·3ANI [1]	2.3	3.2	60.9	33.5	0.1	0	0
2TET·3ANI [2]	1.7	4.9	55.7	34	0.1	0	3.6
2TET·3ANI [3]	0	14.9	51.7	30	0	0	3.5
TET·2CAM[DIS]	0.4	0	83.8	15.8	0.1	0	0
TET·2CAM[2]	0.6	2.7	82.7	14.1	0	0	0
TET·2CAM[1]	0.3	2.4	82.0	15.2	0	0	0
TET·COL	4.1	0	70.9	23	0	2	0

8.4.1 Hirshfeld Surface Analysis of the 2TET·2CAM·ANI Mixed Complex

We analysed the respective Hirshfeld surface determinations for the 2TET·2CAM·ANI mixed complex (Figures 5a–c). A summary of the percentage of each interaction type is displayed graphically in Figure 6, while Table 11 provides the actual values obtained from this figure. Once more, because the third ANI guest is disordered over the nitrogen functional group, we have omitted the H···N/N···H interaction percentage for ANI from this discussion.

From the generated Hirshfeld plot for the ANI guest (Figure 5c, right), it is evident that ANI is not H-bonded in the host framework; the 'spikes' in the plots and the shaded red area in the Hirshfeld surfaces for CAM (Figures 5a and b) shows this interaction type to be present for this guest. ANI, however, experiences a higher percentage of H···C/C···H interactions in comparison to CAM (Figure 6, Table 11, 23% for ANI in

comparison to 20.3 and 15.7% for CAM). However, the CAM guests do experience a greater percentage of H···H/H···H interactions [69.9 and 79.7%, in comparison to ANI (59.2%)].

c)
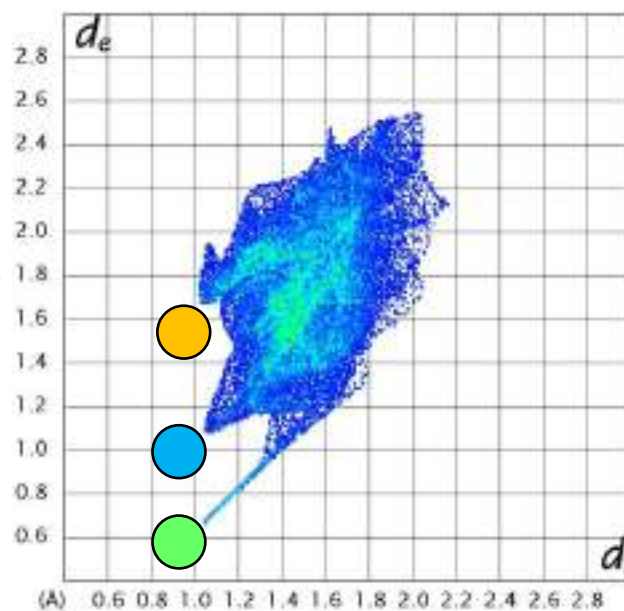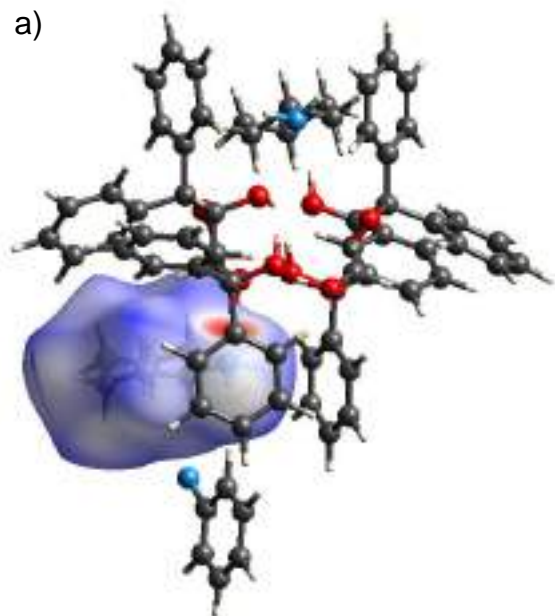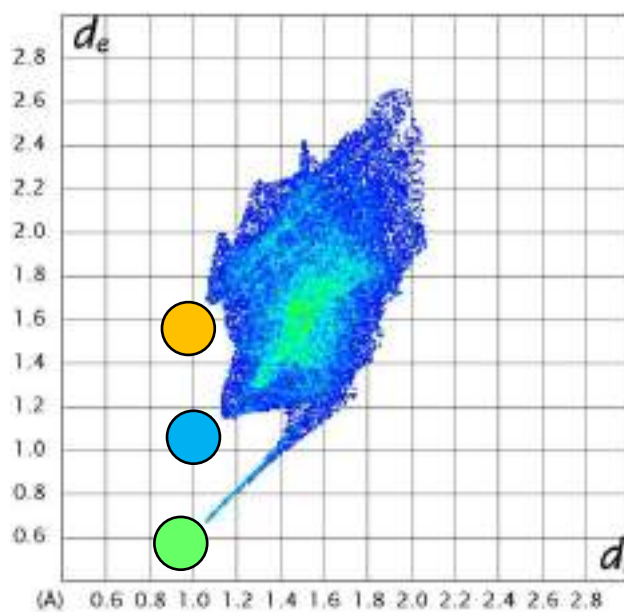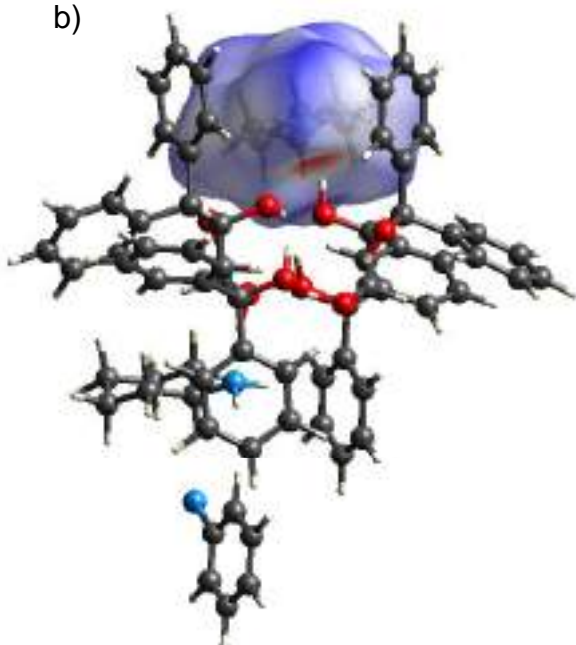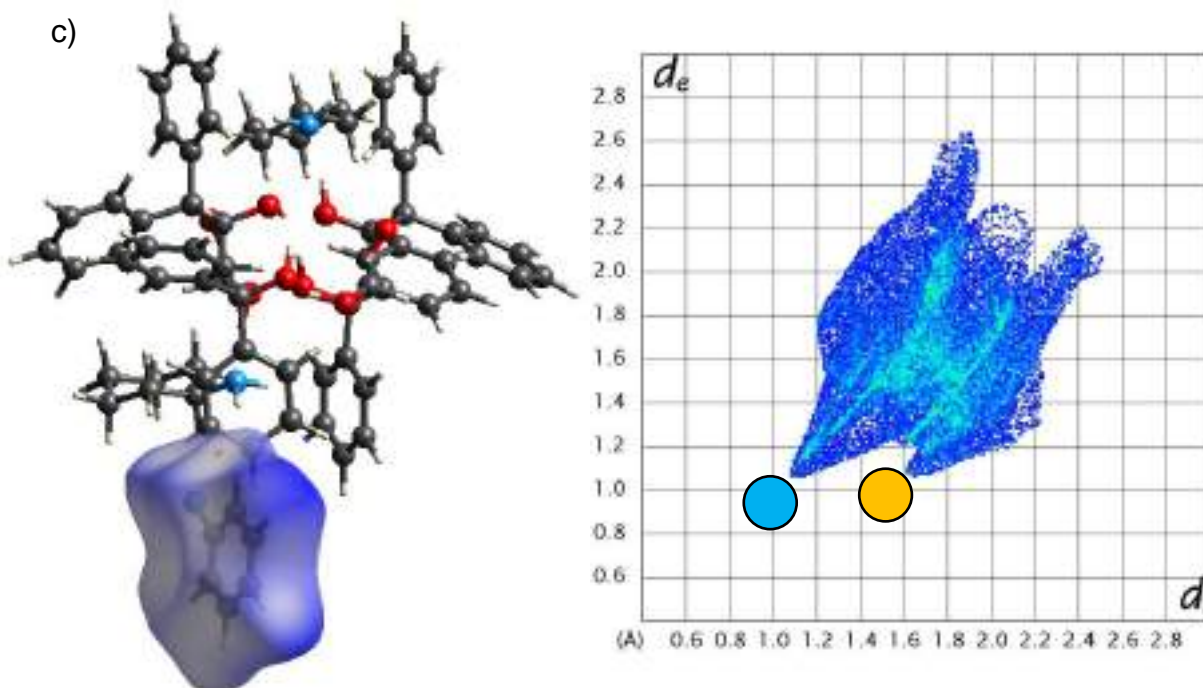
Figure 5: Hirshfeld surfaces (left) and fingerprint plots (right) for a) CAM[1], b) CAM[2] and c) ANI from the 2TET·2CAM·ANI complex; the 'spike' and 'wings' observed in the Hirshfeld plots are colour coded and depict N···H (green), H···H (blue) and C···H (orange) contacts
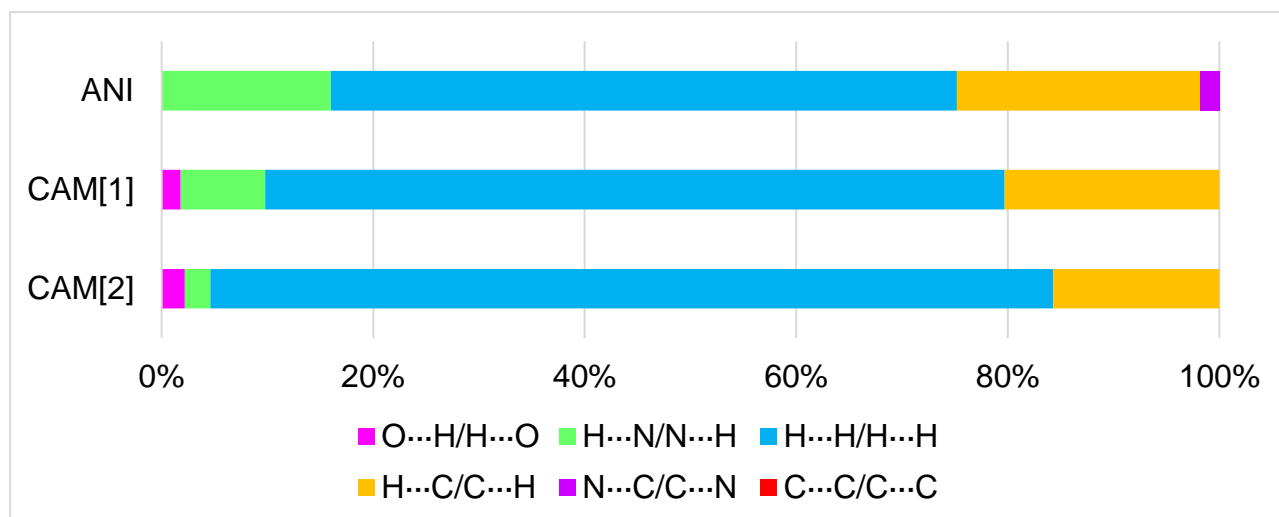
Figure 6: Graphical display showing the percentage intermolecular interactions of each type for the 2TET·2CAM·ANI mixed complex

Table 11: Percentage intermolecular interactions in each inclusion complex (G⋯H/H⋯G)

	O⋯H/H⋯O	H⋯N/N⋯H	H⋯H/H⋯H	H⋯C/C⋯H	N⋯C/C⋯N
ANI	0	16	59.2	23	1.8
CAM[1]	1.8	8	69.9	20.3	0
CAM[2]	2.2	2.4	79.7	15.7	0

8.5　Thermal Analyses

Both DSC and TG experiments of the three 2TET·3ANI, TET·2CAM and TET·COL inclusion complexes have been discussed in previous chapters, but will be briefly analysed here by comparing T_{on} temperatures. (The DSC and TG experiments for the TET·PHO complex did not yield suitable traces and is therefore omitted from this discussion.) Unfortunately, these onset temperatures for the guest release events do not correlate with the preference order of TETROL for these guests (ANI > CAM > COL) (Table 12).

Table 12: Thermal data from DSC/TG traces for the TET·COL, 2TET·3ANI and TET·2CAM complexes

Guest	T_{on} (°C)	T_p (°C)[a]	T_{end} (°C)[b]	Mass loss % (expected)	Mass loss % (actual)
COL	84.5	117.7 135.4	115.9 142.8 147.2	19.0	16.5
ANI	70.9	~98.8 108.8 125.2	~89.8 104.5 127.9	24.7	25.3
CAM	60.0	78.6 ~118.6 134.5	81.4 88.9 ~120.4 139.2	31.7	26.9

[a]T_p values determined from blue DTG traces

[b]T_{end} were obtained from the brown DSC traces

8.6 Conclusion

TETROL proved to be an efficient host for the inclusion of ANI, CAM, COL and PHO. This host showed a high selectivity for ANI when recrystallised from mixtures of the four guests, resulting in a selectivity order of ANI (57.5%) > CAM (37.8%) > COL (3.5%) > PHO (1.3%). Thermal analyses were not helpful in providing evidence for the observed selectivity order of the host, but Hirshfeld analysis showed that 2TET·3ANI experienced a higher degree of N···H/H···N interactions (Table 10, 3.2 and 4.9%) in comparison to TET·COL and TET·2CAM. In SCXRD analyses, it was observed that the 2TET·3ANI complex experienced the shortest stabilising contact in comparison to TET·2CAM (2.69 Å versus 2.81–2.85 Å), which supports the preferred inclusion of ANI over CAM. Once more, it was observed that TETROL has a higher affinity for amine over hydroxy guest types as ANI and CAM were preferentially included over COL and PHO in all competition experiments conducted.

Chapter 9

The Selectivity of TETROL in The Presence of *ortho*-, *meta*- and *para*-Cresol Isomers
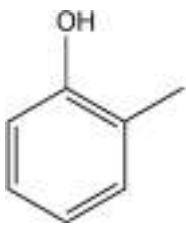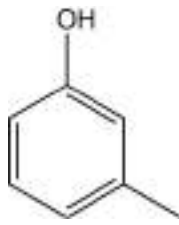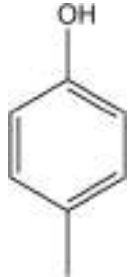
9.1 Introduction

The cresols constitute three isomers, namely *ortho*-, *meta*- and *para*- cresol (OC, MC and PC, respectively). These isomers differ in the relative position of the OH and CH_3 groups on the phenyl ring (Table 1). The cresols are essential for applications in the phenolic resin, explosive, petroleum, photographic, paint and agricultural industries. A mixture of cresols, also known as cresylic acid, is primarily produced as a by-product from coal carbonization plants (18% *o*-cresol, and 30% *m*- and *p*-cresol) or recovered from oil-refinery caustic washes (35% cresols).[203] Each cresol isomer, however, has independent uses: *o*-cresol is applied in tanning, fibre treatment, metal degreasing, and in the production of herbicides and insecticides; *m*-cresol acts as a textile-scouring agent and is used in producing disinfectants and preservatives; *p*-cresol is used as an antioxidant, solvent for wire enamels, and an agent in metal cleaning, ore flotation, synthetic flavouring and perfumes.[198] Isolation of these cresols from one another is a significant challenge in the chemical industry. The *ortho* isomer (190.95 °C) has a boiling point that is slightly different from the *para* (201.9 °C) and *meta* (202.8 °C) isomers (Table 1). Therefore, *o*-cresol is more readily separated from a *m*-, *p*- and *o*-cresol mixture through fractional distillation. Isolation of pure *p*- and *m*-cresols is, however, difficult to achieve due to their very similar boiling points.[204]

Conventional separations of the components of cresol isomer mixtures involve physical and chemical operations requiring expensive equipment, severe processing conditions, and extensive repetition of treatment steps to produce passable yields of marginally-pure products.[204] We therefore explored the selectivity of TETROL for the three cresol isomers. Of the three isomers, only *meta*- and *para*-cresol were enclathrated when crystals of this host compound were grown from each of these isomers, forming 2:1 H:G complexes with these guests. Unfortunately, SCXRD

analysis could not be conducted on the formed complexes due to poor diffraction properties of the crystals.

Table 1: The structure and properties of the three cresol isomers

	o-Cresol	*m*-Cresol	*p*-Cresol
Structure			
Boiling point (°C)	190.95	202.8	201.9

9.2   Competition Experiments

Since MC and PC were enclathrated individually, competition experiments were conducted, and the selectivity of TETROL for these guests investigated to establish if the host would discriminate between them. Note that we added OC to these experiments despite this guest not being included in the single solvent experiment. In Table 2, we summarize data obtained from the recrystallization of TETROL from equimolar binary and ternary combinations of OC, MC and PC. The so-formed crystal inclusions were analysed using proton NMR spectroscopy and GC-MS. The preferred guest species is given in bold red font face.

Table 2: Competition experiments using TETROL and various equimolar mixtures of the cresol guests[a,b]

o-Cresol	*m*-Cresol	*p*-Cresol	Guest ratios (%e.s.d.)	Overall H:G ratio
X	X		_[c]	_[c]
X		X	24.4:**75.6** (1.65)	2:1
	X	X	29.6:**70.4** (1.67)	2:1
X	X	X	11.3:23.8:**64.9** (2.97) (0.84) (3.05)	2:1

[a]Ratios determined using NMR and gas chromatography

[b]Experiments were conducted in triplicate; %e.s.d.'s are provided in parentheses

[c]Crystallization did not occur and a gel remained

From Table 2, it is clear that *p*-cresol was the preferred isomer in all equimolar competition experiments whenever it was present. OC/PC and MC/PC binary experiments showed the selective inclusion of PC with molar ratios of 75.6 and 70.4%, respectively. When PC was absent, the OC/MC mixture did not yield any crystals. The equimolar ternary experiment agreed with these results, showing the preference of TET for the cresol isomers to decrease in the order PC (64.9%) > MC (23.8%) > OC (11.3%) (Table 2). It is interesting that OC was included to some extent here, despite not having been included in the single solvent experiment. The overall host:guest ratio remained 2:1 for all competition experiments conducted.

Binary experiments were also conducted using mixtures of guests with varying molar ratios in order to construct selectivity profiles for this host. Unfortunately, when OC was present in molar ratios greater than 50% in these experiments, crystallization did not occur, and hence selectivity profiles for the OC/MC and OC/PC experiments could not be constructed. We therefore focused on the binary MC/PC experiment, and Figure 1 is the selectivity profile thus obtained. Analyses were carried out using GC-MS as before. The straight-line plot (red data points) is a theoretical one, representing the case where the host is completely unselective towards both guests, and is inserted for ease of comparison with the experimentally-determined data points (blue).

A consistent host preference for PC over MC (Figure 1, $K_{PC:MC} = 3.3$) was observed for the entire concentration range investigated. The host effectively showed high selectivity towards PC even at a very low concentrations of this isomer: a mother liquor compromised of 13.6% PC afforded crystals that already contained 47.2% of this guest.
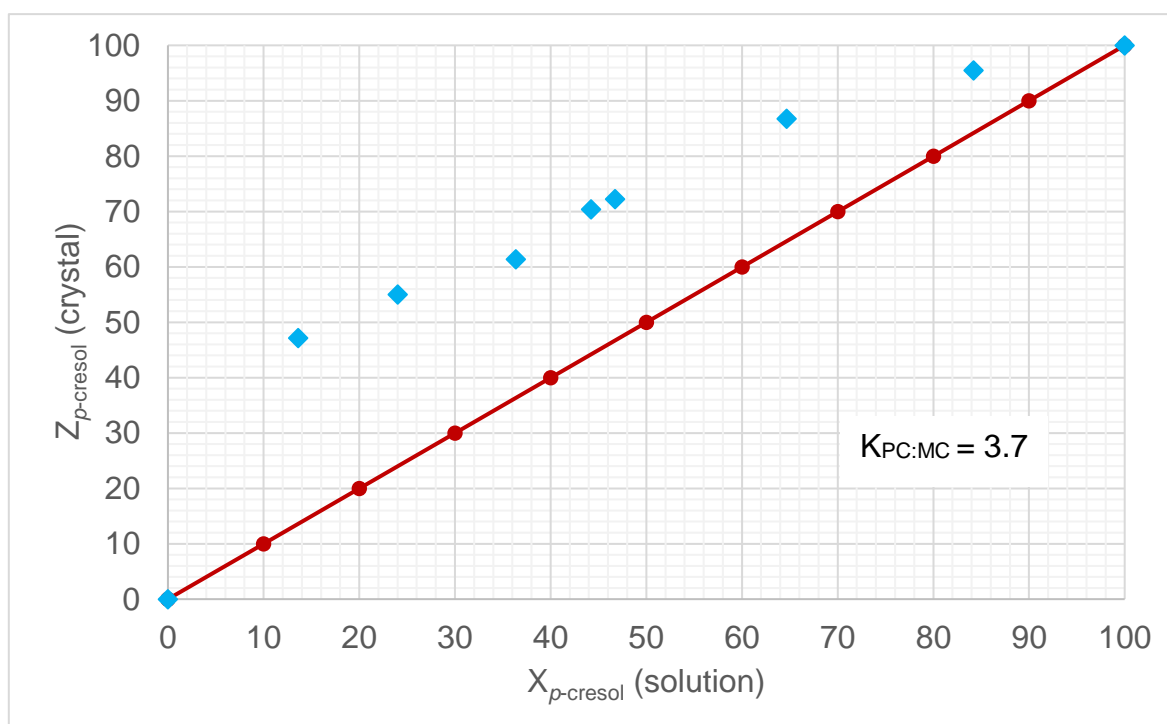
Figure 1: Selectivity curve for the MC/PC binary competition experiment

9.3 Thermal Analyses

Both DSC and TG experiments were carried out on the 2TET·MC and 2TET·PC inclusion complexes. The traces obtained are given in Figures 2a and b. Upon heating of 2TET·PC, the majority of the guest was released just prior to the melting of the host (Figure 2a, 147.2 °C). The guest release onset temperature, T_{on}, was estimated to be 85.5°C (Table 3). The expected mass loss for the 2:1 H:G complex was calculated to be 11.3%, which is in reasonable agreement with the actual mass loss observed (Table 3, 9.3%). In comparison to 2TET·PC, the 2TET·MC complex was unstable as the guest release process occurred rapidly even at room temperature (Figure 2b). T_{on} for this complex could therefore not be identified since the guest is lost from the host

prior to the onset of the experiment (TG), alluding to a guest that is not tightly bound in the crystal. The insert in Figure 2b displays the overlaid traces for the DSC (brown), TG (green) and its derivative (DTG, blue) for the 2TET·MC complex when a fresh sample was prepared for thermal analyses. In this case, the sample was not analysed immediately but left to stand at ambient temperature and pressure for 30 min, after which thermal analysis was carried out. It is clear from this inserted figure that no guest remained after these 30 min, and that only host compound was present (no mass loss was observed at all). The 2TET·MC complex is thus very unstable, and this correlates well with the preference of TET for PC rather than MC (Table 2). The observed mass loss (18.2%, Table 3) is not in agreement with that expected for a 2:1 complex (11.3%), and we currently cannot provide an explanation for this anomaly.

a)

b)
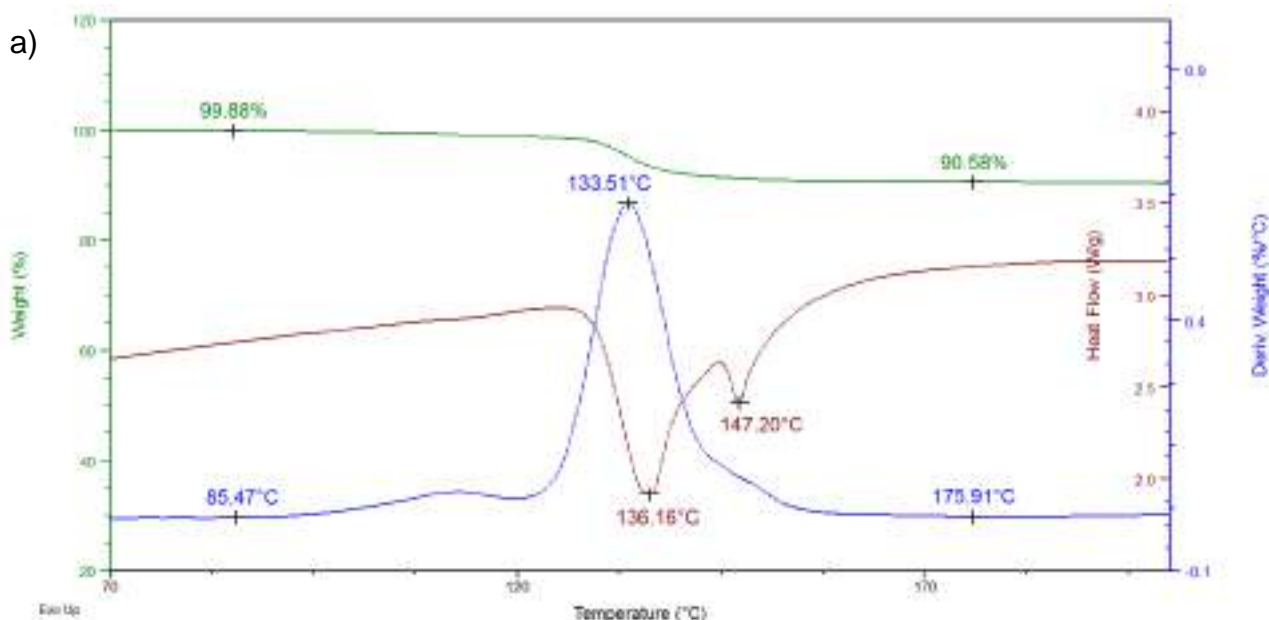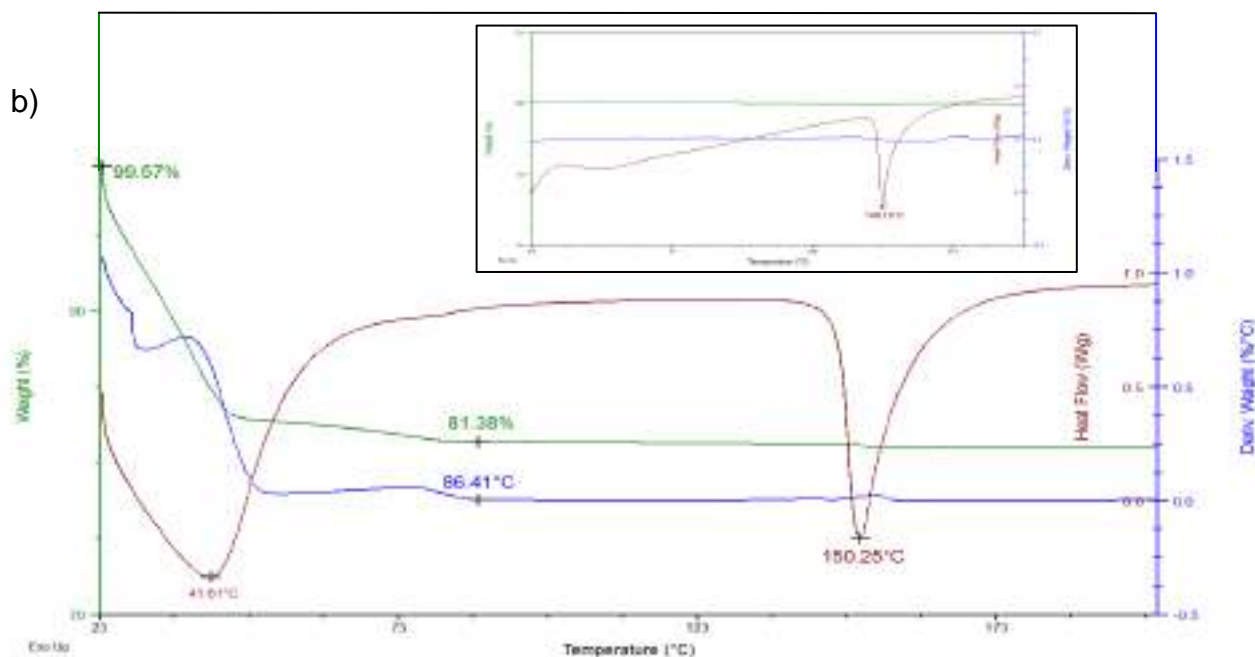
Figure 2: Overlaid traces for the DSC (brown), TG (green) and its derivative (DTG, blue) for the a) 2TET·PC and b) 2TET·MC complexes

Table 3: Thermal data from DSC/TG traces for 2TET·PC and 2TET·MC complexes

Guest	T_{on} (°C)	T_p (°C)^a	T_{end} (°C)^b	Mass loss % (expected)	Mass loss % (actual)
PC	85.47	133.51	136.16 147.20	11.3	9.3
MC	^{c}	–	–	11.3	~18.2^c

^{a}T_p values determined from blue DTG traces

^{b}T_{end} were obtained from the brown DSC traces

^{c}Guest release occurred from the onset of the experiment, and Ton could thus not be identified; the actual mass loss is thus also just an estimation

9.4   Conclusion

The compound TETROL proved to be an effective host for the complexation of *m*-cresol and *p*-cresol. The host showed high selectivity towards *p*-cresol when recrystallised from mixtures of all three isomers, and a host selectivity order of PC (64.9%) > MC (23.8%) > OC (11.3%) was obtained. Thermogravimetric analysis

confirmed that PC was more tightly bound in the crystal compared to MC due to the 2TET·PC complex having a significantly higher T_{on} value (85.5 °C), while MC was released even at room temperature. The aim of this study was to determine whether TETROL has the ability to separate *meta*- and *para*-cresol isomers from one another, and the host does indeed show selectivity towards *p*-cresol (70.4% from a 1:1 mixture with the *meta* isomer), allowing for its possible future application in the purification of mixtures of these guest compounds.

Chapter 10

Competitions Between Two Hosts, TETROL and DMT, in the Presence of Guest Cyclohexanone: TETROL, the Superior Host Material

10.1   Introduction

As previously stated in Chapter 1, a clathrate possesses extramolecular cavities, producing spaces between two or more host molecules which are only present in the crystalline or solid state.[47] Essentially, these hosts form crystal lattice inclusion compounds.[205] Coordinatoclathrates are defined as coordinative group-assisted clathrates, combining the attributes of coordinative complexes and of lattice-dependent clathrates.[206] These host types usually contain functional sensor groups, such as H-bond donor and/or acceptors, and are often highly selective.[207]

During these investigations, we have noted that all crystalline associations between TETROL and guest involve hydrogen bonding, owing to the host's appropriately placed secondary hydroxyl groups. These host-guest complexes may therefore clearly be defined as coordinatoclathrates. To acknowledge the importance of these secondary hydroxyl groups, we will compare TETROL to a related derivative, (−)-(2*R*,3*R*)-2,3-dimethoxy-1,1,4,4-tetraphenylbutane-1,4-diol (DMT) (Figures 1a and b) where these secondary hydroxyl groups are replaced by methoxy groups. DMT has been applied in our laboratories as a host compound, and has recently been shown to have potential for separating the xylene isomers.[208] In this experiment, an equimolar mixture of TET and DMT was recrystallized from cyclohexanone. The resulting crystal was analysed using SCXRD and proton NMR. Individually, TET and DMT form inclusion complexes with cyclohexanone affording TET·CON and 2DMT·CON. Hirshfeld surface analysis could not be conducted on the significantly disordered guest residing in the 2DMT·CON complex.

a)

b)
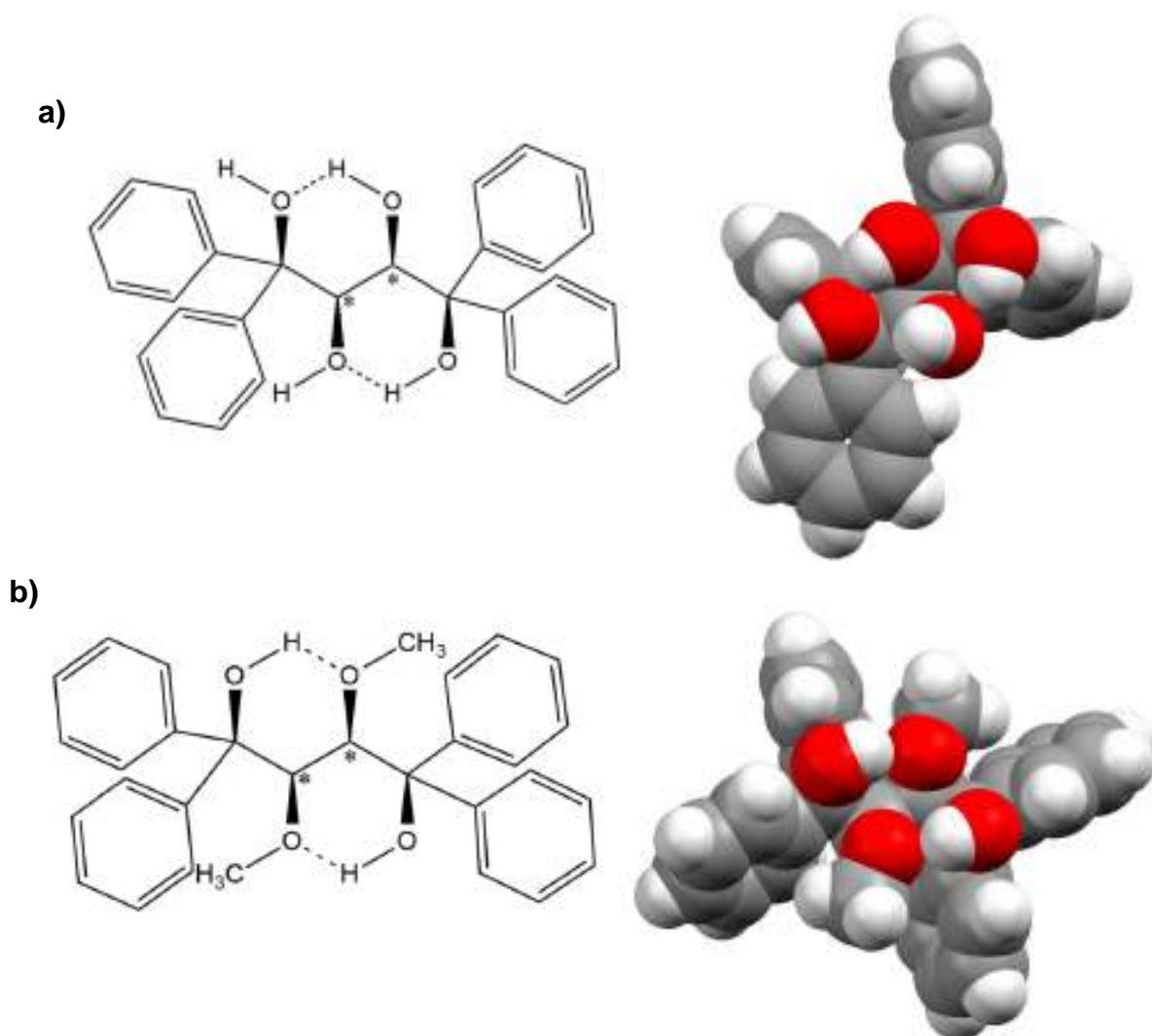
Figure 1: a) Structure of TETROL illustrating 1,3-intramolecular H-bonding array (left) and space-filling model of TETROL (right), and b) structure of DMT illustrating 1,3-intramolecular H-bonding array (left) and space-filling model of DMT (right)

10.2   SCXRD Analyses of TETROL and DMT

It is imperative in this study to initially analyse the fundamental differences between TET and DMT. SCXRD data for TETROL have previously been published by our group, but will be re-presented for ease of comparison. Crystal data and refinement details for TET and DMT are listed in Table 1. Suitable crystals of TET and DMT were obtained by slow recrystallisation from ethanol and citronellol, respectively. TETROL crystallizes in the trigonal crystal system and $P3_1$ space group with $Z = 18$, while DMT

crystallizes in the tetragonal crystal system and $I4_1$ space group with Z = 4. Various diagrams for each host are displayed in Figures 2 and 3.

a)

b)
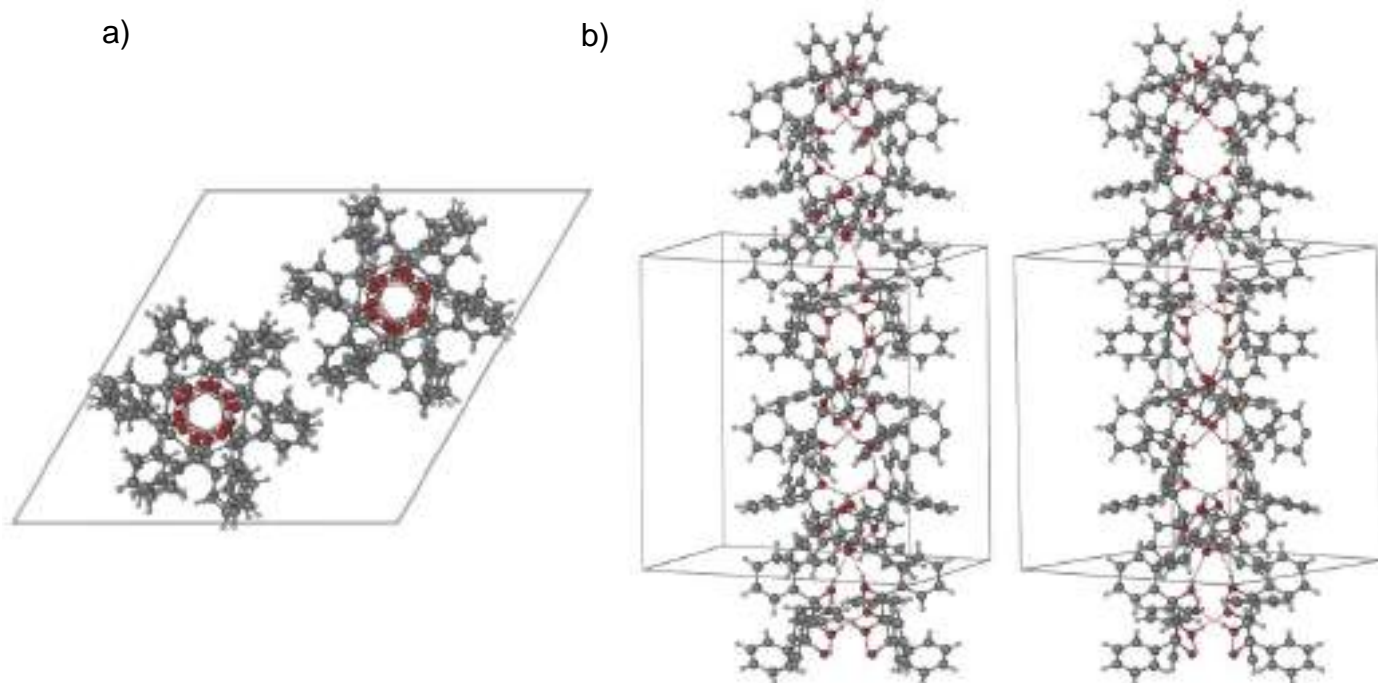
Figure 2: a) The crystal packing of TETROL viewed along the *c*-axis, and b) stereoview of a portion of the crystal packing in TETROL
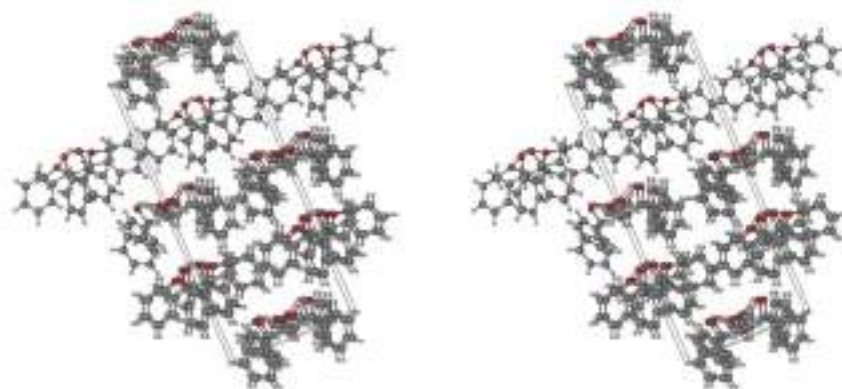
Figure 3: Stereoview of the crystal packing in DMT

Table 1: Relevant single crystal X-ray crystallographic data for TETROL and DMT

	TET	DMT
Chemical formula	$C_{28}H_{26}O_4$	$C_{30}H_{30}O_4$
Formula weight	426.49	454.54
Crystal system	Trigonal	Tetragonal
Space group	$P3_1$	$I4_1$
μ (Mo Kα)/mm^{-1}	0.083	0.078
a/Å	23.7521(12)	10.2823(6)
b/Å	23.7521(12)	10.2823(6)
c/Å	20.5299(10)	23.8173(17)
α/°	90	90
β/°	90	90
γ/°	120	90
V/Å^3	10030.5(9)	2518.1(3)
Z	18	4
F (000)	4068	968
Temp (K)	173(2)	200
Restraints	1	1
Nref	16,611	3129
Npar	1754	156
R1	0.0313	0.0307
wR2	0.0771	0.0826
S	1.004	1.09
Θ min, max/°	1.71, 28.29	2.2, 28.3
Tot. data	152.936	39639
Unique data	16,611	3129
Observed data [I > 2.0σ(I)]	15,808	2982
Rint	0.0511	0.020
Diffrn measured fraction Θ full	0.999	1.000
Min. resd. dens. (e/Å^3)	−0.213	−0.13
Max. resd. dens. (e/Å^3)	0.264	0.16

10.3   Hirshfeld Surface Analyses of TETROL and DMT

Hirshfeld surface analyses will provide for a more comprehensible summary of the interactions associated within the TET and DMT frameworks. From the crystal packing of each host, we chose one TET and DMT molecule and conducted Hirshfeld surface analyses to highlight the respective interactions experienced by each of these (Figures 4 and 5, respectively). A summary of the percentage of each interaction type is displayed graphically in Figure 6.

Upon inspection of the generated 2D Hirshfeld fingerprint plots for each host, obvious differences are noted (Figures 4 and 5). The spikes highlighted in Figure 4a represent O–H···H–O inter- and intra- molecular H-bonding within the crystal framework of TETROL (Figure 4, Table 2, 8.7%). DMT, on the other hand, solely makes use of intramolecular H-bonding and thus experiences a lower percentage of these interactions (Figure 5a, Table 2, 6.0%). This is illustrated in Figures 7a and b; apart from both TET and DMT experiencing 1,3-intramolecular H-bonding, TETROLs secondary hydroxyl groups allow for further stabilisation via intermolecular H-bonding of the type O–H···O. Consequently, the crystal packing of TETROL is made up of dimers where the hydroxyl groups of two TETROL molecules situate opposite one another and hydrogen bond directly (Figures 2 and 7a). The methoxy functional groups replacing these secondary hydroxyl moieties, as in DMT, are relatively uninvolved and only contribute towards intramolecular hydrogen bonding (Figures 3 and 7b). Further stabilisation of TETROL occurs through 27.5% of C–H···H–C interactions (Figure 6, Table 2); a relatively lower percentage of this interaction type is observed for DMT (Figure 6, Table 2, 18.9%). Alternatively, DMT experiences a higher degree of H–H···H–H interactions (Figure 6, Table 2, 73.3%) in comparison to TET (Figure 6, Table 2, 61.4%).
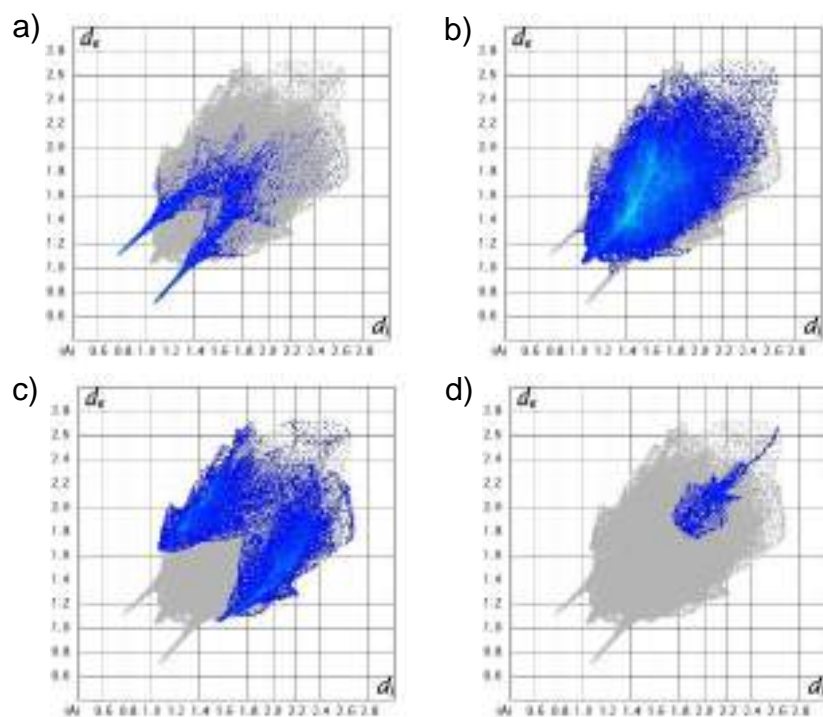
Figure 4: Hirshfeld fingerprint plots for TETROL representing a) O–H···H–O, b) H–H···H–H, c) C–H···H–C and d) C–C···C–C interactions within the host framework
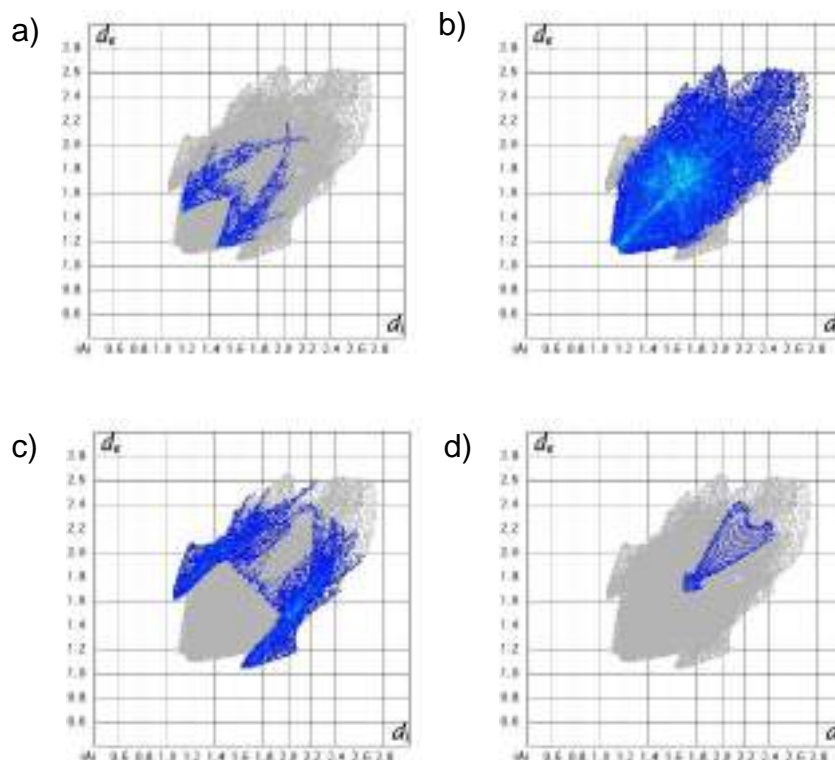
Figure 5: Hirshfeld fingerprint plots for DMT representing a) O–H···H–O, b) H–H···H–H, c) C–H···H–C and d) C–C···C–C interactions within the host framework
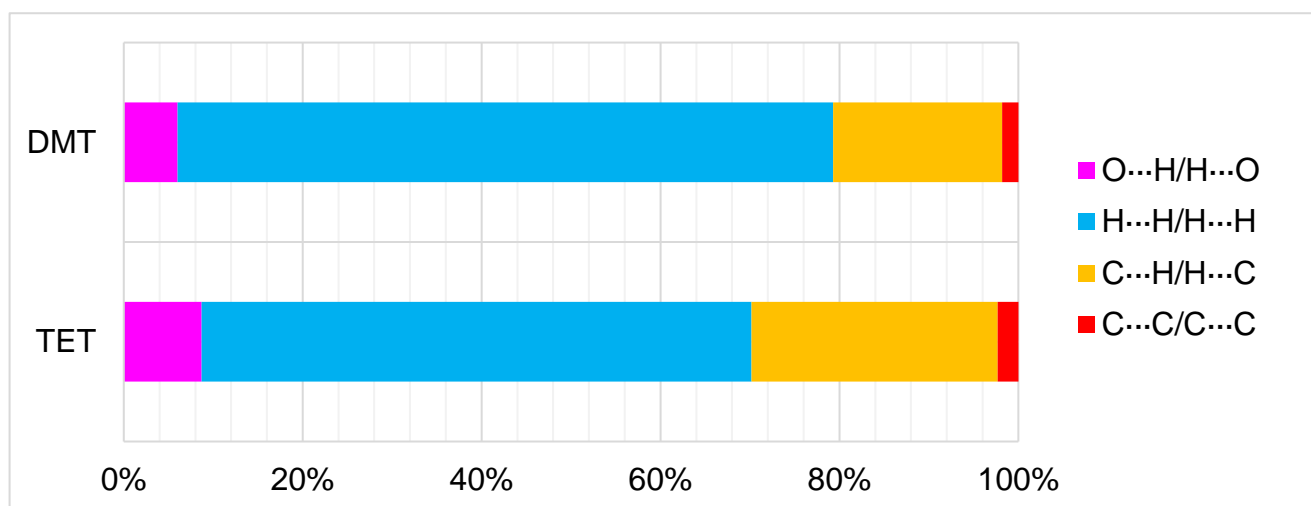
Figure 6: Graphical display showing the percentage intermolecular forces of each type for TET and DMT

Table 2: Percentage intermolecular interactions in TET and DMT (G···H/H···G)

	O···H/H···O	H···H/H···H	H···C/C···H	C···C/C··· C
TET	8.7	61.4	27.5	2.3
DMT	6.0	73.3	18.9	1.8

a)

b)
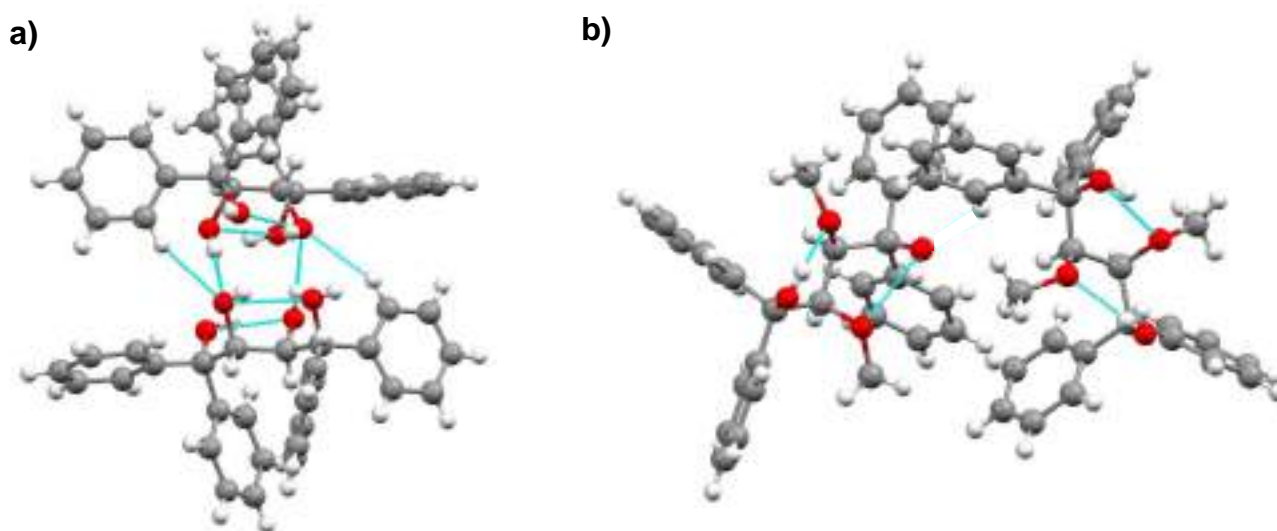
Figure 7: A representation of the intra- and inter- molecular hydrogen bonding in a) TETROL and b) DMT

10.4 SCXRD Analyses Between Hosts (TET and DMT) and Guest (Cyclohexanone)

SCXRD experiments were conducted on suitable crystals of successfully-formed TET·CON and 2DMT·CON complexes. The TET·CON complex was analysed in a previous chapter, but the SCXRD data will be re-stated here for ease of comparison. Crystal data and refinement parameters are listed in Table 3 for the two host complexes with cyclohexanone. Both TET·CON and 2DMT·CON complexes crystallize in the monoclinic crystal system with Z = 2, but with differing space groups of $P2_1$ and $C2$, respectively. SCXRD analysis was also conducted on crystals formed from the TET/DMT/CON mixture; the complex formed was isostructural to TET·CON (Table 3). The respective packing diagrams for each complex are displayed in Figures 4a–c. In all cases, the guest molecules were found to occupy isolated cavities within their respective host frameworks (Figure 8).
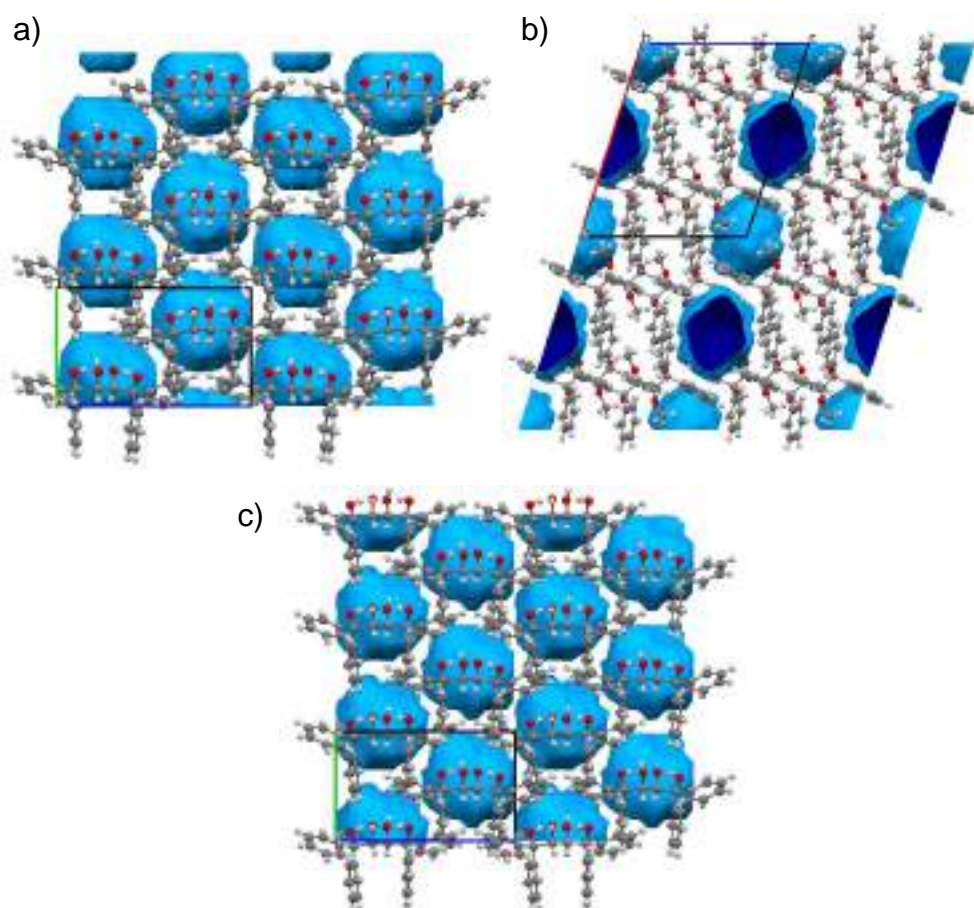
Figure 8: Calculated voids (blue) in a) TET·CON, b) 2DMT·CON and c) crystals from a TET/DMT/CON mixture indicating guest accommodation in isolated cavities (oxygen – red, carbon – grey and hydrogen – light grey)

Table 3: Relevant single crystal X-ray crystallographic data for TET·CON, DMT·CON and crystals formed from a TET/DMT/CON mixture

	TET·CON	2DMT·CON	Crystals from a TET/DMT/CON mixture
Chemical formula	$C_{28}H_{26}O_4$· $C_6H_{10}O$	$2(C_{30}H_{30}O_4)$· $C_6H_{10}O$	$C_{28}H_{26}O_4$· $C_6H_{10}O$
Formula weight	524.63	1007.22	524.63
Crystal system	Monoclinic	Monoclinic	Monoclinic
Space group	$P2_1$	$C2$	$P2_1$
μ (Mo Kα)/mm^{-1}	0.084	0.078	0.083
a/Å	12.5944(4)	17.1864(6)	12.5981(4)
b/Å	8.1531(2)	12.0532(6)	8.1565(2)
c/Å	13.4570(5)	14.1459(6)	13.4580(4)
α/°	90	90	90
β/°	94.025(2)	107.779(2)	93.976(2)
γ/°	90	90	90
V/Å^3	1378.40(8)	2790.4(2)	1379.57(7)
Z	2	2	2
F (000)	560	1076	556
Temp (K)	200	200	200
Restraints	1	1	1
Nref	6501	6181	6680
Npar	356	374	356
R1	0.0388	0.0321	0.0460
wR2	0.1043	0.0821	0.1277
S	1.04	1.04	1.03
Θ min, max/°	1.5, 28.3	1.5, 28.3	2.1, 28.4
Tot. data	13345	25711	23527
Unique data	6501	6181	6680
Observed data [I > 2.0σ(I)]	5554	5614	5232
Rint	0.017	0.018	0.024
Diffrn measured fraction Θ full	1.000	1.000	1.000
Min. resd. dens. (e/Å^3)	−0.21	−0.17	−0.22
Max. resd. dens. (e/Å^3)	0.21	0.22	0.31

10.4.1 H-Bonding Interactions Between Host and Guest Species

From Table 4, it is clear that the TET·CON and crystals from the TET/DMT/CON mixture experience almost identical (guest)C=O···H−O(host) H-bond interactions [2.716(2) and 2.718(3), with angles of 156 and 154°, respectively]. The guest residing in the 2DMT·CON complex does not experience any interactions of this type.

Table 4: Analysis of intermolecular hydrogen bonding interactions between TET·CON, DMT·CON and crystals formed from a mixture of TET/DMT/CON

Host	(host)O···O(host) /Å	(host)H···O(host) /Å	(host)O–H···O(host) /°	Symmetry operator
TET	2.716(2)	1.93	156	x,y,z
DMT	None			
TET/DMT	2.718(3)	1.94	154	−1+x,1+y,z

10.4.2 Short Ring (π···π) and X–H···π Interactions Between Host and Guest Species

Complementing the role of hydrogen bonding are cooperative (guest)CH···π(host) and (guest)C–H···O(host) stabilizing interactions. The host framework for each complex is stabilised by (host)π···π(host) interactions with comparable ranges [Table 5, 4.708(1)–5.912(2) Å]. Once more, TET·CON and crystals from the TET/DMT/CON mixture display virtually identical ranges of this interaction type. The complex from the TET/DMT/CON mixture is, however, devoid of (guest)C–H···π(guest) interactions, which are present in TET·CON (Table 5, 2.84 and 2.94Å, 157 and 145°) and 2DMT·CON (Table 5, 2.99Å, 132°). It is noted that the methoxy groups of DMT are non-functional towards guest inclusion but are utilized for host stabilisation (Table 5). Nonetheless, guest inclusion through this host is assisted via the non-classical (host)C–H···O(guest) short contact (Table 5, 2.54Å, 164°) (Figure 9).

Table 5: Analysis of X–H···π interactions occurring in TET·CON, 2DMT·CON and crystals from the TET/DMT/CON mixture

Interaction	TET·CON	2DMT·CON	Crystals from a TET/DMT/CON mixture
π···π (Host···Guest)	N/A	N/A	N/A
π···π (Host···Host)	4.749(1)–5.911(1) (9 contacts)	4.708(1)–5.673(1) (8 contacts)	4.748(2)–5.912(2) (9 contacts)
π···π (Guest···Guest)	N/A	N/A	N/A
CH···π	2.84 Å, 157° (H···Cg, C–H···Cg) (guest)C–H···π(host) 2.98 Å, 145° (H···Cg, C–H···Cg) (guest)C–H···π(host)	2.90 Å, 147° (H···Cg, C–H···Cg) (host)OMe–H···π(host) 2.88 Å, 148° (H···Cg, C–H···Cg) (host)OMe–H···π(host) 2.80 Å, 152° (H···Cg, C–H···Cg) (host)OMe–H···π(host) 2.80 Å, 144° (H···Cg, C–H···Cg) (host)OMe–H···π(host) 2.87 Å, 169° (H···Cg, C–H···Cg) (host)*m*Ar–H···π(host) 2.99 Å, 132° (H···Cg, C–H···Cg) (guest)C–H···π(host)	None
Short contacts	None	2.54 Å, 164° (H···O, C–H···O) (host)*C–H···O(guest)	None

*denotes the chiral centre
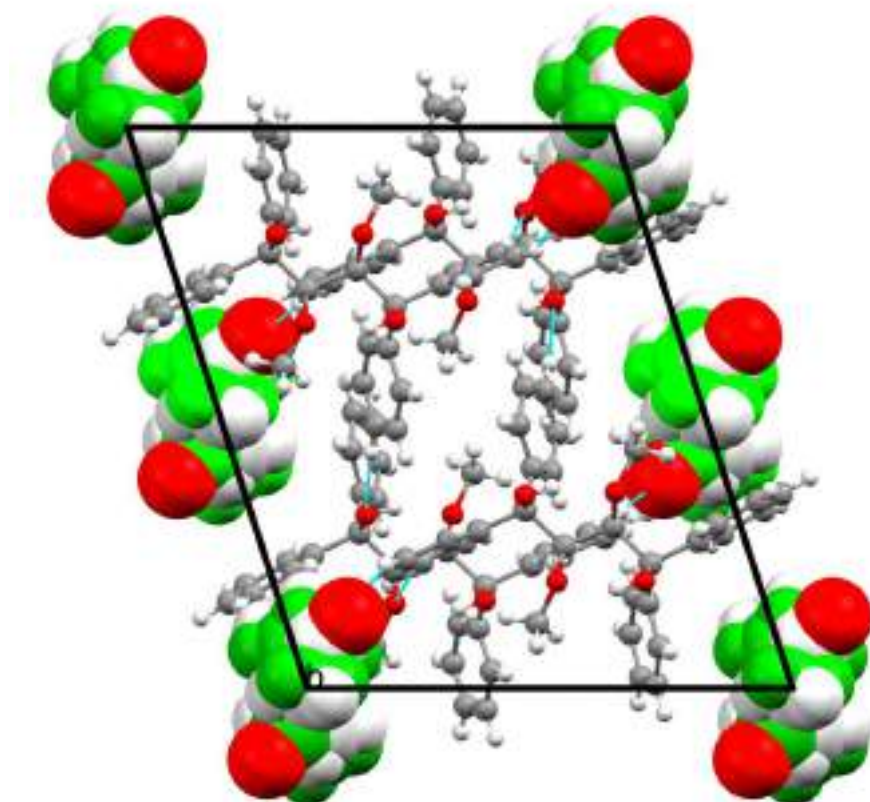
Figure 9: The 2DMT·CON unit cell; the CON guest (spacefilling) is disordered and hence coloured via symmetry operation (the carbonyl functional group is red, and the two disordered cyclic rings are green and white)

10.5 Proton NMR Analysis

The proton NMR spectra for TET, DMT and the complex from the TET/DMT/CON mixture are stacked in Figures 10a–c. It is clear that the latter complex, from the mixture of hosts and guest, is indeed TET·CON. [Note that impurities, such as wash solvent, are present lower field (2.0–0.5 ppm) on the DMT spectrum (Figure 10c).]
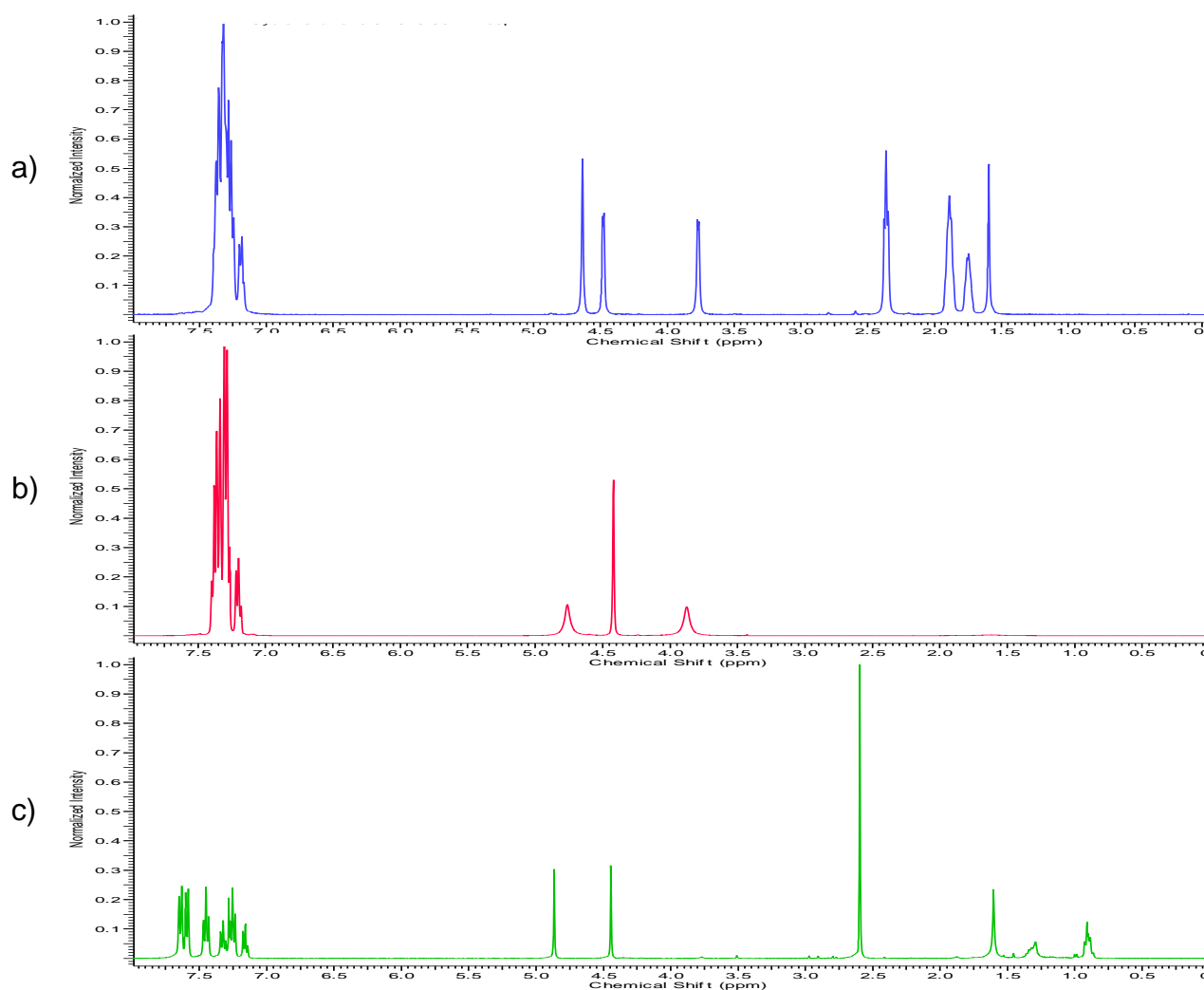
Figure 10: Stacked proton NMR spectra of a) crystals from a TET/DMT/CON mixture, b) TET and c) DMT

10.6 Conclusion

This study proved the efficiency of the secondary hydroxyl group functionality of TETROL. Upon recrystallization of an equimolar mixture of TET and DMT from cyclohexanone, only pure TET·CON crystallized out. As evidence, SCXRD analysis of the resultant solid exhibited identical interactions to that of a previously formed pure TET·CON complex. Proton NMR analysis further proved the formation of a pure TET·CON complex without any residual DMT present. It was concluded that the coordinatoclathrate ability of TETROL was reduced through the substitution of the host's secondary hydroxy groups with that of methoxy. The experiment was repeated for 2- and 4-methylcyclohexanone guests yielding equivalent results: only TETROL crystallized out with these guests. We therefore conclude that TETROL behaves as

the superior host when in competition with DMT solely because of the increased H-bonding capability due to the presence of the secondary hydroxyl groups that it possesses.
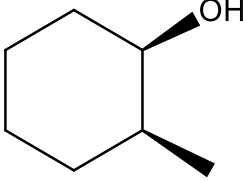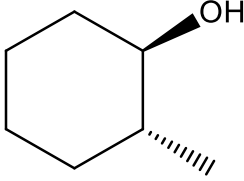
Chapter 11

The Selective Resolution of *cis* and *trans* Isomers of 2-Methylcyclohexanol by TETROL

11.1   Introduction

Geometrical isomers, generally known as *cis* and *trans* isomers, are defined as compounds that can be interconverted only by rotation around a double bond or a bond within a cyclic ring system.[209] These *cis* and *trans* isomers exhibit different physical properties, such as differing reactivities, internal energies, dipole moments, boiling points, melting points and densities.[210] A great deal of research has been conducted in developing methods suited to separate *cis* and *trans* isomers from one another, as each isomer may possess independent advantages within the field of chemical research and/or chemical processing. These methods often rely on intricate azeotropic distillation procedures or arduous chromatography separations.[211,212] Alternatively, for example, isomers such as *cis*- and *trans*- 2-methylcyclohexanol (2-MC) may be separated by means of their hydrogen phthalate solid derivatives [(*cis*-form, m.p. 104°) and (*trans*-form, m.p. 124°)].[213] However, Jackman *et al*[214] stated that separations of this kind usually involve tedious fractional crystallisations; nonetheless, numerous researchers have reported on the preparation of epimeric 2-MC and their solid derivatives. The two isomers of 2-MC are diastereomers of one another and thus differ in their physical properties, making them selected targets for this study. The aim of this investigation is to develop a new method for the separation of *cis*- and *trans*- 2-MC through the possible selective inclusion with TETROL. Table 1 shows the structures and various properties of these two isomers.

Table 1: The structure and properties of the two methylcyclohexanol isomers

	cis-2-MC	*trans*-2-MC
Structure		
Boiling point (°C)	165	167.2–167.6
Melting point (°C)	6–8	−21
Density (g/mL)	0.936	0.924

11.2   The Preparation of 2-Methylcyclohexanol

2-Methylcyclohexanol was prepared by the sodium borohydride reduction of 2-methylcyclohexanone, affording a mixture of *cis*- and *trans*- 2-MC (47.6 and 52.4%, respectively). This compound was analysed using GC-MS methods; the trace for the synthesised product is provided in Figure 1, and the GC peak areas obtained from this figure are given in Table 2.
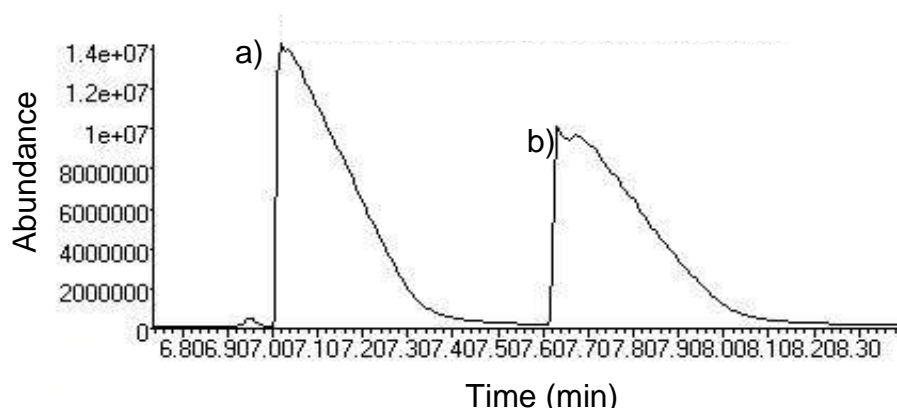
Figure 1: The GC chromatogram of the synthesised 2-methylcyclohexanol product affording a mixture of a) *trans* **(52.4%) and b)** *cis* **(47.6%)**

Table 2: GC data obtained from the chromatogram of the synthesised 2-methylcyclohexanol product

Compound	Peak area	% Yield of isomer	Retention time (min)
cis-2-methylcyclohexnol	1403333732	47.59	7.632
trans-2-methylcyclohexanol	1545185340	52.41	7.020

11.3   SCXRD Analysis

TETROL was recrystallised from the synthesised *cis*:*trans* mixture of 2-methylcyclohexanol, which showed the selective inclusion of 19.8% *cis* and 80.2% *trans* isomers. The GC-MS trace of the inclusion complex is given in Figure 2, with GC peak areas obtained from this figure provided in Table 3.

SCXRD experiments were carried out on suitable crystals of this complex and the crystal data and refinement parameters are listed in Table 4. From these experiments, the site occupancy factors were determined to be 65.9 and 34.1% for the *trans* and *cis* isomers, respectively. This ratio of *cis*:*trans* differs from the result obtained from GC analysis, and future work will be carried out in order to clarify reasons for the discrepancy. The TET·2-MC complex crystallizes in the orthorhombic crystal system and $P2_12_12_1$ space group with Z = 4. Furthermore, the guests are accommodated in discrete cavities in each crystal (Figures 3a and b).
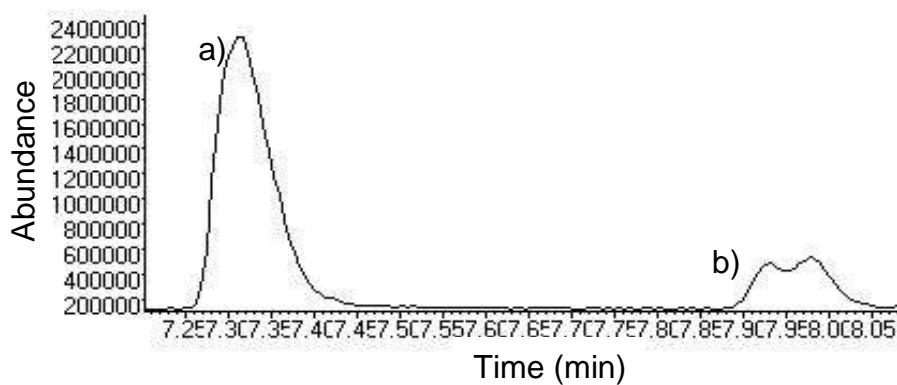
Figure 2: The GC chromatogram of the inclusion complex of a) *trans*-**2-MC (80.2%) and b)** *cis*-**2-MC (19.8%) with TETROL**

Table 3: GC data obtained from the chromatogram of the inclusion complex of TET with 2-MC

Compound	Peak area	% Yield of isomer	Retention time (min)
cis-2-methylcyclohexnol	24422886	19.76	7.977
trans-2-methylcyclohexanol	99161329	80.24	7.315

a)

b)
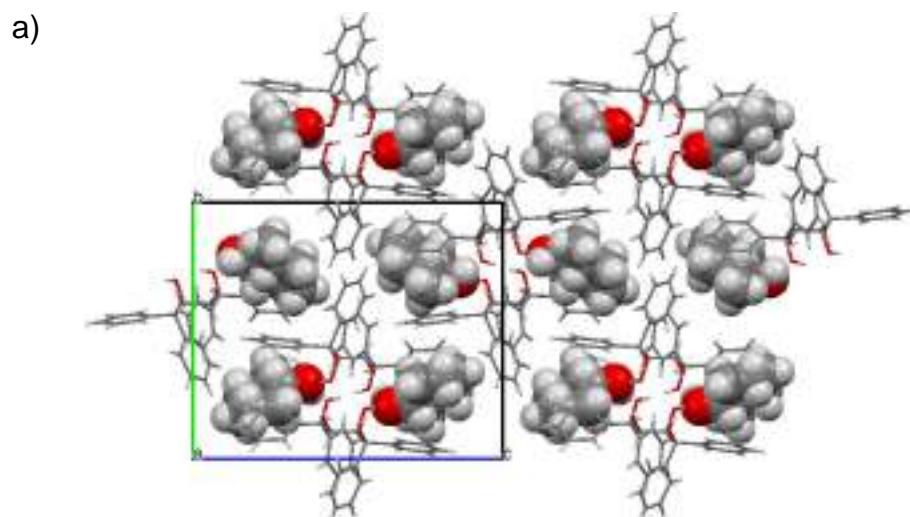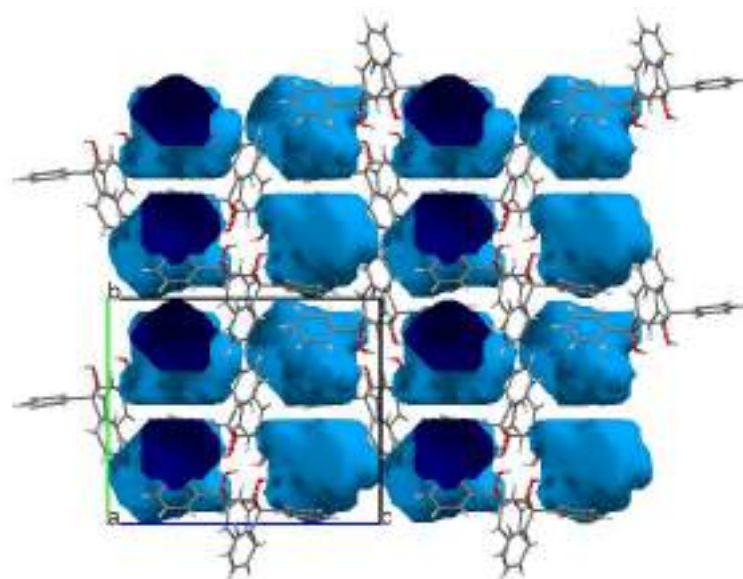
Figure 3: a) Crystal packing of the TET·2-MC inclusion complex with guests in spacefill form, and b) calculated voids (blue) for TET·2-MC indicating guest accommodation in isolated cavities; (oxygen – red, carbon – grey and hydrogen – light grey)

Table 4: Relevant single crystal X-ray crystallographic data for the TET·2-MC complex

	TET·2-MC
Chemical formula	$C_{28}H_{26}O_4 \cdot C_7H_{14}O$
Formula weight	540.67
Crystal system	Orthorhombic
Space group	$P2_12_12_1$
μ (Mo Kα)/mm^{-1}	0.081
a/Å	10.3163(6)
b/Å	15.2803(10)
c/Å	18.4871(11)
α/°	90
β/°	90
γ/°	90
V/Å^3	2914.2(3)
Z	4
F (000)	1160
Temp (K)	200
Restraints	16
Nref	7233
Npar	412
R1	0.0378
wR2	0.1022
S	1.03
Θ min, max/°	2.3, 28.3
Tot. data	60063
Unique data	7233
Observed data [I > 2.0σ(I)]	6654
Rint	0.017
Diffrn measured fraction Θ full	0.999
Min. resd. dens. (e/Å^3)	−0.22
Max. resd. dens. (e/Å^3)	0.31

SCXRD analyses revealed that the hydroxy group of the *cis* isomer occupies an identical position to the hydroxy group of the *trans* isomer. However, the carbon atoms of the rings of these isomers are somewhat displaced from one another (Figure 4). Both these isomers experience H-bonding of the type (guest)O–H···O(host) [Table 5, 2.715(2) and 2.929(2), 173 and 164°, respectively]. The host framework is stabilised by numerous (host)π···π(host) interactions in the range 4.7856(1)–5.7511(1) (Table 6). The *cis* isomer is stabilised within the host framework by a (guest)C–H···π(host) interaction (Table 6, 2.88 Å,140°), as well as by two short contacts of the type (guest)C–H···C$_{Ar}$(host) and (guest)C–H···H(*o*-Ar)(host) (Table 6, 2.79 and 2.21 Å, with angles of 136 and 146°, respectively). The *trans* isomer is stabilised by two (guest)C–H···π(host) interactions of the type 2.97 and 2.72 Å with angles of 129 and 152°, respectively.
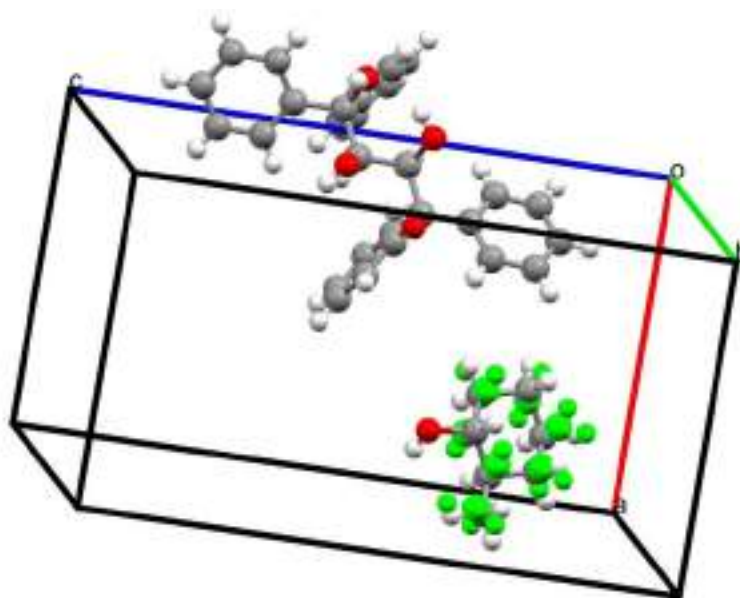
Figure 4: The TET·2-MC complex showing the *cis* isomer highlighted in green, and *trans* isomer in grey; (oxygen – red, carbon – grey and hydrogen – light grey)

Table 5: Analysis of intermolecular hydrogen bonding interactions between TET and 2-MC in the complex

Guest	(host)O⋯O (guest) /Å	(host)H⋯O (guest) /Å	(host)O–H ⋯X(guest) /°	Symmetry operator
2-MCOL	2.715(2)	1.88	173	−1/2+x,1/2−y,1−z
	2.929(2)	2.13	164	−1+x,y,z

Table 6: Analysis of other significant interactions between TETROL and 2-MC

Interaction	TET·2-MC
π⋯π (Host⋯Guest)	N/A
π⋯π (Host⋯Host)	4.7856(1)–5.7511(1) (7 contacts)
π⋯π (Guest⋯Guest)	N/A
CH⋯π	2.97 Å, 129° (H⋯Cg, C–H⋯Cg)[a] (host)C–H⋯π(host) 2.72 Å, 152° (H⋯Cg, C–H⋯Cg)[a] (guest)C–H⋯π(host) 2.85 Å, 142° (H⋯Cg, C–H⋯Cg)[a] (guest)C–H⋯π(host) 2.88 Å, 140° (H⋯Cg, C–H⋯Cg)[b] (guest)C–H⋯π(host)
Short contacts	2.79 Å, 136° (H⋯Cg, C–H⋯Cg)[b] (guest)C–H⋯C_{Ar}(host) 2.21 Å, 146° (H⋯Cg, C–H⋯Cg)[b] (guest)C–H⋯H(o-Ar)(host)

[a]Interaction experienced by the *trans* isomer

[b]Interaction experienced by the *cis* isomer

11.4   Hirshfeld Surface Analysis

Unfortunately, Hirshfeld analyses could not be conducted on the two separate isomers as the hydroxy group of these guests are held in place by H-bonding, while the carbon atoms are disordered. If one were to analyse the *cis* isomer independently, a false percentage interaction data set would be afforded and quantitative comparisons between the two guests would not be viable.

11.5   Thermal Analyses

Both DSC and TG experiments were carried out on the TET·2-MC complex. The overlaid traces obtained are provided in Figure 5. Upon heating of this complex, a simple guest release process ensues, with an onset temperature (T_{on}) of ~31.9 °C (Table 7). The majority of the guest release occurred just prior to the melting of the host (Figure 5, 144.7°C). The expected mass loss for the 1:1 H:G complex was calculated to be 21.1%, which correlates well with the actual mass loss observed (Table 7, 21.0%).
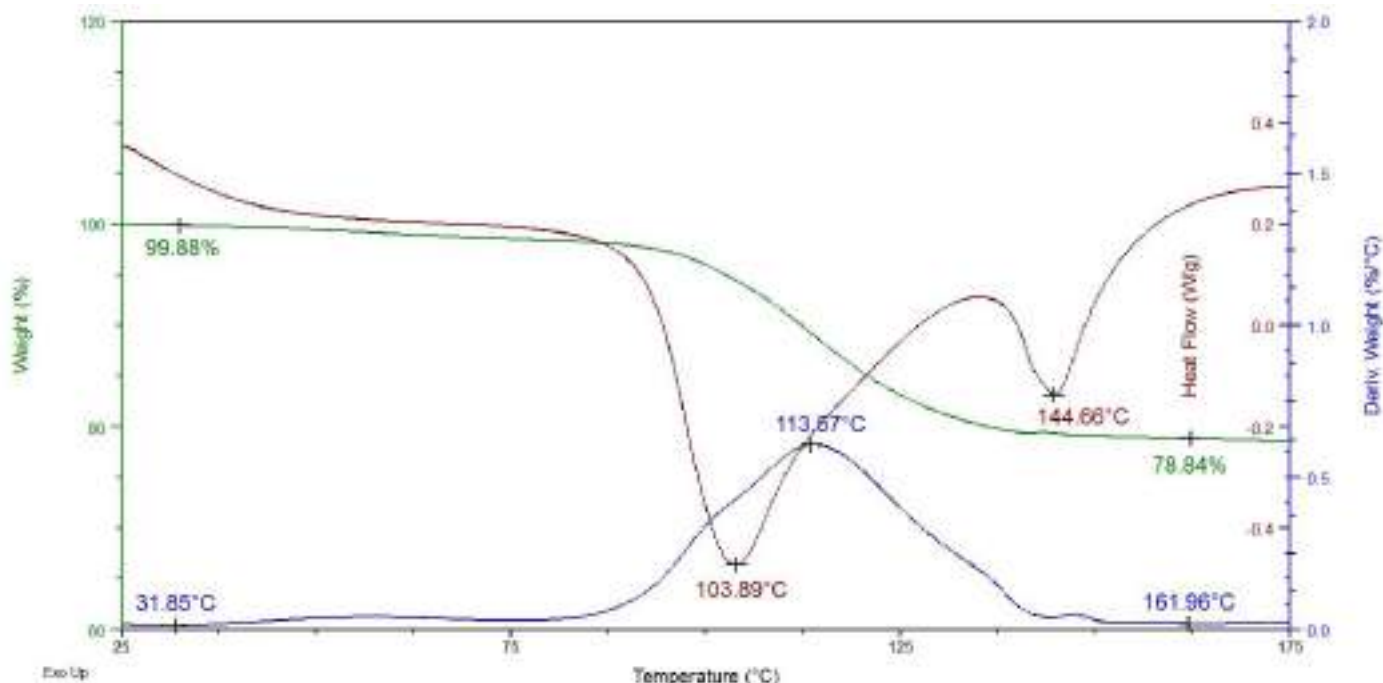
Figure 5: Overlaid traces for the DSC (brown), TG (green) and its derivative (DTG, blue) for the TET·2-MC complex

Table 7: Thermal data from DSC/TG traces of TET·2-MC

Guest	T_{on} (°C)	T_p (°C)[a]	T_{end} (°C)[b]	Mass loss % (expected)	Mass loss % (actual)
2-MCOL	31.9	113.6	103.9 144.7	21.1	21.0

[a]T_p values determined from blue DTG traces
[b]T_{end} were obtained from the brown DSC traces

11.6 Conclusion

The host, TETROL, showed potential for separation of the *trans* isomer (80.2%) of 2-methylcyclohexanol from its *cis* isomer (19.8%) when this host was recrystallized from a 47.59:52.41 mixture of these two guests. These data, obtained from GC-MS experiments, did not correlate with the site occupancy factors (19.8:80.2) of these two guests from SCXRD. Future work will be conducted in order to clarify reasons for this discrepancy. The inclusion complex formed was also qualitatively analysed by SCXRD and thermal analysis, but these analyses could not provide evidence for the favourable inclusion of *trans*-2-MC over *cis*-2-MC.

Chapter 12

Miscellaneous Inclusion Complexes with TETROL

12.1   Introduction

During the analysis of the inclusion abilities of TETROL with various guest species, we prepared inclusion complexes that did not form part of a collective study as in previous chapters, but perhaps may become relevant in future work. For the sake of brevity, we will discuss only three such inclusion complexes formed between TETROL and butyric acid (BA), isobutyric acid (IBA) and 3-chloropropionic acid (3CPA) (Figure 1) affording TET·2BA, TET·2IBA and TET·2[3CPA].

a)   b)   c)
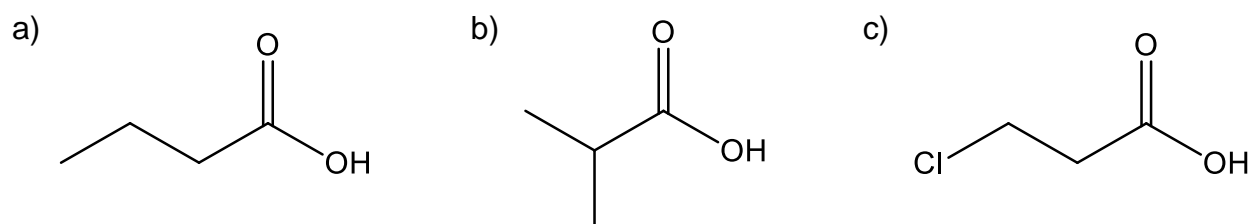
Figure 1: The chemical structures of a) butyric acid, b) isobutyric acid and c) 3-chloropropionic acid

12.2   Single Crystal X-ray Diffraction (SCXRD)

The crystal data and refinement parameters for the three complexes are provided in Table 1. All complexes crystallized in the orthorhombic crystal system and $P2_12_12_1$ space group with $Z = 4$. These complexes crystallized with very similar unit cell dimensions, and their host frameworks were determined to be isostructural (Table 1). This is strikingly evident from Figures 2–4, where the guest accommodation type is characterized by guest molecules occupying isolated cavities within their respective host crystals. The stereoview for each complex with TETROL is displayed in Figure 5.

Table 1: Relevant single crystal X-ray crystallographic data for the complexes of TETROL with BA, IBA and 3CPA

	TET·2BA	TET·2IBA	TET·2[3CPA]
Chemical formula	$C_{28}H_{26}O_4$· $2(C_4H_8O_2)$	$C_{28}H_{26}O_4$· $2(C_4H_8O_2)$	$C_{28}H_{26}O_4$· $2(C_3H_5ClO_2)$
Formula weight	602.70	602.70	643.53
Crystal system	Orthorhombic	Orthorhombic	Orthorhombic
Space group	$P2_12_12_1$	$P2_12_12_1$	$P2_12_12_1$
μ (Mo Kα)/mm^{-1}	0.086	0.085	0.254
a/Å	9.3620(3)	9.2218(6)	9.2108(9)
b/Å	17.6884(8)	18.1796(10)	17.4794(16)
c/Å	19.7085(8)	19.7692(12)	19.8709(19)
α/°	90	90	90
β/°	90	90	90
γ/°	90	90	90
V/Å^3	3263.7(2)	3314.3(3)	3199.2(5)
Z	4	4	4
F (000)	1288	1288	1352
Temp (K)	200	200	200
Restraints	0	18	0
Nref	8128	8264	8005
Npar	405	438	403
R1	0.0410	0.0426	0.0580
wR2	0.1157	0.1191	0.1838
S	1.04	1.04	1.05
Θ min, max/°	2.1, 28.3	2.1, 28.4	2.0, 28.4
Tot. data	39577	60215	66139
Unique data	8128	8264	8005
Observed data [I > 2.0σ(I)]	7009	7285	7333
Rint	0.019	0.019	0.017
Diffrn measured fraction Θ full	1.000	0.999	0.999
Min. resd. dens. (e/Å^3)	–0.30	–0.25	–0.85
Max. resd. dens. (e/Å^3)	0.58	0.29	1.26

a)

b)

Figure 2: a) Crystal packing of the TET·2BA inclusion complex with guests in spacefill form, b) calculated voids (blue) for TET·2BA indicating guest accommodation in channels; (oxygen – red, carbon – grey and hydrogen – light grey)

a)

b)
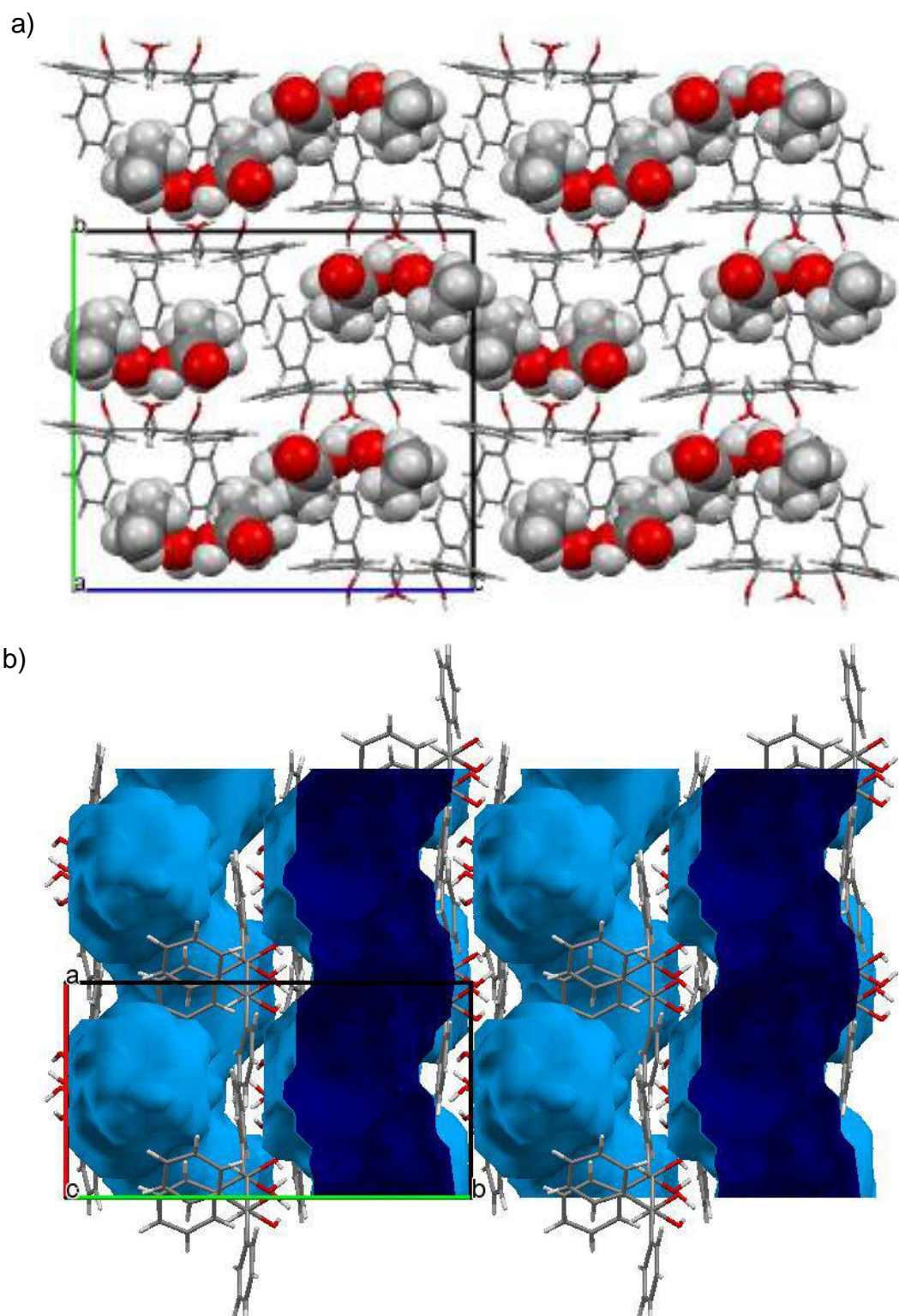
Figure 3: a) Crystal packing of the TET·2IBA inclusion complex with guests in spacefill form, b) calculated voids (blue) for TET·2IBA indicating guest accommodation in channels; (oxygen – red, carbon – grey and hydrogen – light grey)
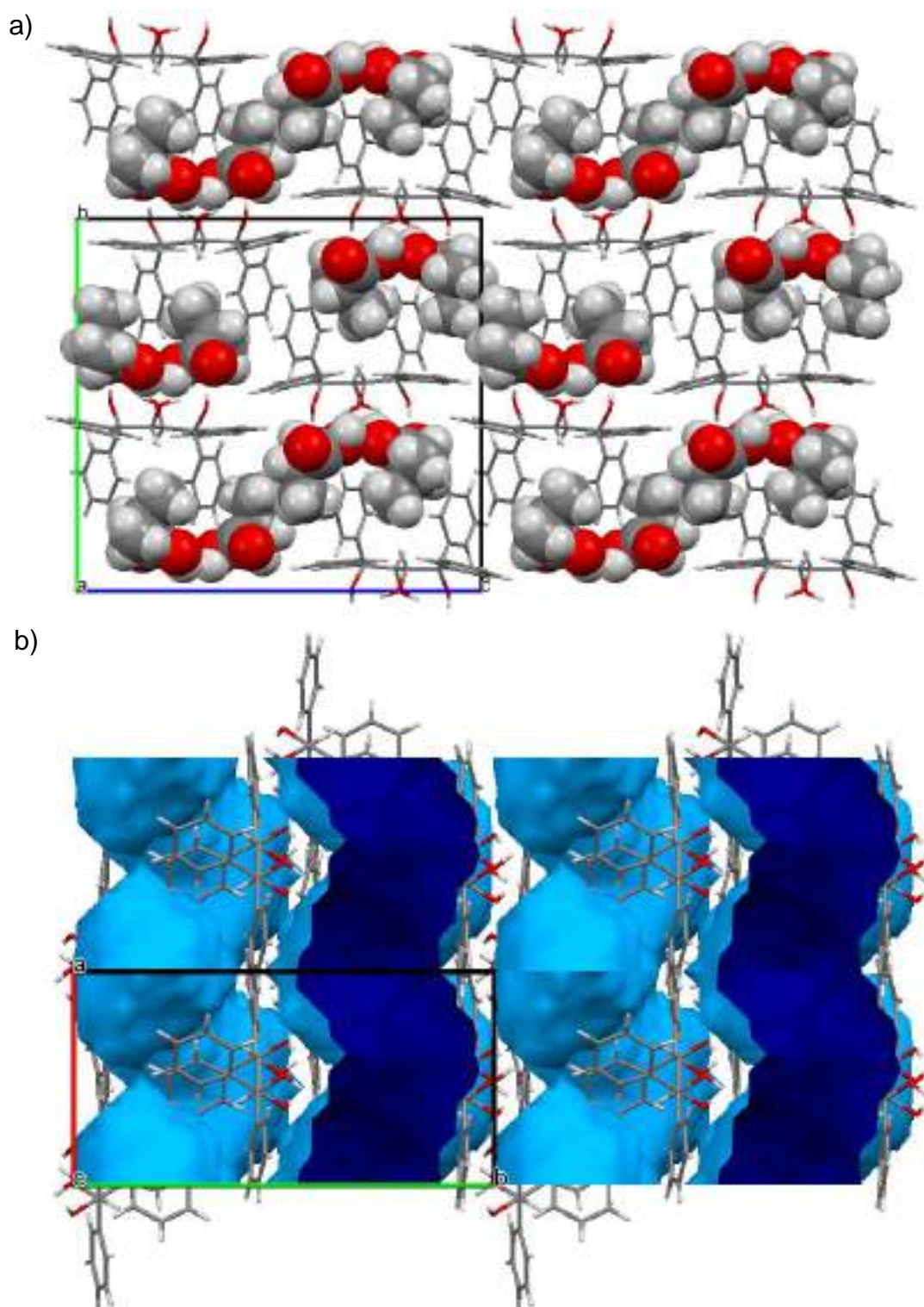
a)

b)
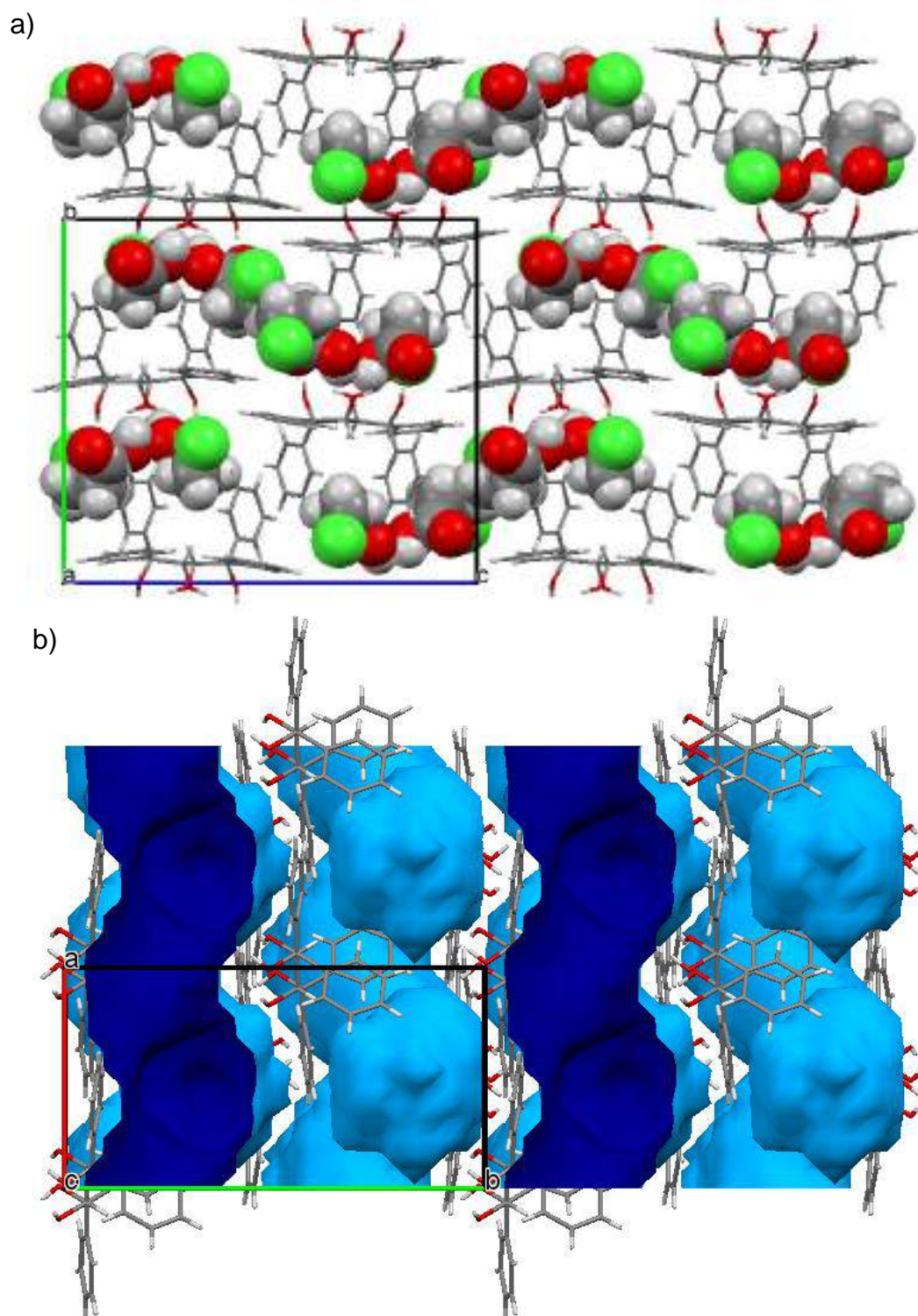
Figure 4: a) Crystal packing of the TET·2[3CPA] inclusion complex with guests in spacefill form, b) calculated voids (blue) for TET·2[3CPA] indicating guest accommodation in channels; (oxygen – red, chlorine – green, carbon – grey and hydrogen – light grey)

245
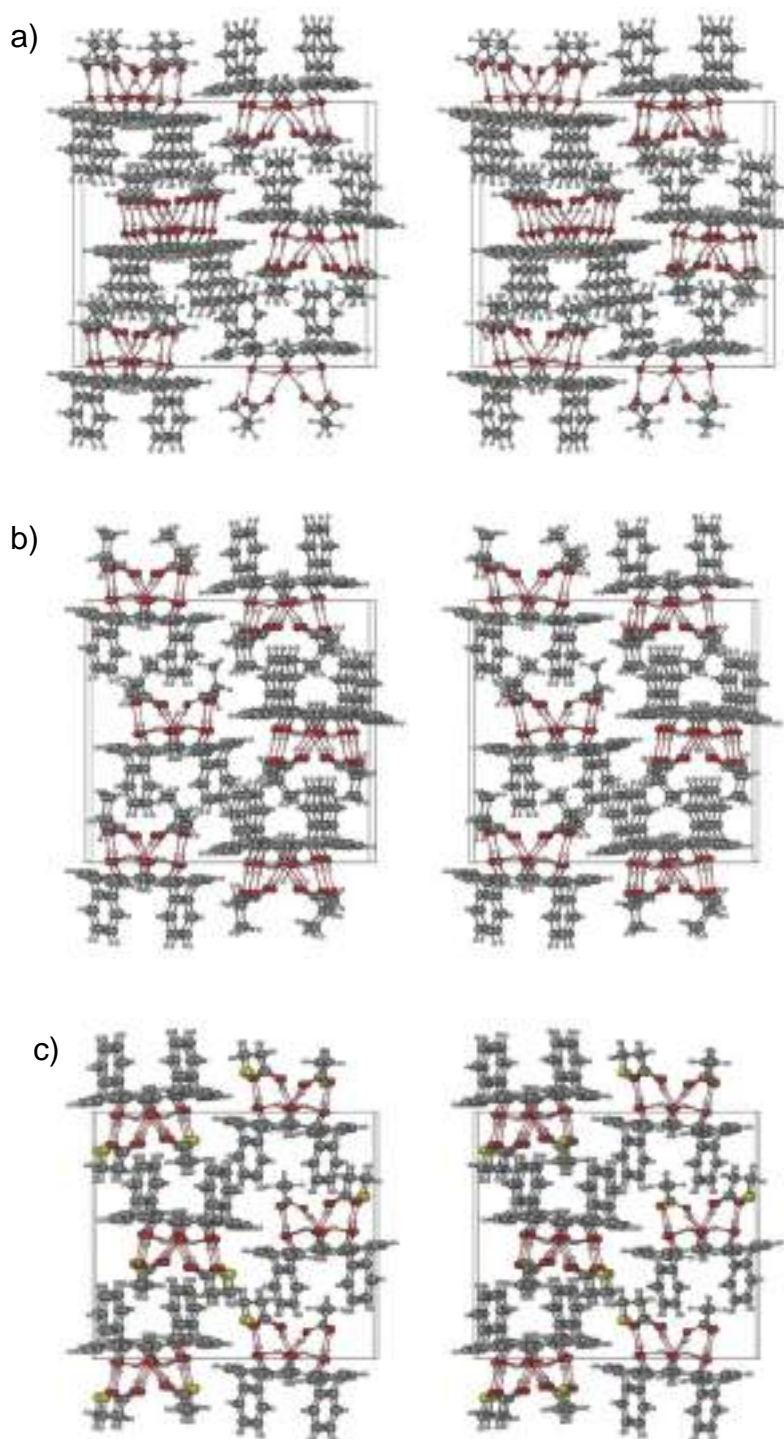
Figure 5: Stereoviews illustrating the unit cells of a) TET·2BA b) TET·2IBA and c) TET·2[3CPA]

12.2.1 H-Bonding Interactions Between Host and Guest Species

Each of the three guests are held in the crystal by means of both (guest)C=O···H−O(host) and (guest)O–H···O(host) hydrogen bonds involving the tertiary outer hydroxy and secondary inner hydroxyl groups of the host, respectively. It is interesting to note that TETROL exhibits bifunctionality as a H-bond donor and acceptor here; also, for the first time, TETROL employs its secondary hydroxyl groups as hydrogen-bond acceptors (Figure 6). Although each guest experiences four H-bonds with TETROL, only two of the shortest of these have been listed in Table 2. The three complexes experience comparable H-bond distances in the range 2.651–2.690 Å with angles of 162–174°.

Table 2: Analysis of intermolecular hydrogen bonding interactions between TETROL and guests BA, IBA and 3CPA

Guest	Unit cell H:G ratio	Guest	(host)O···X(guest) /Å	(host)H···X(guest) /Å	(host)O–H ···X(guest) /°	Symmetry operator
BA	1:2	[1]	2.687(2)[a]	1.85	174	x,y,z
		[2]	2.686(2)[b]	1.87	162	x,y,z
IBA	1:2	[1]	2.684(3)[b]	1.82	169	x,y,z
		[2]	2.651(2)[b]	1.85	171	x,y,z
3CPA	1:2	[1]	2.682(4)[b]	1.86	167	x,y,z
		[2]	2.690(4)[b]	1.87	166	x,y,z

[a]Interaction involving guest carbonyl group
[b]Interaction involving guest hydroxy group

a)

b)

c)
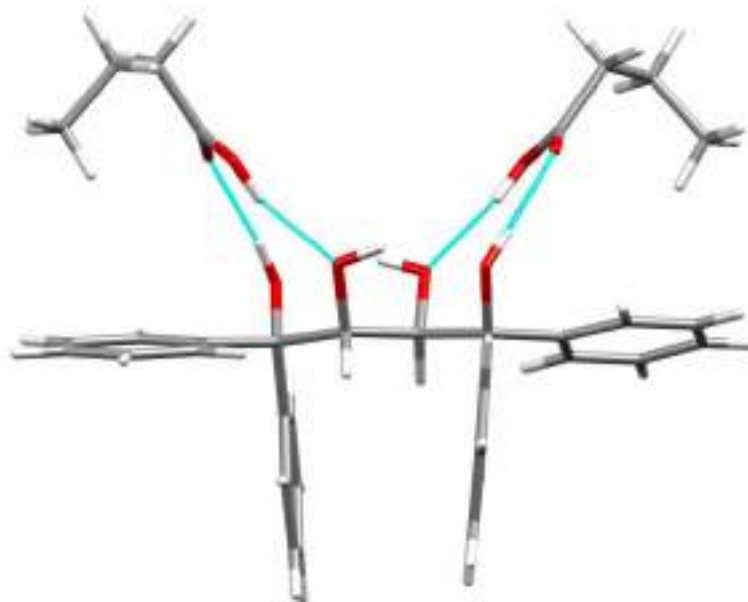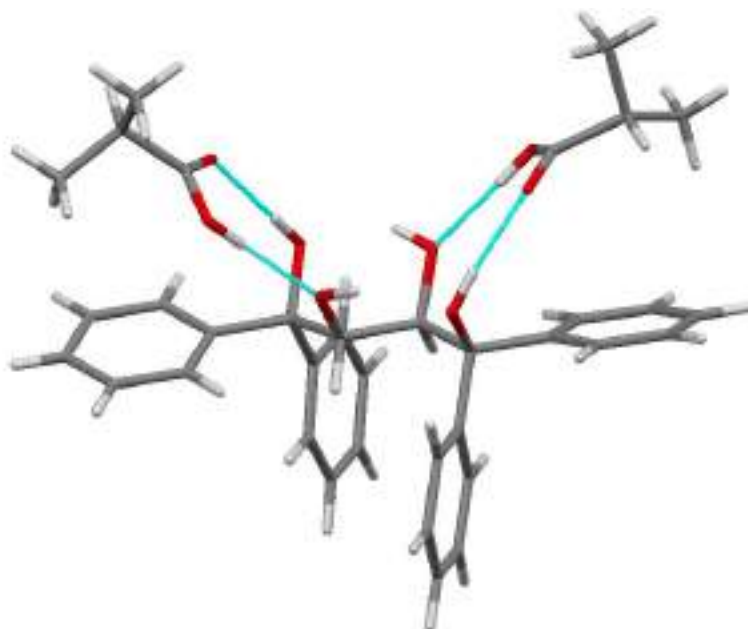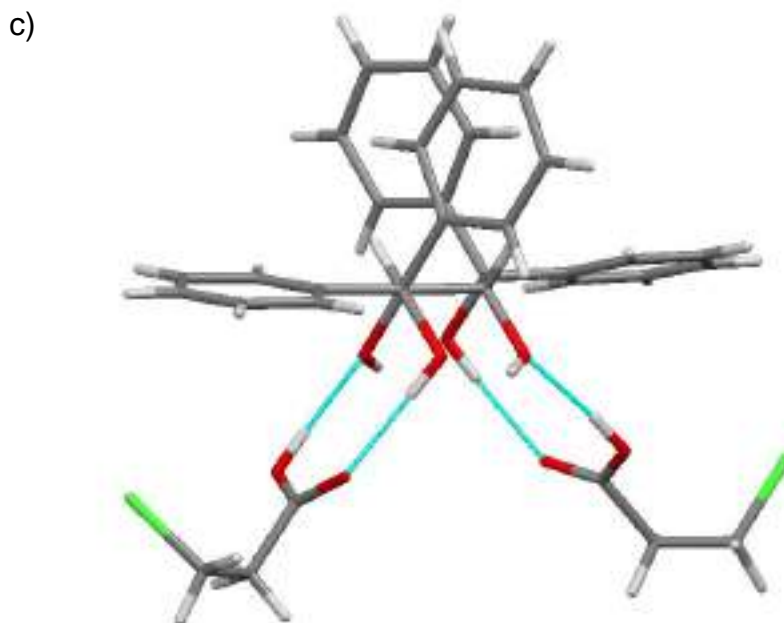
Figure 6: The intermolecular H-bonding in a) TET·2BA, b) TET·2IBA and c) TET·2[3CPA]

12.2.2 Short Ring (π···π) and X–H···π Interactions Between Host and Guest Species

The host framework for each complex is stabilised by (host)π···π(host) interactions in comparable ranges [Table 3, 4.677(2)–5.755(2) Å]. The TET·2BA and TET·2IBA complexes experience further host stabilisation through (host)*p*-ArH···π(host) interactions (Table 6, 2.88 and 2.94 Å, with angles of 139°). These two complexes experience noticeably shorter interactions of the type (host)*m*-ArH···H–C(guest) and (guest)Me–H···H(*p*-Ar)(host), respectively (Table 3, 2.27 and 2.32 Å, both with angles of 146°). The TET·2[3CPA] complex is stabilized by a (guest)Me–H···O=C(guest) interaction of 2.66 Å with angle of 136° (Table 3).

Table 3: Analysis of other significant interactions between TETROL and guests BA, IBA and 3CPA

Interaction	TET·2BA	TET·2IBA	TET·2[3CPA]
π···π (Host···Host)	4.677(2)–5.755(1) (6 contacts)	4.728(1)–5.672(1) (6 contacts)	4.722(2)–5.650(2) (6 contacts)
CH···π	2.88 Å, 139° (H···Cg, C–H···Cg) (host)*p*-ArH···π(host)	2.94 Å, 139° (H···Cg, C–H···Cg) (host)*p*-ArH···π(host)	–
Short contacts	2.27 Å, 146° (H···H, C–H···H) (host)*m*-ArH···H–C(guest)	2.32 Å, 146° (H···H, C–H···H) (guest)Me–H···H(*p*-Ar)(host)	2.66 Å, 136° (H···O, C–H···O) (guest)Me–H···O=C(guest)

12.3   Hirshfeld Surface Analysis

Hirshfeld surface analyses were conducted on the TET·2BA, TET·2IBA and TET·2[3CPA] complexes to assist in summarising, quantitatively, the multiple intermolecular interactions present (Figure 7). A summary of the percentage of each interaction type is displayed graphically in Figure 8, while Table 4 provides the actual values obtained from this figure.

All complexes are predominantly stabilised by H···H interactions (27.7–57.5%) and experience comparable O···H/H···O interactions (23.6–26.9%) (Figure 8, Table 4). These O···H/H···O interactions are observed as two large spikes (marked in magenta) that represent (guest)C=O···H−O(host) and (guest)O–H···O(host) hydrogen bonds, respectively. These are highlighted in red on the calculated Hirshfeld surfaces in Figure 9. Additionally, the TET·2[3CPA] is stabilised by a high number of H···Cl interactions (Table 4, Figure 8, 20.1 and 24.5%).

TET·2BA[1]   **TET·2BA[2]**
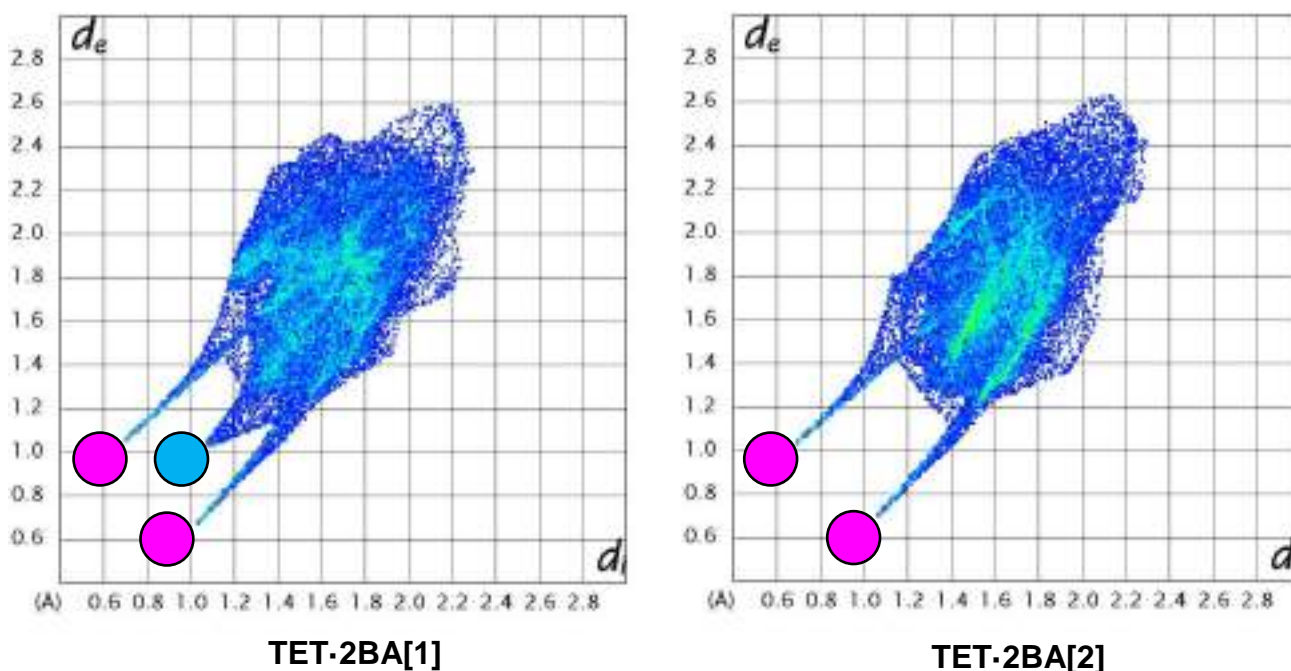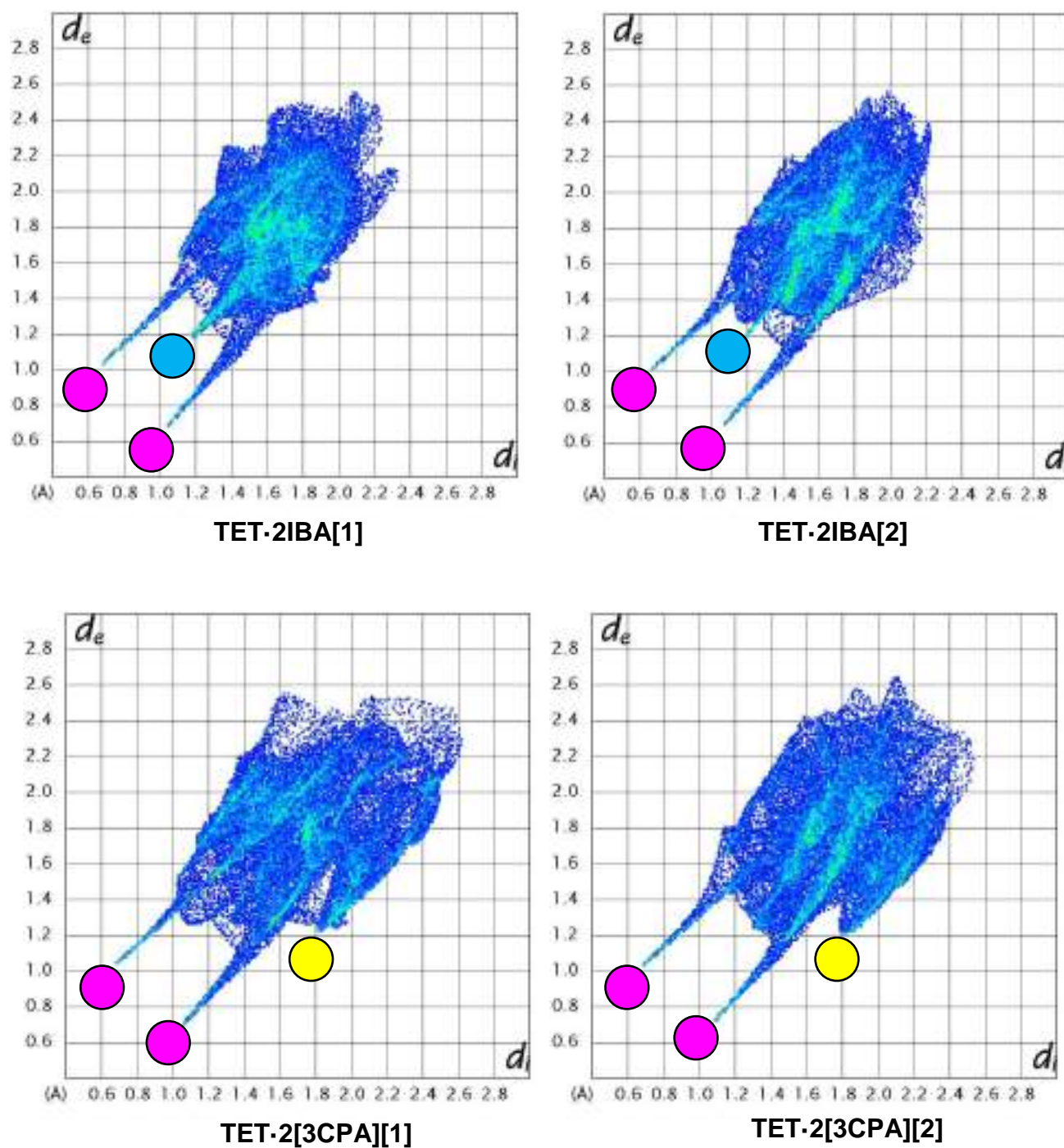
Figure 7: Hirshfeld fingerprint plots for the TET·2BA, TET·2IBA and TET·2[3CPA] complexes; the 'spikes' and 'wings' are colour coded and depict O···H (magenta), H···H (blue) and H···Cl (yellow) contacts
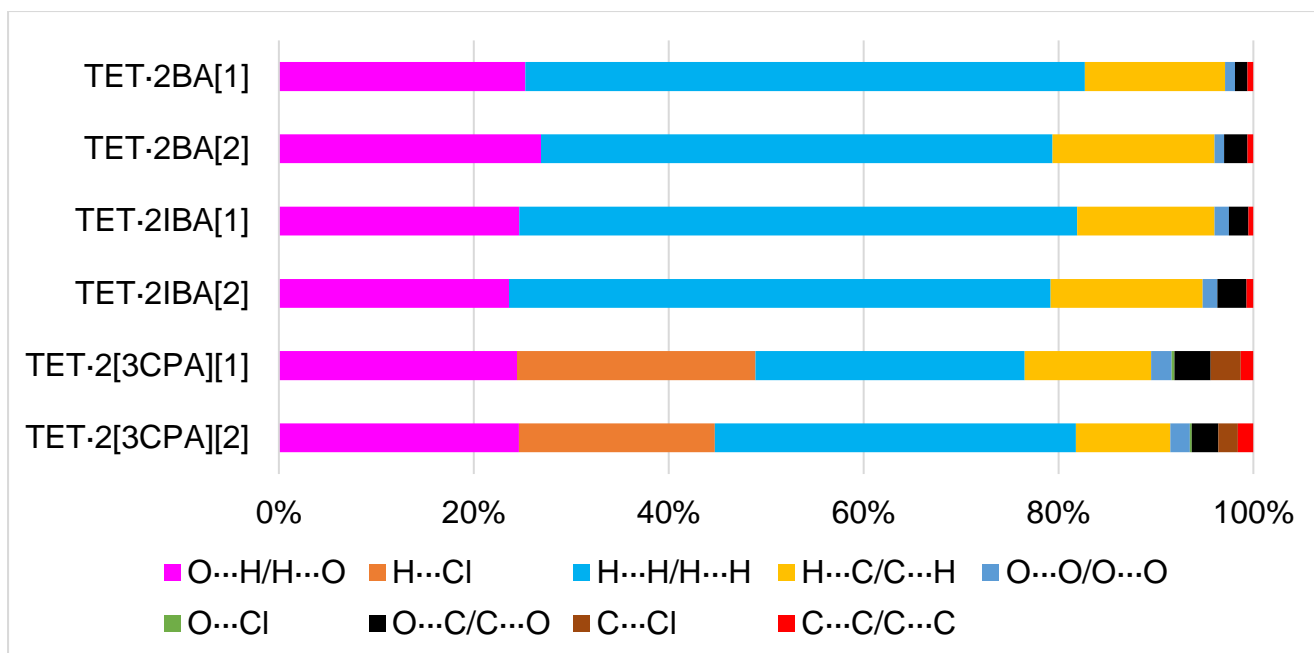
Figure 8: Graphical display showing the percentage intermolecular interactions of each type for the TET·2BA, TET·2IBA and TET·2[3CPA] complexes

Table 4: Percentage intermolecular interactions in each inclusion complex (G···H/H···G)

	O···H/ H···O	H···Cl [a]	H···H/ H···H	H···C/ C···H	O···O/ O···O	O···Cl [a]	O···C/ C···O	C···Cl [a]	C···C/ C···C
TET·2[3CPA][2]	24.6	20.1	37.0	9.7	2.0	0.2	2.7	2.0	1.6
TET·2[3CPA][1]	24.5	24.5	27.7	13.0	2.1	0.3	3.7	3.1	1.3
TET·2IBA[2]	23.6	0.0	55.6	15.6	1.5	0.0	3.0	0.0	0.7
TET·2IBA[1]	24.7	0.0	57.3	14.1	1.5	0.0	2.0	0.0	0.5
TET·2BA[2]	26.9	0.0	52.5	16.6	1.0	0.0	2.4	0.0	0.6
TET·2BA[1]	25.3	0.0	57.5	14.4	1.0	0.0	1.3	0.0	0.6

[a] Only H···G
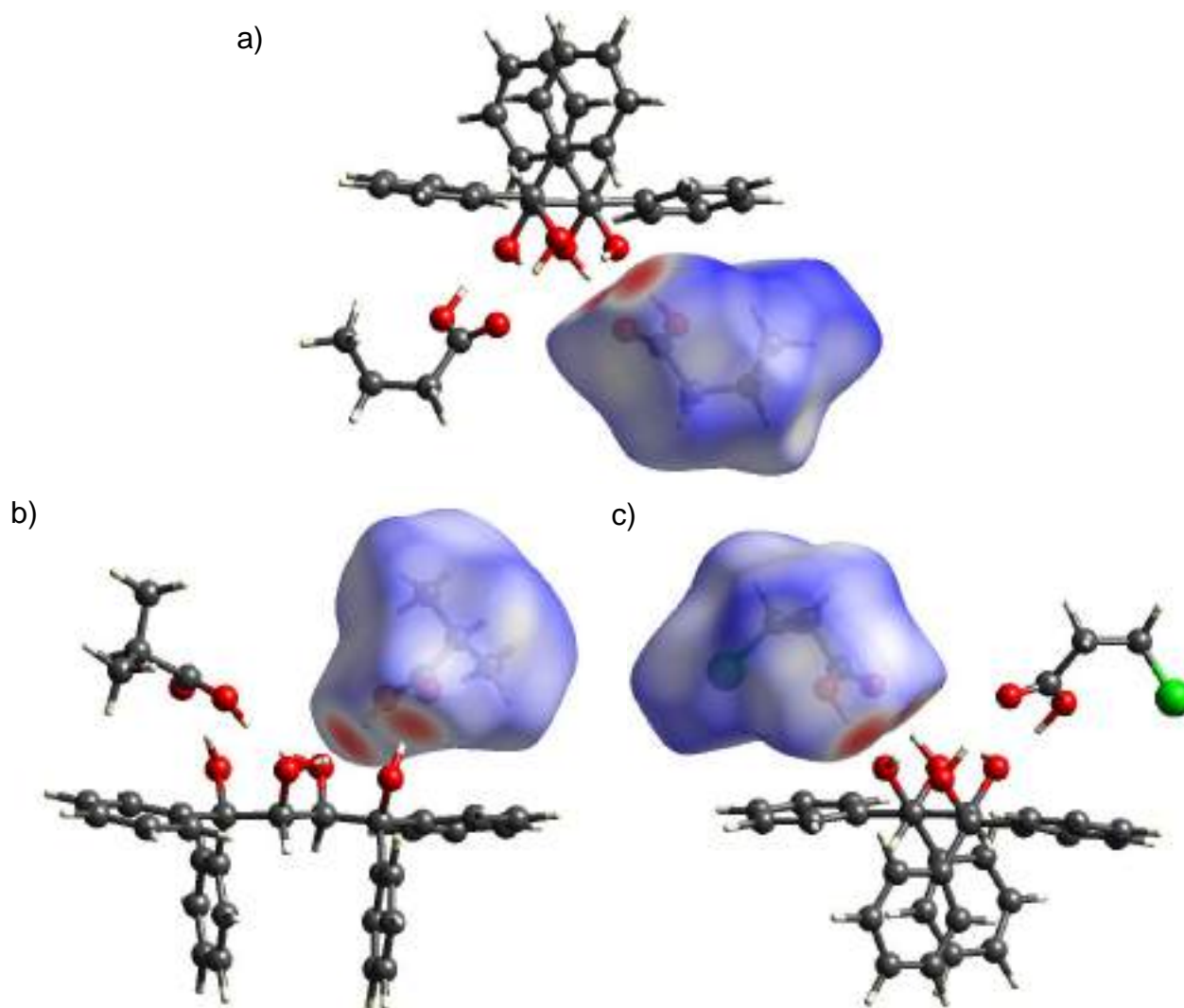
Figure 9: The calculated Hirshfeld surfaces representing (guest)C=O···H−O(host) and (guest)O–H···O(host) hydrogen bonds (shaded red) for the a) TET·2BA, b) TET·2IBA and c) TET·2[3CPA] complexes

12.4 Conclusion

TETROL proved to be an efficient host for the inclusion of three carboxylic acids, namely BA, IBA and CPA. The assessment of these inclusion complexes added to a greater understanding of the host's classification: TETROL has bifunctionality here as both a hydrogen-bond acceptor and donor. We observed, for the first time in this work, that the host's secondary hydroxyl groups behaved as H-bond acceptors (which normally function as H-bond donors). SCXRD and Hirshfeld analyses showed the extent of these H-bond interactions and how well-suited this host is for the inclusion of

carboxylic acid guest types. Future work will be conducted on other carboxylic acids as potential guest species for the host TETROL.

Chapter 13

Conclusion

The objective of this research project was to determine whether TETROL has the ability to serve as a selective host material for the separation of related compounds. This host compound showed selective behaviour when recrystallized from a wide variety of guest mixtures.

In this work, we observed the host's preference for nitrogen-based hydrogen-bond acceptors over oxygen-based ones. TETROL preferentially included CAM over CON and COL [CAM (53.0%) > CON (35.3%) > COL (11.7%)] (Chapter 3, Table 2). Hirshfeld surface analysis showed that the TET·2CAM complex experienced the highest number of H···H interactions (Chapter 3, Table 7, 82.0–83.8%). SCXRD analysis showed evidence for the preferential inclusion of CAM by TET as the TET·2CAM complex experienced the shortest (guest)C–H···π(host) interaction observed (Chapter 3, Table 6, 2.58 Å, 158°), and was the only complex to experience further stabilising short contacts in the form of (host)C_{Ar}···H–N(guest) and (guest)C–H···C_{Ar}(host). The host also had preference for ANI over CAM, COL and PHO [ANI (57.5%) > CAM (37.8%) > COL (3.5%) > PHO (1.3%)] (Chapter 8, Table 2). In these experiments, Hirshfeld surface analysis proved that the 2TET·3ANI complex experienced a higher degree of N···H/H···N interactions (Chapter 8, Table 10, 3.2 and 4.9%) in comparison to TET·COL (0%) and TET·2CAM (0–2.7%). It was observed from SCXRD analyses that this complex, furthermore, experienced the shortest stabilising contact in comparison to TET·2CAM (2.69 Å versus 2.81–2.85 Å), which supported the preferential inclusion of ANI over CAM.

TETROL proved to have selective preference for aniline (67.3%) over its methylated derivatives, *N*-methylaniline (28.4%) and *N,N*-dimethylaniline (4.2%) (Table 2, Chapter 6). As evidence, Hirshfeld surface analysis showed that the 2TET·3ANI complex experienced a higher degree of stabilising N···H/H···N contacts in comparison to 2TET·4NMA (3.2–14.9% versus 1.7–2.8%, Table 6, Chapter 6), which was confirmed by thermal analysis, which indicated that aniline (T_{on} = 70.9 °C) was

more tightly bound in the crystal than NMA (T_{on} = 41.4 °C), and this correlated exactly with the host's selectivity order of ANI > NMA > NNMA. (NNMA was not included in the single solvent experiments.)

The host was, furthermore, recrystallized from a mixture of four selected heterocyclic compounds (MOR, PIP, PYR and DIO) and showed high selectivity in the presence of these guests, with a selectivity order of MOR (75.3%) > PIP (18.2%) > PYR (5.3%) > DIO (1.2%) (Table 2, Chapter 5). Supporting this observation was SCXRD analysis which showed that the TET·MOR complex experienced the strongest host–guest H–bond interactions, while Hirshfeld surface analyses were not useful in this regard. Thermogravimetric analyses confirmed that MOR was more tightly bound in the crystal compared to the other three guests as T_{on} values correlated exactly with the host's selectivity order (MOR 75.4, PIP 73.8 and PYR 48.2 °C, with the DIO complex being unstable at room temperature) (Table 8, Chapter 5).

TETROL also displayed selective behaviour in the presence of mixed isomers. In the presence of the three isomeric methylcyclohexanones (Chapter 4, Table 2), a selectivity order of 2MCON (79%) >> 3MCON (14%) > 4MCON (7%) was obtained. However, adding CON to these experiments resulted in a complete reversal in the host selectivity for the three methylcyclohexanones [Chapter 4, Table 3, CON (52%) > 4MCON (30%) > 3MCON (13%) > 2MCON (5%)]. The host was also efficient in the inclusion and discrimination between the toluidine isomers, resulting in a selectivity order of *p*-TOLU (58.5%) > *m*-TOLU (27.3%) > *o*-TOLU (14.2%) (Table 2, Chapter 7). This same selectivity order was observed in the presence of aniline and toluene, *p*-TOLU (42.8%) > ANI (24.6%) > *m*-TOLU (18.7%) > *o*-TOLU (12.2%) > TOLU (1.8%) (Table 4, Chapter 7). We also analysed the host's selectivity towards the cresol isomers when recrystallised from mixtures of all three isomers, and this resulted in a selectivity order of PC (64.9%) > MC (23.8%) > OC (11.3%) (Table 2, Chapter 9). This result was regarded as significant since the separation of PC from MC remains a significant challenge in the chemical industry. In fact, TETROL was able to separate 70.4% PC from an equimolar binary mixture of PC and MC (Table 2, Chapter 9).

TETROL displayed superior H-bonding ability when comparing it to its derivative, DMT. TETROL alone crystallized out with cyclohexanone when an equimolar mixture

of the two hosts were recrystallized from this guest (Chapter 10); it was noted that this was as a result of the presence of TETROL's secondary hydroxy groups, which frequently behave as H-bond donors. However, during the course of another study, an analysis of the inclusion complexes of TETROL with butyric, isobutyric and 3-chloropropionic acid, showed that the secondary hydroxyl groups now behaved as H-bond acceptors, for the first time, and in each complex (Chapter 12). We therefore characterized TETROL as being a bifunctional H-bond donor and acceptor host compound. This host also showed promise for the separation of a 47.6:52.4 *cis*- and *trans*- 2-methylcyclohexanol mixture by favouring the *trans* isomer (80.24%), but these results still require confirmation since these data did not agree with SCXRD site occupation factors (Chapter 11).

Overall, TETROL is a remarkable host compound that is able to form complexes with very many organic guest molecules. It displays selective behaviour in the presence of similar compounds as well as isomers, both positional and geometrical. The vast majority of results communicated in this thesis are completely novel, and these data have significantly added to the current knowledge base in this realm of chemistry.

Future work will include the assessment of TETROL's ability for guest mixtures not described in this thesis, as well as other geometrical, positional, functional group and chain isomers. TETROL may also have the ability to resolve racemates into their constituent enantiomers, as well as have possible applications in asymmetric syntheses.

References

1. Lehn J. M. *Supramolecular Chemistry: Concepts and Perspectives*. Weinheim, **1995**.

2. Steed, J. W.; Atwood, J.L. *Supramolecular Chemistry*. Wiley, **2000**.

3. Gokel, G. W. *Advances in Supramolecular Chemistry*. Elsevier Science, **2001**.

4. Anslyn, E. V.; Dougherty, D. A. *Modern Physical Organic Chemistry*. University Science, **2006**.

5. Manna, A. K. *I. J. Sci. Res.* **2015**, *4* (4), 892–895.

6. Hasenknopf, B.; Lehn, J.-M.; Kneisel, B. O.; Baum, G.; Fenske, D. *Angew. Chem. Int. Ed.* **1996**, *35* (16), 1838–1840.

7. Madou, M. J. *From MEMS to Bio-MEMS and Bio-NEMS: Manufacturing Techniques and Applications*. CRC Press, **2011**.

8. Kumar, N.; Kumbhat, S. *Essentials in Nanoscience and Nanotechnology*. Wiley, **2016**.

9. Manna, A. K. *I. J. Sci. Res.* **2015**, *4* (4), 897–899.

10. Hadži, D. *Hydrogen Bonding: Papers Presented at the Symposium on Hydrogen Bonding Held at Ljubljana, 29 July–3 August 1957*. Elsevier Science, **2013**.

11. Huang, F.; Anslyn, E. V. *Chem. Rev.* **2015**, *115* (15), 6999–7000.

12. Atwood, J. L.; Steed, J. W. *Encyclopedia of Supramolecular Chemistry*. M. Dekker, **2004**.

13. Keene, F. R. *Chirality in Supramolecular Assemblies: Causes and Consequences*. Wiley, **2017**.

14. Dequan, A. L. *Molecular Self-Assembly: Advances and Applications*. Pan Stanford Publishing, **2012**.

15. Groß, R. *Self Assembly*. Gargaud, M. et al. (eds) Encyclopedia of Astrobiology. Springer Berlin Heidelberg: Berlin, Heidelberg, **2011**, 1496–1497.

16. Whitesides, G. M.; Boncheva, M. *Proc. Natl. Acad. Sci. U.S.A* **2002**, *99* (8), 4769–4774.

17. Karim, A. A.; Dou, Q.; Li, Z.; Loh, X. J. *Chem. Asian J.* **2016***, 11* (9), 1300–1321.

18. Fu, X.-L.; Li, J.-S.; Simpson, J. *Crystals* **2012**, *2* (2), 669–674.

19. Beer, P. D.; Gale, P. A.; Smith, D. K. *Supramolecular Chemistry*. Oxford University Press, New York, **1999**.

20. Steed, J. W.; Turner, D.R.; Wallace, K.J. *Core Concepts in Supramolecular Chemistry and Nanochemistry*. John Wiley & Sons, **2007**.

21.   Steiner, T.; Saenger, W. *J. Am. Chem. Soc.* **1993**, *115* (11), 4540–4547.

22.   Barber, J.; Rostron, C. *Pharmaceutical Chemistry*. OUP Oxford, **2013**.

23.   Piletsky, S. A.; Whitcombe, M. J. *Designing Receptors for the Next Generation of Biosensors*. Springer Berlin Heidelberg, **2012**.

24.   Hubbard, R. E.; Kamran Haider, M. *Hydrogen Bonds in Proteins: Role and Strength*. John Wiley & Sons, Ltd, **2001**.

25.   Crowe, J.; Bradshaw, T. *Chemistry for the Biosciences: The Essential Concepts*. OUP Oxford, **2014**.

26.   Campbell, M. K.; Farrell, S. O.; McDougal, O. M. *Biochemistry*. Cengage Learning, **2016**.

27.   Brunning, A. *The Chemical Structure of DNA*. Compound Interest. **2015**: http://www.compoundchem.com/2015/03/24/dna/

28.   Tiekink, E. R. T.; Zukerman-Schpector, J. *The Importance of Pi-Interactions in Crystal Engineering: Frontiers in Crystal Engineering*. Wiley, **2012**.

29.   Dougherty, D. A. *J. Nutr.* **2007**, *137*, 1504S–1508S.

30.   Grumezescu, A., *Food Packaging*. Elsevier Science, **2016**.

31.   Ma, J. C.; Dougherty, D. A. *Chem. Rev.* **1997**, *97* (5), 1303–1324.

32.   Johnson, D. W.; Hof, F. *Aromatic Interactions: Frontiers in Knowledge and Application*. Royal Society of Chemistry, **2016**.

33.   Levitt, M.; Perutz, M. F. *J. Mol. Biol.* **1988**, *201* (4), 751–754.

34.   Ottiger, P.; Pfaffen, C.; Leist, R.; Leutwyler, S.; Bachorz, R. A.; Klopper, W. *J. Phys. Chem. B* **2009**, *113* (9), 2937–2943.

35.   Burkinshaw, S. M.; Filarowski, A. *Physico-chemical Aspects of Textile Coloration*. Wiley, **2016**.

36.   Steiner, T.; Koellner, G. *J. Mol Biol.* **2001**, *305* (3), 535–557.

37.   Burley, S. K.; Petsko, G. A. *FEBS Lett.* **1986**, *203* (2), 139–143.

38.   Knowles, R. *Aromatic Interactions*. MacMillan Group Meeting, **2005**.

39.   Gupta, G. S.; Gupta, A.; Gupta, R. K. *Animal Lectins: Form, Function and Clinical Applications*. Springer Vienna, **2012**.

40.   Kumar, M.; Balaji, P. V. *J. Mol. Model.* **2014**, *20* (2), 2136.

41.   Boehr, D. D.; Farley, A. R.; Wright, G. D.; Cox, J. R. *Chemistry & Biology* **2002**, *9* (11), 1209–1217.

42.   Pierre, V. C.; Kaiser, J. T.; Barton, J. K. *Proc. Natl. Acad. Sci. U.S.A* **2007**, *104* (2), 429–434.

43. Scheiner, S. *Noncovalent Forces*. Springer International Publishing, **2015**.

44. Mao, L.; Wang, Y.; Liu, Y.; Hu, X. *J. Mol Biol.* **2004**, *336* (3), 787–807.

45. Wilson, K. A.; Kellie, J. L.; Wetmore, S. D. *Nucleic Acids Research* **2014**, *42* (10), 6726–6741.

46. Janiak, C. *J. Chem. Soc., Dalton Trans.* **2000**, (21), 3885–3896.

47. Steed, J. W.; Atwood, J. L. *Supramolecular Chemistry*. Wiley, **2013**.

48. Atwood, J. L.; Steed, J. W. *Encyclopedia of Supramolecular Chemistry*. M. Dekker, **2004**.

49. Hof, F. *Chem. Commun.* **2016**, *52* (66), 10093–10108.

50. Powell, H. M. *J. Chem. Soc. (Resumed)* **1948**, (0), 61–73.

51. Hagan, M. *Clathrate Inclusion Compounds*. Reinhold Publishing Coporation: New York, **1962**.

52. Mandelcorn, L. *Non-stoichiometric Compounds*. Academic Press: New York, **1964**.

53. Coleman, A. W. *Molecular Recognition and Inclusion: Proceedings of the Ninth International Symposium on Molecular Recognition and Inclusion, held at Lyon, 7–12 September 1996*. Springer Netherlands, **2012**.

54. Weber, E.; Csoregh, I.; Stensland, B.; Czugler. *J. Am. Xhem. Soc.* **1984**, *106* (11), 3297–3306.

55. Weber, E. *Molecular Inclusion and Molecular Recognition — Clathrates* I. Topics in Current Chemistry: Springer Verlag, Berlin, *140*, **1987**.

56. Atwood, J. L.; Davies, J. E. D.; MacNicol, D. D. *Inclusion Compounds: Key organic host systems*. Academic Press, **1991**.

57. Carey, C. W. *American Scientists*. Facts On File, Incorporated, **2014**.

58. Izatt, R. M.; Pedersen, C. J. *Chem. Rev.* **2007**, *36* (2), 143–147.

59. Tashiro, S.; Minoda, A.; Yamada, M.; Shionoya, M. *Inorg. Chem.* **2009**, *48* (21), 10093–10101.

60. Garg, R.; Singh, R. D. *Effect of Addition of Crown Ether on the Micellar Behavior of Dodecyltrimethylammonium Chloride in Aqueous Media*. GRIN Verlag, **2011**.

61. Ghany, M. F. A.; Hussein, L. A.; Yamani, H. Z. *J. Appl, Pharm. Sci.* **2014**, *4* (07), 032–037.

62. Gokel, G. W.; Leevy, W. M.; Weber, M. E. *Chem. Rev.* **2004**, *104* (5), 2723–2750.

63. Tsirelson, V. G.; Ozerov, R. P. *Electron Density and Bonding in Crystals: Principles, Theory and X-ray Diffraction Experiments in Solid State Physics and Chemistry*. Taylor & Francis, **1996**.

64.   Kazakevich, Y. V.; LoBrutto, R. *HPLC for Pharmaceutical Scientists*. Wiley, **2007**.

65.   Ball, P., *Designing the Molecular World: Chemistry at the Frontier*. Princeton University Press, **1996**.

66.   Johnson, D. A. *Metals and Chemical Change*. Royal Society of Chemistry, **2002**.

67.   Brown, W. H.; Iverson, B. L.; Anslyn, E.; Foote, C. S. *Organic Chemistry*. Cengage Learning, **2013**.

68.   Ariga, K.; Kunitake, T. *Supramolecular Chemistry - Fundamentals and Applications: Advanced Textbook*. Springer Berlin Heidelberg, **2006**.

69.   Johnson, D. W.; Raymond, K.N.; Wong, E.H. *Inorg. Chem.* **2001**, *40*, 4504–4506.

70.   Schneider, H. *Int. J. Mol. Sci.* **2015**, *16*, 6694–6717.

71.   Pedersen, C. J. *J. Chem. Soc.* **1967**, *89*, 7017–7036.

72.   Izatt, R. M. R., J. H.; Nelson, D. P.; Haymore, B. L.; Christensen, J. J. *Science* **1969**, *164* (3878), 443–444.

73.   Izatt, R. M. T. R. E.; Nelson, D. P.; Chan, Y.; Eatough, D. J.; Bradshaw, J. S.; Hansen, L. D.; Christensen, J. J. *J. Am. Chem. Soc.* **1976**, *98* (24), 7626–7630.

74.   Izatt, R. M. P., K.; Bradshaw, J. S.; Bruening, R. L. *Chem. Rev.* **1995**, *95* (7), 2529–2586.

75.   Schalley, C. A.; Springer, A. *Mass Spectrometry of Non-Covalent Complexes: Supramolecular Chemistry in the Gas Phase*. Wiley, **2009**.

76.   Rodriguez, J. D.; Kim, D.; Tarakeshwar, P.; Lisy, J. M. *J. Phys. Chem. A.* **2010**, *114* (3), 1514–1520.

77.   Skorjanc, T.; Benyettou, F.; Olsen, J.-C.; Trabolsi, A. *Chem. Eur. J* **2017**, *23* (35), 8322–8536.

78.   Lee, S.-F.; Zhu, X.-M.; Wang, Y.-X. J.; Xuan, S.-H.; You, Q.; Chan, W.-H.; Wong, C.-H.; Wang, F.; Yu, J. C.; Cheng, C. H. K.; Leung, K. C.-F. *ACS Appl. Mater. Interfaces* **2013**, *5* (5), 1566–1574.

79.   Yu-rong, T.; Shu-qin, Z.; Yu-ting, W.; Xue-song, F. *Wuhan University Journal of Natural Sciences* **2002**, *7* (2), 217–221.

80.   Steed, J. W.; Turner, D. R.; Wallace, K. *Core Concepts in Supramolecular Chemistry and Nanochemistry*. Wiley, **2007**.

81.   Zhang, M.; Yan, X.; Huang, F.; Niu, Z.; Gibson, H. W. *Acc. Chem. Res* **2014**, *47* (7), 1995–2005.

82.   Bansal, R. K. *Phosphorous Heterocycles I*. Springer, **2009**.

83. Davis, F.; Higson, S. *Macrocycles: Construction, Chemistry and Nanotechnology Applications*. Wiley, **2011**.

84. Bag, B.; Mukhopadhyay, P.; Bharadwaj, P. K. *Curr. Sci.* **2006**, *91* (9), 1166–1175.

85. Katchalski-Katzir, E.; van Binst, G.; Prelog, V. *Design and Synthesis of Organic Molecules Based on Molecular Recognition: Proceedings of the XVIIIth Solvay Conference on Chemistry Brussels, November 28 - December 01, 1983*. Springer Berlin Heidelberg, **2012**.

86. Sapse, A. M.; von R. Schleyer, P. *Lithium Chemistry: A Theoretical and Experimental Overview*. Wiley, **1995**.

87. Tai, Y. F.; Piccini, P. *J. Neurol. Neursurg, Psychiatry.* **2004**, *75* (5), 669–676.

88. Miele, E.; Spinelli, G. P.; Tomao, F.; Zullo, A.; De Marinis, F.; Pasciuti, G.; Rossi, L.; Zoratto, F.; Tomao, S. *J. Exp. Clin. Cancer Res.* **2008**, *27* (1), 52.

89. Foster, B.; Bagci, U.; Mansoor, A.; Xu, Z.; Mollura, D. J. A. *Comput. Biol. Med* **2014**, *0*, 76–96.

90. Fu, Y.; Ong, L.C.; Ranganath, S.H.; Zheng, L.; Kee, I.; Zhan, W.; Yu, S.; Chow, P.K.H.; Wang, C. *PLoS One* **2016**, *11* (2), e0148123.

91. Saha, G. B. *Basics of PET Imaging: Physics, Chemistry, and Regulations*. Springer International Publishing, **2015**.

92. Kuntzsch, M.; Lamparter, D.; Brüggener, N.; Müller, M.; Kienzle, G. J.; Reischl, G. *Pharmaceuticals* **2014**, *7* (5), 621–633.

93. Yu, S. *Biomed Imaging Interv J.* **2006**, *2* (4), e57.

94. Loftsson, T. *J. Incl. Phenom. Macrocycl. Chem.* **2002**, *44* (1), 63–67.

95. Marques, H. M. C. *Flavour Fragr. J.* **2010**, *25*, 313–325.

96. Roux, M.; Perly, B.; Djedaini-Pilard, F. *Eur Biophys J.* **2007**, *36* (8), 861–867.

97. Laza-Knoerr, A. L.; Gref, R.; Couvreur, *J. Drug Target* **2010**, *18* (9), 645–656.

98. Blanford, W. J. *J. Incl. Phenom. Macrocycl. Chem.* **2014**, *79* (1), 57–64.

99. Szejtli, J. *Chem. Rev.* **1998**, *98* (5), 1743–1754.

100. Nasir, A.; Harikumar S.L; Kaur A. *Int. J. Pharm.* **2012**, *3* (4), 44–50.

101. Cheirsilp, B.; Rakmai, J. *Biol Eng Med.* **2016**, *2* (1), 1–6.

102. Otero-Espinar, F. J.; Torres-Labandeira, J.J.; Alvarez-Lorenzo, C.; Blanco- Méndez, J. *J. Drug Deliv. Sci. Technol.* **2010**, *20* (4), 289–301.

103. Kandoth, N.; Choudhury, S.; Mukherjee, T.; Pal, H. *Photochem. Photobiol. Sci.* **2009**, *8*, 82–90.

104. Kandoth, N.; Choudhury, S. D.; Mukherjee, T.; Pal, H. *Photochem. Photobiol. Sci.* **2009**, *8* (1), 82–90.

105. Ezawa, T.; Inoue, Y.; Tunvichien, S.; Suzuki, R.; Kanamoto, I. Int J Med Chem. **2016**, *2016*, 1–9.

106. López-Nicolás, J. M.; Rodríguez-Bonilla, P.;García-Carmona, F. *Crit. Rev. Food Sci. Nutr.* **2014**, *54* (2), 251–276.

107. Mortensen, S. A.; Rosenfeldt, F.; Kumar, A.; Dolliner, P.; Filipiak, K.J.; Pella, D.; Alehagen, U.; Steurer, G.; Littarru, G.P. *JACC Heart Fail.* **2014**, *2* (6).

108. Liu, H.-T.; Cheng, S.-B.; Huang, Y.-C.; Huang, Y.-T.; Lin, P.-T. *Nutrients* **2017**, *9*, 29.

109. Fir, M. M.; Smidovnik, A.; Milivojevic, L.; Zmitek, J.; Prosek, M. *J. Incl. Phenom. Macrocycl. Chem.* **2009**, *64* (3), 225–232.

110. Terao, K.; Nakata, D.; Fukumi, H.; Schmid, G.; Arima, H.; Hirayama, F.; Uekama, K. *Nutr. Res.* **2006**, *26* (10), 503–508.

111. Toda, F. Isolation and Optical Resolution of Materials Utilizing Inclusion Crystallization. In *Molecular Inclusion and Molecular Recognition — Clathrates I*, Weber, E., Ed. Springer Berlin Heidelberg: Berlin, Heidelberg, **1987**

112. Toda, F.; Bishop, R.; Lehn, J. M. *Separations and Reactions in Organic Supramolecular Chemistry*. Wiley, **2004**.

113. Toda, F. *Stud. Surf. Sci. Catal.* **1987**, *54*, 340–351.

114. Afonso, C. A. M.; Crespo, J. P. G.; Anastas, P. T. *Green Separation Processes: Fundamentals and Applications*. Wiley, **2006**.

115. Sykes, N. M.; Su, H.; Weber, E.; Bourne, S. A.; Nassimbeni, L. R. *Cryst. Growth Des.* **2017**, *17* (2), 819–826.

116. Samipillai, M.; Batisai, E.; Nassimbeni, L. R.; Weber, E. *CrystEngComm.* **2015**, *17* (43), 8332–8338.

117. Nassimbeni, L. R.; Marivel, S.; Su, H.; Weber, E. *RSC Adv.* **2013**, *3* (48), 25758–25764.

118. Weatherley, L. R. *Engineering Processes for Bioseparations*. Elsevier Science, **2013**.

119. Whitten, K. W.; Davis, R. E.; Peck, L.; Stanley, G. G. *Chemistry*. Cengage Learning, **2013**.

120. Chaloner, P. *Organic Chemistry: A Mechanistic Approach*. CRC Press, **2014**.

121. Webb, G. A. *Annual Reports on NMR Spectroscopy*. Elsevier Science, **2017**.

122. Arai, Y.; Sako, T.; Takebayashi, Y. *Supercritical Fluids: Molecular Interactions, Physical Properties and New Applications*. Springer Berlin Heidelberg, **2013**.

123. Forecasters, M. S. *Global Cresol Market Growth Opportunities, Driving Factors by Manufacturers, Regions, Type and Application, Forecast Analysis to 2022.* MarketSizeForecasters.com, **2017**.

124. McCombe, K.; Wijayasiri, L. *The Primary FRCA Structured Oral Exam Guide 2, Second Edition.* CRC Press, **2016**.

125. Armarego, W. L. F. *Purification of Laboratory Chemicals.* Elsevier Science, **2017**.

126. Arora, A. *Organic Chemistry: Aromatic, Alcohols Aldehydes & Acids.* Discovery Publishing House, **2006**.

127. Chauhan, B. S. *Engineering Chemistry (M.T.U.).* Laxmi Publications, **2008**.

128. King, C. J. *Separation Processes: Second Edition.* Dover Publications, **2013**.

129. Pivovar, A. M.; Holman, K. T.; Ward, M. D. *Chem. Mater.* **2001**, *13* (9), 3018–3031.

130. Hargittai, M.; Hargittai, I. *Advances in Molecular Structure Research.* Elsevier Science, **1998**.

131. Cragg, P. J. *Supramolecular Chemistry: From Biological Inspiration to Biomedical Applications.* Springer Netherlands, **2010**.

132. Brittain, H. G. *Analytical Profiles of Drug Substances and Excipients.* Elsevier Science, **1993**.

133. Pomeranz, Y. *Food Analysis: Theory and Practice.* Springer US, **2013**.

134. Nassimbeni, L. R. *Acc. Chem. Res.* **2003**, *36* (8), 631–637.

135. Caira, M. R.; Nassimbeni, L. R.; Niven, M. L.; Schubert, W.-D.; Weber, E.; Dorpinghaus, N. *J. Chem. Soc., Perkin Trans. 2* **1990**, (12), 2129–2133.

136. Bourne, S. A.; Nassimbeni, L. R.; Skobridis, K.; Weber, E. *J. Chem. Soc. Chem. Commun.* **1991**, (5), 282–283.

137. Toda, F.; Tanaka, K.; Nagamatsu, S.; Mak, T. C. W. *Isr. J. Chem.* **1985**, *25* (3-4), 346–352.

138. Caira, M. R.; Horne, A.; Nassimbeni, L. R.; Okuda, K.; Toda, F. *J. Chem. Soc., Perkin Trans. 2* **1995**, (6), 1063–1067.

139. Weber, E. *Molecular Inclusion and Molecular Recognition Clathrates I and II.* Topics in Current Chemistry: Springer-Verlag, Berlin, *140*, **1987**.

140. Coetzee, A.; R. Nassimbeni, L.; Su, H. *J. Chem. Res. (S)* **1999**, (7), 436–437.

141. Barbour, L. J.; Caira, M. R.; Nassimbeni, L. R. *J. Chem. Soc., Perkin Trans. 2* **1993**, (12), 2321–2322.

142. Caira, M. R.; Coetzee, A.; Nassimbeni, L. R.; Toda, F. *J. Chem. Res. (S)* **1996**, 280.

143. Coetzee, A.; Nassimbeni, L. R.;. Su, H. *J. Chem. Res. (S)* **1998**, 740–741.

144. Goldberg, I.; Stein, Z.; Tanaka, K.; Toda, F. *J. Incl, Phenom, Macrocycl. Chem.* **1988**, *6* (1), 15–30.

145. Weber E.; Haase D. M. R.; Seichter W.; Rheinwald G. *Supramol. Chem.* **2005**, *17*, 303–314.

146. Weber, E.; Nitsche, S.; Wierig, A.; Csoregh, I. *Eur. J. Org. Chem.* **2002**, 856–872.

147. Nassimbeni, L. R.; Ramon, G.; Weber, E. *J. Therm. Anal. Calorim.* **2007**, *90* (1), 31–37.

148. Seebach, D.; Beck, A. K.; Heckel, A. *Angew. Chem. Int. Ed.* **2001**, *40* (1), 92–138.

149. Zhou, Q. L. *Privileged Chiral Ligands and Catalysts*. Wiley, **2011**.

150. Caira, M. R.; Tanaka, K. *Inclusion and Optical Resolution of Guest Molecules by Selected Synthetic Dihydroxy- and Trihydroxy-Host Compounds Containing Heterocyclic Scaffolds*. In *Heterocyclic Supramolecules II*, Matsumoto, K. et al (eds): Springer, Berlin, **2009**.

151. Barton, B.; Hosten, E. C.; Jooste, D. V. *Tetrahedron* **2017**, *73* (18), 2662–2673.

152. Gawroński, J.; Gawronska, K. *Tartaric and Malic Acids in Synthesis: A Source Book of Building Blocks, Ligands, Auxiliaries, and Resolving Agents*. Wiley, **1999**.

153. Quinkert, G.; Kisakürek, M. V. *Essays in Contemporary Chemistry: From Molecular Structure Towards Biology*. Wiley-VCH, **2001**.

154. Rovis, T. *Handbook of Reagents for Organic Synthesis: Reagents for Organocatalysis*. Wiley, **2016**.

155. Ghazali, N. F.; Ferreira, F. C.; White, A. J. P.; Livingston, A. G. *Tetrahedron: Asymmetry* **2006**, *17* (12), 1846–1852.

156. Clayden, J.; Brown, R.; Cox, L.; Eames, J.; Fader, L. *Science of Synthesis: Houben-Weyl Methods of Molecular Transformations Vol. 36: Alcohols*. Thieme, **2014**.

157. Barton, B.; Caira, M. R.; Hosten, E. C.; McCleland, C. W. *Tetrahedron* **2013**, *69* (41), 8713–8723.

158. Hu, X.; Shan, Z.; Peng, X.; Li, Z. *Tetrahedron: Asymmetry* **2009**, *20* (21), 2474–2478.

159. Barton, B.; Caira, M. R.; Hosten, E. C.; McCleland, C. W.; Weitz, *S. J. Org. Chem.* **2015**, *80* (14), 7184–7192.

160. Barton, B.; Caira, M. R.; Hosten, E. C.; McCleland, C. W.; Weitz, S. *ChemComm* **2014**, *50* (87), 13353–13355.

161. Barton, B.; Hosten, E. C.; Pohl, P. L. Tetrahedron 2016, 72 (49), 8099–8105

162. Barton, B.; Hosten, E. C.; Pohl, P. L. *Aust. J. Chem.*, **2017**, DOI: 10.1071/CH17532

163. Toda, F.; Tanaka, K.; Stein, Z.; Goldberg, I. *J. Chem. Soc. Perkin Trans 2* **1993**, (12), 2359–2361.

164. Haynes, W. M., *CRC Handbook of Chemistry and Physics, 95th Edition*. CRC Press, **2014**.

165. APEX2, SADABS and SAINT; Bruker AXS: Madison, Wisconsin, USA, **2010**.

166. Sheldrick, G. M. *Acta Crystallogr.* **2015**, C71, 3–8.

167. Hübschle, C. B.; Sheldrick, G. M.; Dittrich, B. J. *Appl. Crystallogr.* **2011**, *44*, 1281

168. Wolff, S. K.; Grimwood, D. J.; McKinnon, J. J.; Jayatilaka, D.; Spackman, M. A. Crystalexplorer 17.5; University of Western Australia: Perth, **2007**; hirshfeldsurface.net.

169. ConQuest, A program for the search of the CSD, Version 1.16, **2013**, United Kingdom.

170. PoV-Ray for Windows: *Version 3.le.watcom.win32*, The persistence of Vision Development Team: © **1991-1999**.

171. Bruker **2005**, APEX2, Version 1.0-27, Bruker AXS Inc., Madison, Wisconsin, USA.

172. Plechkova, N. V.; Seddon, K. R. Ionic Liquids Completely UnCOILed: Critical Expert Overviews. Wiley, 2015.

173. Antony, R.; David Manickam, S. T.; Kollu, P.; Chandrasekar, P. V.; Karuppasamy, K.; Balakumar, S. *RSC Adv.* **2014,** *4* (47), 24820–24830.

174. Giesen, J. *Process for separation of cyclohexanol and cyclohexanone*. Google Patents, **1960**.

175. Anderson, J. R.; Boudart, M. *Catalysis: Science and Technology*. Springer Berlin Heidelberg, **2012**.

176. Buhler, D. R.; Reed, D. J. *Nitrogen and Phosphorus Solvents*. Elsevier Science, **2013**.

177. Barker, R. S. *Production of cyclohexylamine*. Google Patents, **1967**.

178. Manghnani, M. H.; Nellis, W. J.; Nicol, M. F.; Science, I. A. f. t. A. o. H. P.; *Technology, Science and Technology of High Pressure: Proceedings of the International Conference on High Pressure Sciene and Technology (AIRAPT-17), Honolulu, Hawaii, 25-30 July, 1999*. Universities Press (India) Limited, **2000**.

179. Bondi, A. *J. Phys. Chem. A* **1964**, *68* (3), 441–451.

180. Barabash, R. I.; Ice, G. E.; Turchi, P. E. A. *Diffuse Scattering and the Fundamental Properties of Materials*. Momentum Press, **2009**.

181. Mooibroek, T. J. *CrystEngComm* **2017**, *19* (31), 4485–4488.

182. Abraham, M. H.; Duce, P. P.; Prior, D. V.; Barratt, D. G.; Morris, J. J.; Taylor, P. J. *J. Chem. Soc. Perkin Trans 2* **1989**, (10), 1355–1375.

181. Schalley, C. A.; Armentrout, P. B. *Modern Mass Spectrometry*. Springer, **2003**.

182. Miller, A.; Solomon, P. H. *Writing Reaction Mechanisms in Organic Chemistry*. Harcourt/Academic Press, **2000**.

183. Neumann, D.; Ritzer, J.; Effenberger, G. *Method for preparing cyclic ketones*. Google Patents, **2014**.

184. Schumann, W. K.; Kut, O. M.; Baiker, A. *Ind. Eng. Chem. Res* **1989**, *28* (6), 693–697.

185. Patnaik, P. *A Comprehensive Guide to the Hazardous Properties of Chemical Substances*. Wiley, **2007**.

186. Weisser, O.; Landa, S. *Sulphide Catalysts, Their Properties and Applications*. Elsevier Science, **2013**.

187. Scriven, E. F. V. *Pyridines: from lab to production*. Elsevier Science, **2013**.

188. Wilbur, S. B.; Jones, D.; Risher, J.F.; Crawford, J.; Tencza, B.; Llados, F.; Diamond, G.L.; Citra, M.; Osier, M.R.; Lockwood, L.O. *Toxicological Profile for 1,4-Dioxane*. Agency for Toxic Substances and Disease Registry (US), **2012**.

189. Dikshith, T. S. S. *Safe Use of Chemicals: A Practical Guide*. CRC Press, **2008**.

190. Hohenstein, E. G.; Sherrill, C. D. *J. Phys. Chem. A* **2009**, *113* (5), 878–886.

191. Buysch, H. J.; Hullmann, M.; Puppe, L. *Process for separating aniline derivatives*. Google Patents, **1990**.

192. Bayer, A. C.; Pittman, C. U.; Wang, L.; Alley, G.; Maliyackel, A. C. *Selective N-alkylation of aniline in the presence of zeolite catalysts*. Google Patents, **1991**.

193. Ivanova, I. I.; Pomakhina, E. B.; Rebrov, A. I.; Wang, W.; Hunger, M.; Weitkamp, J. *Kinetics and Catalysis* **2003**, *44* (5), 701–709.

194. Fleck, R. N.; Wight, C. G. *Separation of toluidine isomers*. Google Patents, **1962**.

195. Franck, H. G.; Stadelhofer, J. W. *Industrial Aromatic Chemistry: Raw Materials · Processes · Products*. Springer Berlin Heidelberg, **2012**.

196. Rase, H. F. *Handbook of Commercial Catalysts: Heterogeneous Catalysts*. Taylor & Francis, **2000**.

197. Cook, J. G. *Handbook of Textile Fibres: Man-Made Fibres*. Elsevier Science, **1984**.

198. Stellman, J. M.; Office, I. L. *Encyclopaedia of Occupational Health and Safety: Guides, indexes, directory*. International Labour Office, **1998**.

199. Kiyuma, T.; Naramoto, I. *Method for production of cyclohexylamines*. Google Patents, **1990**.

200. Lu, X.; Chen, Y.; Zhao, Z.; Deng, H.; Zhou, D.; Wei, C.; Nie, R.; Xia, Q. *Highly selective one-step hydrogenation of nitrobenzene to cyclohexylamine over the supported 10%*

Ni/carbon catalysts doped with 3[per thousand] Rh. RSC Advances **2016**, *6* (19), 15354–15361.

201. Arrigo, J. T.; Christensen, N. J. *Hydrogenation of nitrobenzene*. Google Patents, **1972**.

202. Králik, M.; Turakova, M.; Macak, I.; Wenchich, S. **2012**, *6* (12), 1074–1082.

203. Rase, H. F. *Handbook of Commercial Catalysts: Heterogeneous Catalysts*. CRC Press, **2016**.

204. Mukhopadhyay, A. K. *Industrial Chemical Cresols and Downstream Derivatives*. CRC Press, **2004**.

205. Vögtle, F.; Alfter, F. *Supramolecular chemistry: an introduction*. Wiley, **1991**.

206. Izatt, R. M.; Bradshaw, J. S. *The Pedersen Memorial Issue*. Springer Netherlands, **2012**.

207. Di Silvestro, G.; Adler, G.; Bolognesi, A. *Proceedings of the 9th International Conference on the Chemistry of the Organic Solid State: Held at Lago Como, Italy, July 1989*. Gordon and Breach, **1990**.

208. Barton, B.; Hosten, E. C.; Pohl, P. L. *Tetrahedron* **2016**, *72* (49), 8099–8105.

209. Peters, K. E.; Walters, C. C.; Moldowan, J. M. *The Biomarker Guide*. Cambridge University Press, **2005**.

210. Moore, J. W.; Stanitski, C. L. *Chemistry: The Molecular Science*. Cengage Learning, **2014**.

211. Ray, G. C. *Separation of cis and trans isomers*. Google Patents, **1958**.

212. Singh, R. *Chromatography*. Mittal Publ., **2002**.

213. Coffey, S. *Including the Official Reports of a Number of Learned Societies: The Dental Practitioner and Dental Record*. Elsevier Science, **2013**.

214. Jackman, L. M.; Macbeth, A. K.; Mills, J. A. *J. Chem. Soc (Resumed)* **1949**, (0), 1717–1720.